THE DEVELOPMENT AND APPLICATION OF A NEW SEMI-ANALYTICAL MODEL TO ESTIMATE PERMEABILITY FROM MERCURY INJECTION CAPILLARY PRESSURE

A Thesis

by

SARIN APISAKSIRIKUL

Submitted to the Office of Graduate and Professional Studies of
Texas A&M University
in partial fulfillment of the requirements for the degree of

MASTER OF SCIENCE

Chair of Committee,	Thomas A. Blasingame
Committee Members,	I. Yucel Akkutlu
	Maria A. Barrufet
Head of Department,	A. Daniel Hill

May 2016

Major Subject: Petroleum Engineering

ABSTRACT

In 2005 Huet proposed a semi-analytical model to correlate between rock permeability and capillary pressure data. The model was proposed with the intention to be a "universal" model where the correlation was unique over a wide range of rock types. The objectives of this study are to verify the power-law relationship between permeability and the mercury injection capillary pressure (MICP) parameters in Huet's semi-analytical model and to propose a new correlation to predict permeability from the MICP data. We used a data set consisting of 323 samples from different lithologies including tight, sandstone and carbonate reservoirs. The semi-analytical (Huet) model correlates permeability with porosity (ϕ), irreducible wetting phase saturation (S_{wi}), displacement pressure (p_d), and the pore-size distribution index (λ) obtained from MICP data. The resulting correlation equation generated in this work shows very good coherence for permeabilities higher than 1 md and reasonably good coherence for permeabilities less than 1 md.

In this work we have refitted the Huet model to our database of 323 samples and over the entire range of permeabilities considered (*i.e.*, $1x10^{-7}$ to $1x10^{4}$ md), 95 percent of the data are related to the proposed model by a factor of 9.1 or less, and 58 percent of the data are related to the proposed model by a factor of 2 or less. When the data are "partitioned," we find that our refitted model has a 95% prediction interval within a factor of 3.97 for permeability values greater than 1 md and 12.70 for permeability values less than 1 md. We also showed in this work that our proposed model outperformed the Swanson model to predict permeability from MICP data.

In addition to the statistical work, we performed analytical derivations to establish an analytical relationship between the semi-analytical (Huet) model and the Swanson model. Our derivation results support the application of the semi-analytical model as a viable (and possibly superior) alternative to the Swanson model. Our analytical work also provides an insight into the viability of the Swanson model, which was developed empirically. Based on this derivation, we propose a new method to determine the Brooks-Corey capillary pressure model parameters as an alternative to the regression method.

In short, this work has confirmed the power-law relationship between permeability and the mercury injection capillary pressure data to be valid for both sandstone and carbonate reservoirs. The new correlation model proposed should provide an improvement for the prediction of permeability from the mercury injection capillary pressure data. This work also holds promise in relating the Huet semi-analytical model to the Swanson empirical model directly, and we expect that (eventually) a type of "hybrid" model will evolve which will include the influence of both the Brooks-Corey and the Swanson capillary pressure models.

DEDICATION

This work is dedicated to my father and mother who have always loved me unconditionally.

ACKNOWLEDGEMENTS

I would first like to thank my advisor and the chair of committee, Dr. Blasingame, for his valuable guidance and continuous support throughout my time at Texas A&M University. His tough advice and kind understanding help to push me through challenging times and enabled this research to reach its proper completion.

I would also like to thank Dr. Akkutlu and Dr. Barrufet for their time and support to serve as the members of my committee. I would also like to extend my gratitude to Dr. Chicheng Xu for sharing the data from his work, these data provided a significant contribution to my research.

I also thank my colleagues, the faculty, and the staff at Texas A&M University for making my M.S. studies a great learning experience for me. I would also like to thank all my friends, as well as the Thai Student Association for their friendship — their support helped to make me feel like I am never far from home.

Finally, I must express my profound gratitude to my parents for providing me with unfailing support and continuous encouragement throughout my years of study far away from home. This work would not have been completed without all of their support. Thank you.

TABLE OF CONTENTS

Page

LIST OF FIGURES

FIGURE Page

FIGURE Page

LIST OF TABLES

CHAPTER I

INTRODUCTION

1.1 Introduction

The estimation of formation permeability from mercury injection capillary pressure (MICP) is useful when core samples are not available for routine permeability measurements (Kamath 1992). Estimation of formation permeability from MICP is also beneficial for tight reservoir samples, where permeability measurement using constant-flow equipment becomes very time consuming and possibly/probably inaccurate (Dicker and Smits 1988). Huet (2005) proposed a semi-analytical model with the intention for this to be a "universal" model where the correlation between formation permeability and capillary pressure data was uniquely correlated over a wide range of rock types. While it is possible that there will never be a "universal" relationship, work such as that proposed by Huet (2005) does provide a "semi-analytical" basis for relating permeability. In this work, we provide a verification to the proposed relationship of Huet through the statistical and analytical work. With a comprehensive data set (323 samples are used for our work), we also provide a revised semi-analytical model to predict absolute permeability from MICP data.

1.2 Statement of Problem

Brooks-Corey Capillary Pressure Model

In 1964, Brooks and Corey (1964) observed a power-law relationship in a log-log plot of capillary pressure versus normalized saturation. As such, Brooks and Corey introduced a model to describe capillary pressure as a function of wetting phase saturation — this model is given as:

$$p_C = p_d \, (S_w^*)^{-1/\lambda} \quad \text{.....(1.1)}$$

Where S_w^* is the effective saturation function and is defined as:

$$S_w^* = \left[\frac{S_w - S_{wi}}{1 - S_{wi}} \right] \quad \text{.....(1.2)}$$

Brooks and Corey (1964) proposed the following procedure to determine the three characteristic parameters (λ, S_{wi}, p_d) from capillary pressure data, as follows:

1. Obtain an initial estimate of S_{wi} from a Cartesian plot of p_c vs. S_w. S_{wi} is the wetting phase saturation where the p_c trends "asymptotic" and approaches infinity.
2. Compute the S_w^* function using this initial estimate of S_{wi} and then generate a log-log plot of p_c versus S_w^* — there is an expectation of a straight-line trend (*i.e.*, the power-law model).

3. Near the point of asymptotic capillary pressure, it is possible that the power-law model will deviate (due to the particular value of S_{wi} in the normalized saturation function (S_w^*)) — in such cases the S_{wi}-value should be revised in an attempt to obtain a straight-line trend of log(p_c) versus log(S_w^*).
4. The revision of S_{wi} should be repeated until most of the data points form a straight-line trend of log(p_c) versus log(S_w^*). It should be noted that capillary pressure data are not always uniquely defined by the Brooks-Corey model (*i.e.*, Eq. 1.1) and one must exercise practical judgment as to whether or not the model applies for a specific case.
5. Obtain p_d from the *y*-intercept ($S_w^* = 1$).
6. Obtain λ from the reciprocal slope of the final straight line on the log-log plot (*i.e.*, slope = $-1/\lambda$).

This process is simplified by the use of regression as described by Huet (2005). The three parameters (λ, S_{wi}, p_d) can be determined simultaneously using the Solver Module in Microsoft Excel (2013). However, as noted by Huet (2005), "*... while the data-model fit is good, human intervention is required to ensure that the model is properly applied to the data*".

Thomeer Mercury Injection Capillary Pressure Model

In 1960, Thomeer (1960) proposed and demonstrated that mercury/air capillary pressure curves can be uniquely defined as a hyperbolic function using a log-log plot of capillary pressure (p_c) versus percent bulk volume occupied by mercury (S_b). The "Thomeer" model consists of three parameters (F_g, $S_{b\infty}$, p_d) that are used to characterize the curve and can be written as;

$$\frac{S_b}{S_{b\infty}} = \exp\left[\frac{-F_g}{\ln\left[\frac{p_c}{p_d}\right]}\right] \quad \text{.....(1.3)}$$

Where S_b is the percent bulk volume occupied by mercury and can be written as:

$$S_b = (1 - S_w)\phi \times 100 \quad \text{.....(1.4)}$$

Swanson's Parameter (Based on the Thomeer Model)

In 1981, Swanson (1981) suggested that the "apex" of the Thomeer hyperbolic model is uniquely correlated with parameters such as permeability, and specifically, Swanson defined the apex as $[S_b/p_c]_A$, which is the point where the value $[S_b/p_c]$ is maximum. A detailed derivation of the apex relations are provided in Appendix A. The schematics showing the apex of the Thomeer hyperbolic model and the Swanson apex are shown in **Fig. 1.1** and **1.2**.

The Swanson (1981) study considered 24 clean sandstone samples and 32 carbonate samples, and Swanson's work demonstrated a good correlation between brine permeability and the Swanson parameter $[S_b/p_c]_A$. The correlation for these data is given by:

$$k = 355\left[\frac{S_b}{p_c}\right]_A^{2.005} \quad \text{.....(1.5)}$$

The model proposed by Swanson can be written in a generic form as:

$$k = a_1\left[\frac{S_b}{p_c}\right]_A^{a_2} \quad \text{.....(1.6)}$$

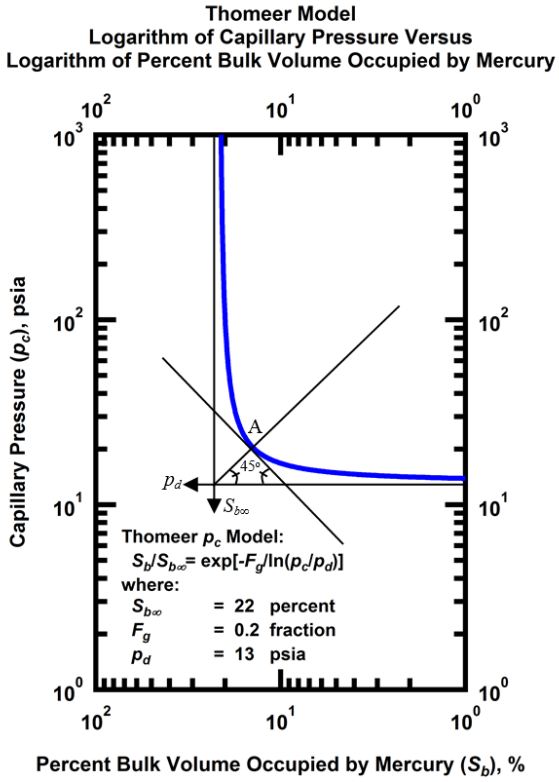

Figure 1.1 — Schematic diagram of the Thomeer (1960) hyperbolic p_c model with the apex shown as point A — which is the intersection of the hyperbola with 45° line passing through the origin of the hyperbolic axis.

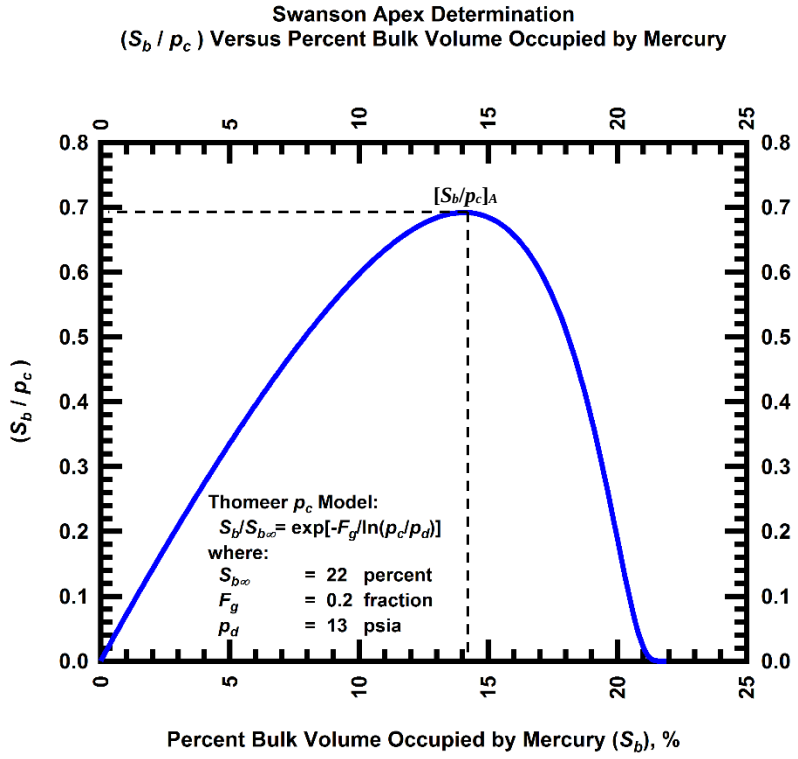

Figure 1.2 — Schematic diagram of $[S_b/p_c]$ plot versus S_b where the Swanson parameter $[S_b/p_c]_A$ (Swanson 1981) is the maximum $[S_b/p_c]$ value, which is the "apex" of the Thomeer hyperbola as shown in **Fig 1.1**.

Semi-Analytical Model to Estimate Permeability from Capillary Pressure

Huet (2005) derived a semi-analytical model to predict absolute permeability from capillary pressure parameters. The model, which is based on the work by Purcell (1949), Burdine (1953), Wyllie-and-Gardner (1958) and Brooks-and-Corey (1964), is given as:

$$k = 10.66\,\alpha(\sigma\cos\theta)^2(1-S_{wi})^4\phi^2\frac{1}{p_d^2}\left[\frac{\lambda}{\lambda+2}\right] \quad \text{.....(1.7)}$$

This derived relationship suggests that permeability should be a power-law function of displacement pressure (p_d), index of pore-size distribution (λ), irreducible wetting phase saturation (S_{wi}), and porosity (ϕ). Expressing Eq. 1.7 in a (generic) correlation form, we have:

$$k = a_1\frac{1}{(p_d)^{a_2}}\left[\frac{\lambda}{\lambda+2}\right]^{a_3}(1-S_{wi})^{a_4}\phi^{a_5} \quad \text{.....(1.8)}$$

In the Huet study (Huet 2005), the model (Eq. 1.8) was correlated using 89 samples from sandstone and carbonate reservoirs. For reference (and for relevance to this study), the Huet study considered only cases where the capillary pressure was obtained using the mercury injection method. The result showed an excellent correlation over a wide range of permeability (0.004 md to 8340 md), which suggests significant potential of this model to predict permeability from capillary pressure.

In the present work, we extended the use of this model to a larger data set to further verify the application of this model using mercury injection capillary pressure (MICP) data. Our study uses data from the original work (Huet 2005) along with additional core samples from tight sand and carbonate reservoirs. This new data set covers permeabilities which range from $1x10^{-7}$ to $1x10^{4}$ md, and porosities which range from 0.009 to 0.371 (or 0.9 to 37.1 percent). Our additional data also covers a number of cases in the mid-range of permeabilities (0.5 to 100 md) which was lacking in the original work by Huet (2005).

For each sample, we matched the MICP data with the Brooks-Corey capillary pressure model using regression (with some hand tuning). The objective parameters p_d, λ and S_{wi} were then correlated to the measured permeabilities using the (Huet) semi-analytical correlation model (Eq. 1.8). The results obtained using the semi-analytical correlation model (Eq. 1.8) were then compared to the results obtained using the Swanson correlation model (Eq. 1.6). For the same set of samples, we determined the Swanson parameter ($[S_b/p_c]_A$) from the MICP data. The obtained values were then correlated with the measured permeabilities using the Swanson correlation model (Eq. 1.6) where the coefficients were optimized to our data sets.

Equivalence of Model Parameters — Brooks-Corey Model and Thomeer-Swanson Model

In this study, the analytical relationship between the Swanson(-Thomeer) parameter ($[S_b/p_c]_A$) and the Brooks-Corey parameters was derived. The pore-size distribution index (λ) and the irreducible wetting phase saturation (S_{wi}) were found to be a function of displacement pressure (p_d) and the Swanson "apex" parameter $[S_b/p_c]_A$, which can be readily determined from MICP data. The derivation of these relations is shown in Appendix B, the results of which are:

$$\left[\frac{S_b}{p_c}\right]_A = 100\frac{1}{p_d}\left[\frac{\lambda}{(1+\lambda)^{(1+\frac{1}{\lambda})}}\right](1-S_{wi})\,\phi \qquad \text{.....(1.9)}$$

Where Eq. 1.9 can be separated into component forms as: (see Appendix B for details)

$$(p_c)_A = p_d\left[\frac{1}{1+\lambda}\right]^{-1/\lambda} \qquad \text{.....(1.10)}$$

$$(S_b)_A = 100\frac{\lambda}{1+\lambda}(1-S_{wi})\,\phi \quad \text{.....(1.11)}$$

Using these results, we formulated the Swanson model (Eq. 1.6) into the same form as the semi-analytical model (Eq. 1.8). We then compared the two models and explained how the Swanson parameter ($[S_b/p_c]_A$) can be correlated with permeability and how the semi-analytical correlation model should (in principle) have a better predictability than the original Swanson correlation model.

In our work, we reviewed hundreds of MICP data cases and determined the Brooks-Corey parameters by plotting techniques. This is time-consuming and can yield multiple realizations (scenarios) for λ and S_{wi}. In contrast, the determination of the threshold/displacement pressure (p_d) is more straightforward (*i.e.*, the extrapolation of the p_c trend to $S_w = 1$). In addition, the majority of the cases we reviewed exhibited a clear maximum value of $[S_b/p_c]$ (*i.e.*, $[S_b/p_c]_A$).

As a practical matter, Eqs. 1.10 and 1.11 can be used to relate the $(p_c)_A$ and $(S_b)_A$ parameters to the Brooks-Corey parameters — in particular, to estimate the λ-parameter. Using these derived relations, we propose a new method to determine the pore-size distribution index (λ) and the irreducible wetting phase saturation (S_{wi}).

1.3 Objectives

The overall objectives of this work are:

- To *verify* the power-law relationship between permeability and capillary pressure proposed by Huet (2005);
- To *develop* a new semi-analytical model based on the relationship proposed by Huet (2005) to predict absolute permeability from mercury injection capillary pressure (MICP);
- To *compare* the semi-analytical (Huet) correlation model to the Swanson correlation model;
- To *derive* an analytical relationship between the semi-analytical (Huet) correlation model and the Swanson correlation model;
- To *propose* an alternative method to determine the Brooks-Corey capillary pressure model parameters from MICP data.

1.4 Results Summary

Development of a New Semi-Analytical Model

To perform our work, we used the mercury injection capillary pressure data sets obtained from the original work of Huet (2005), as well as additional data sets from the literature (Byrnes 2009; Xu 2013). Samples from tight sandstone, conventional sandstone, and carbonate reservoirs were used. We attempted to find relevant "shale" samples, but no comprehensive/complete data sets for shales could be found in the public

literature. In this work, a total of 573 data sets have been reviewed. We selected 323 data sets where the MICP data exhibit a suitably smooth trend sufficient to make parameter estimates. For reference, our working data set has a range of permeability values from $1x10^{-7}$ md to $1x10^{4}$ md; and a range of porosity values from 0.9 to 37.1 percent.

For each sample, the Brooks-Corey model was matched to the MICP data to estimate the p_d, S_{wi}, and λ values. As an observation, we noted that several of the MICP data tended to deviate from the Brooks-Corey model at high mercury saturation (*i.e.*, low wetting phase saturation) — we believe this is due to the ultra-high pressures employed by the MICP device (*i.e.*, greater than 60,000 psia). Because of these deviation features, the selection of a concise data range for matching the data with a model was often subjective. We state that our workflow for this process was both robust and consistent, but we must acknowledge that some of the cases have more "subjective" matches than others. Using the results of the Brooks-Corey matches to the MICP data, along with the other properties (specifically, k and ϕ), regression methods were used to obtain the parameters in Eq. 1.8.

Fig. 1.3 presents the results of the optimized (Huet) correlation for the 323 samples used in this work. As for statistics, 95 percent of the data matched with the new optimized model are within a factor of 9.1 and 58 percent of the data matched with the new optimized model are within a factor of 2. As is evident in **Fig. 1.3**, the new correlation appears to be best suited for cases where the permeability is greater than 1 md — however; it should also be noted that although there is more "scatter" in the optimized results for permeabilities less than 1 md, the scatter is reasonably centered about the "perfect correlation" trend. As a recommendation for future work, we strongly encourage continued investigations for cases where the permeability is less than $1x10^{-3}$ md.

From this regression work, we proposed a new correlation to predict permeability from the mercury injection capillary pressure data. The proposed model is shown in Eq. 1.12. The predicted permeability using the proposed model is expected to be within a factor of 3.97 of the actual permeability for samples with permeability above 1 md. For the lower permeability samples, the error of the predicted permeability is expected to be within a factor of 12.70.

$$k = 3538886 \frac{1}{(p_d)^{1.8873}} \left[\frac{\lambda}{\lambda + 2}\right]^{1.6858} (1 - S_{wi})^{2.9406} \phi^{2.5100} \quad \text{.....(1.12)}$$

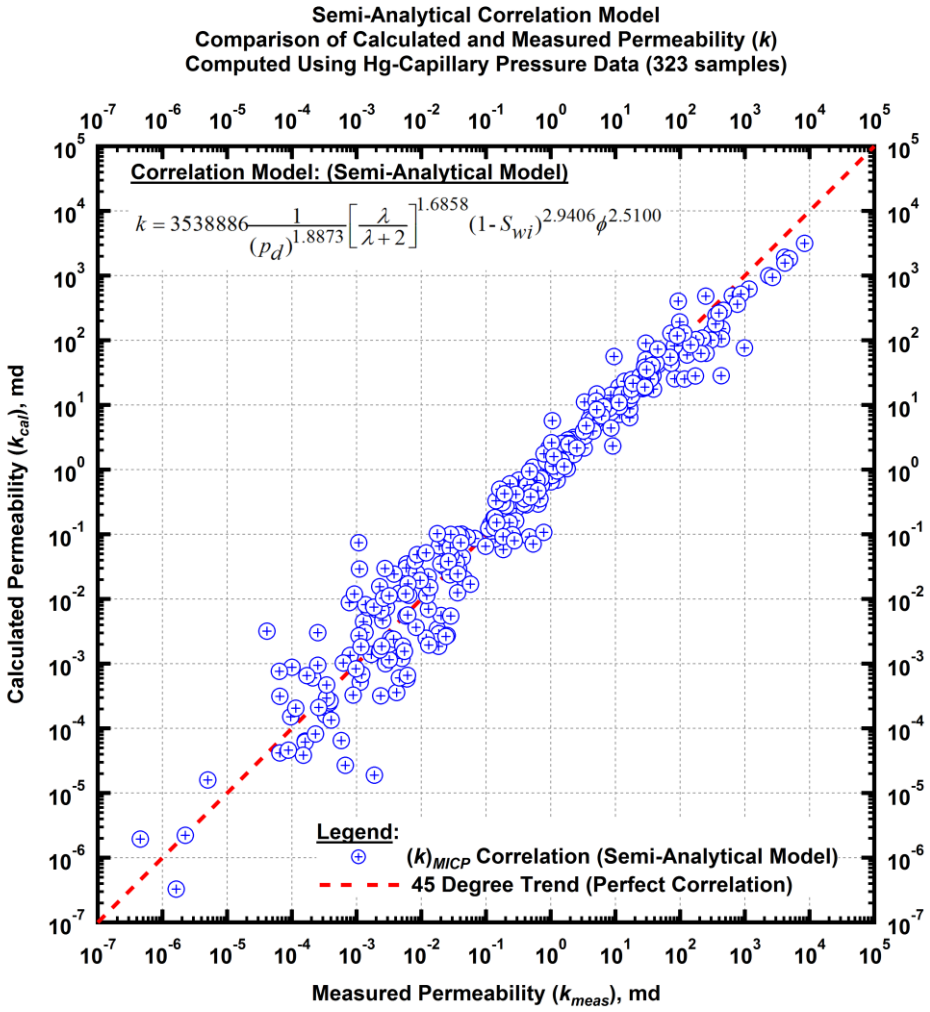

Figure 1.3 — Permeability correlation comparison for the 323 MICP samples used in this work matched with the semi-analytical model of Huet (Huet 2005).

Comparison of the Semi-Analytical Correlation Model to the Swanson Correlation Model

With the same set of data (323 samples), the Swanson parameter $[S_b/p_c]_A$ was determined for each sample by plotting $[S_b/p_c]$ against S_b. The Swanson apex parameter ($[S_b/p_c]_A$) is the maximum value of $[S_b/p_c]$. After estimating the Swanson apex parameter ($[S_b/p_c]_A$) for all of the cases in the data set, the Swanson correlation model (Eq. 1.6) was then optimized using regression with the given core permeability values to provide a permeability prediction model. In **Fig. 1.4** we present the results obtained using the Swanson model and we note that the results are comparable to the semi-analytical (Huet) model. In the case of the Swanson

permeability prediction model, 95 percent of the data are within a factor of 10.4 compared to the Swanson model (compares to 9.1 for the semi-analytical (Huet) model). In addition, 56 percent of the data are within a factor of 2 compared to the Swanson model (compares to 58 percent of the data being within a factor of 2 for the semi-analytical (Huet) model). As with the semi-analytical (Huet) model, the best performance for the Swanson model is for permeabilities greater than 1 md.

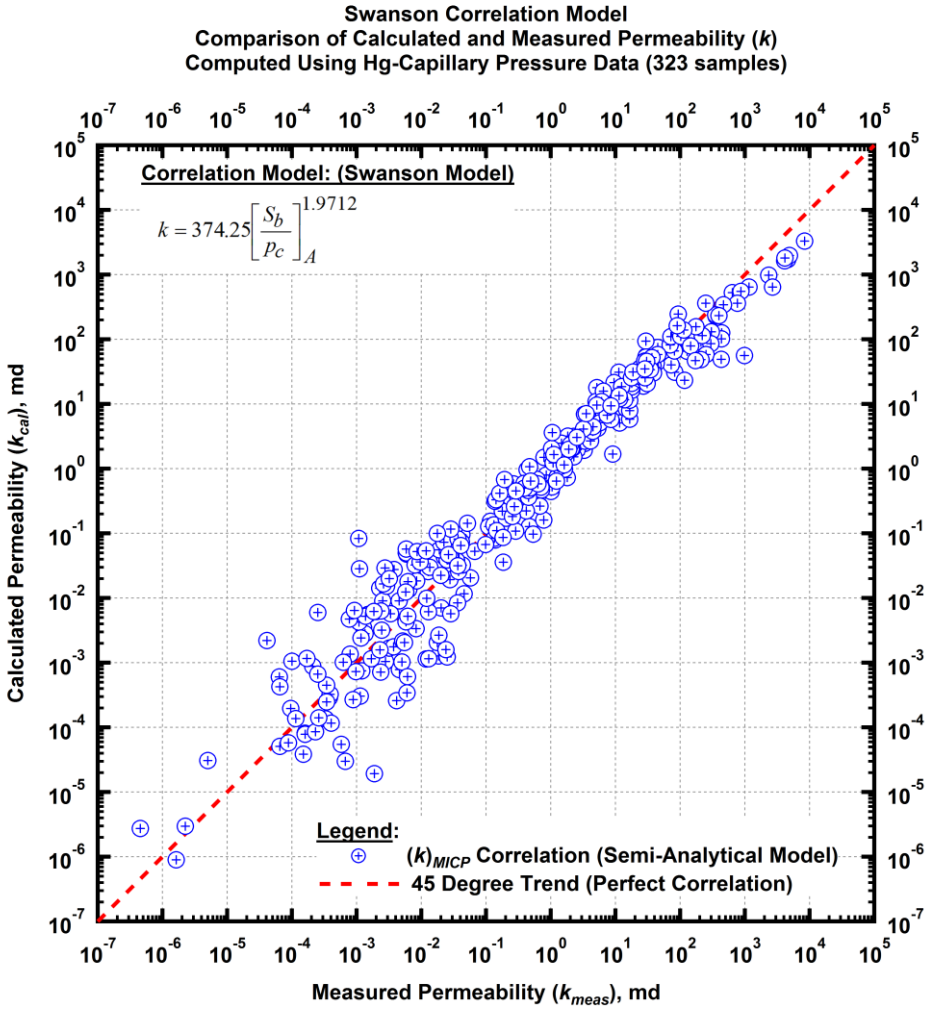

Figure 1.4 — Permeability correlation comparison for the 323 MICP samples used in this work matched with the Swanson model (Swanson 1981).

Analytical Relationship between the Huet and Swanson Correlation Models

Based on the relationship between the Swanson parameter and the Brooks-Corey MICP model parameters (p_d, S_{wi}, λ), the Swanson "apex" parameter can be written as: (see Appendix B for details)

$$\left[\frac{S_b}{p_c}\right]_A = 100\frac{1}{p_d}\left[\frac{\lambda}{(1+\lambda)^{(1+\frac{1}{\lambda})}}\right](1-S_{wi})\,\phi \quad \text{.....(1.9)}$$

Following the assumptions and work performed in Appendix C, the Swanson model (Eq. 1.6) can be written as:

$$k = b_1\frac{1}{(p_d)^{a_2}}\left[\frac{\lambda}{\lambda+2}\right]^{b_2}(1-S_{wi})^{a_2}\,\phi^{a_2} \quad \text{.....(1.13)}$$

In addition, Eq. 1.13 can then be generalized into exactly the same form as the semi-analytical (Huet) model by simply assuming that the parameters in this relation are independent (*i.e.*, unique and non-repeated). This is also shown in Appendix C. The final "Swanson" model is therefore the same as the "Huet" model:

$$k = a_1\frac{1}{(p_d)^{a_2}}\left[\frac{\lambda}{\lambda+2}\right]^{a_3}(1-S_{wi})^{a_4}\,\phi^{a_5} \quad \text{.....(1.8)}$$

Determination of the Brooks-Corey Model Parameters using MICP data

Eq. 1.10 and 1.11 can be used to relate the $(p_c)_A$ and $(S_b)_A$ parameters to the Brooks-Corey parameters, which are given again here as: (these relations are derived in detail in Appendix B)

$$(p_c)_A = p_d\left[\frac{1}{1+\lambda}\right]^{-1/\lambda} \quad \text{.....(1.10)}$$

$$(S_b)_A = 100\frac{\lambda}{1+\lambda}(1-S_{wi})\,\phi \quad \text{.....(1.11)}$$

The Brooks-Corey parameters can be estimated using Eqs. 1.10 and 1.11 using the following workflow:

Step 1 — Estimate p_d using a semilog plot of p_c vs. S_w by extrapolation of the p_c plateau trend to $S_w = 1$.

Step 2 — Calculate for $[S_b/p_c]$ for the data set.

Step 3 — Plot $[S_b/p_c]$ versus S_b on a Cartesian plot.

Step 4 — Estimate $(S_b)_A$ from the Cartesian plot in Step 3 where the $[S_b/p_c]$ trend is maximum (*i.e.*, $[S_b/p_c]_A$).

Step 5 — Calculate $(p_c)_A$ from $[S_b/p_c]_A$ obtained in step 4 using the point $(S_b)_A$. Specifically, use the relation:

$$(p_c)_A = \frac{(S_b)_A}{\left[\frac{S_b}{p_c}\right]_A} \quad \text{.....(1.14)}$$

Step 6 — Solve for λ as a root using Eq. 1.10 or using an approximation function given in Appendix D.

Step 7 — Solve for S_{wi} using Eq. 1.11, which can be rearranged to yield S_{wi} directly:

$$S_{wi} = 1 - \frac{(S_b)_A}{100\phi}\frac{1+\lambda}{\lambda} \quad \text{.....(1.15)}$$

This proposed workflow was performed on all 323 samples in our master data set. This approach forces all of the analyses to be tied to the Swanson parameter ($[S_b/p_c]_A$) — which implies that we can deconstruct the entire capillary pressure curve to a single point (*i.e.*, $[S_b/p_c]_A$), but in reality we should also include the displacement pressure, p_d, and the irreducible wetting phase saturation, S_{wi}. As a comment, this process is valid, but does generate negative S_{wi} values on occasion. This is an aspect of the work that requires additional effort and attention.

CHAPTER II

LITERATURE REVIEW

2.1 Wettability and Capillary Pressure

Wettability is a property of a solid surface to prefer one fluid phase over the others (Agbalaka et al. 2008; Anderson 1986a). When the two immiscible fluids come into contact on a solid substrate, a curved interface between the two fluid phases is formed. This phenomena may be explained by the surface energy balance explained by Young's equation (Lyons and Plisga 2011; Young 1805). An example of oil/water/solid system is shown in **Fig. 2.1**.

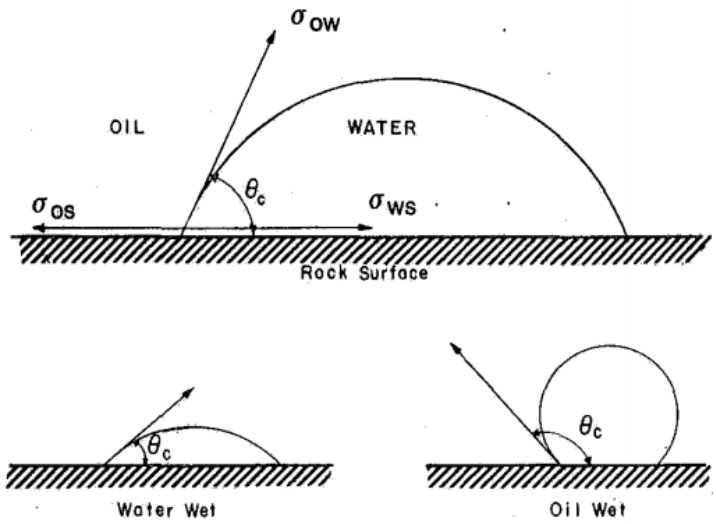

Figure 2.1 — A drop of water on a solid surface immersed in oil to demonstrate the wettability in oil/water/solid system (Anderson 1986b).

The Young equation written for the oil/water/solid system is given as:

$$\sigma_{ow}\cos\theta_c = \sigma_{os} - \sigma_{ws} \quad \text{.....(2.1)}$$

where: (written for an oil/water/solid system)

σ_{ow} = interfacial tension between the oil and water,

σ_{os} = interfacial tension between the oil and solid,

σ_{ws} = interfacial tension between the water and solid, and

θ_c = the angle of the water/oil/solid contact line (contact angle).

The wettability of the solid surface can be determined by the contact angle (θ_c). By convention, the contact angle is measured through the denser phase. In the oil/water/solid system, the solid surface is said to be water-wet if $\theta_c < 90$ degrees, and it is oil-wet if $\theta_c > 90$ degrees. At $\theta_c \approx 90$, neither fluids preferentially wet the solid, and it is said to be neutral-wet (Agbalaka et al. 2008).

The curved interface between the wetting phase and non-wetting phase fluids results in a difference in pressure between each fluid phase. The pressure difference, which is defined as capillary pressure, at any point on the curved interface is related to the principle radii of curvatures through Young-Laplace equation given as (Dake 1983; Pujado et al. 1972):

$$p_C = p_O - p_W = \sigma\left[\frac{1}{r_1} + \frac{1}{r_2}\right] \quad \text{.....(2.2)}$$

where: (written for an oil/water/solid system)

p_c = capillary pressure,

p_o = pressure in oil phase,

p_w = pressure in water phase,

σ = interfacial tension (between the oil and water), and

r_1, r_2 = principal radii of curvature at any point on the interface.

For a cylindrical capillary tube system shown in **Fig. 2.2**, the interface between the wetting phase and non-wetting phase can be approximated as a portion of a sphere. Thus, the two principle radii are equal and they are equal to the radius of the sphere, r_s. The radius r_s can be related to the radius of the capillary tube, r, as a function of the contact angle, θ, as (Anderson 1987):

$$r = r_S \cos\theta \quad \text{.....(2.3)}$$

Eq. 2.2 can then be written as a function of the capillary tube radius (r) and the contact angle (θ) as (Washburn 1921):

$$p_C = \frac{2\sigma\cos\theta}{r} \quad \text{.....(2.4)}$$

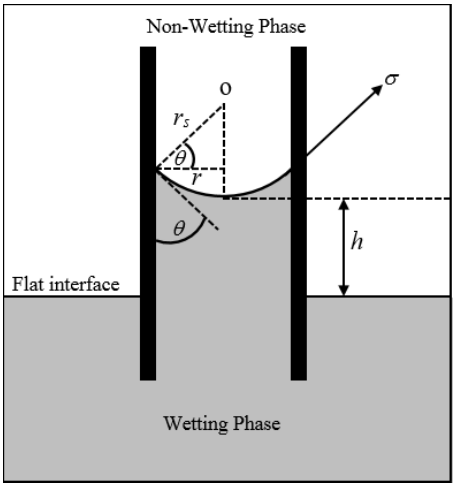

Figure 2.2 — Schematic showing a curved interface between the wetting phase and non-wetting phase fluid in a capillary tube.

The height of the wetting phase fluid to rise up the capillary tube is the result of the balance between the adhesive force (between the wetting phase and the capillary tube) and the gravitational force. The final relationship between the capillary pressure (p_c), the capillary tube radius (r), and the height of wetting phase in the capillary tube (h) for the oil/water system is given as:

$$p_C = \frac{2\sigma\cos\theta}{r} = gh(\rho_W - \rho_O) \quad \text{.....(2.5)}$$

where: (written for an oil/water/solid system)

p_c = capillary pressure = p_o - p_w

p_o = pressure in oil phase,

p_w = pressure in water phase,

ρ_o = density of oil phase,

ρ_w = density of water phase,

σ = interfacial tension (between the oil and water),

θ = contact angle (measured through water phase),

r = capillary tube radius,

h = height of wetting phase in the capillary tube above the flat interface, and

g = standard gravity.

Typical values of the interfacial tension and contact angle of the two immiscible fluids systems commonly encountered in petroleum industry are summarized in **Table 2.1**.

Table 2.1 — Typical values of interfacial tension and contact angle of two immiscible fluid systems (Keelan and Marschall 1979).

System	Interfacial Tension (dyne/cm)	Contact Angle (degree)
Hg-Air	480	140
Water-Oil	~24	20-30
Water-Gas	70-75	0
Oil-Gas	~50	0

The value of the capillary pressure in a capillary tube can be converted between fluids system by the use of Eq. 2.6. For the capillary tubes with the same radius, the capillary pressure of system 1 can be converted into the capillary pressure of system 2 using the equation given as:

$$p_{c2} = \frac{\sigma_2 \cos\theta_2}{\sigma_1 \cos\theta_1} p_{c1} \quad \text{.....(2.6)}$$

This equation is commonly used to convert the capillary pressure measured in the laboratory into the capillary pressure of the reservoir fluids.

2.2 Capillary Pressure Measurement in Porous Medium

In a porous medium such as a reservoir rock, the distribution of multiphase fluids is affected by the capillary phenomena. The capillary pressure of a porous sample can be measured for any particular value of saturation. The earliest method known to be used for measuring the capillary pressure of a column of sand is the gravity drainage method (Hassler and Brunner 1945). A column of sand saturated with a liquid of question is allowed to come to equilibrium by the gravitational force. Saturation of the liquid at each section of the sand column is measured and the associated capillary pressure is calculated from a hydrostatic gradient of the liquid from the free liquid level. This method was proved to be accurate for the sand column, but it is deemed impractical for consolidated sands or small core samples.

Many techniques for capillary pressure measurement have been developed for different purposes (Denney 2008; Newsham et al. 2003; Nguyen et al. 2008; Reitsma and Kueper 1994; Saito 1963). Three commonly used methods for the oil and gas industry are: porous-plate method, centrifuge method, and mercury injection method (Honarpour et al. 2004; PetroWiki 2016).

Porous-Plate Method

As the name suggests, this method requires the use of a permeable membrane of uniform pore-size distribution with the same wettability as the measured sample (Amyx et al. 1960; Honarpour et al. 2004;

PetroWiki 2016). The porous-plate is used to separate the sample chamber and the fluid collector chamber that allows only the wetting phase fluid to flow through. The porous-plate must contain pores of a size small enough that the selected displacing fluid will not penetrate through the plate at the design maximum pressure of investigation. Many materials have successfully been used for the porous-plate, such as fritted glass, porcelain, and cellophane.

To obtain the primary drainage capillary pressure, the sample is saturated with the wetting phase fluid and submerged in the displacing fluid to be in contact with the porous plate saturated with the same wetting fluid. The pressure is then applied stepwise to the displacing fluid surrounding the core sample. For each pressure step, the displacing fluid displaces the saturated fluid in the core sample out through the porous-plate. The core is allowed to approach a state of static equilibrium, and the production of the saturated fluid can be measured for the pressure step. This step could take up 10 to 40 days depending on the samples and the porous-plate used (Honarpour et al. 2004). The process of reaching equilibrium is slower at low-capillary pressure due to the small differential pressure. Provided that the time to reach equilibrium is allowed, the porous-plate method is generally considered as the most accurate of the three methods. The method allows for the measurement of any fluids system, as well as heterogeneous or laminated samples.

This method has been modified to allow for the application of the overburden pressure to simulate the reservoir condition, as well as imbibition capillary pressure curve determination (Fleury et al. 1997; Wilson and Skjæveland 2002). There are also studies on experimental data interpretation during non-equilibrium state to speed up the collection of porous plate/membrane capillary pressure (Dernaika et al. 2010; Shafer and Lasswell 2007). The schematic of the porous-plate method is shown in **Fig. 2.3**.

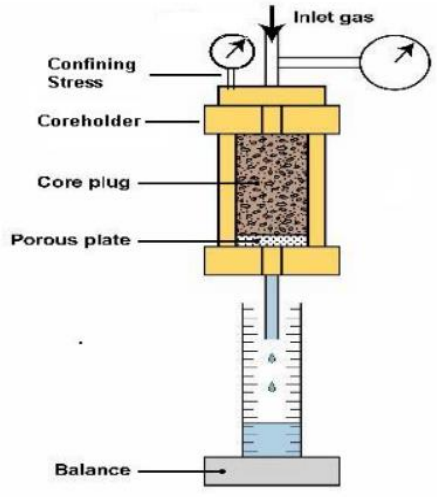

Figure 2.3 — Schematic showing a porous-plate method for capillary pressure measurement (Honarpour et al. 2004).

Centrifuge Method

In the centrifuge method (Amyx et al. 1960; Hassler and Brunner 1945; Honarpour et al. 2004; PetroWiki 2016), centrifugal force is applied to displace the fluid saturating the sample. First, the core sample is saturated with the wetting phase fluid (to measure the primary drainage capillary pressure). The saturated core is then put in the core holder of a centrifuge, in contact with another phase of displacing fluid (**Fig. 2.4**). As the sample is rotated, the centrifugal force generates different pressure gradients in each fluid phase, resulting in the saturated fluid being displaced by the displacing fluid. The displaced fluid accumulates in the liquid collector for the saturation calculation. The capillary pressure is calculated from the fluid densities and the rotating speed. A complete capillary pressure curve can be obtained by performing the experiment at a various constant rotating speed.

The advantage of this method over the porous-plate method is the shorter time required for the system to reach equilibrium, which can be observed by the cease of production. However, by the use of centrifugal force, the core exhibits a gradient of pressure while the obtained saturation is the average saturation of the core. Hassler and Brunner (1945) discussed the method of obtaining the proper capillary pressure and saturation relationship from the centrifuge data. They also discussed on the associated error that may be accumulated from the required process of differentiation on the obtained experimental data and the simplification of the calculation method. This pressure gradient phenomenon in the core also limited the use of the centrifuge method with heterogeneous or laminated rocks (Honarpour et al. 2004).

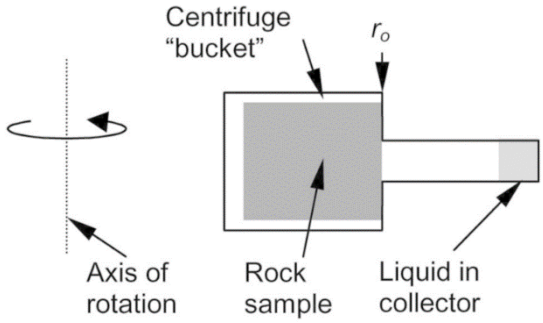

Figure 2.4 — Schematic showing a centrifuge method for capillary pressure measurement (PetroWiki 2016).

Mercury Injection Method

The method of mercury injection was developed to accelerate the determination of the capillary-pressure-saturation relationship over the porous-plate method. Because mercury is normally a non-wetting fluid, this allows the injection of the mercury as a non-wetting phase into the vacuumed samples. This process significantly shortens the time required to reach the equilibrium. However, for the very tight samples the equilibration time as much as one week may still be required (Honarpour et al. 2004).

The mercury injection method also eliminates the use of the porous membrane that has limited the maximum pressure allowable for the measurement of the porous-plate method. The injection pressure of up to 60,000 psia of mercury is possible to allow for the investigation of the micro-pores (Shafer and Neasham 2000). The method also allows the use of non-regular shape samples, such as drill cutting. However, the capillary pressure results were found to be inconsistent, and the effects of the sample size and shape have been discussed (Bolger 1993; Comisky et al. 2011).

The process of the mercury injection method involves evacuating the sample and placing it in the mercury chamber. The mercury is then forced into the sample. The mercury injection pressure is increased by step with time allowed for equilibration between the steps (Giesche 2006). As the sample is vacuumed, the injection pressure is obtained as the mercury injection capillary pressure (MICP) directly. The amount of mercury injected at each pressure step is obtained as the volume of non-wetting phase occupying the pores of the sample, and the wetting phase saturation associated with that capillary pressure can be calculated from the known total pore volume. The nature of the injection process makes the mercury injection method the only method that provides convenient measurement of the entry pressure (Thomas and Katz 1968). The schematic showing the mercury injection method is shown in **Fig. 2.5**.

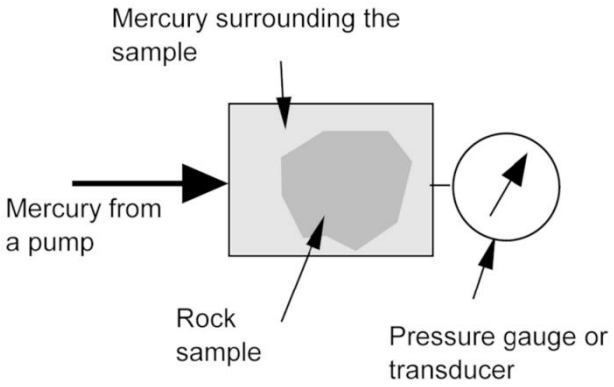

Figure 2.5 — Schematic showing a mercury injection method for capillary pressure measurement (PetroWiki 2016).

Although the measurement of capillary pressure using the mercury injection method seems straightforward, corrections are still required. Data obtained with high pressure mercury injections suffer from two well-known systematic errors — blank errors and conformance errors. Blank errors result in an apparent mercury intrusion due to differential compaction of the mercury, sample and measurement apparatus. Conformance errors result from the mercury not completely filling the measurement container at the start of the measurement. The effects and the corrections to the blank and conformance errors have been studied by many researchers (Comisky et al. 2011; León y León 1998; Richard 2009; Shafer and Neasham 2000). Comisky et al. (2011) study has demonstrated the effects of blank errors and conformance errors very well on different sample sizes as shown in **Fig. 2.6**. Without the corrections, one can see that the resulting mercury injection data could easily be misinterpreted as the actual capillary-pressure-saturation relation of the sample.

Because of the many advantages of the mercury injection method — in particular, this being a simple and rapid process, the method is well-known and widely used. However, caution should be taken when using mercury injection capillary pressure data. The primary disadvantage of this method is the use of non-reservoir fluid (mercury). Specifically, errors are likely to arise from the simple assumption of using the bundle of capillary tubes model to convert the capillary pressure from the mercury-air system into an oil-water or gas-oil system (Anderson 1987). In addition, the method may not replicate the reservoir displacement process correctly, particularly in the low saturation region (Kleinberg et al. 2015; Newsham et al. 2004). Another disadvantage is the loss of samples due to the contamination from mercury.

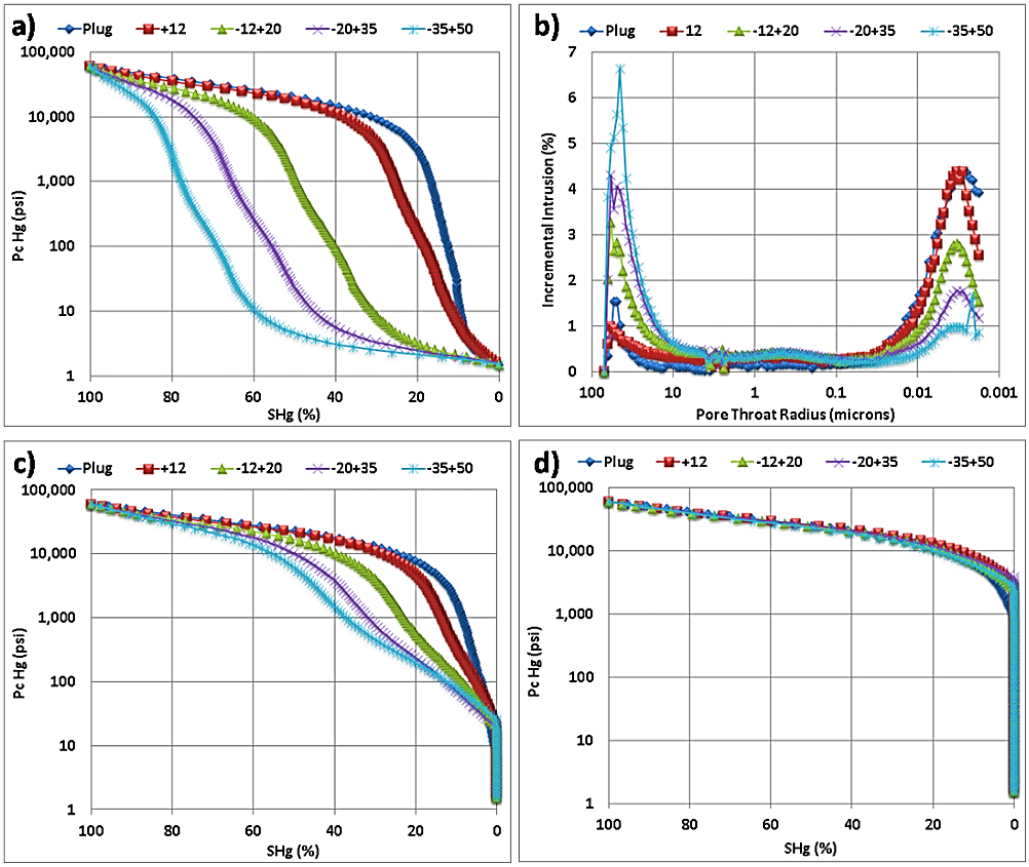

Figure 2.6 — MICP measurements from a single sample with different sample size classes including the plug and the following size ranges (+12, -12+20, -20+25, and -35+50 mesh): **a.** Raw MICP data plotted as mercury saturation (S_{Hg}) vs. mercury intrusion pressure (p_{cHg}), **b.** Pore size distribution of uncorrected MICP measurements, **c.** Conformance-corrected S_{Hg} vs. p_{cHg}, and **d.** Intrusion-corrected S_{Hg} vs. p_{cHg} (Comisky et al. 2011).

2.3 Drainage Capillary Pressure Model

As described above, capillary pressure can be related to the size of a capillary tube as suggested by Washburn (1921). Distribution of various pore and pore-throat sizes in the porous media results in a distribution of capillary pressure values depending on the saturation of the fluids in the media. Capillary pressure can therefore be shown to have a functional relationship with the fluid saturation. Many different types of models have been developed to explain this relationship between the capillary pressure and the fluid saturation as a function of rock and fluid properties.

Leverett (1941) explained the possible relationship between the capillary pressure and the saturation in petroleum reservoirs through the original concept of the pressure difference at the curved interface between the two immiscible fluids. In a vertical column of a reservoir with reservoir fluids assumed initially to be under static equilibrium between the forces due to capillarity and gravitation, interstitial water is found to coexist with oil at all levels throughout the entire reservoir. The pressure difference between the oil and water at any interface (*i.e.* capillary pressure) in the reservoir can be calculated from the hydrostatic pressure gradient in each fluid phase. The curvature of that interface can then be calculated from the determined capillary pressure using the relation of Young-Laplace (Pujado et al. 1972). With a certain pore geometry, a specific curvature of the interface will locate the existence of each fluid phase in the pore. Therefore, the amount of each fluid to occupy the volume of the pore or the saturation of each phase can conceptually be calculated.

Analytical relationships between the saturation and the curvature of a certain pore shape, such as a pack of spheres, were studied (Smith 1933). However, because of the realistically irregular shape of the pores in porous media found in nature, such as reservoir rock, the proposed analytical relationship is not applicable. As a conclusion, <u>any</u> relationship between saturation and the curvature or the capillary pressure of a reservoir rock, or any porous medium in nature thus needs to be determined experimentally.

From the experiment conducted by Leverett (1941), he found a functional relationship between the wetting phase saturation (water in his experiment) and a dimensionless function of capillary pressure, rock and fluid properties for unconsolidated clean sand. He proposed that the interface curvatures normalized by a function of rock properties (permeability and porosity) is constant for each wetting phase saturation. The proposed "*J*-function" from Leverett's work is given as: (Amyx et al. 1960)

$$J(S_w) = \frac{p_c}{\sigma \cos\theta}\sqrt{\frac{k}{\phi}} \quad \text{.....(2.7)}$$

Modifications to this proposed model were studied by many researchers. El-Khatib (1995) proved that the Leverett *J*-function is not a unique function of the wetting phase saturation. He proposed to include the irreducible wetting phase saturation (S_{wi}) and the tortuosity (τ) to better define the relationship. The comparison performed by El-Khatib between the original and the modified *J* function is shown in **Fig. 2.7**. The modified *J*-function (*J**) proposed by El-Khatib is given as:

$$J^*(S_w) = \frac{p_c}{\sigma \cos\theta}\sqrt{\frac{k\tau}{\phi(1-S_{wi})}} \quad \text{.....(2.8)}$$

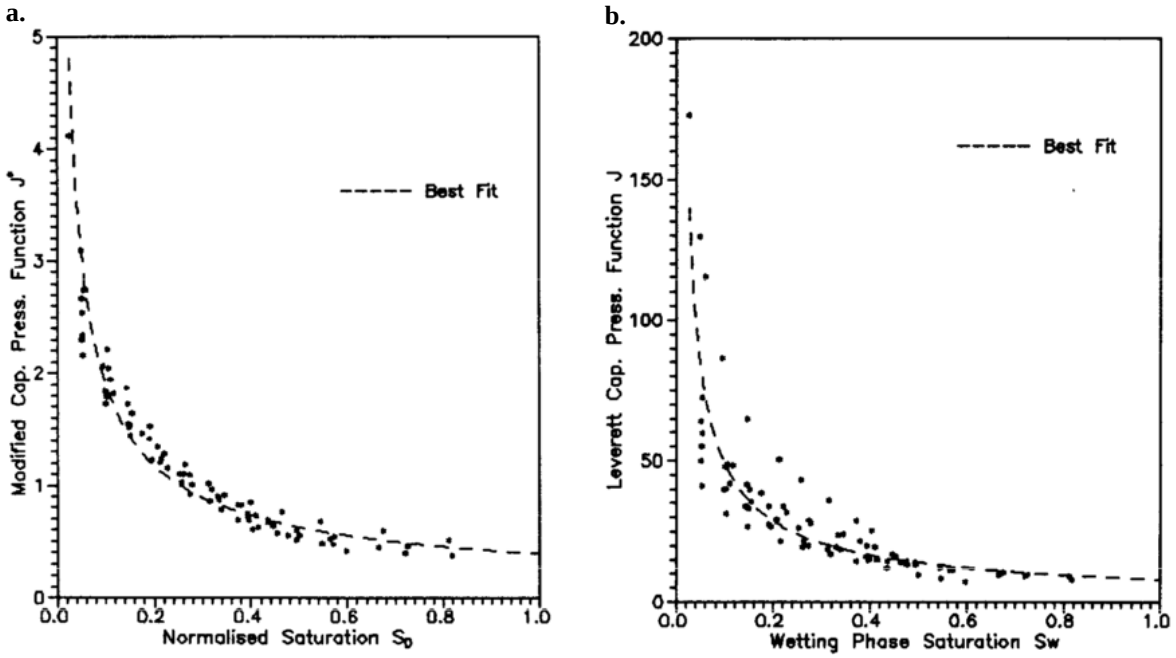

Figure 2.7 — Comparison of the capillary pressure normalization performance using **a.** the modified *J*-function and **b.** the Leverett *J*-function (El-Khatib 1995).

In 1960, Thomeer (1960) proposed and demonstrated that mercury/air capillary pressure curves can be uniquely defined as a hyperbolic function using a log-log plot of capillary pressure (p_c) versus percent bulk volume occupied by mercury (S_b). The Thomeer model consists of three parameters (F_g, $S_{b\infty}$, p_d) that are used to characterize the curve, which can be written as;

$$\frac{S_b}{S_{b\infty}} = \exp\left[\frac{-F_g}{\ln\left[\frac{p_c}{p_d}\right]}\right] \quad \text{.....(2.9)}$$

The parameters $S_{b\infty}$ (bulk volume occupied by mercury at infinite pressure) and p_d (extrapolated displacement pressure) defines the location of the hyperbolic on the log-log plot, and the parameter F_g (pore geometrical factor) defines the curvature of that hyperbolic. Thomeer described the $S_{b\infty}$ parameter as a measure of interconnected pore volume, and the p_d defined the cross-sectional area of the pore first entered by mercury. The parameter F_g represented the interconnection of the pores and the sorting of the pore-sizes.

The schematic showing the Thomeer hyperbolic model is shown in **Fig. 2.8**.

a.

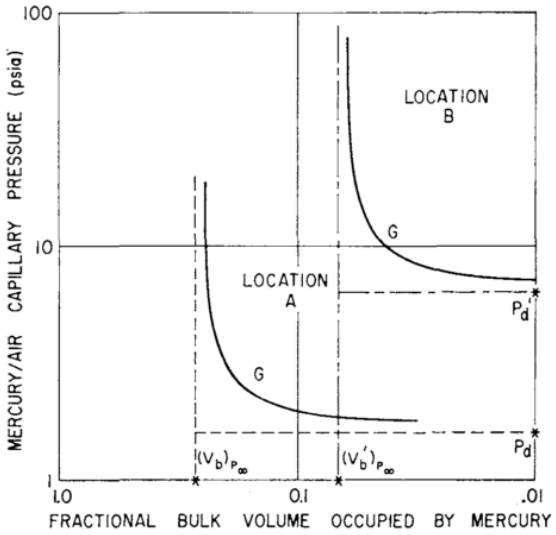

b.

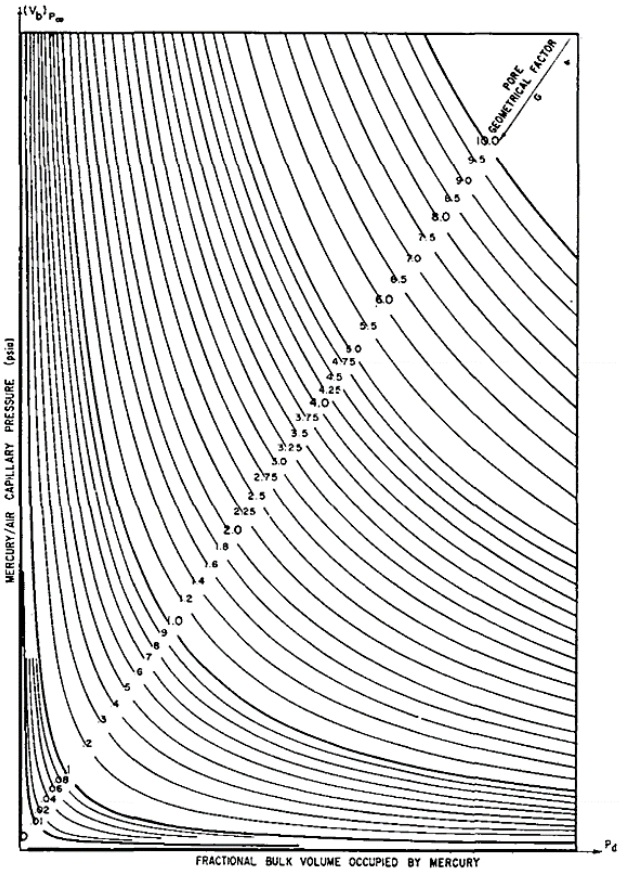

Figure 2.8 — Schematic showing the Thomeer hyperbolic capillary pressure model with **a.** different location on the log-log plot, and **b.** different geometrical factors (Thomeer 1960).

In 1964, Brooks and Corey (1964) observed a power-law behavior in the capillary pressure (air-oil system) versus normalized saturation plot using a large suite of experimental data. As such, Brooks and Corey then created a model to describe capillary pressure as a function of wetting phase saturation — this model is given as:

$$p_c = p_d (S_w^*)^{-1/\lambda} \quad \text{.....(2.10)}$$

where S_w^* is the effective saturation function and is defined as:

$$S_w^* = \left[\frac{S_w - S_{wi}}{1 - S_{wi}} \right] \quad \text{.....(2.11)}$$

The parameter p_d is the displacement pressure, which was defined as the pressure at which the non-wetting phase form a continuous phase in the porous media. The λ–parameter in Eq. 2.10 is designated as "pore-size distribution index". In the Brooks and Corey (1964) experiment, they found that the value of λ–parameter tended to be large for the sample with relatively uniform pore-size, and small for the sample with wide range of pore-size distribution. These two characteristic parameters cannot be physically measured and can only be determined from the capillary pressure data. By plotting the capillary pressure data versus the effective wetting phase saturation in a log-log plot, the data should exhibit a straight line trend. The displacement pressure (p_d) is the extrapolation of that straight line to the effective saturation of 1, and the pore-size distribution index (λ) is a negative reciprocal of the slope of that straight line. Demonstration of the straight line in the log-log plot of the data studied by Brooks and Corey is shown in **Fig. 2.9**.

Despite the empirical origin of the Brooks and Corey model, Kewen (2004) used fractal modeling of the porous media to prove that the Brooks-Corey capillary pressure model can be derived theoretically.

Using the concept of effective wetting phase saturation proposed by Brooks and Corey (1964), Bentsen and Anli (1976) set up a problem as a differential equation with the boundary condition observed from the common capillary pressure curve at effective wetting phase saturation approaching 0 and 1. With the assumption of a finite area under the capillary pressure versus saturation curve as it should represent the work done in creating new boundary surface, the relation between the capillary pressure and wetting phase saturation was proposed as:

$$p_c = p_d - C \ln(S_w^*) \quad \text{.....(2.12)}$$

The parameter "*C*" in Eq. 2.12 is a constant that incorporates the effects of interfacial tension, wettability and pore size distribution. Harris and Goldsmith (2001) proved through dimensional analysis that:

$$C = \sigma \cos\theta \sqrt{\frac{\phi}{k}} \quad \text{.....(2.13)}$$

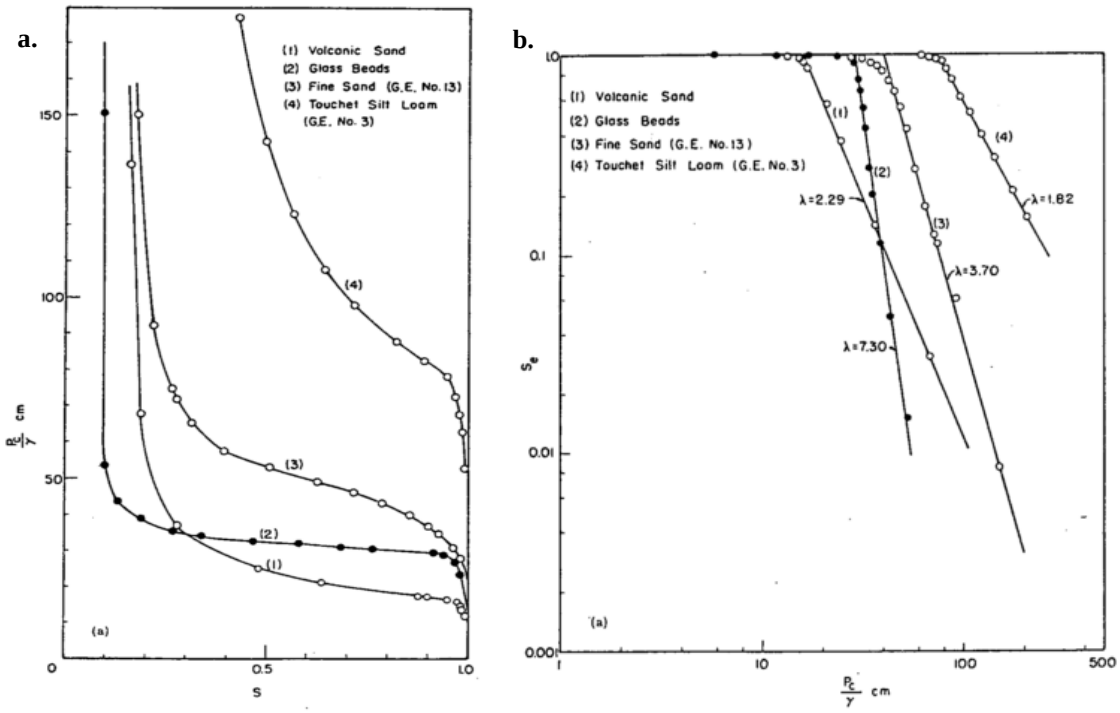

Figure 2.9 — The Brooks and Corey study on characterizing the capillary pressure data as a function of wetting phase saturation: **a.** Cartesian plot of the capillary pressure normalized by the specific weight of the fluid versus wetting phase saturation, and **b.** log-log plot of normalized capillary pressure versus effective wetting phase saturation showing a straight line trend of the data (Brooks and Corey 1964).

Wu (2004) proposed that the use of Eq. 2.12 with Harris and Goldsmith's definition of *C*-parameter could perform very well where the effective wetting phase saturation approaches 0 and 1, but failed to characterize the behavior in between. He then proposed a modified version as:

$$p_C = p_d + \sigma \cos\theta \sqrt{\frac{\phi}{k}} \left[\ln\left[\frac{1}{S_w^*} \right] \right]^{\omega} \quad \text{.....(2.14)}$$

The ω-parameter is added to control the curvature of the capillary pressure versus saturation curve, and this empirical parameter is called a "shape factor". By studying on over 200 samples, he found that the ω-

parameter is a function of lithology and permeability, and ranges narrowly between the values of 1 to 3. A general criteria for ω-parameter was proposed as shown in **Table 2.2**. A default value of 2 works well for a wide range of lithology and permeability.

Table 2.2 — Empirical values of ω-parameter as a function of lithology, pore type, and permeability (Wu 2004).

Lithology	Pore Type	Permeability	ω
Clean Sandstone Carbonate	Intergranular or Intercrystalline Pores	100 – 1000 md	3
Sandstone Shaly sandstone	Micropores, Dissolution Pores	1 – 100 md	2
Shale Tight sandstone	Micropores	< 1 md	1

Xu and Torres-Verdín (2013) used a statistical approach to characterize the capillary pressure data of the studied carbonate reservoir rocks. The problem was set to model the pore-throat size distribution obtained from the capillary pressure data using Washburn relation (Washburn 1921). Using bimodal Gaussian distribution model, six statistical attributes need to be determined to characterize a certain distribution. The process to obtain these attributes from mercury injection capillary pressure data was proposed as shown in the workflow diagram in **Fig. 2.10** along with the example from the study.

Xu and Torres-Verdín (2013) also showed the physical interpretation of each of the six statistical attributes. By using the bimodal distribution model, each distribution of the pore-throat sizes can be referred to as the distribution of the macro-pores and the distribution of the micro-pores. The mean pore-throat size of each distribution mode represents the mean size of flow conduit of that mode, while the standard deviation of each distribution represents the sorting of different pore-throat sizes in that mode. Absolute permeability is mainly controlled by the large pore-throat size mode, or macro-pores mode. It is positively correlated with mean pore-throat radius and the associated pore volume while it negatively correlated with standard deviation. The small pore-throat size mode was found to control the irreducible or critical water saturation. Both are correlated with the mean value of small pore-throat size mode and the associated pore volume fraction. The end point value for gas relative permeability at critical water saturation is mainly controlled by the large pore-throat size mode, especially the mean value.

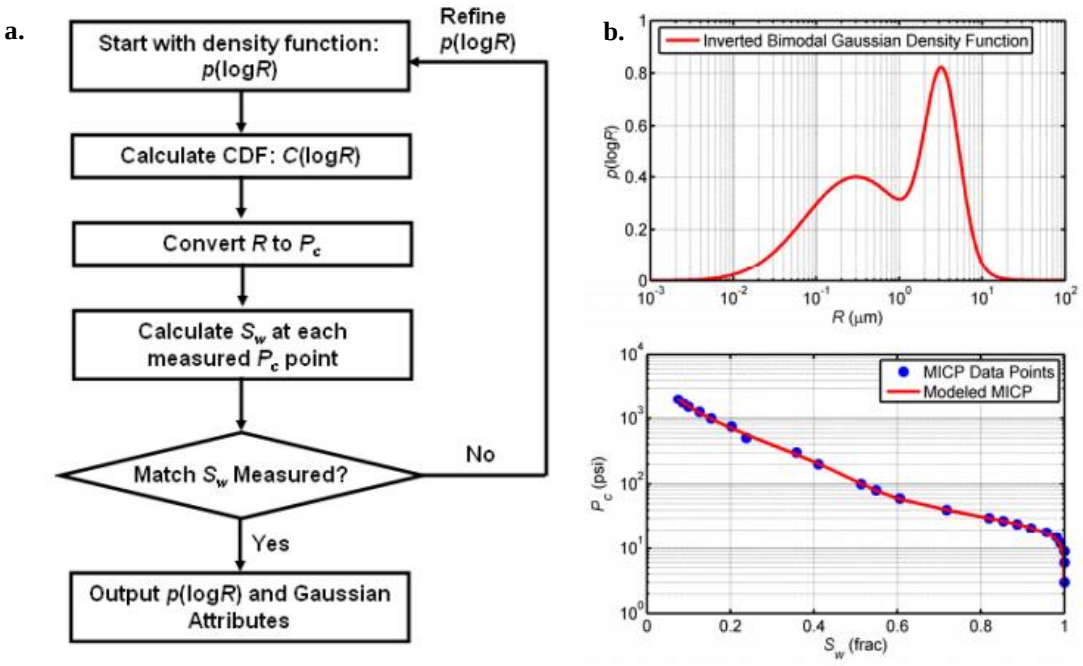

Figure 2.10 — **a.** Workflow used to derive a bimodal Gaussian pore-size distribution by iteratively matching MICP data using inversion. **b**. Example of the derivation of a bimodal Gaussian pore-size distribution from MICP using the proposed method (Xu and Torres-Verdín 2013).

More complex models using the method of pore network modeling have also been developed (Vogel et al. 2005). Despite the complexity of the models, they all suggest a relationship between capillary pressure and the some aspect/dimension of the pore geometry. Therefore, it is logical that information regarding the pore geometry of the sample can be obtained from capillary pressure data. In this study, our goal is to extract a correlation of permeability for a given sample using mercury injection capillary pressure data.

2.4 Permeability Prediction from Drainage Capillary Pressure

Permeability is a measure of the ability of a porous material to allow fluids to pass through it. By analogy to electrical conductors, permeability represents the reciprocal of the resistance that the porous medium offers to fluid flow. Darcy (1856) defined from his experiment that permeability is a constant proportionality of the fluid velocity and the pressure gradient across the porous material. By extending his concept to fluids other than water, under steady-state condition with single phase fluid at constant elevation, Darcy's law is stated as (Amyx et al. 1960):

$$v_x = -\frac{k}{\mu}\frac{dp}{dx} \quad \text{.....(2.15)}$$

where the constant k is the defined permeability, and parameter μ is the viscosity of the flowing fluid. As the flow occurs through the pores of porous medium, one should expect the permeability to be a function of pores and pore network geometry. As demonstrated in the previous sections, capillary pressure and saturation relationship is found to be related to some aspect of the pore structure. As such, there have been many attempts to determine analytically and empirically for permeability using information from the capillary pressure versus saturation curve.

Analytical model

Purcell (1949) applied the concept for a bundle of capillary tubes to represent the porous medium. Distribution of the hypothetical tube sizes could be obtained from the capillary pressure versus saturation curve. Using Poiseuille's flow equation to calculate the flow behavior for a single tube, he then created a relation for a bundle of capillary tubes. Using this approach, the following relationship between permeability and the capillary pressure function was defined analytically. The Purcell model was proposed as:

$$k = 21.32\frac{(\sigma\cos\theta)^2}{2}F_p\phi\int_0^1\frac{1}{p_c^2}dS_w \quad \text{.....(2.16)}$$

An empirical parameter F_p, or the "lithology factor" as called by Purcell, was added to account for the differences between the flow in the hypothetical porous medium and that in naturally occurring rock. Purcell conducted experiments on sandstone samples using the mercury injection method for the capillary pressure with air permeability obtained from conventional flow measurements. Purcell showed that the lithology factor (F_p) varies relative to the magnitude of the permeability. He proposed from his experiments that the average F_p value of 0.216 can give a satisfactory accuracy the prediction of air permeability.

Ma et al. (1991) showed in their study that the permeability prediction using Purcell's model can be improved by using a different lithology factor (F_p) for samples with different Leverett J-function. They also derived a relationship between the Leverett J-function to the tortuosity of the porous medium as given as:

$$\tau^2 = \frac{1}{2}\int_0^1\frac{1}{J(S_w)}dS_w \quad \text{.....(2.17)}$$

They also found that, with their studied set of samples, the exponent of p_c in Purcell's model (Eq. 2.16) should be 1.68 rather than 2.

Burdine et al. (1950) analytically derived the relationship between permeability and the distribution of the size of the pore entries. He used the method proposed by Drake and Ritter (1945) to derive the pore entry size distribution from the mercury injection capillary pressure data. The derivation was on the same basis as Purcell (1949) but proposed in the form of pore entry radii rather than the function of capillary pressure.

Wyllie and Spangler (1952) incorporated the concept of tortuosity, developed by Kozeny and Carman (Schlueter and Witherspoon 1995) into the work by Purcell (1949). To quantify the tortuosity of the sample, Wyllie and Spangler proposed the use of electrical resistivity measurements. By incorporating the Archie formation factor (which is defined as the ratio of the resistivity of the formation at 100 percent wetting phase saturation to the resistivity of the formation brine (Archie 1942)) and the shape factor (to account for the realistic shape of the pores that deviated from the commonly assumed cylindrical shape), Wyllie and Spangler proposed the model given as:

$$k = 21.32(\sigma\cos\theta)^2 \frac{1}{k_0}\frac{1}{F^2\phi}\int_0^1 \frac{1}{p_c^2}dS_w \quad \text{.....(2.18)}$$

where k_0 is the shape factor and F is the Archie formation factor (Archie 1942).

Wyllie and Gardner (1958) added an aspect of randomly connected pores of different sizes into the bundle of capillary tubes model. The final form of the derivation demonstrated by Nakornthap and Evans (1986) is given as:

$$k = 21.32\phi^3(1-S_{wi})^3 \frac{(\sigma\cos\theta)^2}{2}\frac{\beta}{n}\int_0^1 \frac{1}{p_c^2}dS_w^* \quad \text{.....(2.19)}$$

Where S_w^* is the effective wetting phase saturation as defined by Brooks and Corey (1964). The numerical constant n reflects the manner in which the pores are connected. The parameter β is inserted to account for the assumption made by regarding the connectivity of the pores of different sizes. Nakornthap and Evans (1986) described the β–parameter, as follows:

> *The parameter β is inserted to recognize the fact that flow through a pore of radius r overemphasizes the impedance because it ignores the larger areas available for exit flow at either side of the constrictions formed where pores abut. Thus it may be expected that $\beta \sim 1$ and that the actual magnitude of β is a function of the average shape of pores in the medium that the model represents.*

Both n and β were assumed to be constant for all pores for their derivation. **Fig. 2.11** explains the concept of the n and β parameters.

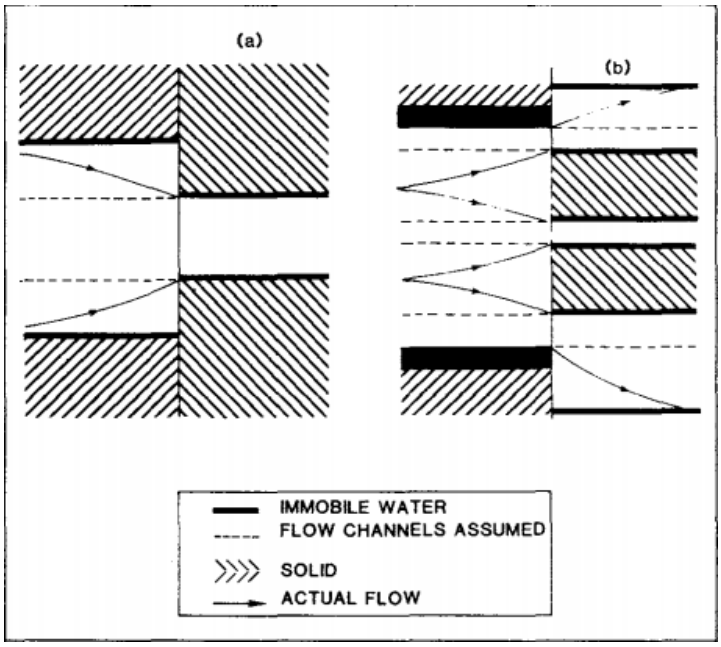

Figure 2.11 — Schematic demonstrating definitions of the parameter n and β: **a.** n =1, the flow exits into one adjacent pore, **b.** n > 1, the flow exits into more than 1 pore (Nakornthap and Evans 1986).

Huet (2005) applied the capillary pressure model of Brooks and Corey (1964) together with the suggestion for the β and n parameters by Ali (1995) into the model derived by Nakornthap and Evans (1986). By solving the integration term and substituting for β and n parameters, the following result is obtained:

$$k = 10.66\alpha(\sigma\cos\theta)^2(1-S_{wi})^4\phi^2\frac{1}{p_d^2}\left[\frac{\lambda}{\lambda+2}\right] \quad \text{.....(2.20)}$$

The empirical parameter, α, was added and noted by Huet (2005) as "to represent any remaining non-idealities that have not been accounted for by any other terms… we would likely assume α = 1, or attempt a calibration of the α-parameter for a particular data set."

Based on this derived relationship (Eq. 2.20), Huet (2005) also proposed a so-called "semi-analytical" model as a correlation model obtained by optimizing the coefficients in Eq. 2.20, which led to the following result:

$$k = 1233562.5(1-S_{wi})^{2.2761}\phi^{1.7296}\frac{1}{p_d^{1.8139}}\left[\frac{\lambda}{\lambda+2}\right]^{1.4385} \quad \text{.....(2.21)}$$

Ruth et al. (2013) used a concept called "representative elemental volume" for their analytical derivation of the relationship between permeability and the capillary pressure function. Instead of assuming a bundle of

different sizes of capillary tubes to represent the porous sample, they assumed a single volume unit consisting of a cylindrical impermeable matrix with a single tortuous tube as a flow path (**Fig. 2.12**). The diameter of the flow tube (δ) is the mean pore-throat size determined from the capillary pressure versus saturation function using Washburn equation (Washburn 1921). With this approach, they were able to use the concept of tortuosity, which can be measured through electrical resistivity measurement, to explain the empirical "lithology factor" of Purcell's model (Purcell 1949).

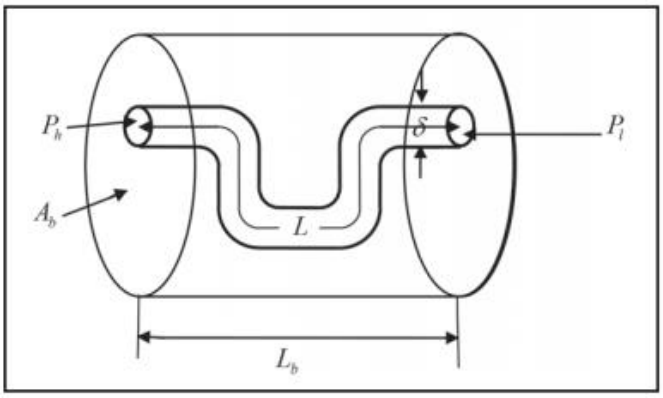

Figure 2.12 — Schematic of the representative elemental volume (REV) (Ruth et al. 2013).

The proposed model written as a function of Archie formation factor (F) is given as:

$$k = 21.32 \frac{(\sigma \cos\theta)^2}{2F} \int_0^1 \frac{1}{p_c^2} dS_w \quad \text{.....(2.22)}$$

In the case where the electrical resistivity data are available, Ruth et al stated that their proposed model can be used to predict permeability with high accuracy. In the case where there are no electrical resistivity data available, Ruth et al proposed an approximation which uses the Archie relation for porosity (Archie 1942). The Ruth et al approximation model is written as:

$$k = 21.32 \frac{\phi^m (\sigma \cos\theta)^2}{2a} \int_0^1 \frac{1}{p_c^2} dS_w \quad \text{.....(2.23)}$$

where a and m (cementation factor) can be determined from correlation of experimental results. An approximation of $a = 1$ and $m = 2$ was proved to give an acceptable prediction (Salimifard et al. 2014).

Katz and Thompson (1986) used concepts of percolation and conductance to derive a relationship for permeability as a function of characteristic length (l_c) and the Archie formation factor (F). The proposed relationship is given as:

$$k = \frac{1}{226}\frac{l_c^2}{F} \quad \text{.....(2.24)}$$

The characteristic length (l_c) defined the threshold pore size to allow the injection of the fluid into the porous medium. They proposed that this parameter can be determined from the threshold pressure (*i.e.*, displacement pressure) of the mercury injection capillary pressure curve using Washburn relation (Washburn 1921).

Katz and Thompson (1987) then extended the concept of percolation to define the hydraulic conductance (l_h) and the electrical conductance (l_e) in term of a length scale. By different weighting of the conduction path way to the conductance for each case, they derived two relationships: (1) for the hydraulic conductance (*i.e.*, the permeability (k)), and (2) for the electrical conductance (*i.e.*, the formation factor (F)). The two relationships are given as:

$$k = \frac{1}{89} l_h^2 \left[\frac{l_h}{l_c}\right] \phi S(l_h) \quad \text{.....(2.25)}$$

$$\frac{1}{F} = \left[\frac{l_e}{l_c}\right] \phi S(l_e) \quad \text{.....(2.26)}$$

By combining Eq. 2.24 and 2.26, permeability may also be calculated as:

$$k = \frac{1}{226} l_c^2 \left[\frac{l_e}{l_c}\right] \phi S(l_e) \quad \text{.....(2.27)}$$

where $S(l_e)$ and $S(l_h)$ are the saturation corresponding to the pore size l_e and l_h, respectively. These two length scales can be determined from the mercury injection capillary pressure as shown in **Fig. 2.13**.

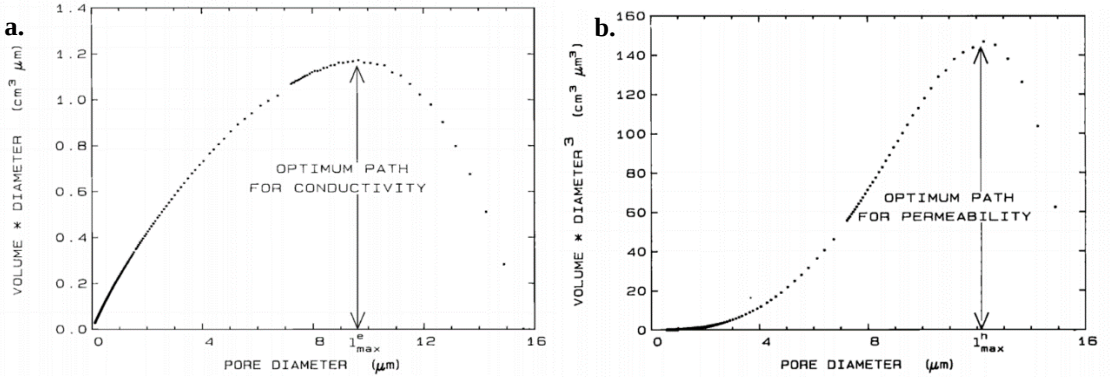

Figure 2.13 — Demonstration of the Katz and Thompson length scales determination from mercury injection capillary pressure data: **a.** length scale of the electrical conductance (l_e), **b.** length scale of the hydraulic conductance (l_h) (Katz and Thompson 1987).

Empirical Models

After defining the hyperbolic capillary pressure model, Thomeer (1983) found a correlation between air permeability and the three characteristic parameters of his model (F_g, p_d, $S_{b\infty}$). Using samples from both sandstone and carbonate reservoirs, Thomeer proposed a correlation model given as:

$$k_a = 3.8068 F_g^{-1.3334} \left[\frac{S_{b\infty}}{p_d} \right]^2 \quad \text{.....(2.28)}$$

In 1981, Swanson (1981) studied the use mercury injection capillary pressure (MICP) together with the initial-residual saturation curve of sandstone and carbonate reservoir samples. Swanson found that, when the MICP data was plotted as a hyperbolic curve proposed by Thomeer (1960), the apex of that hyperbolic curve often coincides with the inflection point of the initial-residual saturation curve (**Fig. 2.14**). Swanson explained the inflection of the initial-residual saturation curve as the point where the distribution of the non-wetting phase is in transition from broadening spatial distribution and trapping to fine structure trapping and/or intrusion of the non-wetting phase into "corners" of pores. The saturation of the non-wetting phase at which the initial-residual curve starts bending should therefore represent the effective pore space contributing to fluid flow. Since the inflection point of the initial-residual curve was found to coincide with the apex point of the capillary pressure curve, the pore size connecting the effective pore space can then be determined from the capillary pressure at the apex point. In concept, considering the Washburn relation (Washburn 1921), the reciprocal of the capillary pressure is proportional to the pore-throat size. Swanson then postulated that the *product of the non-wetting phase bulk saturation and the reciprocal of the capillary pressure at the apex of the hyperbolic capillary pressure curve should be related to the permeability*.

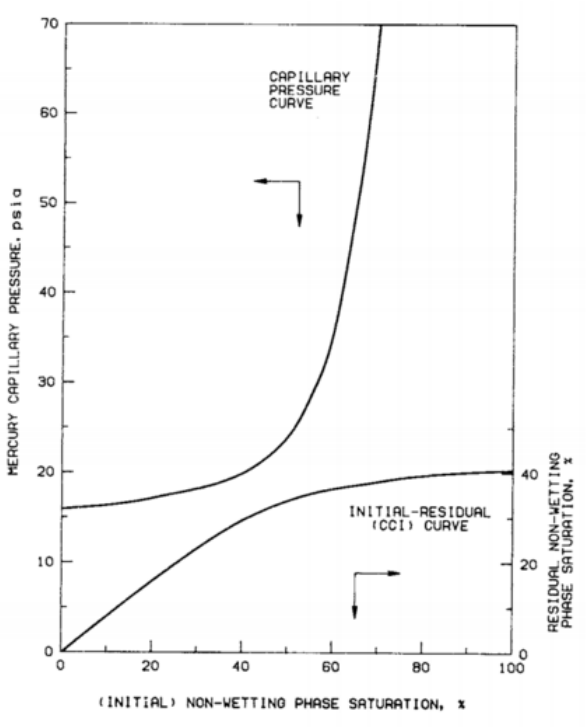

Figure 2.14 — Hypothetical mercury injection capillary pressure curve and the initial-residual saturation curve (Swanson 1981).

As expected, Swanson found a strong correlation between the permeability and his correlating parameter which will be referred to as the Swanson apex parameter ($[S_b/p_c]_A$). Swanson then proposed a correlation with air permeability which is given as:

$$k_a = 339\left[\frac{S_b}{p_c}\right]_A^{1.691} \quad \text{.....(2.29)}$$

Swanson found from his study that his proposed correlation with air permeability became weaker as permeability decreased. He reasoned that the inconsistency in permeability measured at lower region could be due to: (1) the insensitivity of the measuring equipment, (2) stress-sensitivity of the sample, and (3) the Klinkenberg gas slippage effect. His parallel study which considered brine permeability (instead of air permeability) was found to improve the correlation with the Swanson apex parameter ($[S_b/p_c]_A$). Swanson then proposed another correlation for brine permeability as:

$$k_b = 355\left[\frac{S_b}{p_c}\right]_A^{2.005} \quad \text{.....(2.30)}$$

Swanson also provided a nomograph (at 1,000 psia confining stress) to facilitate the determination of permeability from mercury injection capillary pressure curve as shown in **Fig. 2.15**.

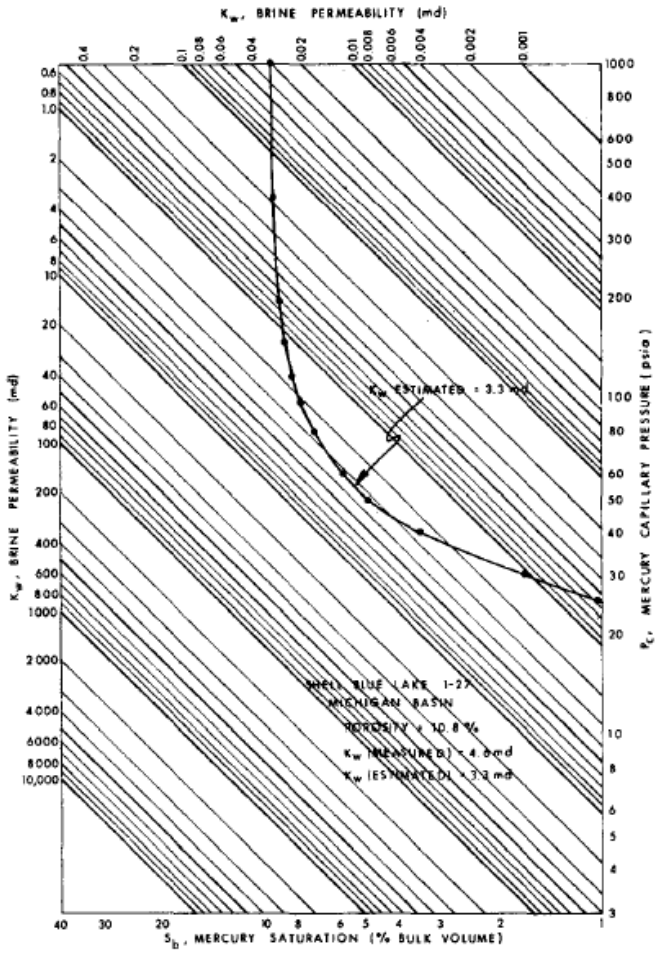

Figure 2.15 — The use of brine permeability/capillary pressure nomograph at 1,000 psia confining stress (Swanson 1981).

Wells and Amaefule (1985) studied the capillary pressure behavior of tight sandstone samples as a means of creating a correlation. They pointed out the challenge in determining the Swanson apex point from an ill-defined trend. To overcome this difficulty, Wells and Amaefule proposed an alternative method to estimate the Swanson apex from the mercury injection capillary pressure data and specifically, they showed that the point at which the value $[p_c/S_b]^{1/2}$ is a minimum, is the same point as the Swanson apex parameter ($[S_b/p_c]_A$). The Swanson apex parameter ($[S_b/p_c]_A$) can be determined from Wells and Amaefule approach as follows:

$$\left[\frac{S_b}{p_c}\right]_A = \psi^{-2} \quad \text{where } \psi = \text{minimum value of } \left[\frac{p_c}{S_b}\right]^{1/2} \qquad (2.31)$$

The Wells and Amaefule study of samples with permeability values less than 0.1 md showed a significant deviation from the Swanson model. As such, they proposed a (slightly) different correlation model for low permeability samples, which is given by:

$$k = 30.5\left[\frac{S_b}{p_c}\right]_A^{1.56} \qquad (2.32)$$

Kamath (1992) had performed an extensive study to compare the correlation of permeability with several length scales based on the models developed by Purcell (1949), Kwon and Pickett (1975), Swanson (1981), and Katz and Thompson (1987). He also proposed two new length scales modified from Swanson's correlating parameter. All six length scales studied are summarized in **Table 2.3**.

The results presented in Kamath's work showed that the correlation model using L_{pd} length scale always have the highest error. The other five length scales appear to be comparable in predictability and Kamath suggested that different researchers may come to different conclusions regarding the best model depending on the specific samples being considered. The difference between the L_{pd} length scale and the other five length scales is that L_{pd} is the only one that scale parameter makes no reference to the Swanson apex parameter ($[S_b/p_c]_A$).

Using samples from sandstone and carbonate reservoirs, Kamath proposed two new correlations using the Swanson apex parameter ($[S_b/p_c]_A$) as a correlating parameter, to be used for permeability estimation below and above 1 md. He also showed that the correlations are invariant to the lithology of the samples (*i.e.*, sandstones versus carbonates). The proposed correlations by Kamath are given as:

$$k = 413\left[\frac{S_b}{p_c}\right]_A^{1.85} \quad \text{for } k < 1\,\text{md} \qquad (2.33)$$

$$k = 347\left[\frac{S_b}{p_c}\right]_A^{1.60} \quad \text{for } k > 1\,\text{md} \qquad (2.34)$$

Table 2.3 — Six length scales for permeability correlation under the study of Kamath (1992).

Length Scale	Based Model
$L_{\max} = \left[\frac{S_b}{p_c}\right]_A$	Swanson (1981)
$L_{\text{int}} = \int_0^1 \left[\frac{S_b}{p_c}\right] dS_b$	Modified Swanson (1981)
$L_{\max, Z} = Z\left[\frac{S_b}{p_c}\right]_A$	Modified Swanson (1981) Z = curvature at $\left[\frac{S_b}{p_c}\right]_A$
$L_{pd} = \frac{\phi}{p_d}$	Kwon and Pickett (1975)
$L_p = \int_0^1 \frac{1}{p_c^2} dS_w$	Purcell (1949)
$L_{klh} = \frac{l_h^3}{l_c}\phi S(l_h)$	Katz and Thompson (1987)

Ma et al. (1991) reformulated Thomeer's hyperbolic model into a function of tangent angle to show that the value of $[S_b/p_c]$ (Swanson's parameter) is insensitive around the Swanson apex point (*i.e.*, the point with tangent angle of 45˚). In other words, *the value of* $[S_b/p_c]$ *at any point in the vicinity of the apex should correlate equally well with permeability*. The results of their study are illustrated in **Fig. 2.16**.

Guo et al. (2004) proposed another correlating parameter that was argued to better correlate with permeability than the Swanson apex parameter ($[S_b/p_c]_A$). Their proposed parameter was based on the permeability model of Purcell (1949). They reasoned that the correlating parameter should carry information about the effective pore size distribution, which was shown as the integral term of Purcell's model. Thus, they proposed a new correlating parameter called "Capillary parachor" — which is the maximum value of $[S_b/p_c^2]$.

The improvement in correlation of capillary parachor over the Swanson apex was also shown in the study of tight gas reservoirs by Xiao et al. (2014). They also demonstrated that in some cases of the very tight samples where the Swanson apex couldn't be observed, the capillary parachor can still be determined as it often exhibits at lower non-wetting phase (mercury) saturation. **Fig. 2.17** shows the comparison between

the Swanson apex parameter ($[S_b/p_c]_A$) and the capillary parachor $[S_b/p_c^2]$ for different capillary pressure curve shapes.

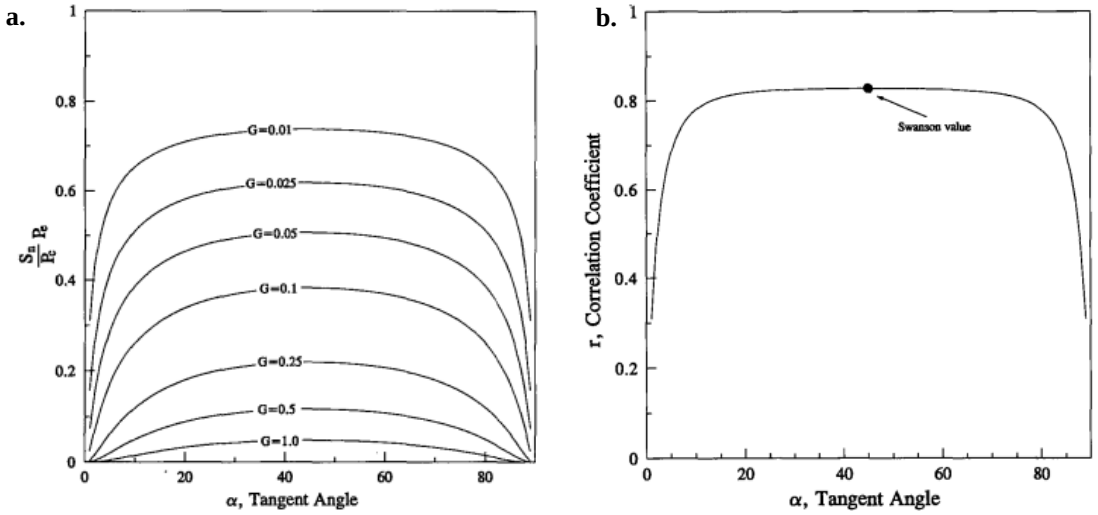

Figure 2.16 — The results of Ma et al. (1991) study: **a.** Dependence of normalized Swanson's parameter on tangent angle, **b.** Correlation coefficient of correlations of Swanson's parameter at different tangent angle (Ma et al. 1991).

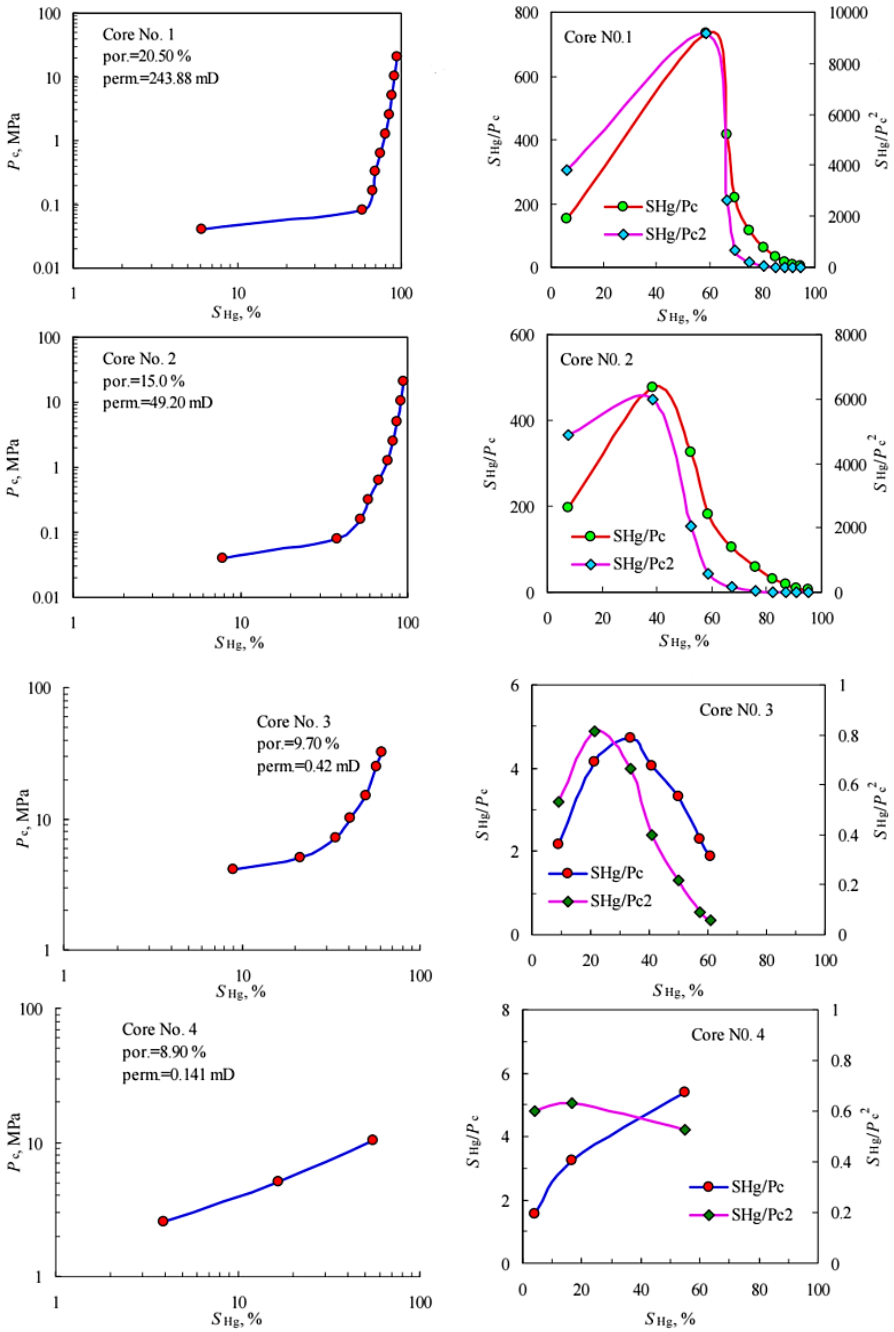

Figure 2.17 — MICP curves and the corresponding Swanson apex and capillary parachor for four representative core samples (Xiao et al. 2014).

Another type of correlation is that between permeability, porosity, and a *representative pore-throat size* obtained from the capillary pressure curve. Such relationships were first introduced by Kwon and Pickett (1975) where they performed an empirical study to determine the relationship between permeability and the mercury injection capillary pressure data. Using a database of >2,500 samples representing various rock types, Kwon and Pickett found that, at different wetting phase saturations, capillary pressure is related to the ratio of permeability over porosity in the form given by:

$$p_C = A\left[\frac{k}{100\phi}\right]^{-B} \quad \text{.....(2.35)}$$

The constant *A* was found to be correlated with wetting phase saturation while the constant *B* was found to be approximately constant at 0.45. By applying the Washburn relation (Washburn 1921), the capillary pressure in Eq. 2.35 can be converted into pore-throat radius. Kwon-Pickett relationship can then be rewritten as a function of pore-throat radius as (Aguilera 2002):

$$r = A^*\left[\frac{k}{100\phi}\right]^{B} \quad \text{.....(2.36)}$$

Taking the logarithm to Eq. 2.36, the model can be formulated as:

$$\log r = A^* + B\log k + B\log 100\phi \quad \text{.....(2.37)}$$

Eq. 2.36 can be generalized by assuming that the parameters in this relation are independent (i.e., unique and non-repeated), this generalized correlation model is written as:

$$\log r = a_1 + a_2\log k + a_3\log 100\phi \quad \text{.....(2.38)}$$

This form of correlation model was first introduced by Winland (Kolodzie Jr 1980). His study on sandstone and carbonate samples (with Klinkenberg corrected permeability for low permeability samples) showed that the correlation was most highly correlated for the pore-throat size at mercury saturation of 35%. The original model was proposed with representative pore-throat size as a dependent variable given as:

$$\log r_{35} = 0.732 + 0.588\log k - 0.864\log 100\phi \quad \text{.....(2.39)}$$

Verification of the Winland model was extensively studied by Gunter et al. (2014) and it is important to note that many correlations with a basis similar to Winland's model have been proposed. Some of the proposed correlations found in the published literature are summarized in **Table 2.4**. From everything that has been reviewed, there is no "analytical" basis to provide support to any of the selected pore-throat size references (e.g., Winland's criteria of 35 percent Hg saturation).

Table 2.4 — Summary of correlations which utilize a representative pore-throat size.

Reference	Correlation Model	Representative pore-throat radius
Winland (Kolodzie Jr 1980)	$\log r_{35} = 0.732 + 0.588\log k - 0.864\log 100\phi$	r_{35} = pore-throat radius at mercury saturation of 35%
Pittman (1992)	$\log k_a = -1.221 + 1.415\log 100\phi + 1.512\log r_{25}$	r_{25} = pore-throat radius at mercury saturation of 25%
Aguilera (2002); (2004)	$\log r_{35} = 0.426 + 0.45\log k - 0.45\log 100\phi$	r_{35} = pore-throat radius at mercury saturation of 35%
Jaya et al. (2005) Limestone	$\log k_a = -0.621 + 4.98\phi + 1.132\log r_{15}$	r_{15} = pore-throat radius at mercury saturation of 15%
Jaya et al. (2005) Sandstone	$\log k_a = -0.422 + 5.19\phi + 1.440\log r_{15}$	r_{15} = pore-throat radius at mercury saturation of 15%
Rezaee et al. (2006) Carbonate	$\log k_a = -1.160 + 1.780\log 100\phi + 0.903\log r_{50}$	r_{50} = pore-throat radius at mercury saturation of 50%
Dastidar et al. (2007)	$\log k = -2.51 + 3.06\log 100\phi + 1.64\log r_{wgm}$	r_{wgm} = weighted geometric mean of the pore-throat radii over the whole range of mercury saturation
Rezaee et al. (2012) Tight gas sand	$\log k_a = -1.92 + 0.949\log 100\phi + 2.18\log r_{10}$	r_{10} = pore-throat radius at mercury saturation of 10%

Studies to compare the performance between different pore throat models have been conducted by numerous researchers (Comisky et al. 2007; Kamath 1992; Nooruddin et al. 2013; Nooruddin et al. 2014). In short, the results were found to be inconclusive between different data sets. An example study from Nooruddin et al. (2013) is shown in **Table 2.5**. These strong correlations explain how different pore throat models may perform equally well.

Table 2.5 — Correlation matrix of air permeability and all extracted parameters in the logarithmic domain (Nooruddin et al. 2013).

	k, mD	$\int_0^1 \frac{dS}{P_c^2}, psi^{-2}$	P_d, psi	$r_{35}, \mu m$	$\left(\frac{S_b}{P_c}\right)_A, psi^{-1}$	$R_{WGM}, \mu m$	$r_{apex}, \mu m$
k, mD	1	0.9422	-0.9199	0.9529	0.9691	0.9526	0.9223
$\int_0^1 \frac{dS}{P_c^2}, psi^{-2}$	0.9422	1	-0.9938	0.9771	0.9792	0.9849	0.9934
P_d, psi	-0.9199	-0.9938	1	-0.9521	-0.9571	-0.9636	-0.9912
$r_{35}, \mu m$	0.9529	0.9771	-0.9521	1	0.9858	0.9949	0.9565
$\left(\frac{S_b}{P_c}\right)_A, psi^{-1}$	0.9691	0.9792	-0.9571	0.9858	1	0.9883	0.9630
$R_{WGM}, \mu m$	0.9526	0.9849	-0.9636	0.9949	0.9883	1	0.9662
$r_{apex}, \mu m$	0.9223	0.9934	-0.9912	0.9565	0.9630	0.9662	1

CHAPTER III

DEVELOPMENT AND APPLICATION OF A NEW SEMI-ANALYTICAL MODEL TO PREDICT PERMEABILITY FROM MICP

3.1 Development of a New Semi-Analytical Model

The development of our new correlation to predict the absolute permeability from mercury injection capillary pressure parameters is based on the semi-analytical model proposed by Huet (2005). Huet's semi-analytical correlation model was developed from the work of Nakornthap and Evans (1986). By re-deriving the classic *k*-model proposed by Purcell (1949) and Burdine (1953) with considerations of the works by Wyllie and Spangler (1952) and Wyllie and Gardner (1958), the derivation result of Nakornthap and Evans work is given as:

$$k = 21.32\frac{\beta}{n}\frac{1}{2}(\sigma_{Hg-air}\cos\theta)^2(1-S_{wi})^3\phi^3\int_0^1\frac{1}{p_c^2}dS_w^* \quad \text{.....(3.1)}$$

where: (written for an Hg-air system (*i.e.*, $S_w = S_{air}$))

k = permeability, md

21.32 = units conversion constant, md-(psia)^2/(dynes/cm)^2

β = pore throat "impedance" factor, dimensionless

n = number of entrances/exits in a pore, dimensionless

$\sigma_{Hg\text{-}air}$ = mercury-air interfacial tension, dynes/cm

θ = contact angle of incidence for wetting phase, radians

ϕ = porosity, fraction of pore volume

p_c = capillary pressure, psia

S_w = wetting phase saturation, fraction of pore volume

S_{wi} = irreducible wetting phase saturation, fraction of pore volume

S_w^* = (S_w-S_{wi})/(1-S_{wi}), "effective" wetting phase saturation function , dimensionless

Huet applied the capillary pressure model of Brooks and Corey (1964) together with the suggestion for the β and n parameters by Ali (1995) into the Nakornthap and Evans (1986) model (Eq. 3.1). The derivation result is given as:

$$k = 10.66\alpha(\sigma\cos\theta)^2(1-S_{wi})^4\phi^2\frac{1}{p_d^2}\left[\frac{\lambda}{\lambda+2}\right] \quad \text{.....(3.2)}$$

The empirical parameter, α, was added and noted by Huet (2005) as

"*to represent any remaining non-idealities that have not been accounted for by any other terms… we would likely assume* $\alpha = 1$*, or attempt a calibration of the α-parameter for a particular data set.*"

The significance of this result is the suggestion of the power-law relationship between the permeability, porosity, and the mercury injection capillary pressure parameters. Eq. 3.2 was recast and proposed as a semi-analytical correlation model as (where a_1, a_2, a_3, a_4, and a_5 are the independent correlation parameters):

$$k = a_1 \frac{1}{(p_d)^{a2}} \left[\frac{\lambda}{\lambda+2}\right]^{a3} (1-S_{wi})^{a4} \phi^{a5} \quad \text{.....(3.3)}$$

To determine the correlation parameters (a_1, a_2, a_3, a_4, and a_5) in Eq. 3.3, we used the mercury injection capillary pressure (MICP) data sets obtained from the original work of Huet (2005), as well as additional data sets from the literature (Byrnes 2009; Xu 2013). These data sets include samples from tight sandstones, as well as conventional sandstone and carbonate reservoirs. We attempted to find relevant "shale" samples, but no comprehensive/complete data sets for shales could be found in the public literature. For consistency, we retained our focus on mercury injection capillary pressure (MIPC) data as studied by Huet.

A total of 573 mercury injection capillary pressure (MICP) data sets were reviewed and considered for use in this work. Ultimately, we selected 323 samples where the MICP data exhibit a suitably smooth trend sufficient to generate parameter estimates. We paid particular attention to the data quality at high wetting-phase saturation region (*i.e.*, low mercury saturation). In addition, all of the selected samples exhibit a clear displacement pressure (p_d). We also made certain that the reported permeabilities of the samples selected were from direct measurements, not calculations from other properties, in order to prevent bias in our analyses.

Our selected samples represent permeabilities ranging from 4.5×10^{-7} md to 8.3×10^{3} md and porosities ranging from 0.9 to 37.1 percent. This new data set covers permeabilities in the mid-range (0.5 to 100 md) which was lacking in the original work by Huet (2005). Histograms showing the distributions of the permeabilities and porosities of the samples in our data set are shown in **Figs. 3.1**.

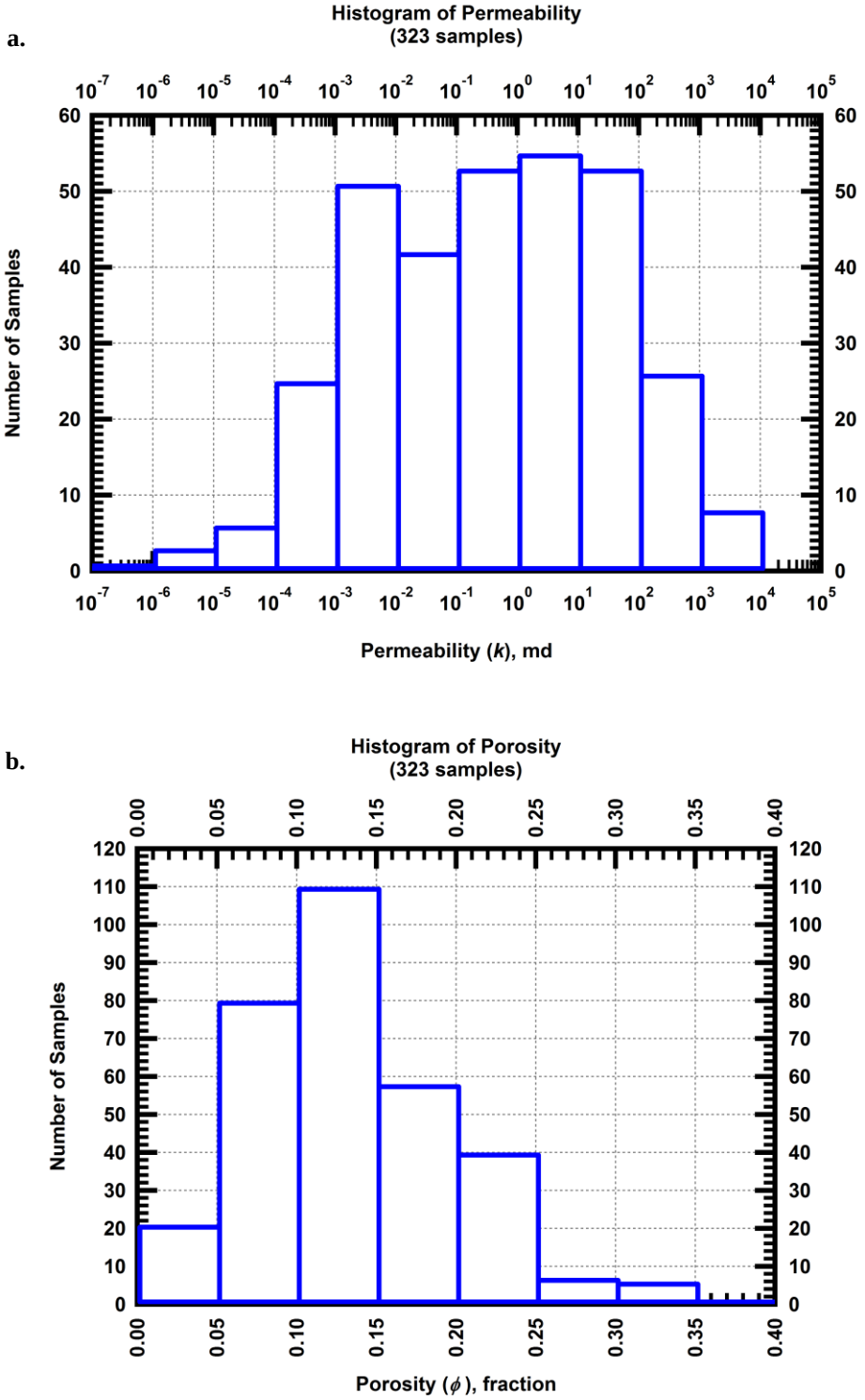

Figure 3.1 — Histograms showing the distributions of **a.** Permeabilities, and **b.** Porosities of 323 selected samples.

Determination of the Brooks-Corey MICP Model Parameters

Using the MICP data set of each sample, we determined the Brooks-Corey MICP model parameters (*i.e.*, the displacement pressure (p_d), pore-size distribution index (λ), and the irreducible wetting phase saturation (S_{wi})) by data-model-matching via regression (with hand corrections when necessary). We utilized the Solver Module in Microsoft Excel (2013) to determine the three Brooks-Corey MICP model parameters (p_d, λ, and S_{wi}) by minimizing the sum-of-squared-residuals (SSR) between the actual and calculated MICP curves.

We also used specialized plots to visually verify the data-model matches. The two plots we used are the semi-log plot of the capillary pressure (p_c) versus the wetting phase saturation (S_w) and the log-log plot of the capillary pressure (p_c) versus the "effective" wetting phase saturation (S_w^*). As originally described by Brooks and Corey (1964), the selected value of S_{wi} should result in most of the points laying sufficiently close to a straight line on the log-log plot of the capillary pressure (p_c) versus the "effective" wetting phase saturation (S_w^*). The λ-parameter is a function of the slope of that straight line (*i.e.*, slope = -1/λ), and the parameter p_d is the capillary pressure at $S_w^* = 1$ extrapolated from the specified straight line. Examples of the semi-log and log-log plots are illustrated in **Figs. 3.2** and **3.3**.

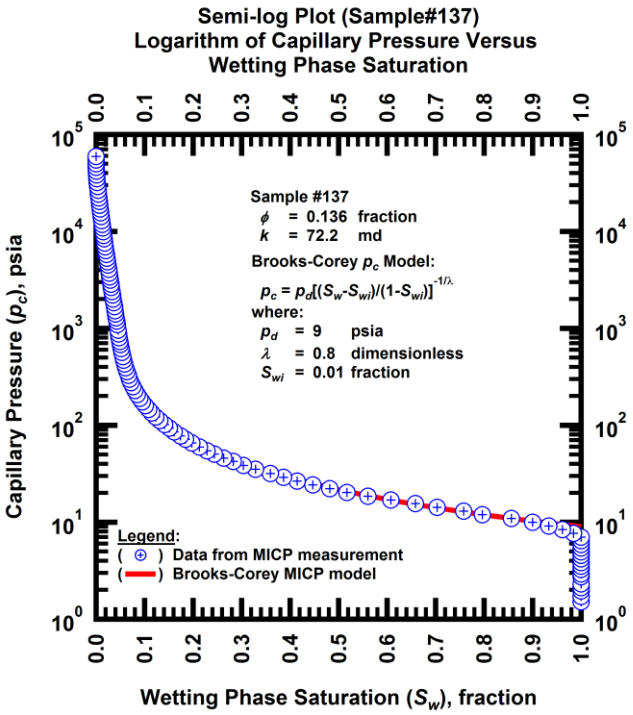

Figure 3.2 — Example of data-model matching on a semi-log plot of capillary pressure (p_c) versus wetting phase saturation (S_w).

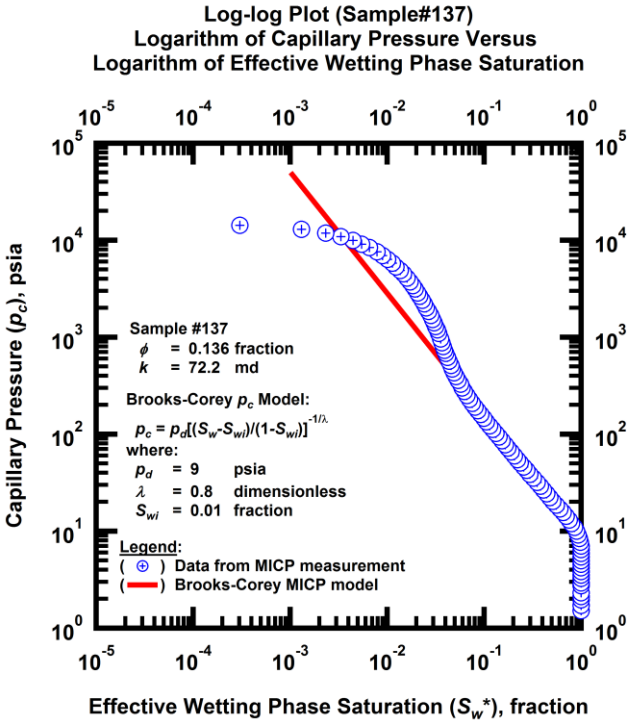

Figure 3.3 — Example of data-model matching on a log-log plot of capillary pressure (p_c) versus "effective" wetting phase saturation (S_w^*).

During this process, we observed that several of the MICP data tended to deviate from the Brooks-Corey capillary pressure model at high mercury saturation (*i.e.*, low wetting phase saturation). Because of these deviation features, the selection of a concise data range for matching the data with the model was often subjective. We stated that our workflow for this process was both robust and consistent, but we must acknowledge that some of the cases have more "subjective" matches than others.

The ranges of the p_d, λ, and S_{wi} determined of the selected 323 samples are summarized below. **Fig. 3.4** shows the histograms of each parameter to illustrate the distributions of the sample properties we used to generate our new correlation.

$2.1 < p_d < 9045.5$ psia
$0.15 < \lambda < 5.22$ dimensionless
$0 < S_{wi} < 0.62$ fraction

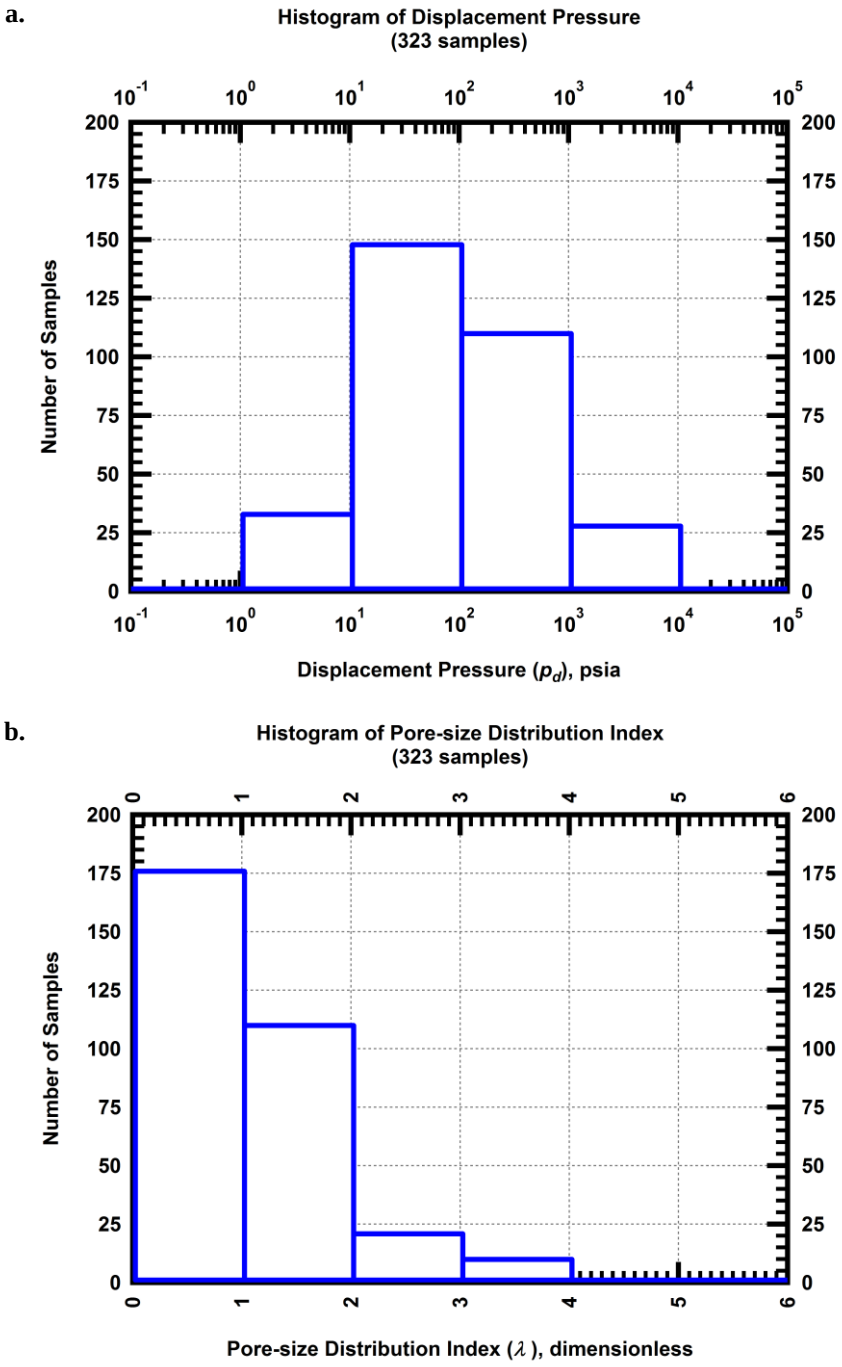

Figure 3.4 — Histograms showing the distributions of **a.** Displacement pressure (p_d), **b.** Pore-size distribution index (λ), and **c.** Irreducible wetting-phase saturation (S_{wi}) determined from data-model matching with regression of 323 selected samples.

c.

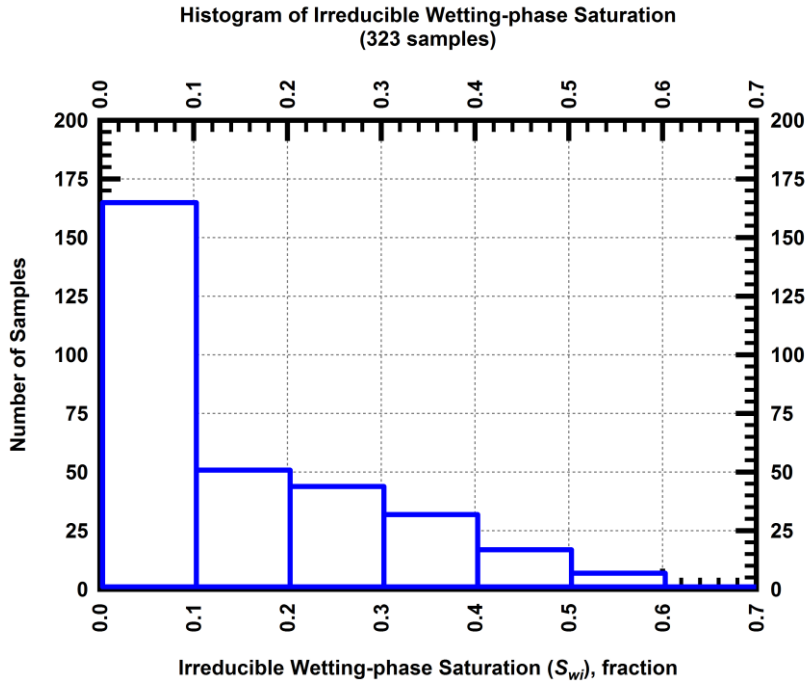

Figure 3.4 — Continued.

Regression Analysis Using the Semi-Analytical Correlation Model

The correlating parameters (a_1, a_2, …, a_5) of the semi-analytical (Huet) correlation model (Eq. 3.3) were optimized by the use of multiple linear regression in the logarithmic domain. By taking the logarithm of Eq. 3.3, the regression model can be written as:

$$\ln(k) = \ln(a_1) + (-a_2)\ln\left[\frac{1}{p_d}\right] + a_3 \ln\left[\frac{\lambda}{\lambda+2}\right] + a_4 \ln(1-S_{wi}) + a_5 \ln(\phi) \quad \text{.....(3.4)}$$

Using a database (323 samples) of permeability (k) and porosity (ϕ), as well as the p_d, λ, and S_{wi} parameters, we then used the correlation model given by Eq. 3.4. The regression analysis was conducted using the statistical software *R* (2015). The regression results are shown on log-log plot where the calculated permeabilities (*i.e.*, permeabilities calculated with the optimized model) are plotted versus the measured permeabilities (see **Fig. 3.5**.) The optimized coefficients and the statistical summary from the regression analysis of Eq. 3.4 are summarized in **Table 3.1**.

Table 3.1 — Regression summary for ln(k) **—** semi-analytical model.

Optimized coefficients for ln(k) **—** *Eq.* 3.4:

Coefficient	Optimized Value
a_1	3538886
a_2	1.88729
a_3	1.68582
a_4	2.94056
a_5	2.50998

Statistical summary for ln(k) **—** *Eq.* 3.4:

Statistical Variable	Value	
Sum of Squared Residuals	367	$\ln(md)^2$
Mean Squared Error	1.1541	$\ln(md)^2$
Residual Standard Error	1.0743	ln(md)
R-Squared	0.9467	dimensionless

Substituting the coefficients from **Table 3.1** into Eq. 3.3, we have:

$$k = 3538886 \frac{1}{(p_d)^{1.8873}} \left[\frac{\lambda}{\lambda + 2} \right]^{1.6858} (1 - S_{wi})^{2.9406} \phi^{2.5100} \quad \text{.....(3.5)}$$

To better illustrate the quality of the correlation, 95 percent of the data matched with the new optimized model lie within a factor of 9.1, and 58 percent of the data matched with the new optimized model lie within a factor of 2 of the measured permeabilities. As is evident in **Fig. 3.5**, the new correlation appears to be best suited for cases where the permeability is greater than 1 md — however; it should also be noted that although there is more "scatter" in the optimized results for permeabilities less than 1 md, the scatter is reasonably centered about the "perfect correlation" trend. As a recommendation for future work, we strongly encourage continued investigations for cases where the permeability is less than 1×10^{-3} md.

As stated earlier, several of the MICP data cases tended to deviate from the Brooks-Corey model at low wetting phase saturations. We have tested the impact of the quality of the MICP data (good quality are classified as the MICP data that follow the Brooks-Corey model) to assess the correlation strength between permeability and the MICP parameters according to the model in Eq. 3.3. *The statistical results suggest that the correlation strength for the samples with good quality MICP data are not significantly different from the correlation strength of the poor quality data sets*. This effort is shown in Appendix E.

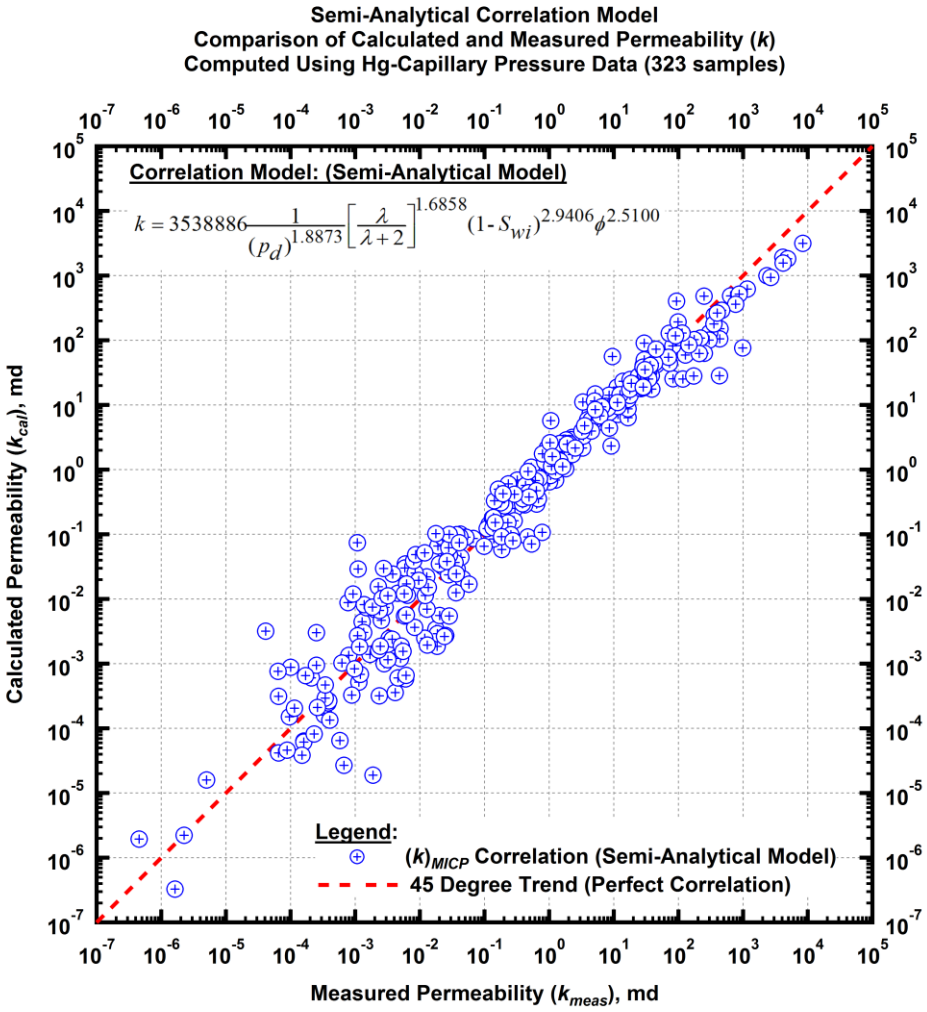

Figure 3.5 — Permeability correlation comparison for the 323 MICP samples used in this work matched with the semi-analytical model of Huet (Huet 2005).

Predictability of the New Semi-Analytical Model

Fig. 3.6 is the same plot as **Fig. 3.5** with the confidence limits plotted as dashed red lines. As noted in the previous section, the variability of the calculated permeabilities using the optimized model to the measured permeabilities was observed to be higher at permeability lower than 1 md. Thus, we separately evaluated the predictability of the model at permeability above and below 1 md.

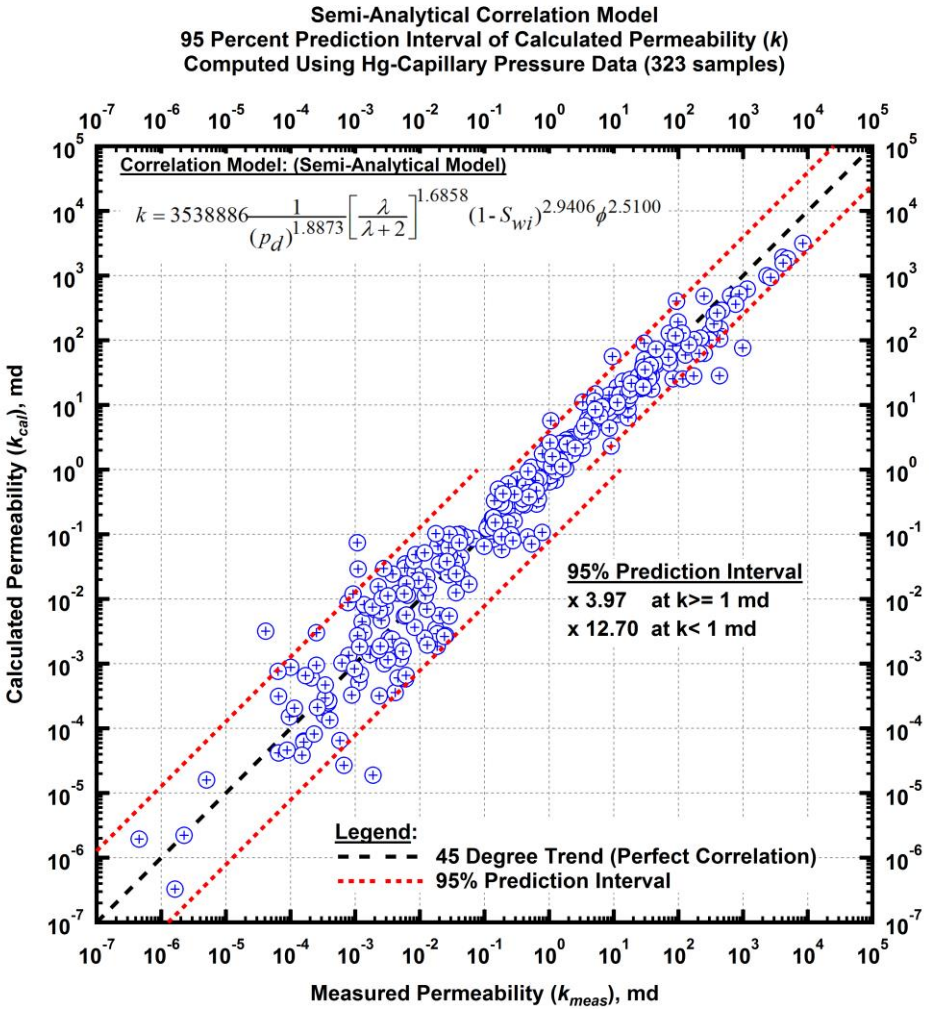

Figure 3.6 — 95 percent prediction intervals of the proposed new semi-analytical model to predict permeability at permeability above and below 1 md.

Dotted lines in **Fig. 3.6** show the 95 percent prediction intervals of the model. At permeability above 1 md, the calculated 95 percent prediction interval is within a factor of 3.97. This means there is 95 percent chance that the actual permeability will be within a factor of 3.97 of the predicted permeability using the proposed model (Eq. 3.5). The 95 percent prediction interval of permeability below 1 md is significantly higher (a factor of 12.70). This could be due to the higher uncertainty in measurement of properties, such as permeability and porosity. To better understand the performance of the model, controlled laboratory measurements will be required for samples with low permeability to reduce the uncertainties of each predicting parameters (*i.e.*, permeability, porosity, and MICP data).

3.2 Comparison to the Swanson Correlation Model

The Swanson (1981) is perhaps the most commonly correlation used to predict permeability from capillary pressure data. Recall that a power-law relationship was observed between the permeability and Swanson's correlating parameter. The correlation model for Swanson's model is given in the general form as:

$$k = a_1\left[\frac{S_b}{p_c}\right]_A^{a_2} \quad \text{.....(3.6)}$$

The parameter $[S_b/p_c]_A$ is Swanson's correlating parameter (*i.e.*, the apex parameter), which is the maximum value of $[S_b/p_c]$ of an MICP data set. The Swanson apex parameter, $[S_b/p_c]_A$ for each of the selected 323 samples was obtained from each MICP data set. The parameter S_b is the percent bulk volume occupied by mercury and can be calculated from the reported wetting phase saturation using the equation given below:

$$S_b = (1 - S_w)\phi \times 100 \quad \text{.....(3.7)}$$

As a quality control mechanism, the Swanson parameter was visually verified by the use of a Cartesian plot of $[S_b/p_c]$ versus S_b. An example of this type of Cartesian plot is shown in **Fig. 3.7**.

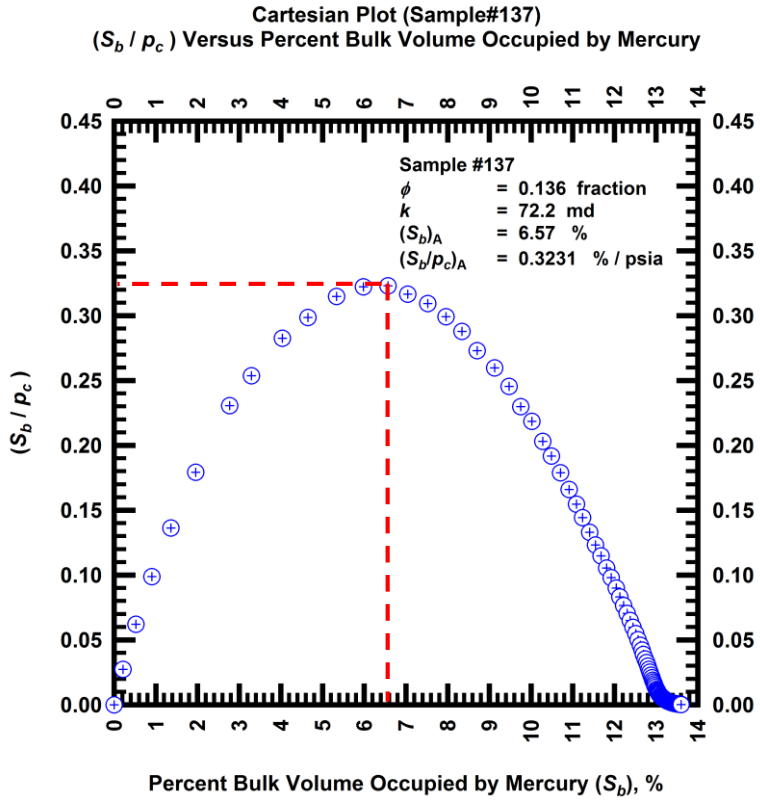

Figure 3.7 — Example of Cartesian plot of $[S_b/p_c]$ versus S_b to determine the Swanson parameter $[S_b/p_c]_A$, which is the maximum value of $[S_b/p_c]$.

Regression Analysis of the Swanson Correlation Model

The correlating parameters (a_1 and a_2) for the Swanson correlation model (Eq. 3.6) were optimized by the use of simple linear regression in the logarithmic domain. By taking the logarithm of Eq. 3.6, the regression model can be written as:

$$\ln(k) = \ln(a_1) + a_2 \ln\left[\frac{S_b}{p_c}\right]_A \quad \text{.....(3.8)}$$

Eq. 3.8 was used as a regression model for permeability and the Swanson apex parameter ($[S_b/p_c]_A$) — the regression was conducted using the statistical software *R* (2015). The regression results are shown as a log-log plot of the calculated permeability (*i.e.*, permeability calculated with the optimized Swanson model) versus the measured permeability in **Fig. 3.8**. The optimized coefficients and the statistical summary from the regression analysis of Eq. 3.8 are summarized in **Table 3.2**.

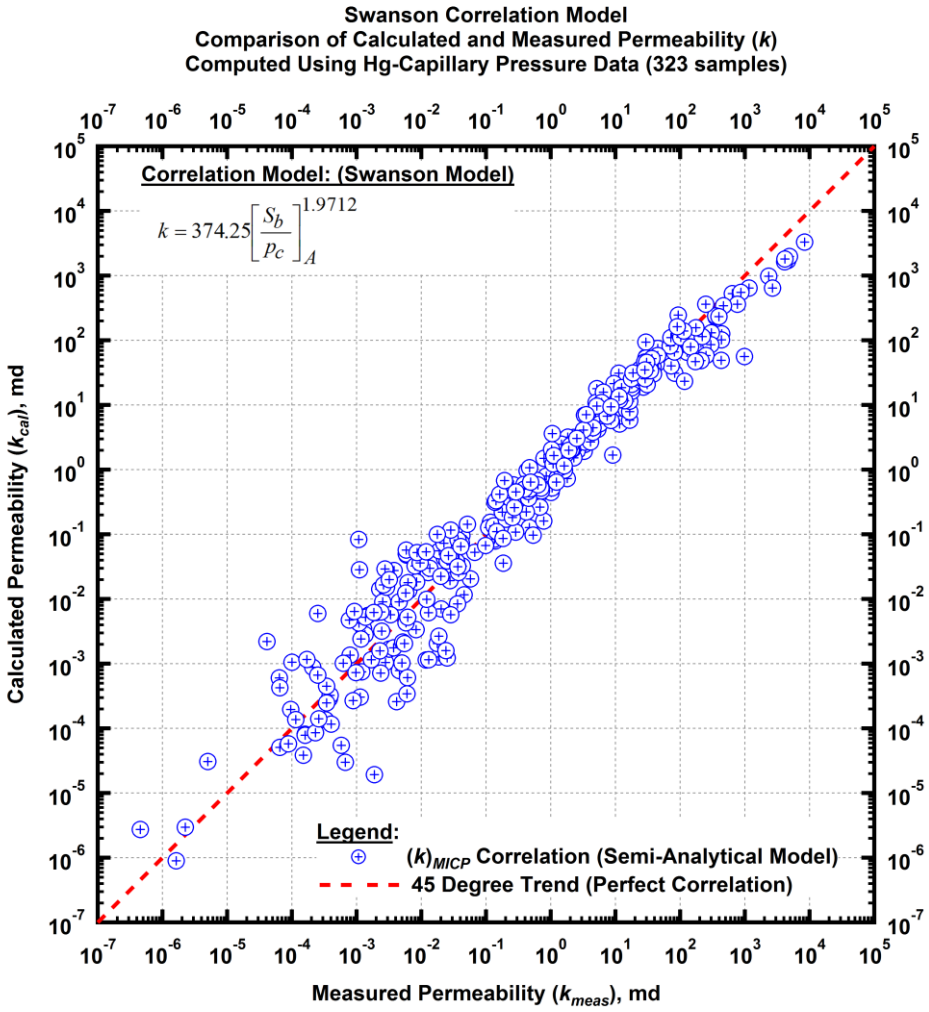

Figure 3.8 — Permeability correlation comparison for the 323 MICP samples used in this work matched with the Swanson model (Swanson 1981).

Table 3.2 — Regression summary for ln(k) **—** Swanson model.

Optimized coefficients for ln(k) **—** *Eq.* 3.8:

Coefficient	Optimized Value
a_1	374.25
a_2	1.9712

Statistical summary for ln(k) — Eq. 3.8:

Statistical Variable	Value	
Sum of Squared Residuals	392	$\ln(md)^2$
Mean Squared Error	1.2207	$\ln(md)^2$
Residual Standard Error	1.1048	ln(md)
R-Squared	0.9431	dimensionless

Substituting the coefficients from **Table 3.2** into Eq. 3.6, we have:

$$k = 374.25\left[\frac{S_b}{p_c}\right]_A^{1.9712} \quad \text{.....(3.9)}$$

Comparison of the Regression Results

The regression results summary of the semi-analytical (Huet) correlation model (Eq. 3.4) and the Swanson correlation model (Eq. 3.7) are summarized again in **Table 3.3** for comparison. The sum-of-squared-residuals, mean-squared-error, and residual-standard-error obtained for the (Huet) semi-analytical correlation model were all shown to be (slightly) lower than those of the Swanson correlation model. The value of R-squared for the semi-analytical (Huet) correlation model was shown to be (slightly) higher than the R-squared of the Swanson correlation model. These results suggest that the semi-analytical (Huet) model is a better permeability correlator than the Swanson correlation model. In other words, the optimized semi-analytical model (Eq. 3.5) can give a better permeability prediction than the optimized Swanson model (Eq. 3.9). We do note that the significance of the statistics for the Huet model is only slightly better than that for the Swanson model.

For the Swanson model, 95 percent of the data matched with the optimized model (Eq. 3.9) is within a factor of 10.4 (compared to 9.1 of the optimized semi-analytical model (Eq. 3.5)), and 56 percent of the data matched with the optimized model (compared to 58 percent of the optimized semi-analytical model (Eq. 3.5)) is within a factor of 2.

Table 3.3 — Comparison of statistical regression results for ln(k) of the semi-analytical model (Eq. 3.4) and the Swanson model (Eq. 3.8).

Statistical Variable	Semi-Analytical Model		Swanson Model	
Sum of Squared Residuals	367	$\ln(md)^2$	392	$\ln(md)^2$
Mean Squared Error	1.1541	$\ln(md)^2$	1.2207	$\ln(md)^2$
Residual Standard Error	1.0743	ln(md)	1.1048	ln(md)
R-Squared	0.9467	dimensionless	0.9431	dimensionless

CHAPTER IV

ANALYTICAL RELATIONSHIP BETWEEN THE SEMI-ANALYTICAL CORRELATION MODEL AND THE SWANSON CORRELATION MODEL

4.1 Analytical Relationship between the Swanson and Brooks-Corey Models

Swanson (1981) studied the mercury injection capillary pressure (MICP) data for a large number of sandstone and carbonate reservoirs. Swanson found a correlation between permeability and the maximum value of the ratio of percent bulk volume occupied by mercury (S_b) divided by the capillary pressure (p_c) — where this parameter is defined as the "Swanson apex" ($[S_b/p_c]_A$). The proposed Swanson correlation, in generic form, is given as:

$$k = a_1\left[\frac{S_b}{p_c}\right]_A^{a_2} \quad \text{.....(4.1)}$$

We will demonstrate that by applying the Brooks-Corey capillary pressure model (Brooks and Corey 1964), the maximum value of $[S_b/p_c]$ can be solved analytically as a function of the Brooks-Corey model parameters. Brooks and Corey (1964) proposed a "power-law" model to describe capillary pressure (p_c) as a function of "effective" wetting phase saturation as:

$$p_c = p_d\,(S_w^*)^{-1/\lambda} \quad \text{.....(4.2)}$$

Where S_w^* is the effective saturation function and is defined as a function of the wetting phase saturation (S_w) and the irreducible wetting phase saturation (S_{wi}) as follows:

$$S_w^* = \left[\frac{S_w - S_{wi}}{1 - S_{wi}}\right] \quad \text{.....(4.3)}$$

The Brooks-Corey power law capillary pressure model can then be written as a function of wetting phase saturation (S_w) as:

$$p_c = p_d\left[\frac{S_w - S_{wi}}{1 - S_{wi}}\right]^{-1/\lambda} \quad \text{.....(4.4)}$$

Eq. 4.4 shows that the Brooks-Corey capillary pressure model is a function of wetting phase saturation with three characteristic parameters — the displacement pressure (p_d), the index of pore-size distribution (λ), and the irreducible wetting phase saturation (S_{wi}). The function $[S_b/p_c]$ can therefore be formulated as a function of the Brooks-Corey capillary pressure model's characteristic parameters (p_d, λ, S_{wi}). The maximum value of $[S_b/p_c]$, or the Swanson apex parameter ($[S_b/p_c]_A$), can then be analytically determined by differentiating

the [S_b/p_c] function. The detailed derivation for this work is shown in Appendix B. The final form of the Swanson apex parameter ([S_b/p_c]$_A$) as a function of the model parameters for the Brooks-Corey capillary pressure relation is given as:

$$\left[\frac{S_b}{p_c}\right]_A = 100\frac{1}{p_d}\left[\frac{\lambda}{(1+\lambda)^{(1+\frac{1}{\lambda})}}\right](1-S_{wi})\,\phi \quad \text{.....(4.5)}$$

4.2 Analytical Relationship between the Semi-Analytical Correlation and Swanson Model

By substituting Eq. 4.5 into Eq. 4.1, Swanson's correlation model can be written as a function of the Brooks-Corey model parameters as:

$$k = a_1\left[\frac{1}{p_d}\left[\frac{\lambda}{(1+\lambda)^{(1+\frac{1}{\lambda})}}\right](1-S_{wi})\,\phi\right]^{a_2}$$

$$= a_1\frac{1}{(p_d)^{a_2}}\left[\frac{\lambda}{(1+\lambda)^{(1+\frac{1}{\lambda})}}\right]^{a_2}(1-S_{wi})^{a_2}\,\phi^{a_2}$$

.....(4.6)

Comparing Eq. 4.6 to the semi-analytical model proposed by Huet (2005), we have:

$$k = a_1\frac{1}{(p_d)^{a_2}}\left[\frac{\lambda}{\lambda+2}\right]^{a_3}(1-S_{wi})^{a_4}\,\phi^{a_5} \quad \text{.....(4.7)}$$

In our statistical work, we found that the λ-term proposed in Eq. 4.6 is well correlated with the λ-term given in Eq. 4.7 with the "power-law" relationship over the entire range of λ-values in our data sets. This may seem obvious at first, but this observation allows us to relate the empirical correlation model of Swanson to the analytically derived, semi-analytical model proposed by Huet (2005). Following the assumptions and work performed in Appendix C, Eq. 4.6 can be written as:

$$k = b_1\frac{1}{(p_d)^{a_2}}\left[\frac{\lambda}{\lambda+2}\right]^{b_2}(1-S_{wi})^{a_2}\,\phi^{a_2} \quad \text{.....(4.8)}$$

Eq. 4.8 can then be generalized into exactly the same form as the semi-analytical (Huet) model (Eq. 4.7) by simply assuming that the correlation parameters in this relation are independent (*i.e.*, unique and non-

repeated). This is also shown in Appendix C. Therefore, the final form of the "Swanson" model is the same as the "Huet" model:

$$k = a_1 \frac{1}{(p_d)^{a_2}} \left[\frac{\lambda}{\lambda+2}\right]^{a_3} (1-S_{wi})^{a_4} \phi^{a_5} \quad \text{.....(4.7)}$$

This derivation has demonstrated how the Swanson apex can be correlated with the permeability by re-formulating Swanson's correlating parameter (the Swanson apex) into the form that is comparable to the semi-analytical model. This derivation has also shown that the semi-analytical model is the more generic form of the Swanson correlation model, and should better represent the relationship between the capillary pressure and the permeability.

4.3 Determination of λ and S_{wi} using the Brooks-Corey-Swanson Relationship

During our matching work to estimate the Brooks-Corey model parameters described in Chapter 3, we observed that the displacement pressure (p_d) can easily be obtained from the semi-log plot of the capillary pressure versus the wetting phase saturation. However; the pore-size distribution index (λ) and the irreducible wetting phase saturation (S_{wi}) are often ambiguous. The (very) high pressures of the mercury injected at higher mercury saturations (*i.e.*, lower wetting phase saturation) during the laboratory measurement process may impact the original geometry of the pore network, which would likely mask the true irreducible wetting phase saturation.

From our observations in the study, the Swanson apex parameter ($[S_b/p_c]_A$) almost always clearly visible in the MICP data. As such, the maximum value of $[S_b/p_c]$ can easily be obtained from the Cartesian plot of the calculated $[S_b/p_c]$ versus the percent bulk volume occupied by mercury (S_b). Our derived relationship in Eq. 4.5 allows us to utilize the benefit of using a clearly defined value of the Swanson apex parameter ($[S_b/p_c]_A$) to determine the more uncertain parameters — *i.e.*, the pore-size distribution index (λ) and the irreducible wetting phase saturation (S_{wi}).

From the derived relationship between the Swanson apex and the Brooks-Corey MICP model parameters, Eq. 4.5 can be separated into component forms as: (see Appendix B for details)

$$(p_c)_A = p_d \left[\frac{1}{1+\lambda}\right]^{-1/\lambda} \quad \text{.....(4.8)}$$

$$(S_b)_A = 100 \frac{\lambda}{1+\lambda} (1-S_{wi})\,\phi \quad \text{.....(4.9)}$$

The Brooks-Corey parameters can be estimated using Eqs. 4.8 and 4.9 with the following workflow:

Step 1 — Estimate p_d using a semilog plot of p_c vs. S_w by extrapolation of the p_c plateau trend to $S_w = 1$. Example of this step is illustrated in **Fig. 4.1**.

Step 2 — Calculate for $[S_b/p_c]$ for the data set.

Step 3 — Plot $[S_b/p_c]$ versus S_b on a Cartesian plot.

Step 4 — Estimate $(S_b)_A$ from the Cartesian plot in Step 3 where the $[S_b/p_c]$ trend is maximum (*i.e.*, $[S_b/p_c]_A$). Example of this step is illustrated in **Fig. 4.2**.

Step 5 — Calculate $(p_c)_A$ from $[S_b/p_c]_A$ obtained in step 4 using the point $(S_b)_A$. Specifically, use the relation:

$$(p_c)_A = \frac{(S_b)_A}{\left[\frac{S_b}{p_c}\right]_A} \quad \text{.....(4.10)}$$

Step 6 — Solve for λ as a root using Eq. 4.8 or using an approximation function given in Appendix D.

Step 7 — Solve for S_{wi} using Eq. 4.9, which can be rearranged to yield S_{wi} directly:

$$S_{wi} = 1 - \frac{(S_b)_A}{100\phi}\frac{1+\lambda}{\lambda} \quad \text{.....(4.11)}$$

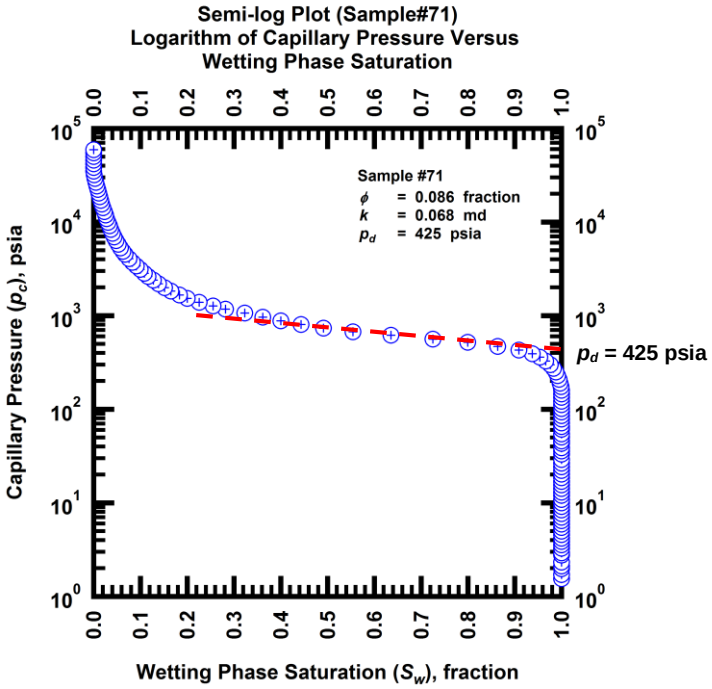

Figure 4.1 — Example of the displacement pressure determination from the semi-log plot of capillary pressure versus wetting phase saturation.

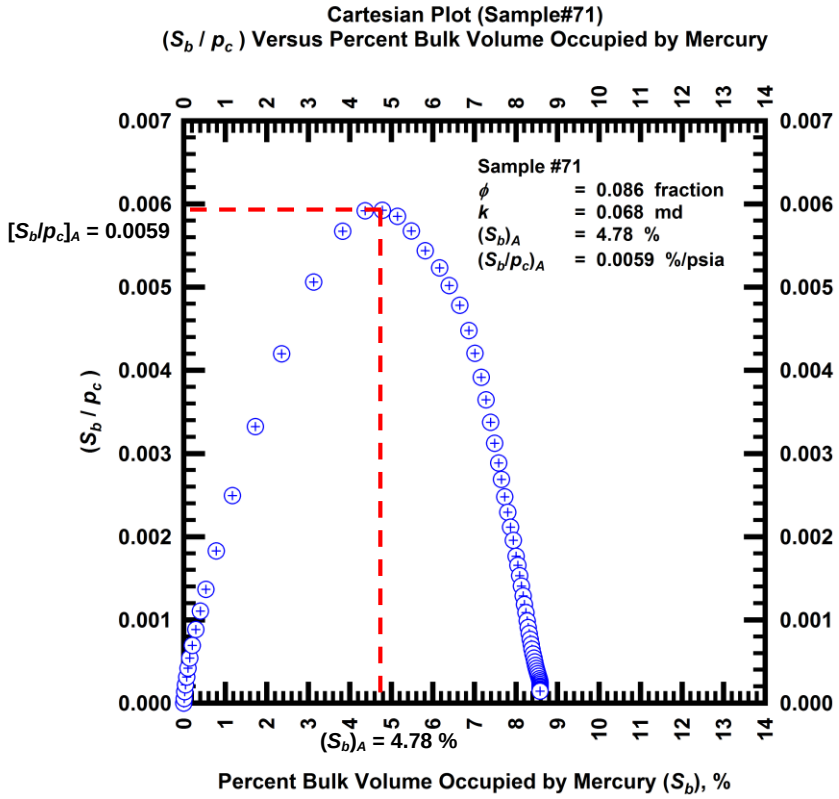

Figure 4.2 — Example of the Swanson apex $[S_b/p_c]_A$ determination from the Cartesian plot of $[S_b/p_c]$ versus the percent bulk volume occupied by mercury (S_b).

This approach forces all of the analyses to be tied to the Swanson apex parameter ($[S_b/p_c]_A$) — which implies that we can in essence, deconstruct the entire capillary pressure curve to a single point (*i.e.*, $[S_b/p_c]_A$), but from a completely rigorous standpoint we must also include the displacement pressure, p_d, and the irreducible wetting phase saturation (S_{wi}). Assuming that the capillary pressure at the apex $(p_c)_A$ can only be equal or higher than the displacement pressure (p_d), we note that this calculation allows the λ-value to be any number from 0 to infinity — which may result in the calculation of a negative S_{wi} value.

Verification of the Proposed Method

To verify the applicability of the proposed method of determining the Brooks-Corey MICP model parameters, we applied this method using the samples in our database. **Figs. 4.3** to **4.5** show example of the case where our method can be applied with confidence. The determination of the displacement pressure (p_d) and the Swanson apex ($[S_b/p_c]_A$) are shown in **Fig. 4.1** and **4.2**. This sample exhibits an excellent quality of MICP data.

The displacement pressure is clearly shown in the semi-log plot (**Fig. 4.1**) and can be obtained with high certainty. There are sufficient data around the Swanson apex in the Cartesian plot (**Fig. 4.2**) to reduce the uncertainty of the maximum value of $[S_b/p_c]$ together with the associated $(S_b)_A$ obtained. The λ and S_{wi}-parameters are then calculated with the proposed method. The results show an excellent match between the data and the capillary pressure computed using the Brooks-Corey capillary pressure model with our p_d, λ, and S_{wi} parameters determined for this case. This example has verified that our proposed method can be used to determine the Brooks-Corey MICP model parameters of the MICP data set.

We did find cases where the calculated S_{wi} were negative. Such cases require a re-evaluation of the displacement pressure (p_d) and the Swanson apex values ($[S_b/p_c]_A$ and $(S_b)_A$). The accuracy of the measured MICP data for those cases are likely the cause in such cases of where negative S_{wi} values are obtained. We acknowledge that the problem with negative S_{wi} is still an aspect of the work that requires additional effort and attention.

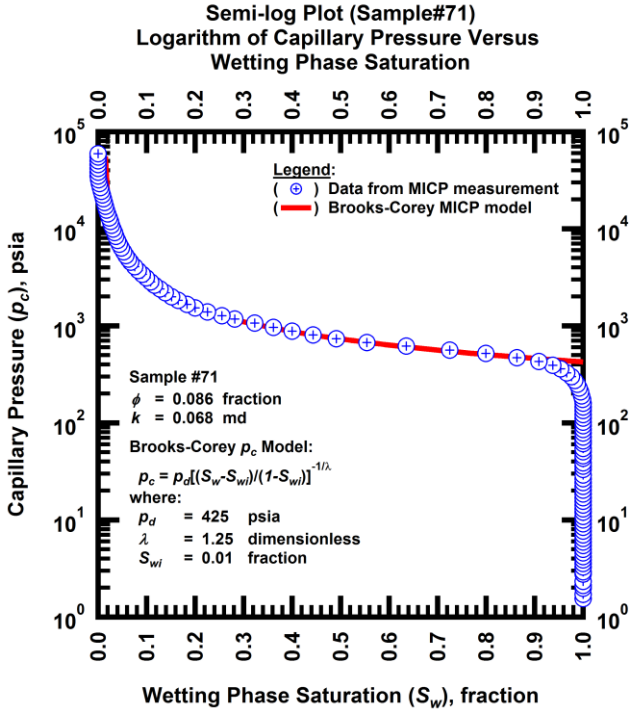

Figure 4.3 — Semi-log plot of the capillary pressure (p_c) versus wetting phase saturation (S_w) of sample #71 to show an excellent match between the data and the determined Brooks-Corey MICP model.

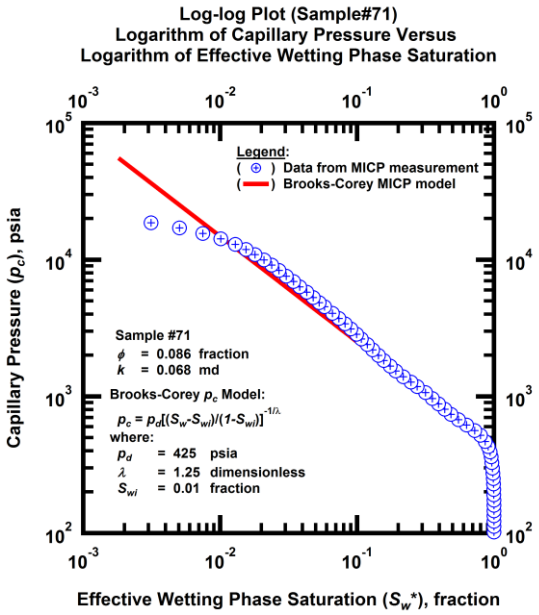

Figure 4.4 — Log-log plot of the capillary pressure (p_c) versus effective wetting phase saturation (S_w^*) of sample #71 to show an excellent match between the data and the determined Brooks-Corey MICP model.

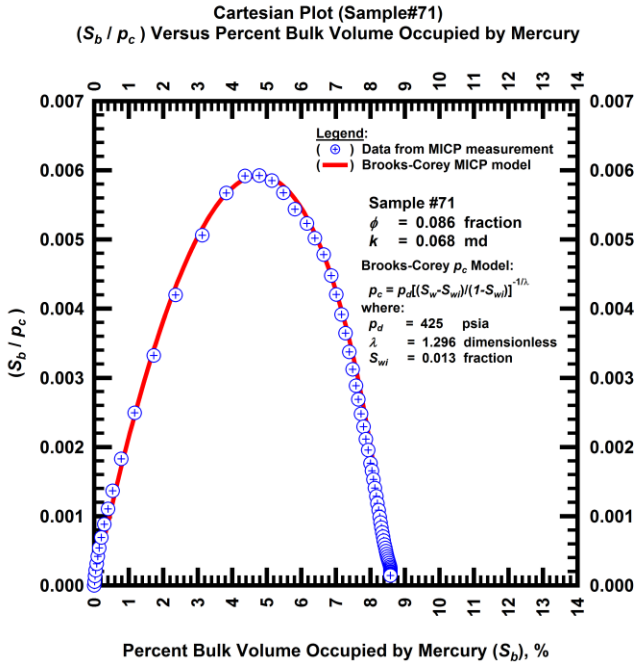

Figure 4.5 — Cartesian plot of the [S_b/p_c] versus percent bulk volume occupied by mercury (S_b) of sample #71 to show an excellent match between the data and the determined Brooks-Corey MICP model.

Recalling Eq. 4.8, we have:

$$(p_c)_A = p_d \left[\frac{1}{1+\lambda} \right]^{-1/\lambda} \quad \text{.....(4.8)}$$

We have studied this function in detail (as shown in Appendix D) and found that the ratio of $(p_c)_A/p_d$ is a limited function with a value between 1 and the exponential of 1 (Euler's number, 2.718281828459). The methodology proposed in Appendix D serves as a mechanism that is used to crosscheck the selected displacement pressure (p_d) and the Swanson apex values ($[S_b/p_c]_A$ and $(S_b)_A$). Using the 323 data sets in our database we investigated the ratio $(p_c)_A/p_d$ and established a few cases where we needed to re-estimate the behavior of the p_d values and the Swanson apex values ($[S_b/p_c]_A$ and $(S_b)_A$).

As a final note, since this method calculates the pore-size distribution index (λ) and the irreducible wetting phase saturation (S_{wi}) from a single point on the mercury injection capillary pressure curve (at the Swanson apex), we propose this method only as an alternative method to check the results obtained by regression. This approach is not intended to replace the regression method. This alternative methodology may serve as an initial evaluation tool, prior to applying the Brooks-Corey relation as a regression model.

As a final comment, we recommend that the laboratory data set have as many data points as practically possible (particularly in the region near the Swanson apex) in order to reduce the uncertainty in estimating the Swanson apex values ($[S_b/p_c]_A$ and $(S_b)_A$).

CHAPTER V

SUMMARY, CONCLUSIONS, AND RECOMMENDATIONS FOR FUTURE WORK

5.1 Summary

Using the relation proposed by Huet (2005), we have developed a new correlation model to predict absolute permeability from the mercury injection capillary pressure (MICP) data — our proposed model for permeability prediction is given as:

$$k = 3538886 \frac{1}{(p_d)^{1.8873}} \left[\frac{\lambda}{\lambda + 2} \right]^{1.6858} (1 - S_{wi})^{2.9406} \phi^{2.5100} \quad \text{.....(5.1)}$$

This power-law correlation was proved over 11 log-cycles of permeability (from $1x10^{-7}$ to $1x10^{4}$ md). The data sets used to construct the proposed correlation consisted of 323 samples from tight sandstones, conventional sandstone and carbonate reservoirs. Each data set includes the measured k and ϕ data — as well as the p_d, λ, and S_{wi} parameters obtained from the MICP data using the process of regression with the Brooks-Corey capillary pressure model (Brooks and Corey 1964) given as:

$$p_c = p_d \, (S_w^*)^{-1/\lambda} \quad \text{.....(5.2)}$$

Where S_w^* is the effective saturation function and is defined as:

$$S_w^* = \left[\frac{S_w - S_{wi}}{1 - S_{wi}} \right] \quad \text{.....(5.3)}$$

The permeability predicted by our proposed correlation model is expected to be within a factor of 3.97 of the actual permeability at 95% confidence level for the samples with permeability above 1 md. For samples with permeability less than 1 md, the predicted permeability was shown to be less accurate (within a factor of 12.70). Since there is higher uncertainty in the laboratory measurements of samples with low permeability, the error from the measurement is arguably the source of error for this portion of data in the correlation model.

We compared the correlation results using the semi-analytical (Huet) correlation model to the correlation results using the empirical correlation model proposed by Swanson (1981). The results showed that the semi-analytical (Huet) model was better correlated with the permeabilities in all statistical measures. We also proved analytically that the semi-analytical (Huet) correlation model is of a more generic form than the Swanson correlation model, which should (in general) allow for a better correlation to be obtained.

Our analytical derivations also provided insight into the viability of Swanson's empirical correlation parameter ($[S_b/p_c]_A$) to be correlated with permeability. The results of our analytical work are summarized as:

$$\left[\frac{S_b}{p_c}\right]_A = 100\frac{1}{p_d}\left[\frac{\lambda}{(1+\lambda)^{(1+\frac{1}{\lambda})}}\right](1-S_{wi})\,\phi \quad \text{.....(5.4)}$$

$$(p_c)_A = p_d\left[\frac{1}{1+\lambda}\right]^{-1/\lambda} \quad \text{.....(5.5)}$$

$$(S_b)_A = 100\frac{\lambda}{1+\lambda}(1-S_{wi})\,\phi \quad \text{.....(5.6)}$$

We use these derived results to propose an alternative method to estimate the Brooks-Corey MICP model parameters (p_d, λ, and S_{wi}). We validated the proposed method with our MICP database. This method is expected to be an alternative method to avoid, but not to replace, the use of regression. We acknowledge that our proposed method may generate physically unrealistic (*i.e.*, negative) estimates of the irreducible wetting phase saturation (S_{wi}). This is an aspect of work that will require additional effort and attention.

5.2 Conclusions

The following conclusions have been derived from this work:

1. The power-law relationship between the permeability (k), porosity (ϕ), capillary displacement pressure (p_d), index of pore-size distribution (λ), and the irreducible wetting phase saturation (S_{wi}) in the form of the semi-analytical model (Huet 2005) is proved over 11 log-cycles of permeability ($1x10^{-7}$ - $1x10^{4}$ md).

2. A new correlation to predict the absolute permeability from mercury injection capillary pressure (MICP) data based on the semi-analytical (Huet) model is provided with the predictability of a factor of 3.97 for permeability above 1 md and 12.70 for permeability below 1 md. The 323 data sets from our database were used to obtain this correlation.

3. The semi-analytical (Huet) model is shown to be better both statistically and analytically for correlating the permeability (k) with the mercury injection capillary pressure data as compared to the Swanson model (Swanson 1981).

4. The relationship between Swanson's correlating parameter (Swanson apex — $[S_b/p_c]_A$) and the Brooks-Corey capillary pressure model parameters (p_d, λ, and S_{wi}) can be derived. This derivation provides

insight into the viability of the correlation between Swanson's empirical correlating parameter (*i.e.*, the Swanson apex parameter — $[S_b/p_c]_A$) and the permeability (k). The results of this derivation also provide for the calculation of the pore-size distribution index (λ) and the irreducible wetting phase saturation (S_{wi}) from the Swanson apex parameter ($[S_b/p_c]_A$).

5.3 Recommendations for Future Work

The following recommendations for future work are proposed:

1. Verification of the correlation results in this work to samples with permeability values lower than $1x10^{-3}$ md, including samples from the shale reservoirs. The measurements of the permeability, porosity, and mercury injection capillary pressure (MICP) for the samples to be studied should be carefully selected and analyzed to avoid additional uncertainty in the resulting correlations.

2. Extension of the results of this work to capillary pressure measurement using methods other than the mercury-air system (*e.g.*, the porous plate and centrifuge methods).

3. Detailed study of cases where our proposed "alternative" method for determining the Brooks-Corey capillary pressure model parameters using the Brooks-Corey-Swanson correlation yields negative values of the irreducible wetting phase saturation (S_{wi}).

NOMENCLATURE

Field Variables

$(p_c)_A$ = capillary pressure at Swanson's apex, psia

$(S_b)_A$ = percent bulk volume occupied by mercury at Swanson's apex, percent

$[S_b/p_c]_A$ = Swanson apex, percent/psia

C = Bentsen and Anli empirical parameter

F = formation factor (Archie "definition"), dimensionless

F_g = pore geometrical factor (Thomeer "definition"), dimensionless

F_p = lithology factor (Purcell "definition"), dimensionless

k = absolute permeability, md

k_a = air permeability, md

k_o = pore shape factor (Wyllie and Spangler "definition"), dimensionless

l_c = characteristic length (Katz and Thompson "definition"), μm

l_h = hydraulic conductivity length scale (Katz and Thompson "definition"), μm

l_e = electrical conductivity length scale (Katz and Thompson "definition"), μm

p_c = capillary pressure, psia

p_d = displacement pressure, psia

p_o = pressure in oil phase, psia

p_w = pressure in water phase, psia

n = number of entrances/exits in a pore (Nakornthap and Evans "definition"), dimensionless

r = pore-throat radius, μm

S_b = percent bulk volume occupied by mercury at a given capillary pressure, percent

$S_{b\infty}$ = percent bulk volume occupied by mercury at infinite capillary pressure, percent

S_w = wetting phase saturation, fraction

S_w^* = $(S_w-S_{wi})/(1-S_{wi})$, effective wetting phase saturation, fraction

S_{wi} = irreducible wetting phase saturation, fraction

Greek Variables

α = empirical parameter (Huet "definition"), dimensionless

β = pore throat impedance factor (Nakornthap and Evans "definition"), dimensionless

ϕ = porosity, fraction

λ = pore-size distribution index (Brooks-Corey "definition"), dimensionless

θ, θ_c = contact angle, degree

σ = interfacial tension, dynes/cm

σ_{ow} = interfacial tension between oil and water, dynes/cm

σ_{os} = interfacial tension between oil and solid, dynes/cm

σ_{ws} = interfacial tension between water and solid, dynes/cm

τ = tortuosity, dimensionless

ω = shape factor (Wu "definition"), dimensionless

REFERENCES

Agbalaka, C. C., Dandekar, A. Y., Patil, S. L. et al. 2008. The Effect of Wettability on Oil Recovery: A Review. Presented at the SPE Asia Pacific Oil and Gas Conference and Exhibition, Perth, Australia, 20-22 October. SPE-114496-MS. http://dx.doi.org/10.2118/114496-MS.

Aguilera, R. 2002. Incorporating Capillary Pressure, Pore Throat Aperture Radii, Height above Free-Water Table, and Winland R35 Values on Pickett Plots. *AAPG bulletin* **86** (4): 605-624.

Aguilera, R. 2004. Integration of Geology, Petrophysics, and Reservoir Engineering for Characterization of Carbonate Reservoirs through Pickett Plots. *AAPG bulletin* **88** (4): 433-446.

Ali, L. 1995. Personal Communication with T. Blasingame.

Amyx, J. W., Bass, D. M., Whiting, R. L. 1960. *Petroleum Reservoir Engineering: Physical Properties*. New York: McGraw-Hill.

Anderson, W. G. 1986a. Wettability Literature Survey- Part 1: Rock/Oil/Brine Interactions and the Effects of Core Handling on Wettability. *Journal of Petroleum Technology* **38** (10): 1125-1144. SPE-13932-PA. http://dx.doi.org/10.2118/13932-PA.

Anderson, W. G. 1986b. Wettability Literature Survey- Part 2: Wettability Measurement. *Journal of Petroleum Technology* **38** (11): 1,246 - 1,262. SPE-13933-PA. http://dx.doi.org/10.2118/13933-PA.

Anderson, W. G. 1987. Wettability Literature Survey- Part 4: Effects of Wettability on Capillary Pressure. *Journal of Petroleum Technology* **39** (10): 1,283 - 1,300. SPE-15271-PA. http://dx.doi.org/10.2118/15271-PA.

Archie, G. E. 1942. The Electrical Resistivity Log as an Aid in Determining Some Reservoir Characteristics. *Transactions of the AIME* **146** (01): 54-62.

Bentsen, R. G., Anli, J. 1976. A New Displacement Capillary Pressure Model. *Journal of Canadian Petroleum Technology* **15** (03). PETSOC-76-03-10. http://dx.doi.org/10.2118/76-03-10.

Blasingame, T. A. 2014. Petrophysics Lecture 4 – Capillary Pressure. In *Petroleum Engineering 620 Course Notes*. Texas A&M University.

Bolger, G. 1993. The Use of Small Rock Samples to Determine Reservoir Parameters and Seal Capacity. *Bulletin Houston Geological Society*: 56-57.

Brooks, R. H., Corey, A. T. 1964. Hydraulic Properties of Porous Media and Their Relation to Drainage Design. *Transactions of the ASAE* **7** (1): 0026-0028.

Burdine, N. 1953. Relative Permeability Calculations from Pore Size Distribution Data. *Journal of Petroleum Technology* **5** (03): 71-78. SPE-225-G. http://dx.doi.org/10.2118/225-G.

Burdine, N. T., Gournay, L. S., Reichertz, P. P. 1950. Pore Size Distribution of Petroleum Reservoir Rocks. *Journal of Petroleum Technology* **2** (07): 195 - 204. SPE-950195-G. http://dx.doi.org/10.2118/950195-G.

Byrnes, A., Cluff, R., Webb, J. 2009. *Analysis of Critical Permeability, Capillary Pressure, and Electrical Properties for Mesaverde Tight Gas Sandstones from Western Us Basins: Final Report Submitted by Kansas Geological Survey for United States Department of Energy (Doe) Contract De-Fc26-05nt42660*, Technical Report: pdf document and spreadsheets downloaded February 2013 from website: http://www.kgs.ku.edu/mesaverde.

Comisky, J. T., Newsham, K., Rushing, J. A. et al. 2007. A Comparative Study of Capillary-Pressure-Based Empirical Models for Estimating Absolute Permeability in Tight Gas Sands. Presented at the SPE Annual Technical Conference and Exhibition, Anaheim, California, U.S.A., 11-14 November. SPE-110050-MS. http://dx.doi.org/10.2118/110050-MS.

Comisky, J. T., Santiago, M., McCollom, B. et al. 2011. Sample Size Effects on the Application of Mercury Injection Capillary Pressure for Determining the Storage Capacity of Tight Gas and Oil Shales. Presented at the Canadian Unconventional Resources Conference, Calgary, Alberta, Canada, 15-17 November. http://dx.doi.org/10.2118/149432-MS.

Dake, L. P. 1983. *Fundamentals of Reservoir Engineering*. Amsterdam: Elsevier Science.

Darcy, H. 1856. *Les Fontaines Publiques De La Ville De Dijon*. Dalmont, Paris.

Agbalaka, C. C., Dandekar, A. Y., Patil, S. L. et al. 2008. The Effect of Wettability on Oil Recovery: A Review. Presented at the SPE Asia Pacific Oil and Gas Conference and Exhibition, Perth, Australia, 20-22 October. SPE-114496-MS. http://dx.doi.org/10.2118/114496-MS.

Aguilera, R. 2002. Incorporating Capillary Pressure, Pore Throat Aperture Radii, Height above Free-Water Table, and Winland R35 Values on Pickett Plots. *AAPG bulletin* **86** (4): 605-624.

Aguilera, R. 2004. Integration of Geology, Petrophysics, and Reservoir Engineering for Characterization of Carbonate Reservoirs through Pickett Plots. *AAPG bulletin* **88** (4): 433-446.

Ali, L. 1995. Personal Communication with T. Blasingame.

Amyx, J. W., Bass, D. M., Whiting, R. L. 1960. *Petroleum Reservoir Engineering: Physical Properties*. New York: McGraw-Hill.

Anderson, W. G. 1986a. Wettability Literature Survey- Part 1: Rock/Oil/Brine Interactions and the Effects of Core Handling on Wettability. *Journal of Petroleum Technology* **38** (10): 1125-1144. SPE-13932-PA. http://dx.doi.org/10.2118/13932-PA.

Anderson, W. G. 1986b. Wettability Literature Survey- Part 2: Wettability Measurement. *Journal of Petroleum Technology* **38** (11): 1,246 - 1,262. SPE-13933-PA. http://dx.doi.org/10.2118/13933-PA.

Anderson, W. G. 1987. Wettability Literature Survey- Part 4: Effects of Wettability on Capillary Pressure. *Journal of Petroleum Technology* **39** (10): 1,283 - 1,300. SPE-15271-PA. http://dx.doi.org/10.2118/15271-PA.

Archie, G. E. 1942. The Electrical Resistivity Log as an Aid in Determining Some Reservoir Characteristics. *Transactions of the AIME* **146** (01): 54-62.

Bentsen, R. G., Anli, J. 1976. A New Displacement Capillary Pressure Model. *Journal of Canadian Petroleum Technology* **15** (03). PETSOC-76-03-10. http://dx.doi.org/10.2118/76-03-10.

Blasingame, T. A. 2014. Petrophysics Lecture 4 – Capillary Pressure. In *Petroleum Engineering 620 Course Notes*. Texas A&M University.

Bolger, G. 1993. The Use of Small Rock Samples to Determine Reservoir Parameters and Seal Capacity. *Bulletin Houston Geological Society*: 56-57.

Brooks, R. H., Corey, A. T. 1964. Hydraulic Properties of Porous Media and Their Relation to Drainage Design. *Transactions of the ASAE* **7** (1): 0026-0028.

Burdine, N. 1953. Relative Permeability Calculations from Pore Size Distribution Data. *Journal of Petroleum Technology* **5** (03): 71-78. SPE-225-G. http://dx.doi.org/10.2118/225-G.

Burdine, N. T., Gournay, L. S., Reichertz, P. P. 1950. Pore Size Distribution of Petroleum Reservoir Rocks. *Journal of Petroleum Technology* **2** (07): 195 - 204. SPE-950195-G. http://dx.doi.org/10.2118/950195-G.

Byrnes, A., Cluff, R., Webb, J. 2009. *Analysis of Critical Permeability, Capillary Pressure, and Electrical Properties for Mesaverde Tight Gas Sandstones from Western Us Basins: Final Report Submitted by Kansas Geological Survey for United States Department of Energy (Doe) Contract De-Fc26-05nt42660*, Technical Report: pdf document and spreadsheets downloaded February 2013 from website: http://www.kgs.ku.edu/mesaverde.

Comisky, J. T., Newsham, K., Rushing, J. A. et al. 2007. A Comparative Study of Capillary-Pressure-Based Empirical Models for Estimating Absolute Permeability in Tight Gas Sands. Presented at the SPE Annual Technical Conference and Exhibition, Anaheim, California, U.S.A., 11-14 November. SPE-110050-MS. http://dx.doi.org/10.2118/110050-MS.

Comisky, J. T., Santiago, M., McCollom, B. et al. 2011. Sample Size Effects on the Application of Mercury Injection Capillary Pressure for Determining the Storage Capacity of Tight Gas and Oil Shales. Presented at the Canadian Unconventional Resources Conference, Calgary, Alberta, Canada, 15-17 November. http://dx.doi.org/10.2118/149432-MS.

Dake, L. P. 1983. *Fundamentals of Reservoir Engineering*. Amsterdam: Elsevier Science.

Darcy, H. 1856. *Les Fontaines Publiques De La Ville De Dijon*. Dalmont, Paris.

Dastidar, R., Sondergeld, C. H., Rai, C. S. 2007. An Improved Empirical Permeability Estimator from Mercury Injection for Tight Clastic Rocks. *Petrophysics* **48** (03).

Denney, D. 2008. Capillary Pressure Measurement on Cores by Mri. *Journal of Petroleum Technology* **60** (08): 63 - 66. SPE-0808-0063-JPT. http://dx.doi.org/10.2118/0808-0063-JPT.

Dernaika, M., Wilson, O. B., Skjæveland, S. M. et al. 2010. Drainage Capillary Pressure and Resistivity Index from Short-Wait Porous Plate Experiments. *GeoArabia, Journal of the Middle East Petroleum Geosciences* **16** (02).

Dicker, A., Smits, R. 1988. A Practical Approach for Determining Permeability from Laboratory Pressure-Pulse Decay Measurements. Presented at the International Meeting on Petroleum Engineering, Tianjin, China, 1-4 November. SPE-17578-MS.

Drake, L., Ritter, H. 1945. Macropore-Size Distributions in Some Typical Porous Substances. *Industrial & Engineering Chemistry Analytical Edition* **17** (12): 787-791.

El-Khatib, N. 1995. Development of a Modified Capillary Pressure J-Function. Presented at the Middle East Oil Show, Bahrain, 11-14 March. SPE-29890-MS. http://dx.doi.org/10.2118/29890-MS.

Fleury, M., Doevle, M., Longeron, D. 1997. Full Imbibition Capillary Pressure Measurements on Preserved Samples Using the Micropore Membrane Technique. Presented at the the International Symposium of the Society of Core Analysts, Calgary, AB, Canada, 7 September.

Giesche, H. 2006. Mercury Porosimetry: A General (Practical) Overview. *Particle & particle systems characterization* **23** (1): 9-19.

Gunter, G., Spain, D., Viro, E. et al. 2014. Winland Pore Throat Prediction Method-a Proper Retrospect: New Examples from Carbonates and Complex Systems. Presented at the SPWLA 55th Annual Logging Symposium, Abu Dhabi, United Arab Emirates, 18-22 May. SPWLA-2014-KKK.

Guo, B., Ghalambor, A., Duan, S. 2004. Correlation between Sandstone Permeability and Capillary Pressure Curves. *Journal of Petroleum Science and Engineering* **43** (3): 239-246.

Harris, R. G., Goldsmith, P. J. 2001. Water Saturation Analysis and Interpretation of a Tilted Free-Water Level in the Joanne/Judy Chalk Field, U.K. North Sea. Presented at the SPWLA 42nd Annual Logging Symposium, Houston, Texas, 17-20 June.

Hassler, G. L., Brunner, E. 1945. Measurement of Capillary Pressures in Small Core Samples. *Transactions of the AIME* **160** (01): 114 - 123. SPE-945114-G. http://dx.doi.org/10.2118/945114-G.

Honarpour, M. M., Djabbarah, N. F., Kralik, J. G. 2004. Expert-Based Methodology for Primary Drainage Capillary Pressure Measurements and Modeling. Presented at the Abu Dhabi International Conference and Exhibition, Abu Dhabi, United Arab Emirates, 10-13 October. http://dx.doi.org/10.2118/88709-MS.

Huet, C. C. 2005. *Semi-Analytical Estimates of Permeability Obtained from Capillary Pressure*. MS thesis, Texas A&M University, College Station, Texas (December 2005).

Jaya, I., Sudaryanto, A., Widarsono, B. 2005. Permeability Prediction Using Pore Throat and Rock Fabric: A Model from Indonesian Reservoirs. Presented at the SPE Asia Pacific Oil and Gas Conference and Exhibition, Jakarta, Indonesia, 5-7 April. SPE-93363-MS. http://dx.doi.org/10.2118/93363-MS.

Kamath, J. 1992. Evaluation of Accuracy of Estimating Air Permeability from Mercury-Injection Data. *SPE Formation evaluation* **7** (04): 304-310.

Katz, A., Thompson, A. 1986. Quantitative Prediction of Permeability in Porous Rock. *Physical review B* **34** (11): 8179.

Katz, A., Thompson, A. 1987. Prediction of Rock Electrical Conductivity from Mercury Injection Measurements. *Journal of Geophysical Research: Solid Earth* **92** (B1): 599-607.

Keelan, D.K. and Marschall, D.M. 1979 : *The Fundamentals of Core Analysis*, Core Laboratories, Inc., Dallas.

Kewen, L. 2004. Theoretical Development of the Brooks-Corey Capillary Pressure Model from Fractal Modeling of Porous Media. Presented at the SPE/DOE Symposium on Improved Oil Recovery, Tulsa, Oklahoma, 17-21 April. http://dx.doi.org/10.2118/89429-MS.

Kleinberg, R. L., Ferreira, F. D. C., Boyd, A. et al. 2015. Method for Estimating Irreducible Water Saturation from Mercury Injection Capillary Pressure. U.S. Patent No. 14/595,904.

Kolodzie Jr, S. 1980. Analysis of Pore Throat Size and Use of the Waxman-Smits Equation to Determine Ooip in Spindle Field, Colorado. Presented at the SPE Annual Technical Conference and Exhibition, Dallas, Texas, 21-24 September. SPE-9382-MS. http://dx.doi.org/10.2118/9382-MS.

Kwon, B., Pickett, G. 1975. A New Pore Structure Model and Pore Structure Interrelationships. Presented at the SPWLA 16th Annual Logging Symposium, New Orleans, Louisiana, 4-7 June. SPWLA-1975-P.

León y León, C. A. 1998. New Perspectives in Mercury Porosimetry. *Advances in Colloid and Interface Science* **76–77**: 341-372. http://dx.doi.org/10.1016/S0001-8686(98)00052-9.

Leverett, M. C. 1941. Capillary Behavior in Porous Solids. *Transactions of the AIME* **142** (01): 152 - 169. SPE-941152-G. http://dx.doi.org/10.2118/941152-G.

Lyons, W. C., Plisga, G. J. 2011. *Standard Handbook of Petroleum and Natural Gas Engineering*, second edition. Burlington, MA: Gulf Professional Publishing.

Ma, S., Jiang, M.-X., Morrow, N. 1991. Correlation of Capillary Pressure Relationships and Calculations of Permeability. Presented at the SPE Annual Technical Conference and Exhibition, Dallas, Texas, 6-9 October. SPE-22685-MS. http://dx.doi.org/10.2118/22685-MS.

Nakornthap, K., Evans, R. D. 1986. Temperature-Dependent Relative Permeability and Its Effect on Oil Displacement by Thermal Methods. *SPE Reservoir Engineering* **1** (03): 230 - 242. SPE-11217-PA. http://dx.doi.org/10.2118/11217-PA.

Newsham, K., Rushing, J., Lasswell, P. 2003. Use of Vapor Desorption Data to Characterize High Capillary Pressures in a Basin-Centered Gas Accumulation with Ultra-Low Connate Water Saturations. Presented at the SPE Annual Technical Conference and Exhibition, Denver, Colorado, 5-8 October. SPE-84596-MS. http://dx.doi.org/10.2118/84596-MS.

Newsham, K. E., Rushing, J. A., Lasswell, P. M. et al. 2004. A Comparative Study of Laboratory Techniques for Measuring Capillary Pressures in Tight Gas Sands. Presented at the SPE Annual Technical Conference and Exhibition, Houston, Texas, 26-29 September. SPE-89866-MS. http://dx.doi.org/10.2118/89866-MS.

Nguyen, T. V., Lin, G., Ohn, H. et al. 2008. Measurement of Capillary Pressure Property of Gas Diffusion Media Used in Proton Exchange Membrane Fuel Cells. *Electrochemical and Solid-State Letters* **11** (8): B127-B131. http://dx.doi.org/10.1149/1.2929063.

Nooruddin, H. A., Anifowose, F., Abdulraheem, A. 2013. Applying Artificial Intelligence Techniques to Develop Permeability Predictive Models Using Mercury Injection Capillary-Pressure Data. Presented at the SPE Saudi Arabia Section Technical Symposium and Exhibition, Al-Khobar, Saudi Arabia, 19-22 May. SPE-168109-MS. http://dx.doi.org/10.2118/168109-MS.

Nooruddin, H. A., Hossain, M. E., Al-Yousef, H. et al. 2014. Comparison of Permeability Models Using Mercury Injection Capillary Pressure Data on Carbonate Rock Samples. *Journal of Petroleum Science and Engineering* **121**: 9-22.

PetroWiki. 2016. *Measurement of Capillary Pressure and Relative Permeability*. http://petrowiki.org/index.php?title=Measurement_of_capillary_pressure_and_relative_permeability&oldid=51664 (accessed 1 February 2016).

Pittman, E. D. 1992. Relationship of Porosity and Permeability to Various Parameters Derived from Mercury Injection-Capillary Pressure Curves for Sandstone (1). *AAPG bulletin* **76** (2): 191-198.

Pujado, P. R., Huh, C., Scriven, L. E. 1972. On the Attribution of an Equation of Capillarity to Young and Laplace. *Journal of Colloid and Interface Science* **38** (3): 662-663. http://dx.doi.org/10.1016/0021-9797(72)90410-9.

Purcell, W. 1949. Capillary Pressures-Their Measurement Using Mercury and the Calculation of Permeability Therefrom. *Journal of Petroleum Technology* **1** (02): 39-48. SPE-949039-G. http://dx.doi.org/10.2118/949039-G.

R: A Language and Environment for Statistical Computing, version 3.2.3. 2015. Vienna, Austria: R Foundation for Statistical Computing. https://www.R-project.org/.

Reitsma, S., Kueper, B. H. 1994. Laboratory Measurement of Capillary Pressure-Saturation Relationships in a Rock Fracture. *Water Resources Research* **30** (4): 865-878.

Rezaee, M., Jafari, A., Kazemzadeh, E. 2006. Relationships between Permeability, Porosity and Pore Throat Size in Carbonate Rocks Using Regression Analysis and Neural Networks. *Journal of Geophysics and Engineering* **3** (4): 370.

Rezaee, R., Saeedi, A., Clennell, B. 2012. Tight Gas Sands Permeability Estimation from Mercury Injection Capillary Pressure and Nuclear Magnetic Resonance Data. *Journal of Petroleum Science and Engineering* **88**: 92-99.

Richard, F. S. 2009. A Methodology for Blank and Conformance Corrections for High Pressure Mercury Porosimetry. *Measurement Science and Technology* **20** (4).

Ruth, D., Lindsay, C., Allen, M. 2013. Combining Electrical Measurements and Mercury Porosimetry to Predict Permeability. *Petrophysics* **54** (06): 531-537.

Saito, H. 1963. Capillary Pressure Measurement of Porous Medium by Vapor Pressure Method. Presented at the 6th World Petroleum Congress, Frankfurt am Main, Germany, 19-26 June.

Salimifard, B., Ruth, D. W., Green, D. et al. 2014. Developing a Model to Estimate Permeability from Other Petrophysical Data. Presented at the International Symposium of the Society of Core Analysts, Avignon, France, 8-11 September. SCA2014-063.

Schlueter, E. M., Witherspoon, P. A. 1995. Note on the Validity of the Kozeny-Carman Formulas for Consolidated Porous Media. Presented at the SEG Annual Meeting, Houston, Texas, 8-13 October.

Shafer, J., Lasswell, P. 2007. Modeling Porous Plate Capillary Pressure Production Data: Shortening Test Duration and Quality Controlling Data. Presented at the 48th Annual Logging Symposium, Austin, Texas, 3-6 June.

Shafer, J., Neasham, J. 2000. Mercury Porosimetry Protocol for Rapid Determination of Petrophysical and Reservoir Quality Properties. *Society of Core Analysis, SCA* **21**: 2001.

Smith, W. O. 1933. The Final Distribution of Retained Liquid in an Ideal Uniform Soil. *Journal of Applied Physics* **4** (12): 425-438. doi:http://dx.doi.org/10.1063/1.1745156.

Swanson, B. F. 1981. A Simple Correlation between Permeabilities and Mercury Capillary Pressures. *Journal of Petroleum Technology* **33** (12): 2,498-2,504. SPE-8234-PA. http://dx.doi.org/10.2118/8234-PA.

Thomas, L., Katz, D., Tek, M. 1968. Threshold Pressure Phenomena in Porous Media. *Society of Petroleum Engineers Journal* **8** (02): 174-184. SPE-1816-PA. http://dx.doi.org/10.2118/1816-PA.

Thomeer, J. 1983. Air Permeability as a Function of Three Pore-Network Parameters. *Journal of Petroleum Technology* **35** (04): 809-814. SPE-10922-PA. http://dx.doi.org/10.2118/10922-PA.

Thomeer, J. H. M. 1960. Introduction of a Pore Geometrical Factor Defined by the Capillary Pressure Curve. *Journal of Petroleum Technology* **12** (03): 73 - 77. SPE-1324-G. http://dx.doi.org/10.2118/1324-G.

Vogel, H.-J., Tölke, J., Schulz, V. P. et al. 2005. Comparison of a Lattice-Boltzmann Model, a Full-Morphology Model, and a Pore Network Model for Determining Capillary Pressure–Saturation Relationships. *Vadose Zone Journal* **4** (2). http://dx.doi.org/10.2136/vzj2004.0114.

Washburn, E. W. 1921. Note on a Method of Determining the Distribution of Pore Sizes in a Porous Material. *Proceedings of the National Academy of Sciences of the United States of America* **7** (4): 115-116.

Wells, J., Amaefule, J. 1985. Capillary Pressure and Permeability Relationships in Tight Gas Sands. Presented at the SPE/DOE Low Permeability Gas Reservoirs Symposium, Denver, Colorado, 19-22 March. SPE-13879-MS. http://dx.doi.org/10.2118/13879-MS.

Wilson, O., Skjæveland, S. 2002. Porous Plate Influence on Effective Imbibition Rates in Capillary Pressure Experiments. Presented at the International Symposium of the Society of Core Analysts, Monterey, CA, USA,

Wu, T. 2004. *Permeability Prediction and Drainage Capillary Pressure Simulation in Sandstone Reservoirs*. Doctoral dissertation, Texas A&M University, College Station, Texas (December 2004).

Wyllie, M., Gardner, G. 1958. The Generalized Kozeny-Carman Equation. *World oil* **146** (4): 121-128.

Wyllie, M., Spangler, M. 1952. Application of Electrical Resistivity Measurements to Problem of Fluid Flow in Porous Media. *AAPG Bulletin* **36** (2): 359-403.

Xiao, L., Liu, X.-P., Zou, C.-C. et al. 2014. Comparative Study of Models for Predicting Permeability from Nuclear Magnetic Resonance (Nmr) Logs in Two Chinese Tight Sandstone Reservoirs. *Acta Geophysica* **62** (1): 116-141.

Xu, C. 2013. *Reservoir Description with Well-Log-Based and Core-Calibrated Petrophysical Rock Classification*. Doctorial dissertation, University of Texas at Austin (August 2013).

Xu, C., Torres-Verdín, C. 2013. Pore System Characterization and Petrophysical Rock Classification Using a Bimodal Gaussian Density Function. *Mathematical Geosciences* **45** (6): 753-771.

Young, T. 1805. An Essay on the Cohesion of Fluids. *Philosophical Transactions of the Royal Society of London* **95**: 65-87. http://dx.doi.org/10.1098/rstl.1805.0005.

APPENDIX A

DERIVATION OF THE THOMEER-SWANSON APEX TERM

Introduction

In 1981, Swanson (1981) suggested that the "apex" of the Thomeer hyperbolic model is uniquely correlated with parameters such as permeability, and specifically, Swanson defined the apex as $[S_b/p_c]_A$, which is the point where the value $[S_b/p_c]$ is maximum. In this appendix, we showed that the apex of the Thomeer hyperbolic model is the point where the value $[S_b/p_c]$ is maximum.

Derivation of the Thomeer-Swanson Apex Term

From Thomeer (1960), the basic "hyperbolic" relationship for capillary pressure:

$$\frac{S_b}{S_{b\infty}} = \exp\left[\frac{-F_g}{\ln\left[\frac{p_c}{p_d}\right]}\right] \quad \text{.....(A-1)}$$

Taking the logarithm of Eq. A-1

$$\ln\left[\frac{S_b}{S_{b\infty}}\right] = \frac{-F_g}{\ln\left[\frac{p_c}{p_d}\right]}$$

Rearranging, we have

$$\ln\left[\frac{S_b}{S_{b\infty}}\right] = \frac{-F_g}{\ln\left[\frac{p_c}{p_d}\right]}$$

$$\ln\left[\frac{p_c}{p_d}\right] = \frac{-F_g}{\ln\left[\frac{S_b}{S_{b\infty}}\right]}$$

$$\ln(p_c) - \ln(p_d) = \frac{-F_g}{\ln(S_b) - \ln(S_{b\infty})}$$

$$\ln(p_c) = \ln(p_d) - \frac{F_g}{\ln(S_b) - \ln(S_{b\infty})}$$

.....(A-2)

The apex of $\ln(p_c)$ as a hyperbolic function of $\ln(S_b)$ in Eq. A-2 is where the slope of $\ln(p_c)$ with respect to $\ln(S_b)$ is equal to 1. The required derivative function is defined as:

$$\frac{d\ln(p_c)}{d\ln(S_b)} = \frac{d}{d\ln(S_b)}\left[\ln(p_d) - \frac{F_g}{\ln(S_b) - \ln(S_{b\infty})}\right]$$

$$= -F_g \frac{d}{d\ln(S_b)}\left[\frac{1}{\ln(S_b) - \ln(S_{b\infty})}\right]$$

$$= \frac{F_g}{[\ln(S_b) - \ln(S_{b\infty})]^2} \frac{d}{d\ln(S_b)}[\ln(S_b) - \ln(S_{b\infty})]$$

$$= \frac{F_g}{[\ln(S_b) - \ln(S_{b\infty})]^2}$$

.....(A-3)

Setting Eq. A-3 to unity (1), we have:

$$\frac{d\ln(p_c)}{d\ln(S_b)} = 1$$

$$= \frac{F_g}{[\ln(S_b)_A - \ln(S_{b\infty})]^2}$$

Rearranging:

$$[\ln[(S_b)_A] - \ln(S_{b\infty})]^2 = F_g$$

Solving for $\ln[(S_b)_A]$, we obtain:

$$\ln[(S_b)_A] = \sqrt{F_g} + \ln(S_{b\infty})$$

Exponentiating for $(S_b)_A$, we obtain our desired result:

$$(S_b)_A = \exp[\sqrt{F_g} + \ln(S_{b\infty})]$$ .....(A-4)

Exponentiating the relation given by Eq. A-2, yields:

$$p_c = \exp\left[\ln(p_d) - \frac{F_g}{\ln(S_b) - \ln(S_{b\infty})}\right]$$ .....(A-5)

Dividing the function S_b by Eq. A-5, we obtain

$$\frac{S_b}{p_c} = \frac{S_b}{\exp\left[\ln(p_d) - \frac{F_g}{\ln(S_b) - \ln(S_{b\infty})}\right]}$$ .....(A-6)

The objective is to estimate the location (*i.e.*, the S_b-value) where the $[S_b/p_c]$ function is at a maximum. As such, we first take the derivative of Eq. A-6 with respect to S_b.

$$\frac{d}{dS_b}\left[\frac{S_b}{p_c}\right] = \frac{d}{dS_b}\left[\frac{S_b}{\exp\left[\ln(p_d) - \frac{F_g}{\ln(S_b)-\ln(S_{b\infty})}\right]}\right]$$

$$= S_b \frac{d}{dS_b}\left[\frac{1}{\exp\left[\ln(p_d) - \frac{F_g}{\ln(S_b)-\ln(S_{b\infty})}\right]}\right] + \left[\frac{1}{\exp\left[\ln(p_d) - \frac{F_g}{\ln(S_b)-\ln(S_{b\infty})}\right]}\right]\frac{d}{dS_b}(S_b)$$

$$= S_b \frac{-1}{\left[\exp\left[\ln(p_d) - \frac{F_g}{\ln(S_b)-\ln(S_{b\infty})}\right]\right]^2}\frac{d}{dS_b}\exp\left[\ln(p_d) - \frac{F_g}{\ln(S_b)-\ln(S_{b\infty})}\right] + \left[\frac{1}{\exp\left[\ln(p_d) - \frac{F_g}{\ln(S_b)-\ln(S_{b\infty})}\right]}\right]$$

$$= S_b \frac{-\exp\left[\ln(p_d) - \frac{F_g}{\ln(S_b)-\ln(S_{b\infty})}\right]}{\left[\exp\left[\ln(p_d) - \frac{F_g}{\ln(S_b)-\ln(S_{b\infty})}\right]\right]^2}\frac{d}{dS_b}\left[\ln(p_d) - \frac{F_g}{\ln(S_b)-\ln(S_{b\infty})}\right] + \left[\frac{1}{\exp\left[\ln(p_d) - \frac{F_g}{\ln(S_b)-\ln(S_{b\infty})}\right]}\right]$$

$$= S_b \frac{-1}{\exp\left[\ln(p_d) - \frac{F_g}{\ln(S_b)-\ln(S_{b\infty})}\right]}(-F_g)\frac{d}{dS_b}\left[\frac{1}{[\ln(S_b)-\ln(S_{b\infty})]}\right] + \left[\frac{1}{\exp\left[\ln(p_d) - \frac{F_g}{\ln(S_b)-\ln(S_{b\infty})}\right]}\right]$$

$$= S_b \frac{F_g}{\exp\left[\ln(p_d) - \frac{F_g}{\ln(S_b)-\ln(S_{b\infty})}\right]}\frac{-1}{[\ln(S_b)-\ln(S_{b\infty})]^2}\frac{d}{dS_b}[\ln(S_b)-\ln(S_{b\infty})] + \left[\frac{1}{\exp\left[\ln(p_d) - \frac{F_g}{\ln(S_b)-\ln(S_{b\infty})}\right]}\right]$$

$$= S_b \frac{F_g}{\exp\left[\ln(p_d) - \frac{F_g}{\ln(S_b)-\ln(S_{b\infty})}\right]}\frac{-1}{[\ln(S_b)-\ln(S_{b\infty})]^2}\frac{1}{S_b} + \left[\frac{1}{\exp\left[\ln(p_d) - \frac{F_g}{\ln(S_b)-\ln(S_{b\infty})}\right]}\right]$$

$$= \frac{1}{\exp\left[\ln(p_d) - \frac{F_g}{\ln(S_b)-\ln(S_{b\infty})}\right]}\left[\frac{-F_g}{[\ln(S_b)-\ln(S_{b\infty})]^2} + 1\right]$$

.....(A-7)

Setting Eq. A-7 to zero yields the value of S_b where (S_b/p_c) is a maximum.

$$\frac{d}{dS_b}\left[\frac{S_b}{p_c}\right] = 0$$

$$= \frac{1}{\exp\left[\ln(p_d) - \dfrac{F_g}{\ln(S_b)_{\text{Max}} - \ln(S_{b\infty})}\right]}\left[\frac{-F_g}{[\ln(S_b)_{\text{Max}} - \ln(S_{b\infty})]^2} + 1\right]$$

$$= \frac{-F_g}{[\ln(S_b)_{\text{Max}} - \ln(S_{b\infty})]^2} + 1$$

Which yields the following identity:

$$1 = \frac{F_g}{[\ln(S_b)_{\text{Max}} - \ln(S_{b\infty})]^2}$$

Rearranging and solving for the "maximum" point (*i.e.*, $\ln(S_b)_{\text{Max}}$), we have:

$$[\ln(S_b)_{\text{Max}} - \ln(S_{b\infty})]^2 = F_g$$

$$\ln(S_b)_{\text{Max}} - \ln(S_{b\infty}) = \sqrt{F_g}$$

$$\ln(S_b)_{\text{Max}} = \sqrt{F_g} + \ln(S_{b\infty})$$

Exponentiating the $\ln(S_b)_{\text{Max}}$ formulation yields the "maximum" point:

$$(S_b)_{\text{Max}} = \exp[\sqrt{F_g} + \ln(S_{b\infty})] \quad \text{.....(A-8)}$$

Where we noted that $(S_b)_{\text{Max}} = S_b$ where (S_b/p_c) is at its maximum.

Recalling Eq. A-4 — *i.e.*, the expression for $(S_b)_A$:

$$(S_b)_A = \exp[\sqrt{F_g} + \ln(S_{b\infty})] \quad \text{.....(A-4)}$$

Comparing Eqs. A-4 and A-8, we have:

$$(S_b)_A = (S_b)_{\text{Max}} = \exp[\sqrt{F_g} + \ln(S_{b\infty})] \quad \text{.....(A-9)}$$

Equation A-9 proves that the apex of the hyperbolic function of the Thomeer capillary pressure model is the point where the (S_b/p_c) function is maximum.

References

A.1. Swanson, B. F. 1981. A Simple Correlation Between Permeabilities and Mercury Capillary Pressures. Journal of Petroleum Technology 33 (12): 2498-2504. doi:10.2118/8234-PA.

A.2. Thomeer, J.H.M. 1960. Introduction of a Pore Geometrical Factor Defined by the Capillary Pressure Curve. JPT 12(3): 73-77. doi:10.2118/1324-G.

Nomenclature

F_g = Pore geometrical factor (Thomeer "definition"), dimensionless

k = Permeability, md

p_d = Displacement pressure, psia

p_c = Capillary pressure, psia

S_b = Percent bulk volume occupied by mercury at a given capillary pressure, percent

$(S_b)_A$ = Percent bulk volume occupied by mercury at the apex of the Thomeer model, percent

$(S_b)_{Max}$ = Percent bulk volume occupied by mercury at the point where $[S_b/p_c]$ is maximum, percent

$S_{b\infty}$ = Percent bulk volume occupied by mercury at infinite capillary pressure, percent

APPENDIX B

DERIVATION OF THE ANALYTICAL RELATIONSHIP BETWEEN THE MODEL PARAMETERS FOR THE SWANSON AND BROOKS-COREY MODELS

Introduction

In 1964, Brooks and Corey (1964) observed a "power-law" behavior in the capillary pressure versus normalized saturation plot using quite a large suite of experimental data. As such, Brooks and Corey introduced a model to describe capillary pressure as a function of wetting phase saturation. The model consists of three parameters: irreducible wetting phase saturation (S_{wi}), displacement pressure (p_d), and the pore-size distribution index (λ). In 1981, Swanson (1981) suggested that the point where the value $[S_b/p_c]$ is maximum is uniquely correlated with parameters such as permeability, and specifically, Swanson defined the point as $[S_b/p_c]_A$. In this appendix, we derived the relationship between Swanson's parameter $[S_b/p_c]_A$ and the Brooks-Corey model parameters (S_{wi}, p_d, λ).

Derivation of the Relationship between the Swanson Model Parameter and the Brooks-Corey Model Parameters

Recalling the Brooks-Corey capillary pressure-normalized saturation model (Brooks and Corey 1964)

$$
\begin{aligned}
p_c &= p_d (S_w^*)^{-1/\lambda} \\
&= p_d \left[\frac{S_w - S_{wi}}{1 - S_{wi}} \right]^{-1/\lambda} \\
&= p_d \left[\frac{1 - S_{nw} - S_{wi}}{1 - S_{wi}} \right]^{-1/\lambda} \\
&= p_d \left[1 - \frac{S_{nw}}{1 - S_{wi}} \right]^{-1/\lambda}
\end{aligned}
$$

.....(B-1)

Multiplying through Eq. B-1 by $\phi^{-1/\lambda}$ — we have:

$$
\begin{aligned}
p_c \phi^{-1/\lambda} &= p_d \left[\phi - \frac{\phi S_{nw}}{1 - S_{wi}} \right]^{-1/\lambda} \\
&= p_d \left[\phi - \frac{S_b}{1 - S_{wi}} \right]^{-1/\lambda}
\end{aligned}
$$

.....(B-2)

Where, we use the Swanson definitions, given as

S_b = ϕS_{nw} = Non-wetting phase saturation referenced to the BULK volume, percent

ϕ = Porosity, percent.

Solving Eq. B-2 for the reciprocal capillary pressure ($1/p_c$), we obtain:

$$\frac{1}{p_c} = \frac{\phi^{-1/\lambda}}{p_d\left[\phi - \frac{S_b}{1-S_{wi}}\right]^{-1/\lambda}}$$

Multiplying through this result by the non-wetting phase saturation, S_b:

$$\frac{S_b}{p_c} = \frac{\phi^{-1/\lambda}}{p_d\left[\phi - \frac{S_b}{1-S_{wi}}\right]^{-1/\lambda}}\ S_b \quad \text{.....(B-3)}$$

We note that Swanson's "apex" is the point on capillary pressure curve where (S_b/p_c) as a function of S_b is at its maximum. We propose to determine the Swanson apex point by differentiation of Eq. B-3 with respect to S_b and setting that derivative to 0.

Differentiating Eq. B-3 with respect to S_b, we have:

$$\begin{aligned}
\frac{d}{dS_b}\left[\frac{S_b}{p_c}\right] &= \frac{d}{dS_b}\left[\frac{\phi^{-1/\lambda}}{p_d\left[\phi - \frac{S_b}{1-S_{wi}}\right]^{-1/\lambda}} S_b\right] \\
&= \frac{\phi^{-1/\lambda}}{p_d}\frac{d}{dS_b}\left[\left[\phi - \frac{S_b}{1-S_{wi}}\right]^{1/\lambda} S_b\right] \\
&= \frac{\phi^{-1/\lambda}}{p_d}\left[\left[\phi - \frac{S_b}{1-S_{wi}}\right]^{1/\lambda} + S_b\frac{d}{dS_b}\left[\phi - \frac{S_b}{1-S_{wi}}\right]^{1/\lambda}\right] \\
&= \frac{\phi^{-1/\lambda}}{p_d}\left[\left[\phi - \frac{S_b}{1-S_{wi}}\right]^{1/\lambda} + S_b\frac{1}{\lambda}\left[\phi - \frac{S_b}{1-S_{wi}}\right]^{(1/\lambda)-1}\frac{d}{dS_b}\left[\phi - \frac{S_b}{1-S_{wi}}\right]\right] \\
&= \frac{\phi^{-1/\lambda}}{p_d}\left[\left[\phi - \frac{S_b}{1-S_{wi}}\right]^{1/\lambda} - \frac{S_b}{1-S_{wi}}\frac{1}{\lambda}\left[\phi - \frac{S_b}{1-S_{wi}}\right]^{(1/\lambda)-1}\right]
\end{aligned}$$

.....(B-4)

Continuing to reduce Eq. B-4, we obtain:

$$\frac{d}{dS_b}\left[\frac{S_b}{p_c}\right] = \frac{\phi^{-1/\lambda}}{p_d}\left[\left[\phi - \frac{S_b}{1-S_{wi}}\right]^{1/\lambda} - \frac{S_b}{1-S_{wi}}\frac{1}{\lambda}\left[\phi - \frac{S_b}{1-S_{wi}}\right]^{(1/\lambda)-1}\right]$$

$$= \frac{\phi^{-1/\lambda}}{p_d}\left[\phi - \frac{S_b}{1-S_{wi}}\right]^{1/\lambda}\left[1 - \frac{S_b}{1-S_{wi}}\frac{1}{\lambda}\left[\phi - \frac{S_b}{1-S_{wi}}\right]^{-1}\right]$$

$$= \frac{\phi^{-1/\lambda}}{p_d}\left[\phi - \frac{S_b}{1-S_{wi}}\right]^{1/\lambda}\left[\phi - \frac{S_b}{1-S_{wi}}\right]^{-1}\left[\left[\phi - \frac{S_b}{1-S_{wi}}\right] - \left[\frac{S_b}{1-S_{wi}}\frac{1}{\lambda}\right]\right]$$

$$= \frac{\phi^{-1/\lambda}}{p_d}\left[\phi - \frac{S_b}{1-S_{wi}}\right]^{1/\lambda}\left[\phi - \frac{S_b}{1-S_{wi}}\right]^{-1}\left[\phi - \frac{S_b}{1-S_{wi}}\left[1+\frac{1}{\lambda}\right]\right]$$

.....(B-5)

Where Eq. B-5 is the "most reduced" form of the $d/dS_b[S_b/p_c]$ formulation. This form will be set = 0 and solved for the point at which (S_b/p_c) is a maximum, *i.e.*, $(S_b)_A$.

Setting Eq. B-5 to zero as a means to determine the point S_b where (S_b/p_c) is maximum. This gives:

$$\frac{d}{dS_b}\left[\frac{S_b}{p_c}\right] = 0$$

$$= \frac{\phi^{-1/\lambda}}{p_d}\left[\phi - \frac{(S_b)_A}{1-S_{wi}}\right]^{1/\lambda}\left[\phi - \frac{(S_b)_A}{1-S_{wi}}\right]^{-1}\left[\phi - \frac{(S_b)_A}{1-S_{wi}}\left[1+\frac{1}{\lambda}\right]\right]$$

$$= \phi - \frac{(S_b)_A}{1-S_{wi}}\left[1+\frac{1}{\lambda}\right]$$

Solving for the point $(S_b)_A$ yields:

$$(S_b)_A = \phi(1-S_{wi})\frac{1}{\left[1+\frac{1}{\lambda}\right]}$$

$$= \phi(1-S_{wi})\frac{\lambda}{\lambda+1}$$

.....(B-6)

Where Eq. B-6 represents the inter-relation of the Thomeer-Swanson parameter $[(S_b)_A]$ with the Brooks-Corey parameter (λ). Substituting Eq. B-6 into Eq. B-3, we have:

$$\left[\frac{S_b}{p_c}\right]_A = \left[\frac{\phi^{-1/\lambda}}{p_d\left[\phi - \frac{\phi(1-S_{wi})\frac{\lambda}{\lambda+1}}{1-S_{wi}}\right]^{-1/\lambda}}\right]\left[\phi(1-S_{wi})\frac{\lambda}{\lambda+1}\right]$$

$$= \left[\frac{\phi^{-1/\lambda}}{p_d\,\phi^{-1/\lambda}\left[1-\frac{\lambda}{1+\lambda}\right]^{-1/\lambda}}\right]\left[\phi(1-S_{wi})\frac{\lambda}{\lambda+1}\right]$$

$$= \frac{1}{p_d}\left[\frac{\lambda}{(1+\lambda)^{(1+\lambda)/\lambda}}\right](1-S_{wi})\,\phi$$

.....(B-7)

Substituting Eq. B-6 into Eq. B-2 and reducing terms yields:

$$(p_c)_A\,\phi^{-1/\lambda} = p_d\left[\phi - \frac{(S_b)_A}{1-S_{wi}}\right]^{-1/\lambda}$$

$$= p_d\left[\phi - \frac{\phi(1-S_{wi})\frac{\lambda}{\lambda+1}}{1-S_{wi}}\right]^{-1/\lambda}$$

$$= p_d\left[1-\frac{\lambda}{\lambda+1}\right]^{-1/\lambda}\phi^{-1/\lambda}$$

.....(B-8)

Dividing through Eq. B-8 by $\phi^{-1/\lambda}$, we obtain:

$$(p_c)_A = p_d\left[\frac{1}{\lambda+1}\right]^{-1/\lambda} \quad \text{.....(B-9)}$$

Where Eq. B-9 represents the inter-relation of the Thomeer-Swanson parameter [$(p_c)_A$] with the Brooks-Corey parameters (p_d and λ).

References

B.1. Brooks, R.H., Corey, A. T. 1964. Hydraulic Properties of Porous Media 3(3), Colorado State University Hydrology Papers.

B.2. Swanson, B. F. 1981. A Simple Correlation Between Permeabilities and Mercury Capillary Pressures. Journal of Petroleum Technology 33 (12): 2498-2504. doi:10.2118/8234-PA.

B.3. Thomeer, J.H.M. 1960. Introduction of a Pore Geometrical Factor Defined by the Capillary Pressure Curve. JPT 12(3): 73-77. doi:10.2118/1324-G.

Nomenclature

k = Permeability, md

p_d = Displacement pressure, psia

p_c = Capillary pressure, psia

$(p_c)_A$ = Capillary pressure at Swanson's apex, psia

S_b = Percent bulk volume occupied by mercury at a given capillary pressure, percent

$(S_b)_A$ = Percent bulk volume occupied by mercury at Swanson's apex, percent

$S_{b\infty}$ = Percent bulk volume occupied by mercury at infinite capillary pressure, percent

S_{wi} = Irreducible wetting phase saturation, fraction

S_w = Wetting phase saturation, fraction

S_w^* = Non-wetting phase saturation, fraction

S_{nw} = Non-wetting phase saturation, fraction

ϕ = Porosity, percent

λ = Pore-size distribution index (Brooks-Corey "definition"), dimensionless

APPENDIX C

DERIVATION OF THE ANALYTICAL RELATIONSHIP BETWEEN THE PROPOSED SEMI-ANALYTICAL MODEL AND THE SWANSON MODEL

Introduction

In 1981, Swanson proposed an empirical model to predict permeability by the use of parameter $[S_b/p_c]_A$, which is the maximum value of $[S_b/p_c]$. In 2005, Huet (2005) has developed an analytical model based on the work by Purcell, Burdine, Wyllie-and-Gardner and Brooks-and-Corey to calculate for permeability from MICP data. The Huet model suggested a relationship between parameters which led to the proposed semi-analytical model to be correlated with permeabilities. In this Appendix, we show that the Swanson model can be directly related to the semi-analytical model proposed by Huet.

Derivation of the Analytical Relationship between the Huet (semi-analytical) Model and the Swanson Model

Based on Swanson's correlation model and the derived relationship between Swanson's parameter and the Brooks-Corey MICP model parameters (p_d, S_{wi}, and λ) in Appendix B, we have the following results:

$$k = a_1 \left[\frac{S_b}{p_c} \right]_A^{a_2} \quad \text{.....(C-1)}$$

$$\left[\frac{S_b}{p_c} \right]_A = 100 \frac{1}{p_d} \left[\frac{\lambda}{(1+\lambda)^{(1+\frac{1}{\lambda})}} \right] (1 - S_{wi})\, \phi \quad \text{.....(C-2)}$$

Substituting Eq. C-2 into the Swanson correlation model (Eq. C-1) gives:

$$k = a_1 \left[\frac{1}{p_d} \left[\frac{\lambda}{(1+\lambda)^{(1+\frac{1}{\lambda})}} \right] (1 - S_{wi})\, \phi \right]^{a_2}$$

$$k = a_1 \frac{1}{(p_d)^{a_2}} \left[\frac{\lambda}{(1+\lambda)^{(1+\frac{1}{\lambda})}} \right]^{a_2} (1 - S_{wi})^{a_2}\ \phi^{a_2} \quad \text{.....(C-3)}$$

The semi-analytical correlation model provided by Huet is given as:

$$k = a_1 \frac{1}{(p_d)^{a2}} \left[\frac{\lambda}{\lambda + 2} \right]^{a3} (1 - S_{wi})^{a4} \phi^{a5} \quad \text{.....(C-4)}$$

In our statistical work we found that the λ-term proposed in Eq. C-3 is well correlated with the λ-term given in Eq. C-4 over the entire range of λ-values in our data sets. For reference, Swanson's λ-term is given as:

$$\text{Swanson's } \lambda - \text{term} = \frac{\lambda}{(1+\lambda)^{(1+\frac{1}{\lambda})}} \quad \text{.....(C-5)}$$

And the Huet λ-term is given as:

$$\text{Huet's } \lambda - \text{term} = \frac{\lambda}{\lambda + 2} \quad \text{.....(C-6)}$$

In Fig. C-1, the Swanson λ-term is plotted versus the Huet λ-term, and a correlation is imposed

$$\frac{\lambda}{(1+\lambda)^{(1+\frac{1}{\lambda})}} = A \left[\frac{\lambda}{\lambda + 2} \right]^{B} = 0.7871 \left[\frac{\lambda}{\lambda + 2} \right]^{1.0381} \quad \text{.....(C-7)}$$

Substitution of Eq. C-7 into Eq. C-3 yields:

$$k = a_1 \frac{1}{(p_d)^{a2}} \left[A \left[\frac{\lambda}{\lambda + 2} \right]^{B} \right]^{a2} (1 - S_{wi})^{a2} \ \phi^{a2}$$

$$= a_1 (A)^{a2} \frac{1}{(p_d)^{a2}} \left[\frac{\lambda}{\lambda + 2} \right]^{a2 \times B} (1 - S_{wi})^{a2} \ \phi^{a2}$$

.....(C-8)

Where Eq. C-8 can be generalized into <u>exactly the same form</u> as the semi-analytical (Huet) model by simply stating that the coefficients a_1, a_2, … a_5 are independent (*i.e.*, unique and non-repeated), which yields:

$$k = a_1 \frac{1}{(p_d)^{a2}} \left[\frac{\lambda}{\lambda + 2} \right]^{a3} (1 - S_{wi})^{a4} \phi^{a5} \quad \text{.....(C-9)}$$

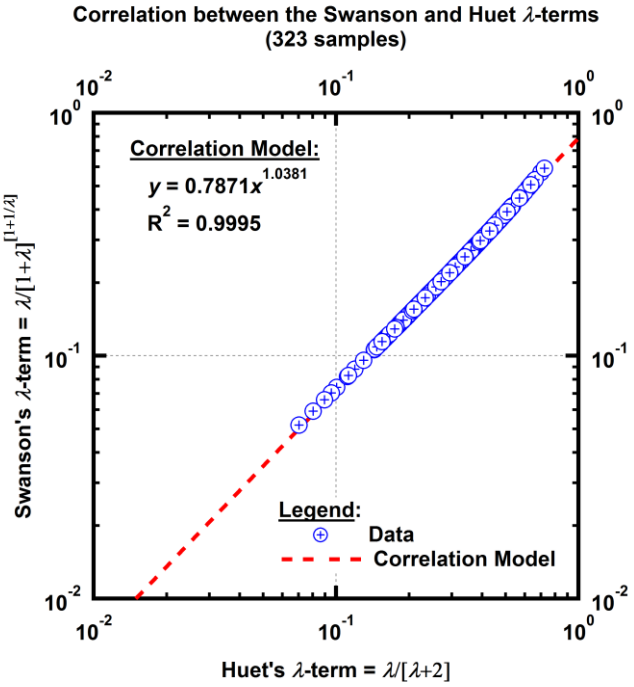

Figure C-1 — Correlation between the Swanson and Huet λ-terms.

References

C.1. Brooks, R.H., Corey, A. T. 1964. Hydraulic Properties of Porous Media 3(3), Colorado State University Hydrology Papers.

C.2. Swanson, B. F. 1981. A Simple Correlation Between Permeabilities and Mercury Capillary Pressures. Journal of Petroleum Technology 33 (12): 2498-2504. doi:10.2118/8234-PA.

C.3. Huet, C. C. 2005. Semi-Analytical Estimates of Permeability Obtained from Capillary Pressure. MS thesis, Texas A&M University, College Station, Texas (December 2005).

Nomenclature

k = Permeability, md

p_d = Displacement pressure, psia

p_c = Capillary pressure, psia

S_b = Percent bulk volume occupied by mercury at a given capillary pressure, percent

S_{wi} = Irreducible wetting phase saturation, fraction

S_w = Wetting phase saturation, fraction

ϕ = Porosity, fraction

λ = Pore-size distribution index (Brooks-Corey "definition"), dimensionless

APPENDIX D

CORRELATION FUNCTION FOR THE BROOKS-COREY PORE-SIZE DISTRIBUTION INDEX

Introduction

The relationship between Brooks-Corey MICP model (Brooks and Corey 1964) parameters displacement pressure (p_d) and the pore-size distribution index (λ), and the Swanson parameter $(S_b/p_c)_A$ was derived in this study as:

$$\left[\frac{S_b}{p_c}\right]_A = 100\frac{1}{p_d}\left[\frac{\lambda}{(1+\lambda)^{(1+\frac{1}{\lambda})}}\right](1-S_{wi})\,\phi \quad \text{.....(D-1)}$$

Where Eq. D-1 can be separated into component forms as:

$$(p_c)_A = p_d\left[\frac{1}{1+\lambda}\right]^{-1/\lambda} \text{ or } y = \frac{(p_c)_A}{p_d} = \left[\frac{1}{1+\lambda}\right]^{-1/\lambda} \quad \text{.....(D-2)}$$

$$(S_b)_A = 100\frac{\lambda}{1+\lambda}(1-S_{wi})\,\phi \quad \text{.....(D-3)}$$

The pore-size distribution index (λ) can be solved using Eq. D-2 as a root solution. Alternatively, the λ-parameter can be calculated using an approximation function which will be derived in this Appendix.

Development of the Correlation Function for the Brooks-Corey Pore-Size Distribution Index

Eq. D-2 is written as a function of λ as:

$$y = \frac{(p_c)_A}{p_d} = \left[\frac{1}{1+\lambda}\right]^{-1/\lambda} \quad \text{.....(D-2)}$$

It can be shown that the y function is a bounded function with maximum value at λ reaching 0 and minimum value at λ reaching infinity. The y-function is plotted in Fig. D-1 and the limits of the function are shown as:

$$y_{\max} = \lim_{\lambda\to 0} y = \lim_{\lambda\to 0}\left[\frac{1}{1+\lambda}\right]^{-1/\lambda} = e \quad \text{.....(D-4)}$$

$$y_{\min} = \lim_{\lambda\to \infty} y = \lim_{\lambda\to \infty}\left[\frac{1}{1+\lambda}\right]^{-1/\lambda} = 1 \quad \text{.....(D-5)}$$

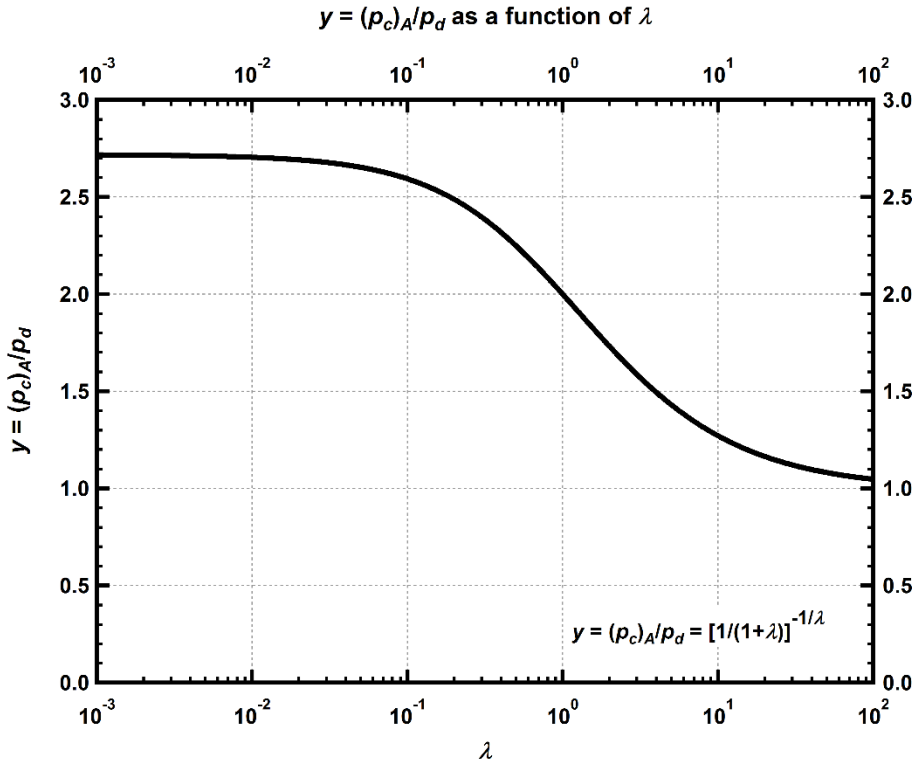

Figure D-1 — Plot of the *y*-function versus the λ-parameter. The *y*-function is bounded with a maximum value of *e* at λ approaching 0, and a minimum value of 1 at λ approaching infinity.

The *y*-function can be written in dimensionless form in terms of the maximum and minimum values as follows:

$$y_D = \frac{y_{\max} - y}{y_{\max} - y_{\min}} = \frac{e - \left[\frac{1}{1+\lambda}\right]^{-1/\lambda}}{e-1} \quad \text{.....(D-6)}$$

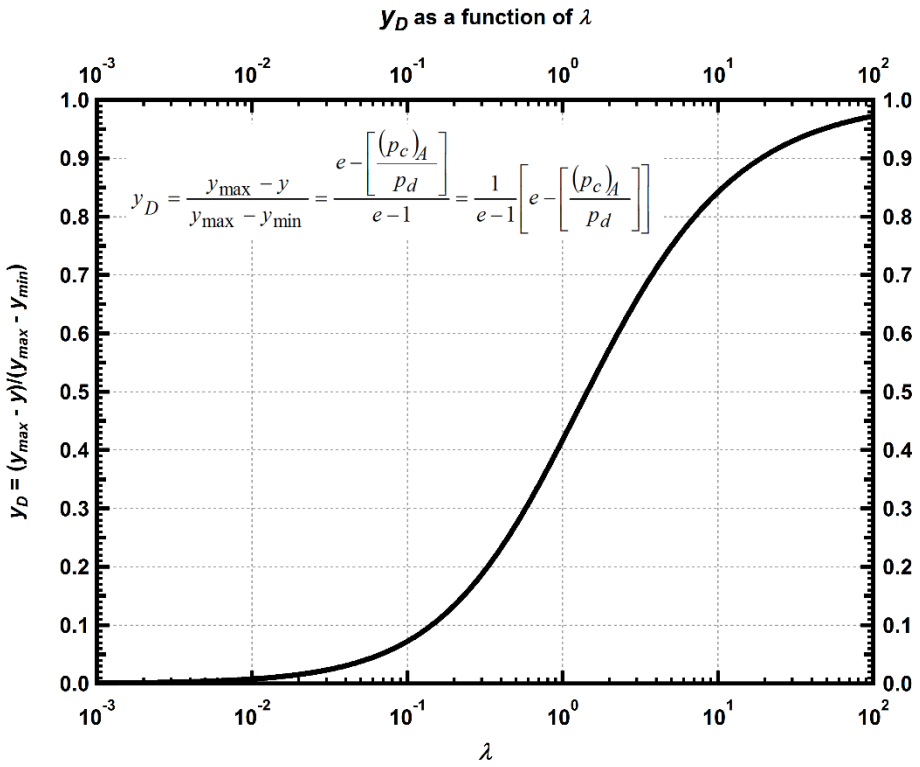

Figure D-2 — Plot of y_D as a function of λ. The dimensionless function y_D is bounded function; with a maximum value of 1 at λ approaching infinity, and a minimum value of 0 at λ approaching 0.

Using regression, the following model was created to approximate the value of λ as a function of y_D as follows:

$$\lambda = \frac{n_1 + n_2 y_D + n_3 y_D^2 + n_4 y_D^3 + n_5 y_D^4}{d_1 + d_2 y_D + d_3 y_D^2 + d_4 y_D^3 + d_5 y_D^4} \quad \text{.....(D-7)}$$

Where the correlating function, $y_D(\lambda)$, is defined as:

$$y_D = \frac{y_{max} - y}{y_{max} - y_{min}} = \frac{e - \left[\frac{(p_c)_A}{p_d}\right]}{e-1} = \frac{1}{e-1}\left[e - \left[\frac{(p_c)_A}{p_d}\right]\right] \quad \text{.....(D-8)}$$

The optimized coefficients of Eq. D-7 (n_1, n_2, … n_5 and d_1, d_2, … d_5) are shown in Table D-1 together with the statistical summary. The comparison of the regression model to the original analytical solution (Eq. D-2) is shown in Fig. D-3.

Table D-1 — Regression summary for λ.

Optimized coefficients for λ **(***Eq. D*-7**)**:

Coefficient	Optimized Value
n_1	0.000013
n_2	-4.338365
n_3	0.322016
n_4	-0.105426
n_5	-0.129459
d_1	-3.424593
d_2	3.995668
d_3	0.000049
d_4	-0.149015
d_5	-0.405945

Statistical summary for λ **(***Eq. D*-7**)**:

Statistical Variable	Value
Sum of Squared Residuals	5.9624 ln(dimensionless)^2
Average Absolute Error	0.5949 percent

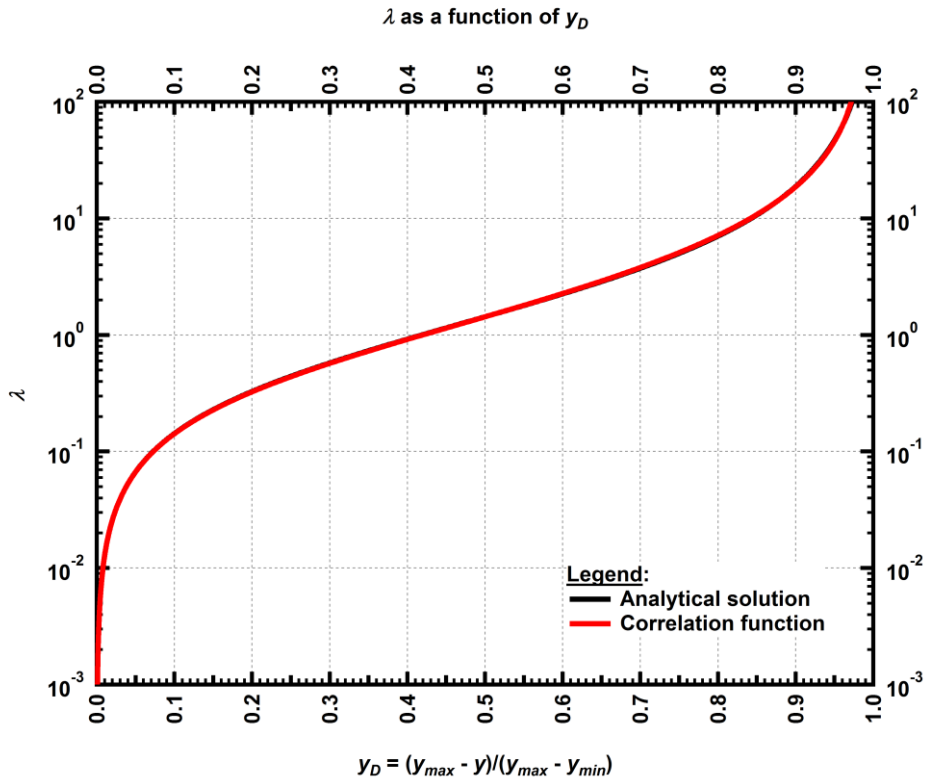

Figure D-3 — Regression model to predict λ-parameter from $(p_c)_A/p_d$ ratio (note that the correlating function $y_D = \frac{1}{e-1}\left[e - \left[\frac{(p_c)_A}{p_d}\right]\right]$).

References

D.1. Brooks, R.H., Corey, A. T. 1964. Hydraulic Properties of Porous Media 3(3), Colorado State University Hydrology Papers.

Nomenclature

e = Euler's number

p_d = Displacement pressure, psia

p_c = Capillary pressure, psia

$(p_c)_A$ = Capillary pressure at Swanson's apex, psia

S_b = Percent bulk volume occupied by mercury at a given capillary pressure, percent

$(S_b)_A$ = Percent bulk volume occupied by mercury at Swanson's apex, percent

S_{wi} = Irreducible wetting phase saturation, fraction

ϕ = Porosity, fraction

λ = Pore-size distribution index (Brooks-Corey "definition"), dimensionless

APPENDIX E

IMPACT OF THE QUALITY OF THE MICP DATA TO THE CORRELATION OF THE SEMI-ANALYTICAL MODEL

Introduction

During the matching process using the Brooks-Corey capillary pressure model (Brooks and Corey 1964), we observed that several of the mercury injection capillary pressure (MICP) data tended to deviate from the Brooks-Corey capillary pressure model at high mercury saturations (*i.e.*, low wetting phase saturation). Because of these deviation features, the selection of a concise data range for matching the data with the model was often subjective. While some samples have the MICP data follow the Brooks-Corey capillary pressure model very well, some samples clearly deviate from the expected behavior. The attempt to verify the impact of the MICP data quality on the correlation of the semi-analytical model (Huet 2005) will be shown in this Appendix.

MICP Data Quality Determination

We have visually reviewed the matches between the MICP data and the calculated capillary pressure using the Brooks-Corey capillary pressure model of the 323 samples in this study. The score of 1 to 5 was given to each sample to quantify the quality of the MICP data with 5 being the highest quality (*i.e.*, excellent match with the Brooks-Corey model). The criteria of each score is given in **Table E-1**.

Table E-1 — MICP data quality scoring criteria.

Score	Criteria
1	Unable to match the Brooks-Corey model
2	Deviation occurs at $S_w \geq 0.4$
3	Deviation occurs at $S_w < 0.4$
4	Nearly perfect match
5	Perfect match with Brooks-Corey model

The evaluation results of 323 samples are summarized in **Table E-2**.

Table E-2 — Evaluation results summary of 323 samples.

Score	Number of Samples
1	0
2	56
3	147
4	99
5	21
Total	323

To study for the impact of the quality of the MICP data on the correlation of the semi-analytical model, we separated the samples into two groups. To clearly differentiate the quality of the MICP data between the two study groups, we selected the samples with the score of 1 and 2 to represent the sample group with poor MICP data quality, and the samples with the score of 4 and 5 to represent the sample group with good quality of the MICP data. **Fig. E-1** shows the example MICP data of each sample group.

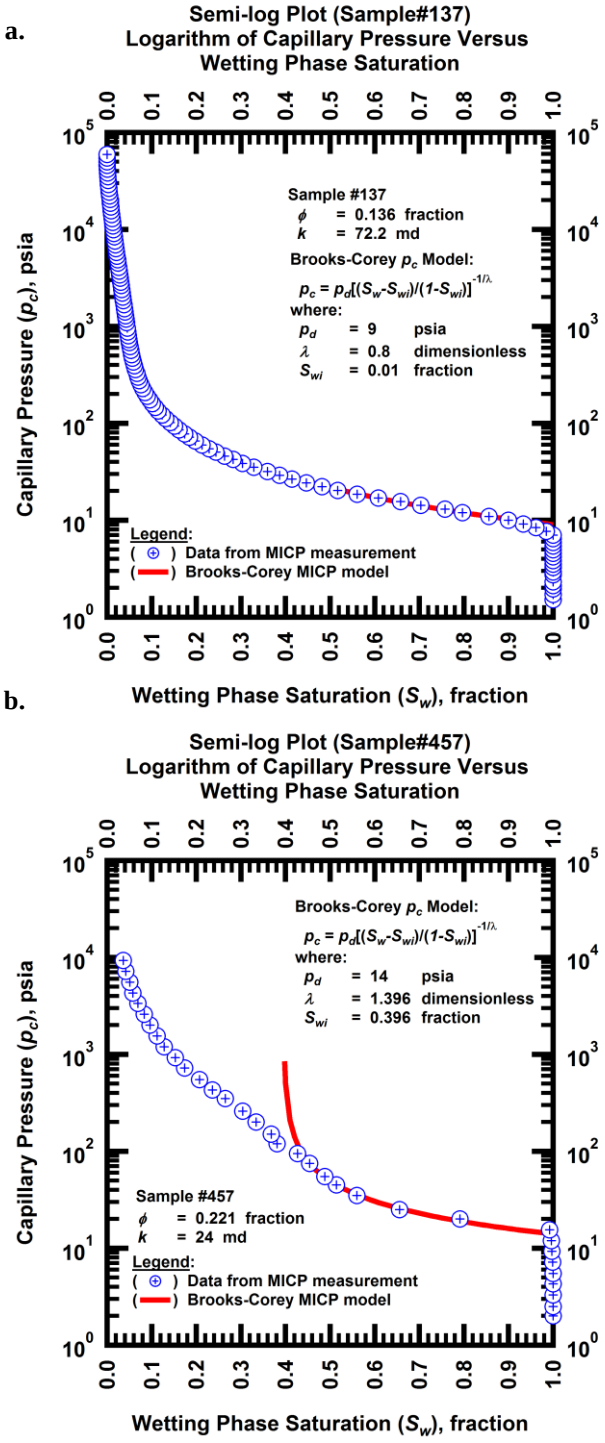

Figure E-1 — Examples of data-model matching on semi-log plot of capillary pressure (p_c) versus wetting phase saturation (S_w) — compared between the two study groups: **a.** Good quality MICP data, and **b.** Poor quality MICP data.

Regression Results and Comparison

The semi-analytical correlation model proposed by Huet (2005) is given as:

$$k = a_1 \frac{1}{(p_d)^{a_2}} \left[\frac{\lambda}{\lambda + 2} \right]^{a_3} (1 - S_{wi})^{a_4} \phi^{a_5} \quad \text{.....(E-1)}$$

The correlating parameters (a_1, a_2, …, a_5) of the semi-analytical (Huet) correlation model (Eq. E-1) were optimized by the use of multiple linear regression in the logarithmic domain. By taking the logarithm of Eq. E-1, the regression model can be written as:

$$\ln(k) = \ln(a_1) + (-a_2) \ln\left[\frac{1}{p_d} \right] + a_3 \ln\left[\frac{\lambda}{\lambda + 2} \right] + a_4 \ln(1 - S_{wi}) + a_5 \ln(\phi) \quad \text{.....(E-2)}$$

The measured permeabilities of the samples in each group were regressed on their measured porosities (ϕ) and the determined p_d, λ, and S_{wi} using the regression model in Eq. E-2. The regression analysis was conducted using R statistical software (2015).

The regression results of each sample group are shown as a log-log plot of the calculated permeabilities (*i.e.*, permeabilities calculated with the optimized model) versus the measured permeabilities in **Fig. E-2**. The optimized coefficients are shown in **Table E-3**, and the statistical summary from the regression analyses of both study groups are compared in **Table E-4**.

Table E-3 — Optimized coefficients for ln(k) of the samples with good and poor MICP data quality.

Coefficient	Good MICP quality samples	Poor MICP quality samples
a_1	9484052	589556
a_2	1.8703	1.9154
a_3	2.7358	1.0540
a_4	3.0323	1.8508
a_5	2.4284	2.0503

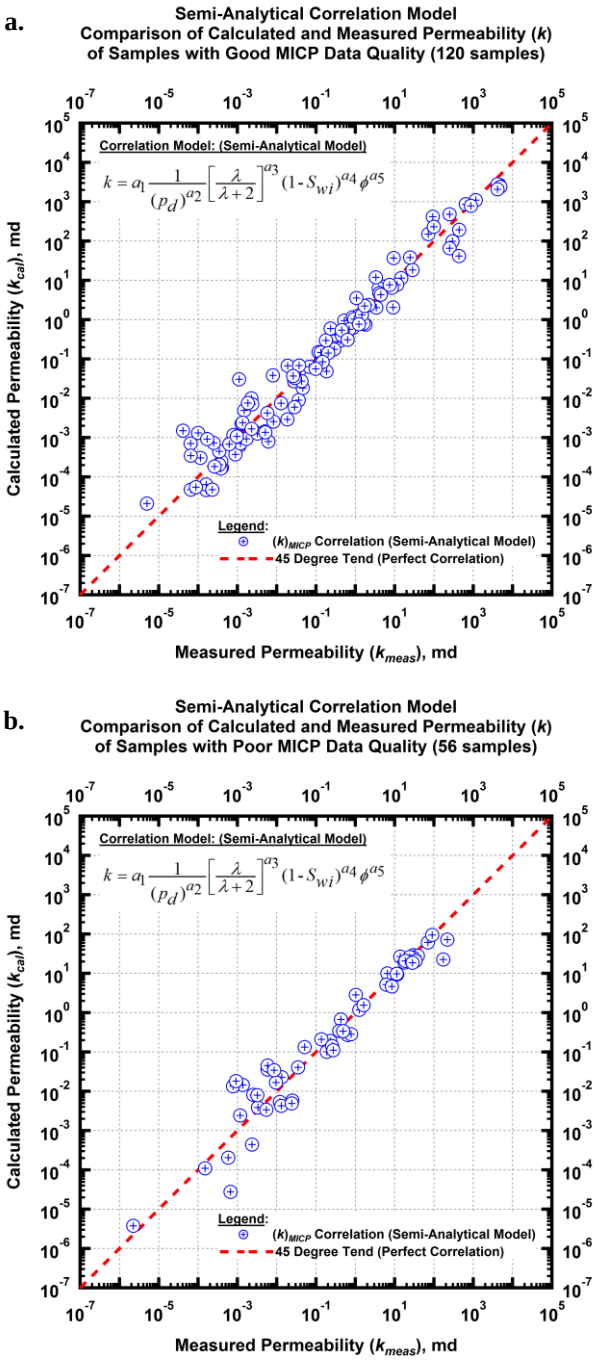

Figure E-2 — Permeability correlation comparison for the MICP samples matched with the semi-analytical model of Huet (Huet 2005) — compared between the two study groups: **a.** Good quality MICP data, and **b.** Poor quality MICP data.

Table E-4 — Comparison of regression summary for ln(k) between the samples with good and poor MICP data quality.

Statistical Variable	Good MICP quality samples		Poor MICP quality samples	
Number of Samples	120	samples	56	samples
Sum of Squared Residuals	118.48	$\ln(md)^2$	69.47	$\ln(md)^2$
Mean Squared Error	1.0303	$\ln(md)^2$	1.3621	$\ln(md)^2$
Residual Standard Error	1.0150	ln(md)	1.1671	ln(md)
R-Squared	0.9579	dimensionless	0.9314	dimensionless
Correlation Coefficients	0.9787	dimensionless	0.9651	dimensionless

From the values of the mean squared error, residual standard error, R-squared, and the correlation coefficient, the samples with good quality MICP data were shown to better correlate with permeability using the semi-analytical model. However, these two groups contain different number of samples and thus these statistical variables may not be compared directly. We applied the procedure developed by Fisher (Fisher 1921; Kenny 1946) to determine if the difference in the correlation coefficients between the two sample groups are significant. Using the statistical software *R*, the result suggests that the difference in the correlation coefficient (0.9787 versus 0.9651) are statistically insignificant at 5% level (p-value = 0.065). In simple terms, there is not enough evidence to prove that the correlation of the samples with good MICP data quality is better than the samples with poor MICP data quality.

References

E.1. Brooks, R.H., Corey, A. T. 1964. Hydraulic Properties of Porous Media 3(3), Colorado State University Hydrology Papers.

E.2. Fisher, R.A. 1921. On the "Probable Error" of a Coefficient of Correlation Deduced from a Small Sample. 1, *Metron*: 3-32.

E.3. Huet, C. C. 2005. Semi-Analytical Estimates of Permeability Obtained from Capillary Pressure. MS thesis, Texas A&M University, College Station, Texas (December 2005).

E.4. Kenny, D. 1987. Testing Measures of Association. In *Statistics for the social and behavioral sciences*, Chap. 16, 270-291. Boston, Massachusetts: Little, Brown.

E.5. R: A Language and Environment for Statistical Computing, version 3.2.3. 2015. Vienna, Austria: R Foundation for Statistical Computing. https://www.R-project.org/.

Nomenclature

k = Permeability, md

p_d = Displacement pressure, psia

p_c = Capillary pressure, psia

S_{wi} = Irreducible wetting phase saturation, fraction

S_w = Wetting phase saturation, fraction

ϕ = Porosity, fraction

λ = Pore-size distribution index (Brooks-Corey "definition"), dimensionless

APPENDIX F

SUMMARY OF DATA USED IN THIS STUDY

Table F-1 — Summary of data used in this study (323 samples).

		Input Data		p_d, S_{wi} and λ Calibration Results			Swanson Apex
Item	Sample No.	ϕ (fraction)	k (md)	S_{wi} (fraction)	p_d (psia)	λ (dim-less)	$[S_b/p_c]_A$ (%/psia)
1	40	0.166	0.046	0.01	652.50	0.75	0.0052
2	41	0.162	0.184	0.01	348.00	0.70	0.0092
3	42	0.068	0.004	0.01	1450.00	0.59	0.0008
4	43	0.095	0.018	0.02	942.50	0.60	0.0017
5	44	0.085	0.006	0.01	1305.00	0.48	0.0009
6	45	0.123	0.018	0.01	797.50	0.45	0.0021
7	46	0.139	0.636	0.30	108.75	1.46	0.0309
8	47	0.125	0.187	0.30	152.25	1.20	0.0172
9	48	0.111	0.036	0.02	406.00	0.56	0.0044
10	49	0.129	0.020	0.30	725.00	1.20	0.0040
11	50	0.073	0.019	0.02	638.00	0.81	0.0024
12	51	0.079	0.028	0.05	522.00	0.93	0.0036
13	52	0.117	0.057	0.18	406.00	1.00	0.0069
14	53	0.050	0.005	0.07	964.25	1.06	0.0013
15	54	0.124	0.465	0.30	159.50	1.25	0.0174
16	75	0.235	438.000	0.10	12.00	1.50	0.5759
17	76	0.204	82.300	0.20	17.00	1.00	0.2828
18	77	0.234	244.000	0.20	15.00	2.20	0.5577
19	78	0.207	434.000	0.26	8.00	1.20	0.5163
20	79	0.214	303.000	0.14	11.00	1.60	0.5876
21	80	0.209	210.000	0.21	14.00	2.00	0.4876
22	81	0.265	8340.000	0.10	3.80	3.00	3.0175
23	82	0.287	640.000	0.17	10.00	3.00	1.1936
24	83	0.316	1150.000	0.17	10.00	3.00	1.3142
25	84	0.320	868.000	0.16	10.00	2.15	1.2153
26	85	0.335	4570.000	0.10	6.00	2.10	2.1646
27	86	0.297	764.000	0.18	10.00	1.90	0.9843
28	87	0.272	296.000	0.12	14.00	1.01	0.4731
29	88	0.309	4110.000	0.06	5.50	2.00	2.1177

Table F-1 — Summary of data used in this study (323 samples).

		Input Data		p_d, S_{wi} and λ Calibration Results			Swanson Apex
Item	Sample No.	ϕ (fraction)	k (md)	S_{wi} (fraction)	p_d (psia)	λ (dim-less)	$[S_b/p_c]_A$ (%/psia)
30	89	0.266	250.000	0.16	17.00	1.10	0.3892
31	90	0.313	4890.000	0.10	5.00	1.70	2.3254
32	115	0.216	430.000	0.35	18.00	2.00	0.3564
33	116	0.371	14.600	0.10	53.00	0.78	0.1466
34	117	0.265	11.500	0.01	70.00	1.12	0.1130
35	119	0.311	4130.000	0.14	5.00	1.70	2.2275
36	120	0.188	357.000	0.04	6.33	1.06	0.7780
37	121	0.202	218.000	0.23	10.53	1.95	0.5469
38	122	0.081	0.005	0.02	1348.50	1.02	0.0015
39	123	0.062	0.006	0.01	1305.00	1.00	0.0012
40	124	0.108	0.025	0.01	321.06	0.15	0.0017
41	125	0.104	0.012	0.01	321.05	0.15	0.0016
42	126	0.085	0.013	0.01	314.47	0.17	0.0016
43	127	0.089	0.024	0.01	346.77	0.22	0.0019
44	128	0.115	985.000	0.01	3.00	0.35	0.3818
45	129	0.110	128.000	0.01	4.50	0.55	0.4138
46	130	0.133	44.800	0.02	8.00	0.69	0.4415
47	131	0.132	467.000	0.02	3.00	0.75	0.9566
48	132	0.110	351.000	0.07	2.80	0.75	0.7975
49	133	0.125	174.000	0.11	7.30	2.10	0.6432
50	134	0.148	117.000	0.06	15.00	1.08	0.2438
51	135	0.126	16.500	0.06	24.00	1.00	0.1210
52	136	0.109	16.600	0.01	14.50	0.70	0.1411
53	137	0.136	72.200	0.01	9.00	0.80	0.3231
54	138	0.153	209.000	0.01	9.00	0.84	0.3561
55	139	0.146	81.300	0.01	5.00	0.48	0.4157
56	141	0.218	2321.000	0.04	2.70	0.65	1.6299
57	183	0.125	0.612	0.00	73.69	0.83	0.0377
58	184	0.158	11.169	0.37	16.79	3.27	0.2831
59	185	0.162	0.809	0.24	95.74	1.59	0.0428
60	187	0.175	5.320	0.11	46.66	1.48	0.1025
61	194	0.168	1.490	0.25	64.23	1.48	0.0630
62	197	0.171	3.288	0.20	53.67	1.14	0.0690
63	202	0.129	0.846	0.07	68.65	0.80	0.0371

Table F-1 — Summary of data used in this study (323 samples).

		Input Data		p_d, S_{wi} and λ Calibration Results			Swanson Apex
Item	Sample No.	ϕ (fraction)	k (md)	S_{wi} (fraction)	p_d (psia)	λ (dim-less)	$[S_b/p_c]_A$ (%/psia)
64	207	0.176	26.866	0.03	9.25	0.39	0.2200
65	216	0.132	2.117	0.11	36.74	0.78	0.0660
66	217	0.202	69.784	0.45	7.32	1.36	0.4640
67	218	0.225	3.330	0.00	65.82	0.83	0.0782
68	220	0.059	0.003	0.02	1103.46	1.23	0.0015
69	223	0.050	0.000	0.00	1014.10	1.37	0.0015
70	224	0.066	0.013	0.00	387.36	0.89	0.0037
71	228	0.193	0.526	0.17	77.90	0.81	0.0417
72	229	0.125	0.322	0.07	85.84	0.67	0.0268
73	239	0.140	0.854	0.05	54.27	0.77	0.0442
74	244	0.091	0.028	0.14	120.79	0.64	0.0126
75	250	0.208	28.288	0.00	12.24	0.45	0.2712
76	252	0.153	4.277	0.00	21.74	0.57	0.1156
77	255	0.144	8.418	0.09	10.24	0.44	0.1717
78	256	0.126	4.909	0.19	18.09	0.86	0.1254
79	272	0.131	1.243	0.11	36.42	0.67	0.0556
80	318	0.066	0.023	0.07	150.68	0.86	0.0101
81	333	0.161	5.728	0.10	16.40	0.42	0.1135
82	334	0.130	29.712	0.37	8.93	2.17	0.3770
83	336	0.139	0.774	0.57	42.44	0.47	0.0196
84	337	0.243	28.284	0.08	22.58	1.16	0.2630
85	341	0.090	0.116	0.15	95.59	0.96	0.0192
86	342	0.161	1.253	0.30	95.85	1.94	0.0427
87	344	0.078	0.028	0.00	269.63	1.00	0.0067
88	345	0.127	0.934	0.00	24.35	0.37	0.0592
89	346	0.099	0.038	0.00	474.16	2.00	0.0077
90	348	0.206	15.681	0.17	32.02	1.94	0.2087
91	349	0.161	1.014	0.03	115.89	0.98	0.0328
92	354	0.022	0.000	0.00	9045.54	1.46	0.0001
93	356	0.059	0.000	0.00	2672.53	1.03	0.0005
94	357	0.053	0.002	0.00	195.21	0.49	0.0038
95	358	0.103	0.234	0.00	97.15	0.64	0.0179
96	359	0.042	0.002	0.00	6140.62	1.35	0.0002
97	360	0.091	0.264	0.26	46.01	1.00	0.0377

Table F-1 — Summary of data used in this study (323 samples).

		Input Data		p_d, S_{wi} and λ Calibration Results			Swanson Apex
Item	Sample No.	ϕ (fraction)	k (md)	S_{wi} (fraction)	p_d (psia)	λ (dim-less)	$[S_b/p_c]_A$ (%/psia)
98	362	0.109	0.295	0.22	87.74	1.12	0.0267
99	363	0.098	0.138	0.01	192.05	1.07	0.0137
100	364	0.058	0.535	0.22	40.50	0.45	0.0152
101	365	0.195	16.649	0.15	37.18	1.95	0.1699
102	366	0.058	0.000	0.00	2964.02	1.08	0.0005
103	367	0.145	29.283	0.17	5.06	0.80	0.4968
104	368	0.145	29.283	0.19	7.64	0.98	0.3715
105	369	0.139	5.140	0.30	11.54	1.07	0.2141
106	370	0.139	5.140	0.16	14.19	0.69	0.1595
107	371	0.121	2.267	0.19	25.29	0.95	0.0889
108	372	0.212	13.056	0.22	28.32	1.55	0.1899
109	373	0.141	0.677	0.00	66.73	0.34	0.0253
110	374	0.137	1.803	0.00	55.17	0.60	0.0421
111	375	0.063	0.001	0.00	6373.66	0.79	0.0003
112	376	0.182	17.827	0.18	28.06	1.89	0.2043
113	377	0.225	42.429	0.19	21.52	2.06	0.3332
114	378	0.202	3.932	0.06	47.26	1.04	0.1045
115	379	0.211	3.295	0.04	38.56	1.10	0.1328
116	380	0.149	1.616	0.00	56.80	0.58	0.0491
117	381	0.191	2.550	0.13	65.84	1.17	0.0696
118	382	0.102	0.001	0.00	3016.76	1.05	0.0008
119	383	0.148	1.403	0.06	55.70	0.78	0.0516
120	384	0.152	1.054	0.05	74.05	0.69	0.0357
121	385	0.151	0.718	0.06	113.23	1.08	0.0337
122	388	0.073	0.006	0.12	330.00	1.19	0.0056
123	389	0.070	0.001	0.00	2181.84	0.94	0.0008
124	390	0.039	0.000	0.00	1430.05	0.86	0.0007
125	391	0.088	0.000	0.00	4771.02	1.41	0.0005
126	392	0.026	0.000	0.00	6478.74	0.65	0.0001
127	393	0.059	0.026	0.00	76.00	0.53	0.0139
128	394	0.113	0.417	0.00	111.89	0.91	0.0231
129	395	0.137	37.835	0.23	12.18	1.78	0.3178
130	396	0.132	0.286	0.00	195.43	1.00	0.0160
131	397	0.087	0.229	0.43	72.70	2.24	0.0278

Table F-1 — Summary of data used in this study (323 samples).

		Input Data		p_d, S_{wi} and λ Calibration Results			Swanson Apex
Item	Sample No.	ϕ (fraction)	k (md)	S_{wi} (fraction)	p_d (psia)	λ (dim-less)	$[S_b/p_c]_A$ (%/psia)
132	398	0.149	17.757	0.28	17.01	1.61	0.2174
133	399	0.071	0.012	0.00	280.55	0.69	0.0048
134	400	0.166	397.000	0.08	3.25	0.58	0.7854
135	401	0.196	2670.000	0.00	2.06	0.47	1.3156
136	402	0.097	0.109	0.13	116.49	0.93	0.0174
137	403	0.009	0.000	0.00	6553.25	1.26	0.0000
138	404	0.160	2.275	0.24	42.91	0.86	0.0613
139	405	0.122	0.132	0.03	126.35	0.68	0.0180
140	406	0.130	0.306	0.00	77.59	0.62	0.0285
141	407	0.155	3.385	0.00	31.15	0.50	0.0813
142	408	0.128	0.204	0.00	75.77	0.39	0.0202
143	409	0.157	8.480	0.08	23.47	0.76	0.1207
144	410	0.112	0.309	0.10	58.48	0.70	0.0318
145	411	0.270	38.645	0.62	9.74	1.10	0.2782
146	412	0.237	13.816	0.00	12.28	0.27	0.1715
147	413	0.191	26.154	0.23	19.31	1.55	0.2506
148	414	0.147	2.175	0.00	39.35	0.71	0.0717
149	415	0.111	0.134	0.00	110.27	0.49	0.0141
150	416	0.148	25.588	0.22	8.76	0.83	0.2815
151	417	0.180	71.391	0.06	8.89	1.26	0.5367
152	418	0.236	9.456	0.03	12.94	0.58	0.2344
153	419	0.210	4.086	0.01	66.70	1.10	0.0819
154	422	0.121	0.319	0.00	48.64	0.46	0.0308
155	423	0.193	45.130	0.14	9.22	0.86	0.3887
156	424	0.160	17.827	0.10	15.38	1.06	0.2317
157	425	0.154	5.017	0.24	15.09	0.87	0.1661
158	426	0.135	0.702	0.00	69.17	0.65	0.0355
159	427	0.195	24.600	0.17	30.38	2.75	0.2479
160	428	0.176	4.437	0.00	31.90	0.63	0.0974
161	429	0.121	0.453	0.00	88.68	0.78	0.0296
162	430	0.127	0.178	0.00	121.33	0.86	0.0230
163	431	0.097	0.043	0.00	157.29	0.47	0.0087
164	432	0.115	1.819	0.11	40.27	1.79	0.0890
165	433	0.208	34.181	0.19	20.15	1.81	0.3150

Table F-1 — Summary of data used in this study (323 samples).

		Input Data		p_d, S_{wi} and λ Calibration Results			Swanson Apex
Item	Sample No.	ϕ (fraction)	k (md)	S_{wi} (fraction)	p_d (psia)	λ (dim-less)	$[S_b/p_c]_A$ (%/psia)
166	434	0.215	93.017	0.06	5.60	1.06	0.8072
167	435	0.223	249.233	0.04	5.41	1.03	0.9816
168	436	0.247	98.275	0.04	11.91	1.36	0.5689
169	437	0.175	0.782	0.28	67.32	1.84	0.0608
170	438	0.243	101.820	0.17	15.66	2.22	0.5406
171	439	0.090	0.042	0.19	82.13	0.63	0.0151
172	440	0.164	4.488	0.30	31.00	1.23	0.1058
173	441	0.143	1.458	0.00	64.80	0.87	0.0541
174	442	0.132	0.609	0.20	73.97	1.28	0.0409
175	443	0.185	7.429	0.04	27.29	0.72	0.1301
176	444	0.179	1.221	0.09	69.47	0.62	0.0397
177	445	0.169	1.709	0.00	53.75	0.77	0.0656
178	446	0.152	0.233	0.04	105.05	0.91	0.0296
179	447	0.174	9.038	0.15	46.51	0.80	0.0644
180	448	0.125	0.446	0.00	80.67	0.81	0.0334
181	449	0.132	34.545	0.23	10.84	1.84	0.3413
182	450	0.117	12.366	0.21	11.89	1.18	0.2182
183	451	0.144	143.885	0.11	5.06	0.65	0.4554
184	454	0.217	29.000	0.38	14.67	1.48	0.3064
185	455	0.199	11.500	0.38	21.05	1.25	0.1751
186	456	0.192	7.960	0.29	23.74	1.07	0.1596
187	457	0.221	24.000	0.40	14.03	1.40	0.3041
188	458	0.198	2.070	0.23	45.85	0.79	0.0713
189	459	0.209	3.180	0.32	38.42	1.09	0.1014
190	460	0.177	26.100	0.35	13.95	1.27	0.2549
191	461	0.187	28.100	0.29	10.50	1.06	0.3460
192	462	0.114	0.137	0.43	88.91	1.96	0.0275
193	463	0.083	0.000	0.00	401.69	0.34	0.0022
194	464	0.106	0.013	0.29	245.51	0.99	0.0077
195	465	0.066	0.001	0.01	750.62	0.67	0.0017
196	466	0.033	0.000	0.00	1235.39	0.49	0.0004
197	467	0.030	0.000	0.00	1484.83	0.75	0.0004
198	470	0.062	0.001	0.13	947.21	0.85	0.0013
199	471	0.042	0.000	0.08	701.19	0.46	0.0008

Table F-1 — Summary of data used in this study (323 samples).

		Input Data		p_d, S_{wi} and λ Calibration Results			Swanson Apex
Item	Sample No.	ϕ (fraction)	k (md)	S_{wi} (fraction)	p_d (psia)	λ (dim-less)	$[S_b/p_c]_A$ (%/psia)
200	472	0.042	0.000	0.00	1021.57	0.70	0.0008
201	473	0.032	0.000	0.00	859.12	0.38	0.0004
202	474	0.058	0.008	0.00	313.26	0.51	0.0028
203	475	0.050	0.002	0.00	406.82	0.47	0.0016
204	477	0.026	0.000	0.00	1605.99	0.83	0.0003
205	479	0.073	0.025	0.00	134.40	0.63	0.0095
206	480	0.043	0.000	0.27	421.36	0.70	0.0014
207	484	0.057	0.000	0.00	1142.29	0.49	0.0007
208	486	0.034	0.000	0.00	882.41	0.21	0.0003
209	487	0.045	0.000	0.31	201.17	0.90	0.0037
210	488	0.127	0.001	0.29	180.82	1.15	0.0140
211	489	0.078	0.006	0.25	105.96	0.63	0.0106
212	490	0.102	0.002	0.00	301.76	0.49	0.0057
213	491	0.114	0.429	0.40	48.68	1.66	0.0487
214	492	0.120	1.460	0.22	20.97	0.66	0.0783
215	495	0.102	0.029	0.00	96.12	0.39	0.0136
216	497	0.087	0.006	0.50	142.52	1.73	0.0108
217	498	0.086	0.006	0.40	130.01	1.13	0.0116
218	499	0.077	0.003	0.33	842.65	1.37	0.0019
219	501	0.069	0.001	0.00	277.30	0.36	0.0028
220	502	0.090	0.001	0.03	372.02	0.51	0.0036
221	503	0.245	113.000	0.34	6.94	1.06	0.6054
222	505	0.055	0.000	0.00	1111.84	0.73	0.0010
223	507	0.062	0.001	0.00	422.40	0.59	0.0025
224	508	0.030	0.000	0.00	1928.02	0.89	0.0004
225	510	0.204	1.250	0.55	50.64	1.56	0.0603
226	511	0.062	0.001	0.33	390.71	1.30	0.0031
227	513	0.154	0.067	0.00	242.27	0.60	0.0111
228	514	0.224	1.030	0.28	38.79	0.60	0.0712
229	516	0.137	1.080	0.33	43.87	1.22	0.0549
230	517	0.175	1.110	0.35	50.79	1.32	0.0640
231	518	0.167	2.020	0.30	29.39	0.73	0.0768
232	521	0.100	0.008	0.01	202.55	0.43	0.0065
233	522	0.121	0.387	0.47	71.35	2.30	0.0379

Table F-1 — Summary of data used in this study (323 samples).

		Input Data		p_d, S_{wi} and λ Calibration Results			Swanson Apex
Item	Sample No.	ϕ (fraction)	k (md)	S_{wi} (fraction)	p_d (psia)	λ (dim-less)	$[S_b/p_c]_A$ (%/psia)
234	523	0.121	0.479	0.29	49.24	0.73	0.0351
235	526	0.096	0.254	0.45	81.12	1.42	0.0209
236	527	0.154	1.610	0.36	32.98	0.65	0.0530
237	529	0.098	0.051	0.38	82.88	0.95	0.0184
238	530	0.095	0.042	0.10	69.70	0.35	0.0132
239	532	0.072	0.001	0.00	183.05	0.30	0.0034
240	535	0.031	0.001	0.00	555.74	0.20	0.0003
241	537	0.083	0.003	0.49	269.33	1.18	0.0045
242	538	0.076	0.005	0.00	227.56	0.48	0.0046
243	540	0.102	0.019	0.00	206.96	0.88	0.0115
244	541	0.102	0.022	0.00	170.19	0.85	0.0131
245	542	0.050	0.003	0.39	304.59	1.63	0.0036
246	545	0.078	0.000	0.00	1036.19	0.57	0.0012
247	546	0.100	0.004	0.14	376.27	1.55	0.0080
248	547	0.212	17.700	0.45	14.32	1.36	0.2561
249	548	0.116	0.001	0.00	291.21	0.25	0.0033
250	549	0.116	0.035	0.28	216.15	1.00	0.0094
251	550	0.088	0.029	0.00	142.64	0.52	0.0103
252	551	0.101	0.146	0.01	79.05	0.42	0.0162
253	552	0.215	6.500	0.52	20.33	2.14	0.2009
254	554	0.068	0.000	0.00	2084.75	0.65	0.0006
255	555	0.130	0.028	0.09	176.69	0.51	0.0103
256	557	0.106	0.037	0.08	112.14	0.54	0.0139
257	558	0.187	30.700	0.05	9.79	0.40	0.2304
258	559	0.201	28.500	0.54	13.65	2.72	0.3005
259	560	0.041	0.000	0.40	2687.97	1.15	0.0003
260	561	0.106	0.013	0.54	208.17	1.77	0.0084
261	563	0.084	0.001	0.34	633.48	1.08	0.0023
262	564	0.065	0.003	0.31	391.61	3.52	0.0059
263	565	0.105	0.008	0.01	268.93	0.82	0.0087
264	566	0.132	0.028	0.24	244.39	2.13	0.0166
265	567	0.102	0.010	0.39	382.52	4.65	0.0092
266	568	0.109	0.003	0.20	220.69	0.74	0.0082
267	573	0.055	0.001	0.00	546.18	0.47	0.0015

Table F-1 — Summary of data used in this study (323 samples).

		Input Data		p_d, S_{wi} and λ Calibration Results			Swanson Apex
Item	Sample No.	ϕ (fraction)	k (md)	S_{wi} (fraction)	p_d (psia)	λ (dim-less)	$[S_b/p_c]_A$ (%/psia)
268	574	0.217	33.800	0.43	18.89	3.90	0.3264
269	575	0.200	11.300	0.35	22.65	1.37	0.1853
270	576	0.187	6.100	0.41	34.64	3.67	0.1666
271	577	0.160	1.900	0.11	37.27	0.62	0.0704
272	578	0.174	28.600	0.32	14.19	1.28	0.2561
273	579	0.182	170.900	0.41	15.26	3.47	0.3487
274	580	0.089	0.006	0.00	496.40	0.59	0.0031
275	581	0.120	0.020	0.00	196.19	0.37	0.0072
276	582	0.115	0.142	0.00	75.68	0.55	0.0283
277	583	0.082	0.000	0.00	1447.14	0.72	0.0012
278	584	0.026	0.000	0.00	556.46	0.84	0.0010
279	589	0.049	0.001	0.00	894.07	1.08	0.0013
280	592	0.098	0.002	0.00	675.51	0.91	0.0038
281	593	0.045	0.000	0.31	566.71	1.32	0.0016
282	594	0.128	0.001	0.00	445.36	0.92	0.0081
283	595	0.073	0.006	0.15	198.83	0.79	0.0065
284	596	0.100	0.002	0.01	613.78	0.85	0.0038
285	597	0.112	0.470	0.23	43.30	1.07	0.0513
286	598	0.114	1.060	0.01	15.38	0.50	0.0950
287	599	0.105	0.026	0.42	126.53	0.90	0.0105
288	600	0.119	0.163	0.00	53.48	0.43	0.0318
289	601	0.136	0.018	0.01	217.99	0.78	0.0154
290	602	0.077	0.003	0.00	596.00	0.47	0.0019
291	604	0.243	90.100	0.41	8.83	2.25	0.6553
292	605	0.181	36.500	0.26	10.58	1.13	0.3692
293	606	0.170	34.600	0.26	14.39	1.43	0.2965
294	607	0.147	2.530	0.28	39.64	1.28	0.0872
295	608	0.173	5.150	0.23	27.13	1.34	0.1566
296	610	0.166	3.530	0.35	28.84	1.55	0.1339
297	611	0.131	0.041	0.00	166.86	0.43	0.0123
298	616	0.178	30.200	0.27	13.22	1.53	0.3446
299	617	0.120	0.390	0.28	69.04	1.03	0.0348
300	618	0.121	0.633	0.00	64.27	0.52	0.0377
301	619	0.096	0.182	0.07	106.38	0.57	0.0143

Table F-1 — Summary of data used in this study (323 samples).

		Input Data		p_d, S_{wi} and λ Calibration Results			Swanson Apex
Item	Sample No.	ϕ (fraction)	k (md)	S_{wi} (fraction)	p_d (psia)	λ (dim-less)	$[S_b/p_c]_A$ (%/psia)
302	620	0.098	0.098	0.01	167.61	0.69	0.0126
303	621	0.090	0.036	0.09	229.08	0.74	0.0086
304	623	0.069	0.002	0.00	1278.76	0.43	0.0013
305	626	0.084	0.004	0.00	729.03	0.61	0.0020
306	627	0.078	0.006	0.00	586.23	1.03	0.0034
307	628	0.090	0.274	0.56	89.44	3.92	0.0250
308	629	0.117	8.500	0.45	20.31	3.41	0.1541
309	630	0.051	0.005	0.00	389.35	0.53	0.0022
310	631	0.070	0.002	0.00	864.61	0.83	0.0019
311	635	0.098	0.006	0.11	618.01	1.94	0.0053
312	639	0.215	18.600	0.44	15.07	1.65	0.2838
313	640	0.099	0.005	0.41	388.08	0.42	0.0021
314	641	0.117	0.001	0.00	251.29	0.25	0.0038
315	642	0.141	0.487	0.41	100.00	2.79	0.0396
316	643	0.148	0.288	0.25	102.24	1.30	0.0331
317	644	0.201	28.500	0.51	15.09	3.00	0.3005
318	646	0.067	0.003	0.23	369.92	2.66	0.0062
319	647	0.107	0.003	0.31	689.33	5.22	0.0068
320	648	0.118	0.009	0.09	347.47	1.51	0.0111
321	649	0.117	0.012	0.12	364.58	2.06	0.0112
322	650	0.061	0.002	0.25	780.47	2.66	0.0027
323	651	0.111	0.192	0.31	92.92	3.50	0.0408

APPENDIX G

LIBRARY OF CAPILLARY PRESSURE VERSUS WETTING PHASE SATURATION PLOTS — CARTESIAN CAPILLARY PRESSURE FORMAT

This Appendix presents the calibration of the capillary displacement pressure (p_d), irreducible wetting phase saturation (S_{wi}), and the index of pore-size distribution (λ) on a sample-by-sample basis using the Brooks-Corey $p_c(S_w)$ model. In this Appendix, we provide example plots of capillary pressure (p_c) vs. wetting phase saturation (S_w) of 50 (fifty) samples used in this study.

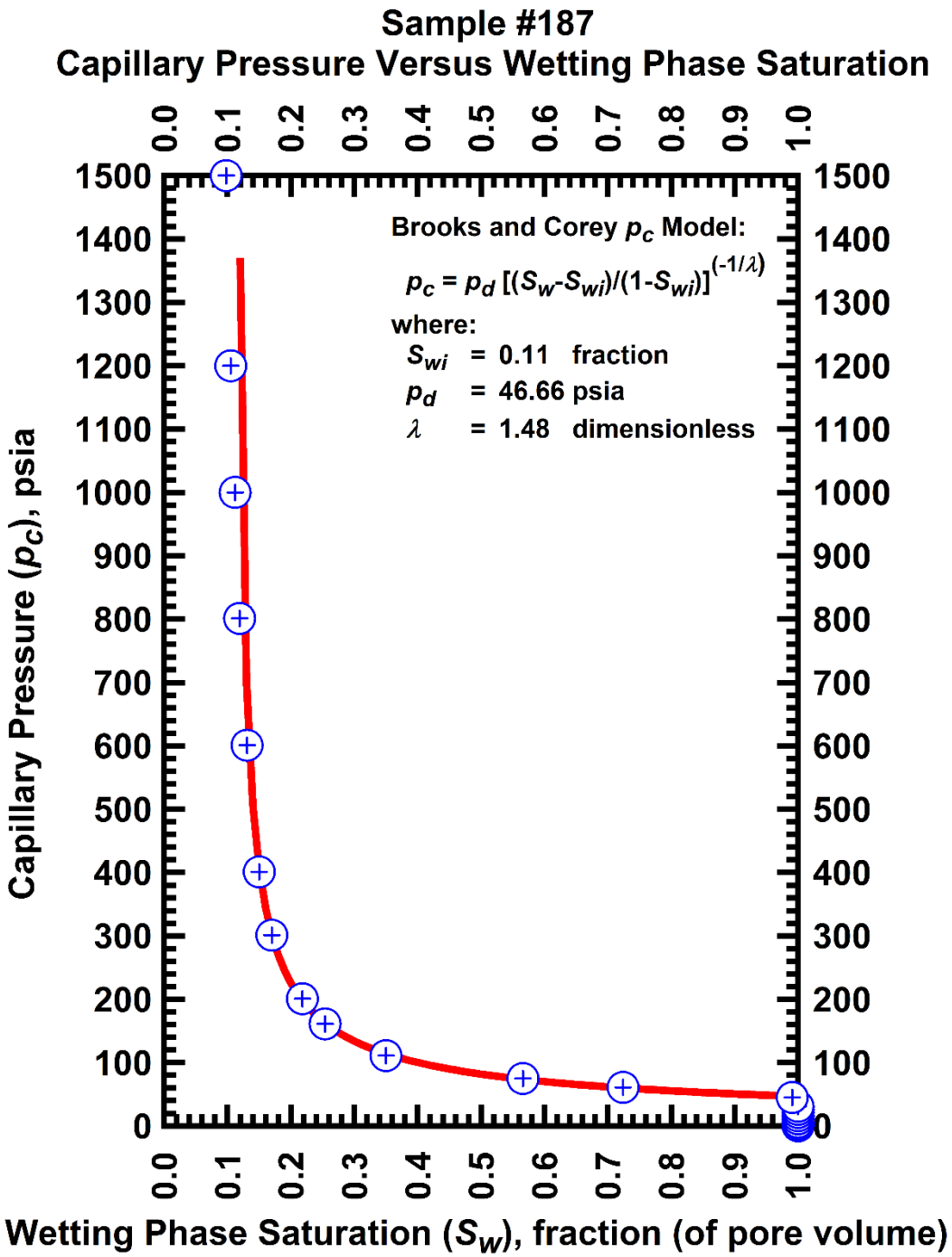

Figure G-1 — Plot of capillary pressure (p_c) vs. wetting phase saturation (S_w) — Sample #187.

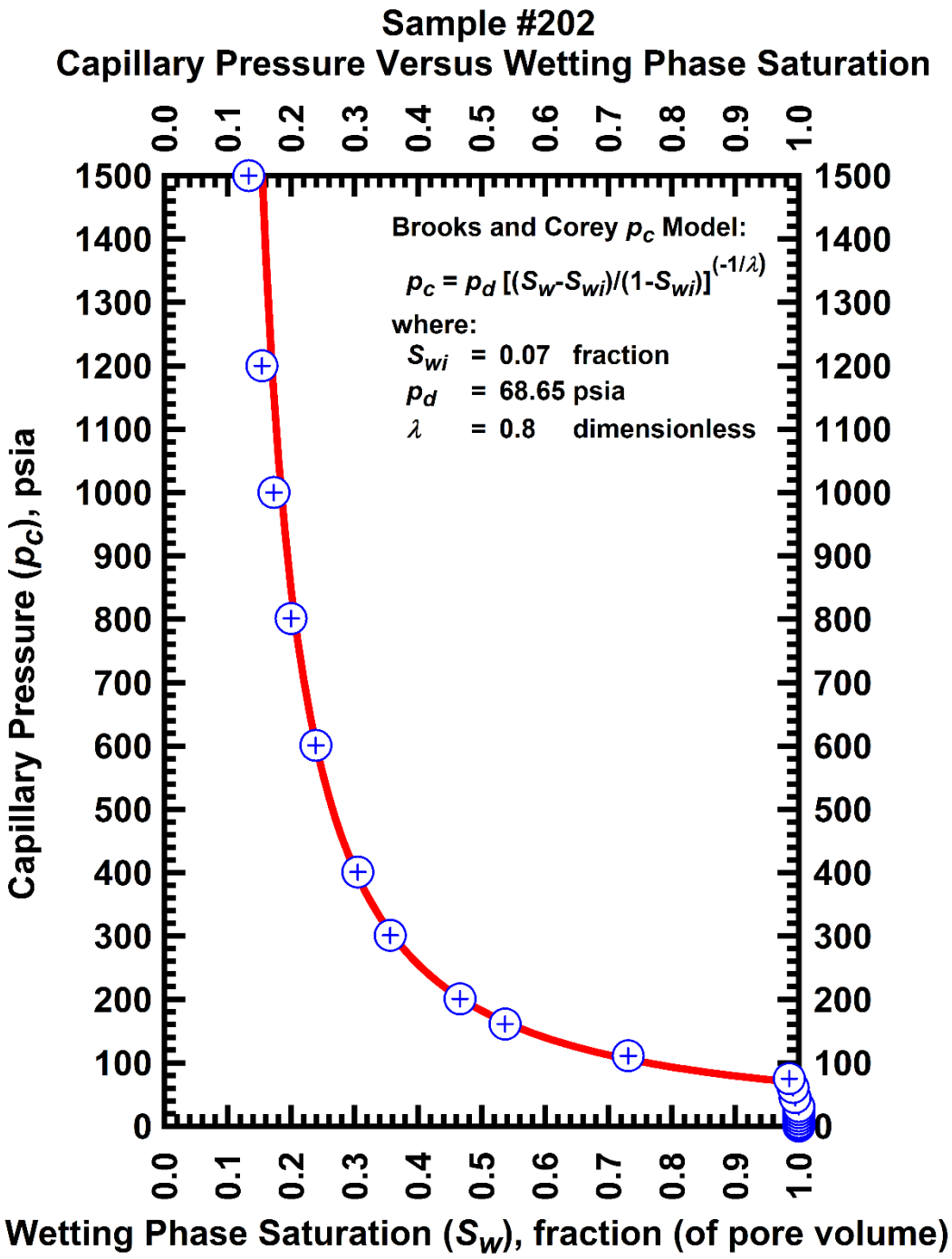

Figure G-2 — Plot of capillary pressure (p_c) vs. wetting phase saturation (S_w) — Sample #202.

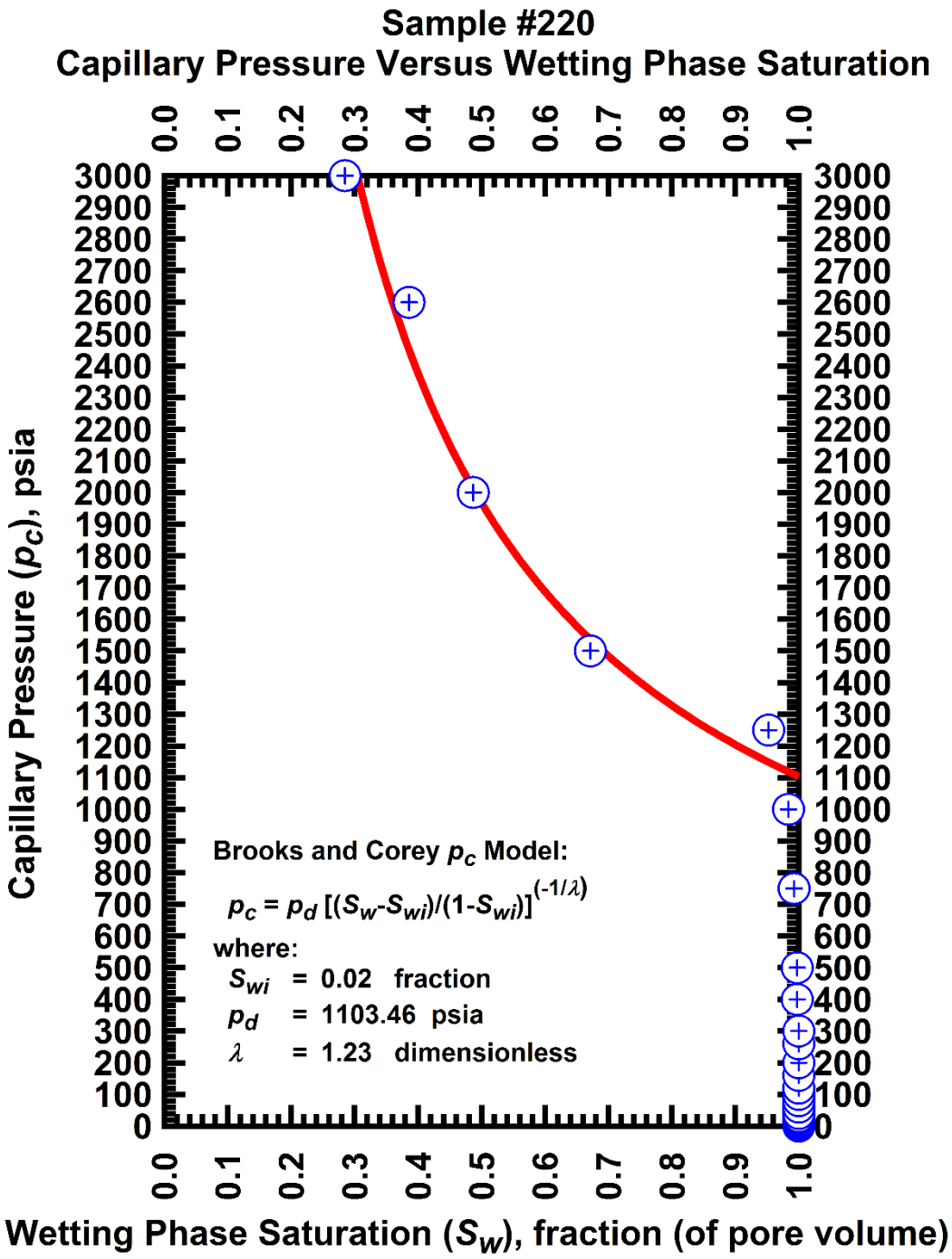

Figure G-3 — Plot of capillary pressure (p_c) vs. wetting phase saturation (S_w) — Sample #220.

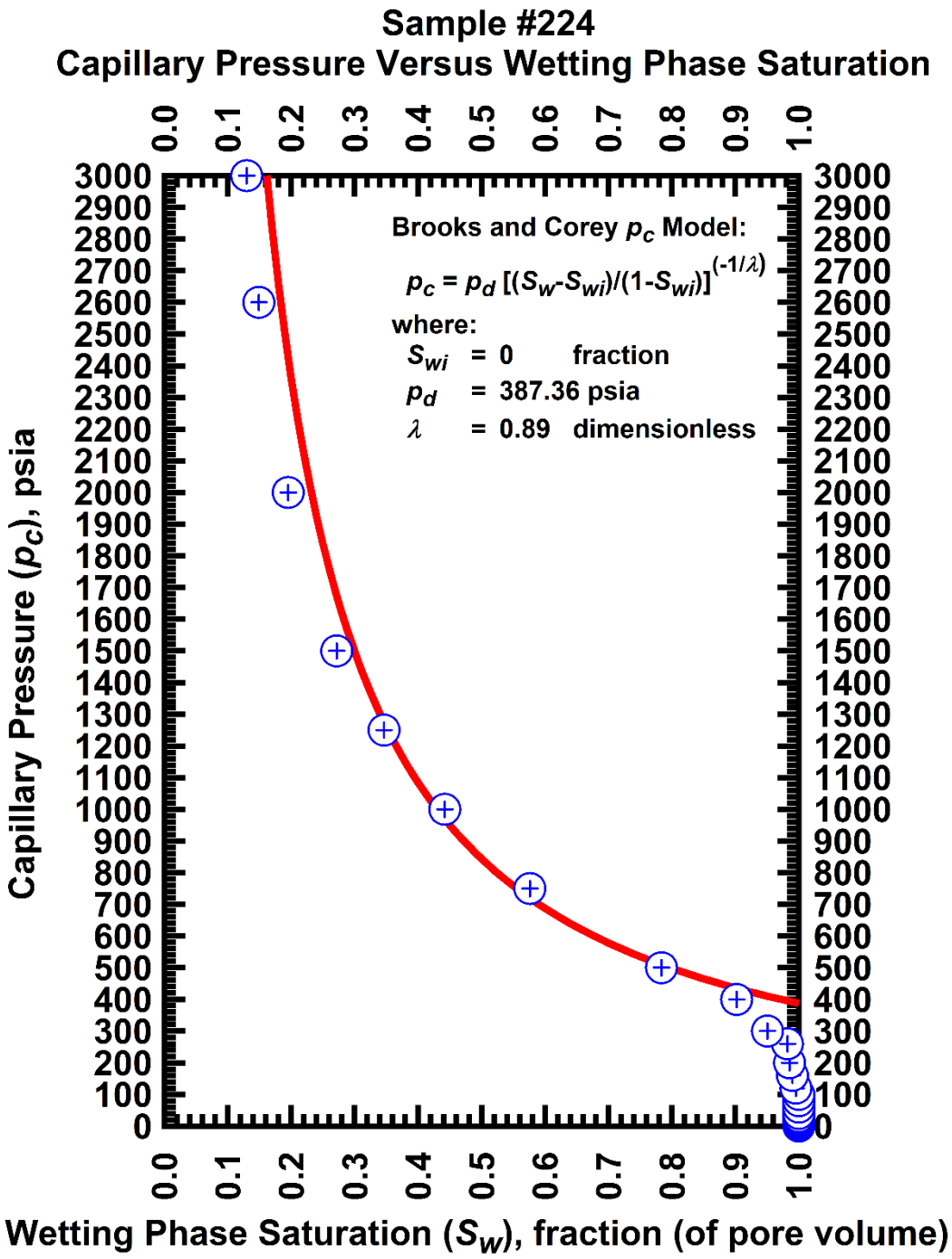

Figure G-4 — Plot of capillary pressure (p_c) vs. wetting phase saturation (S_w) — Sample #224.

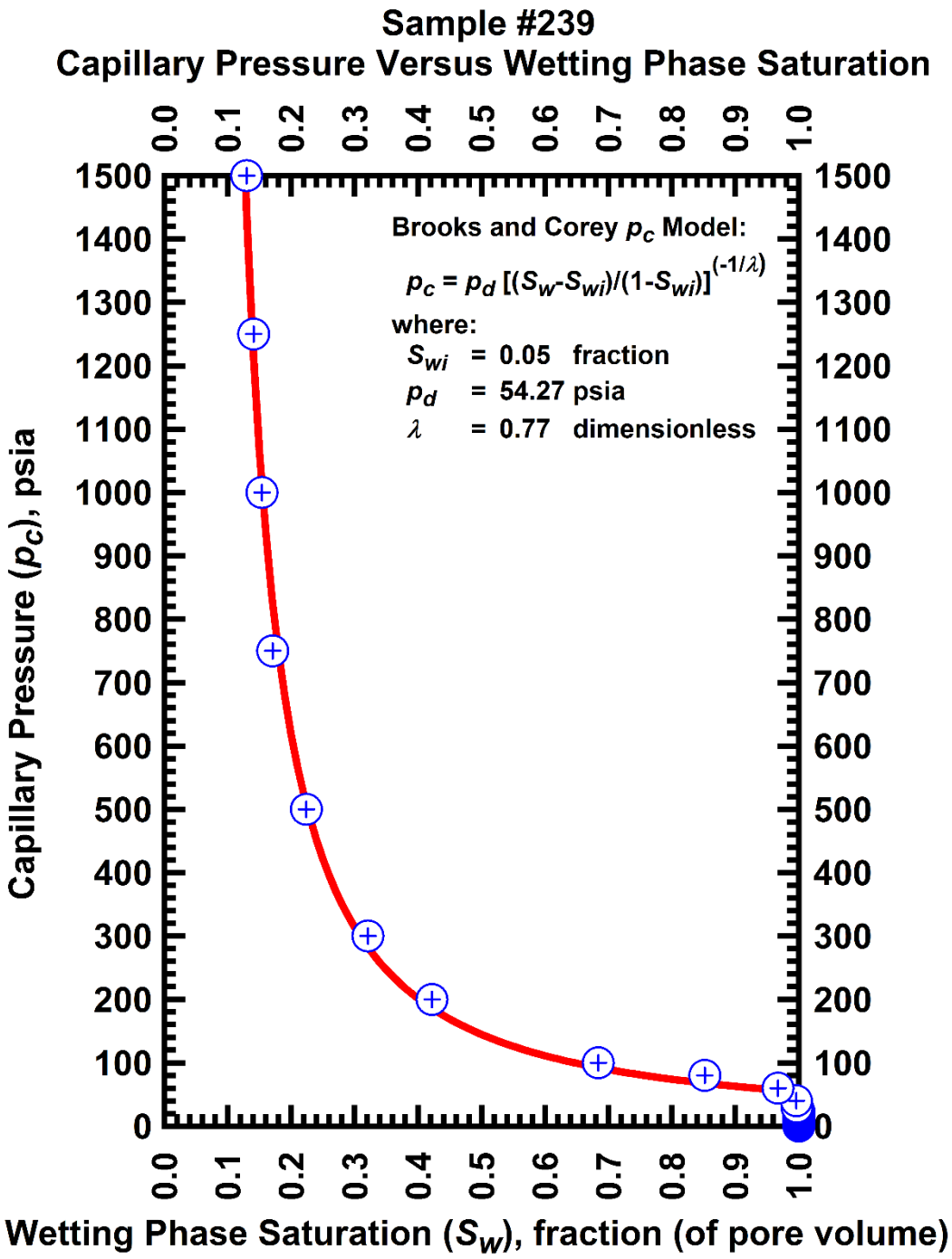

Figure G-5 — Plot of capillary pressure (p_c) vs. wetting phase saturation (S_w) — Sample #239.

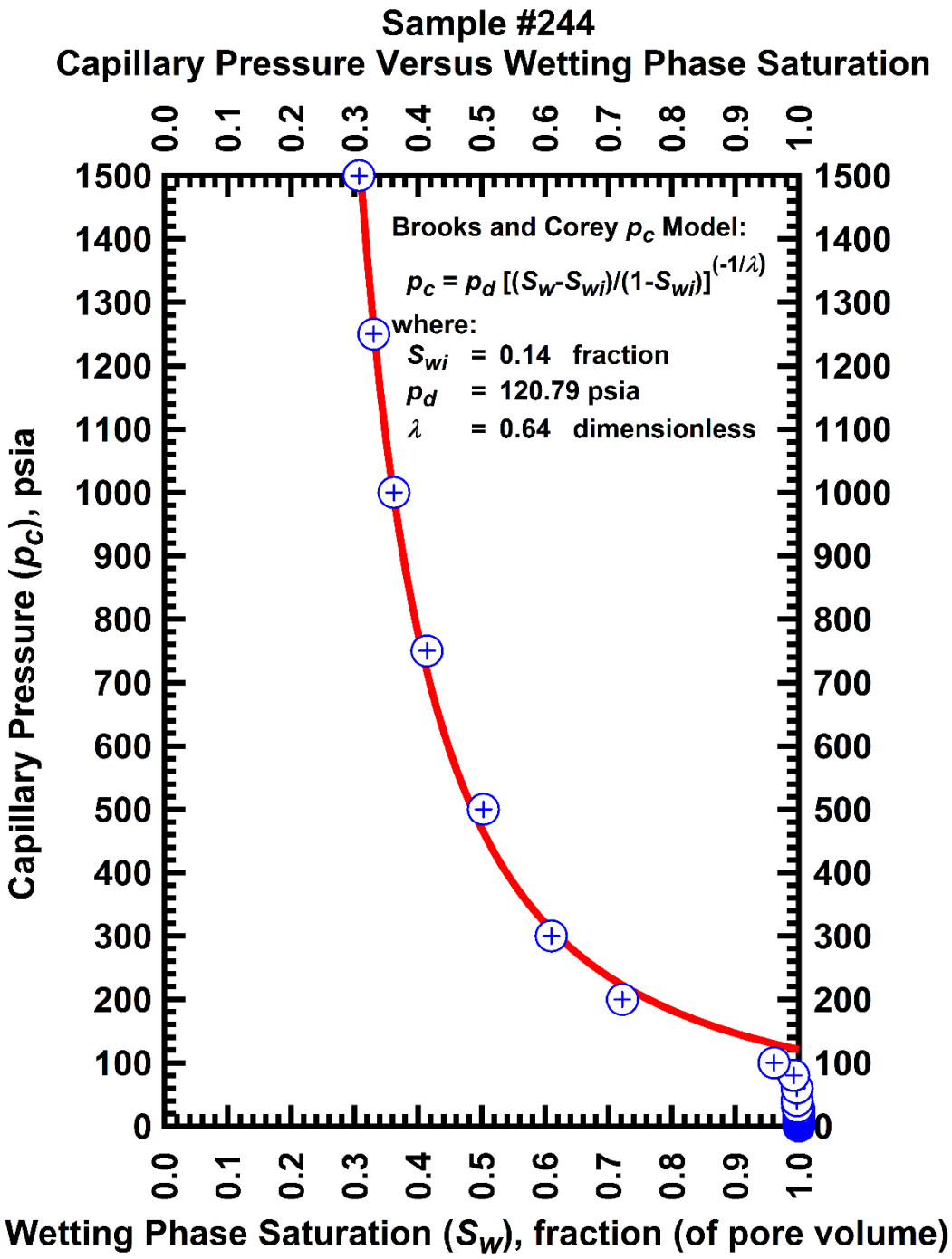

Figure G-6 — Plot of capillary pressure (p_c) vs. wetting phase saturation (S_w) — Sample #244.

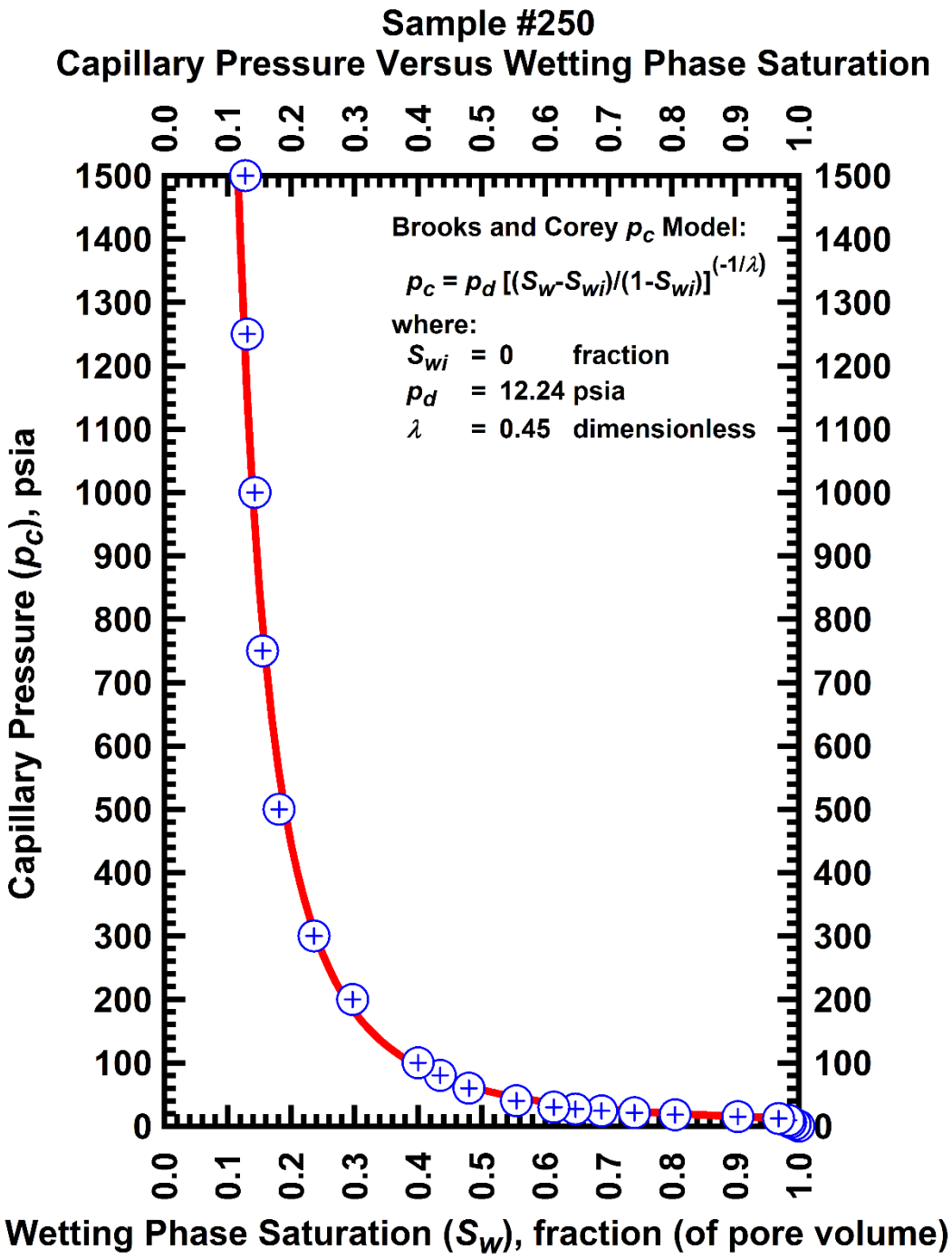

Figure G-7 — Plot of capillary pressure (p_c) vs. wetting phase saturation (S_w) — Sample #250.

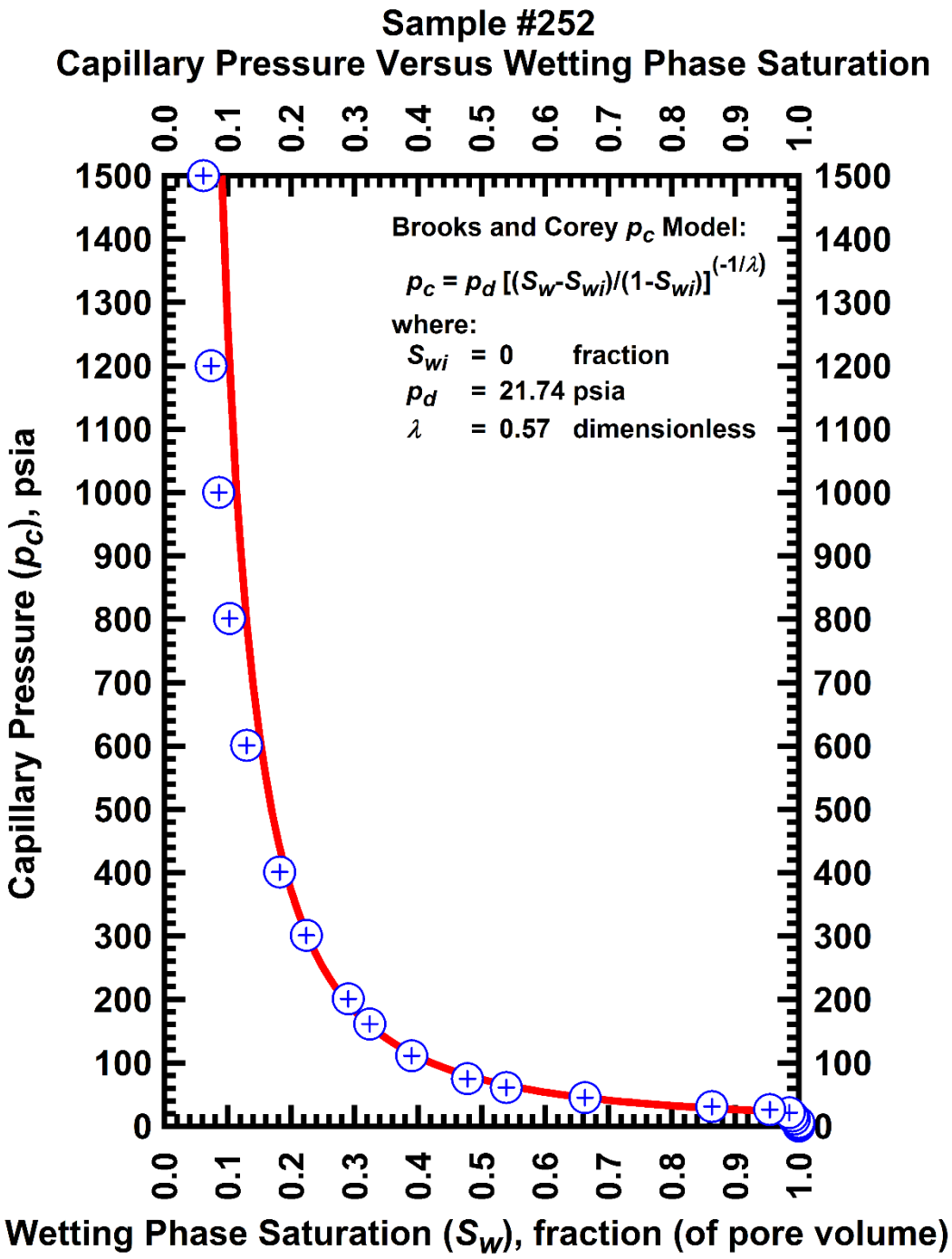

Figure G-8 — Plot of capillary pressure (p_c) vs. wetting phase saturation (S_w) — Sample #252.

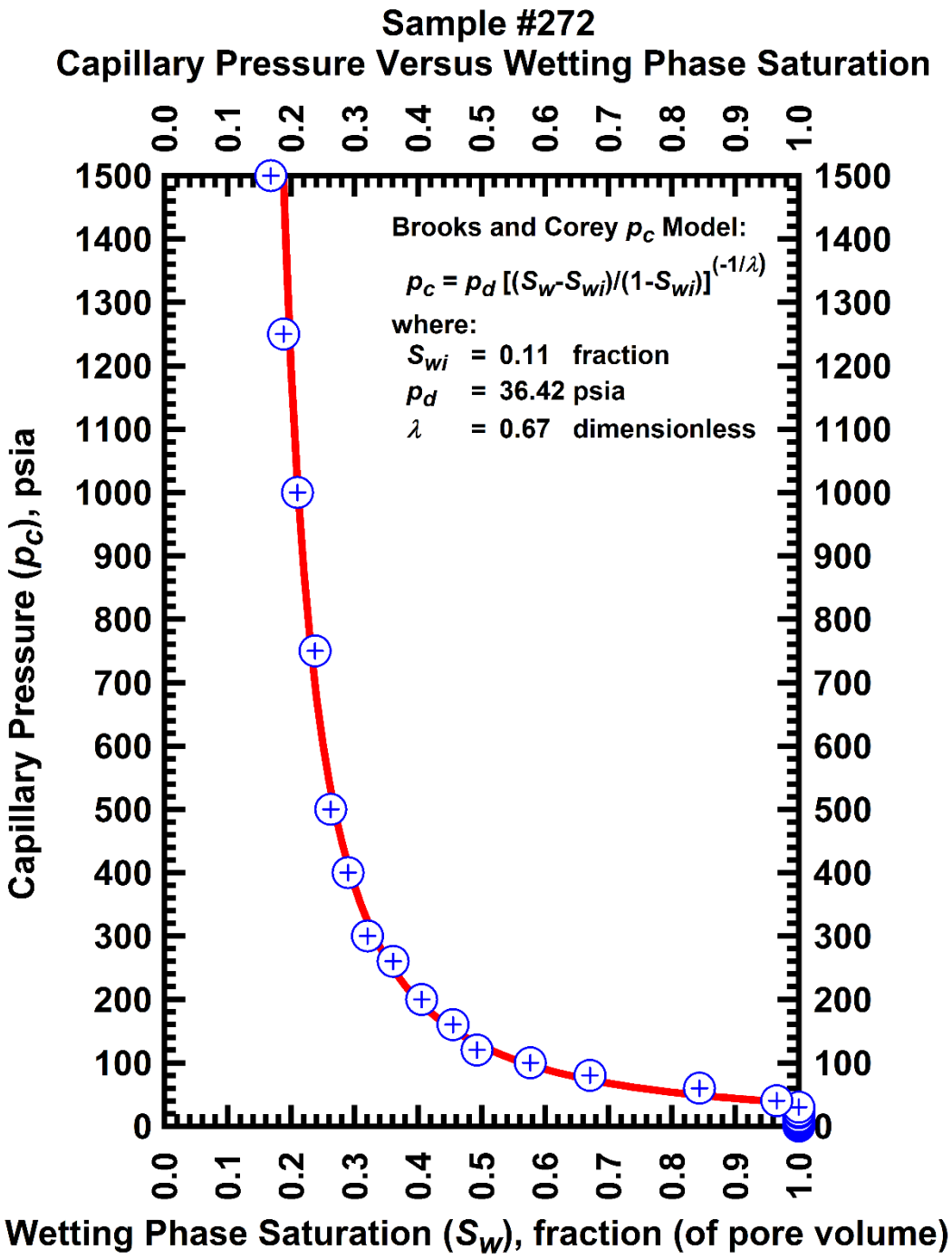

Figure G-9 — Plot of capillary pressure (p_c) vs. wetting phase saturation (S_w) — Sample #272.

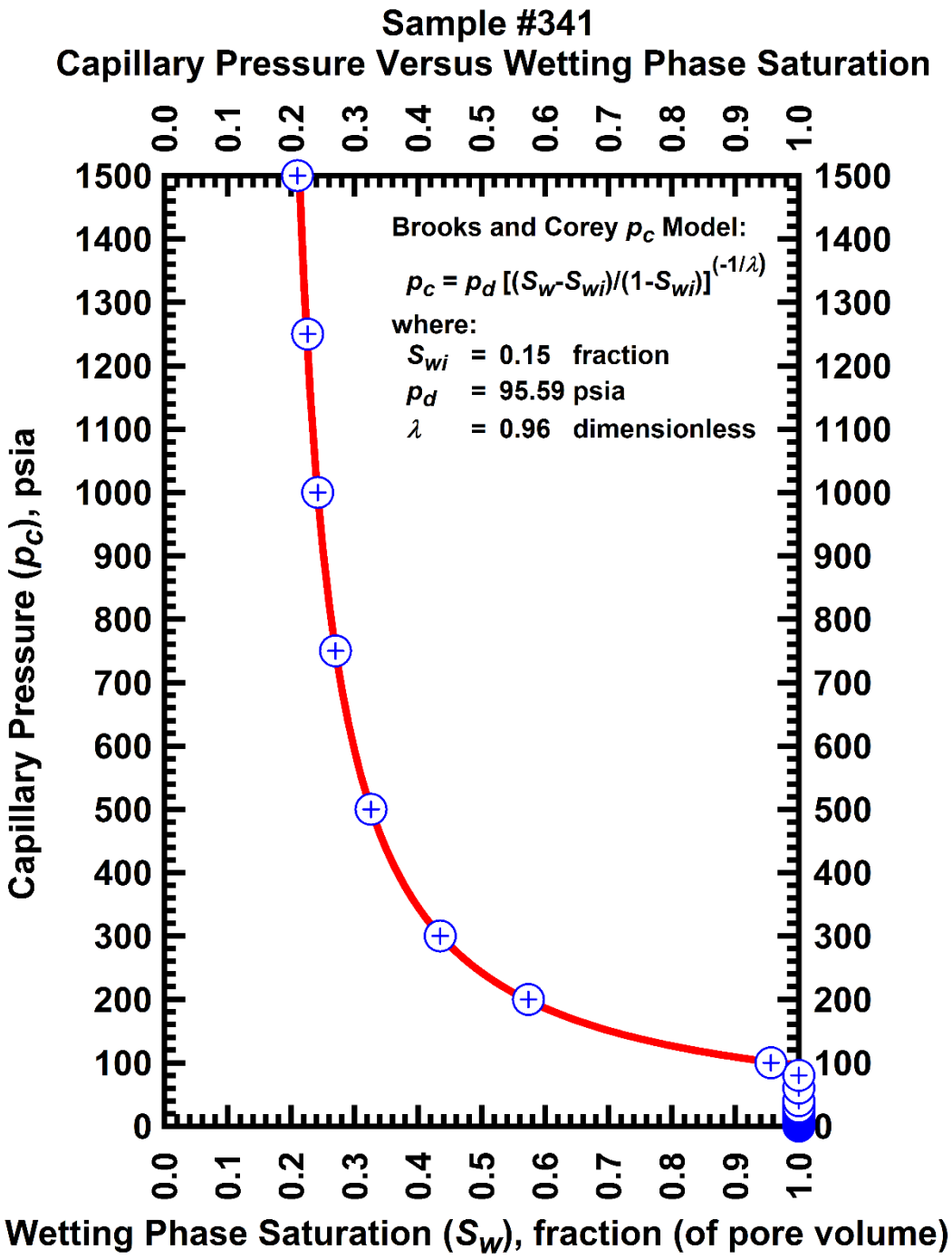

Figure G-10 — Plot of capillary pressure (p_c) vs. wetting phase saturation (S_w) — Sample #341.

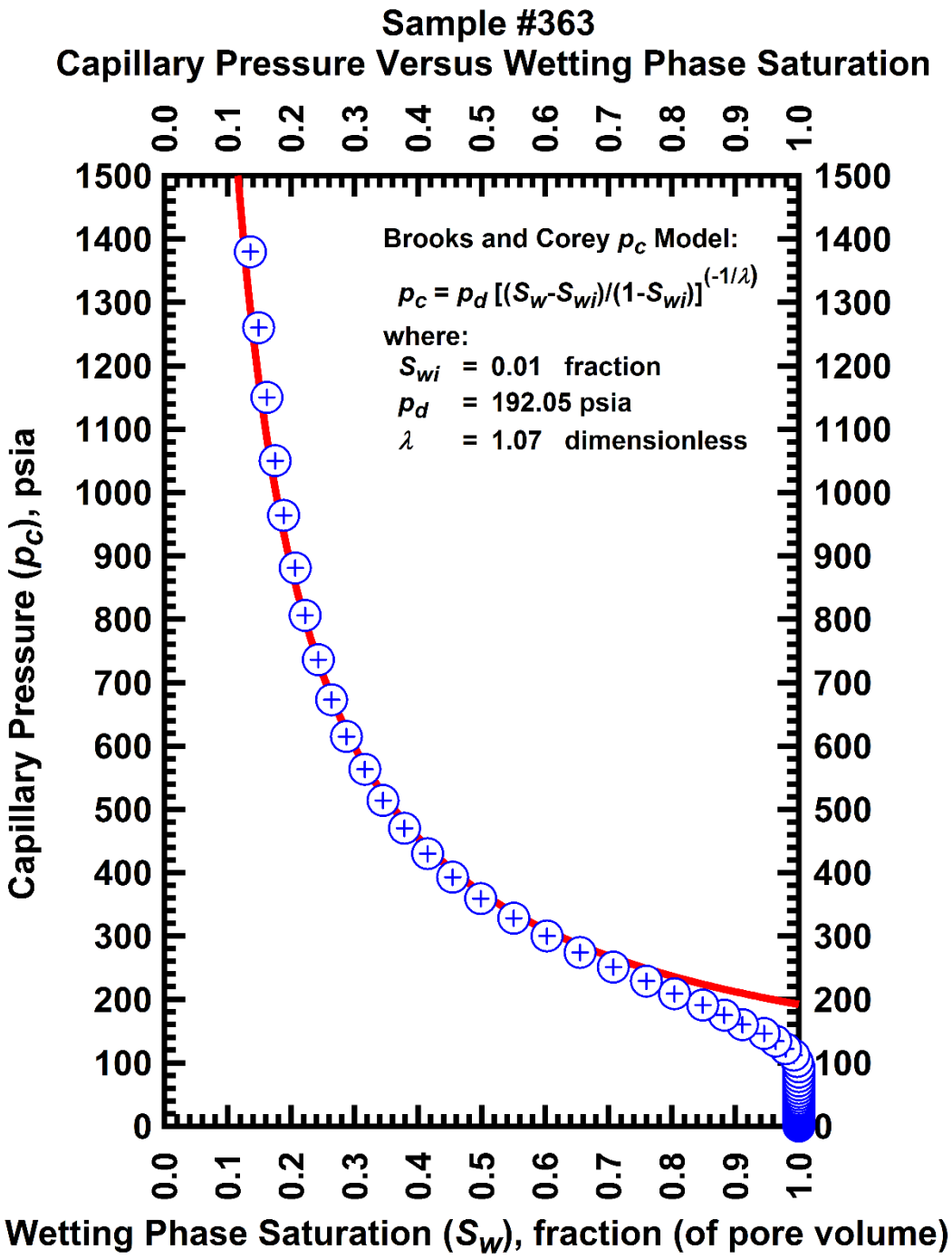

Figure G-11 — Plot of capillary pressure (p_c) vs. wetting phase saturation (S_w) — Sample #363.

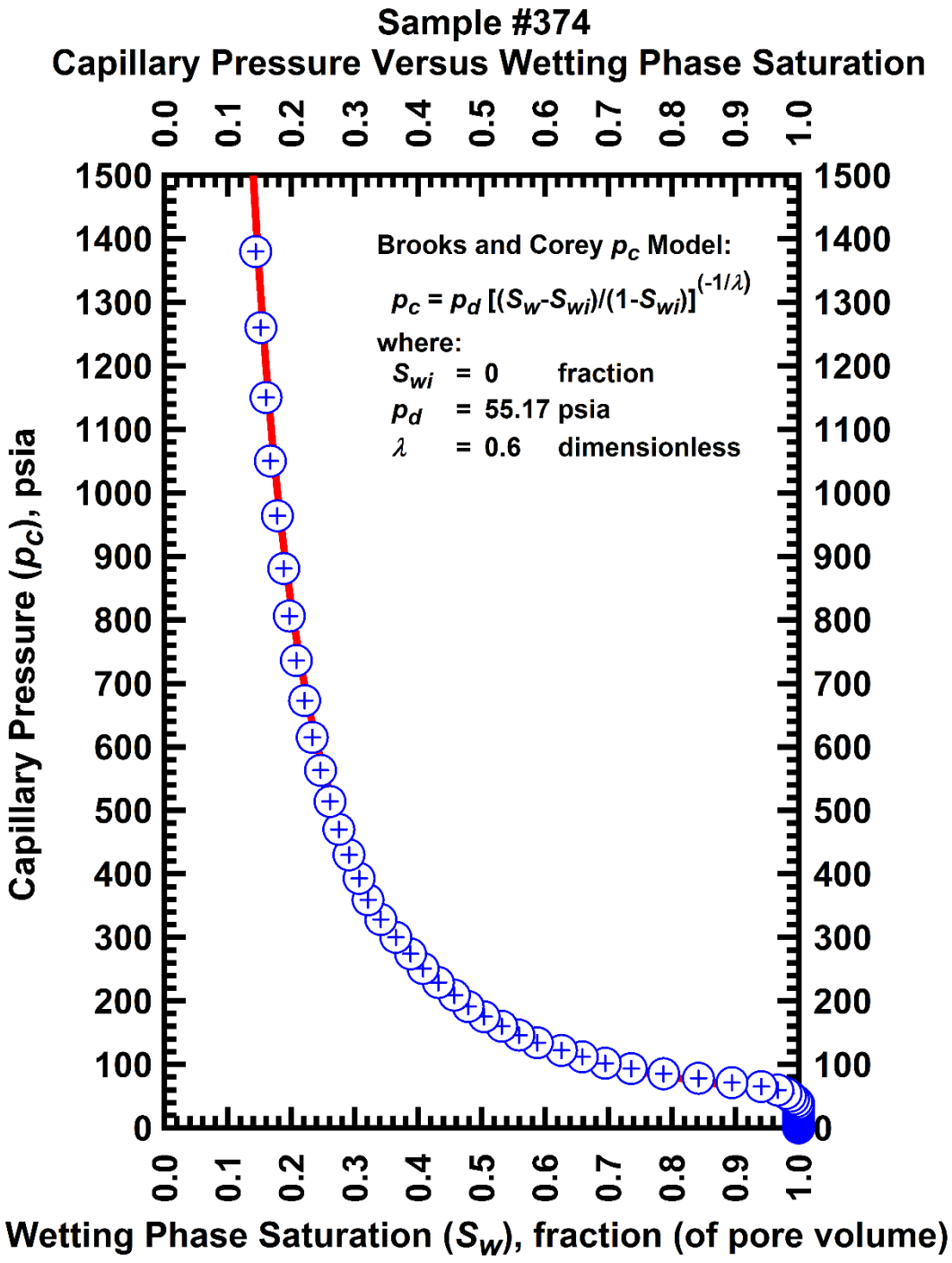

Figure G-12 — Plot of capillary pressure (p_c) vs. wetting phase saturation (S_w) — Sample #374.

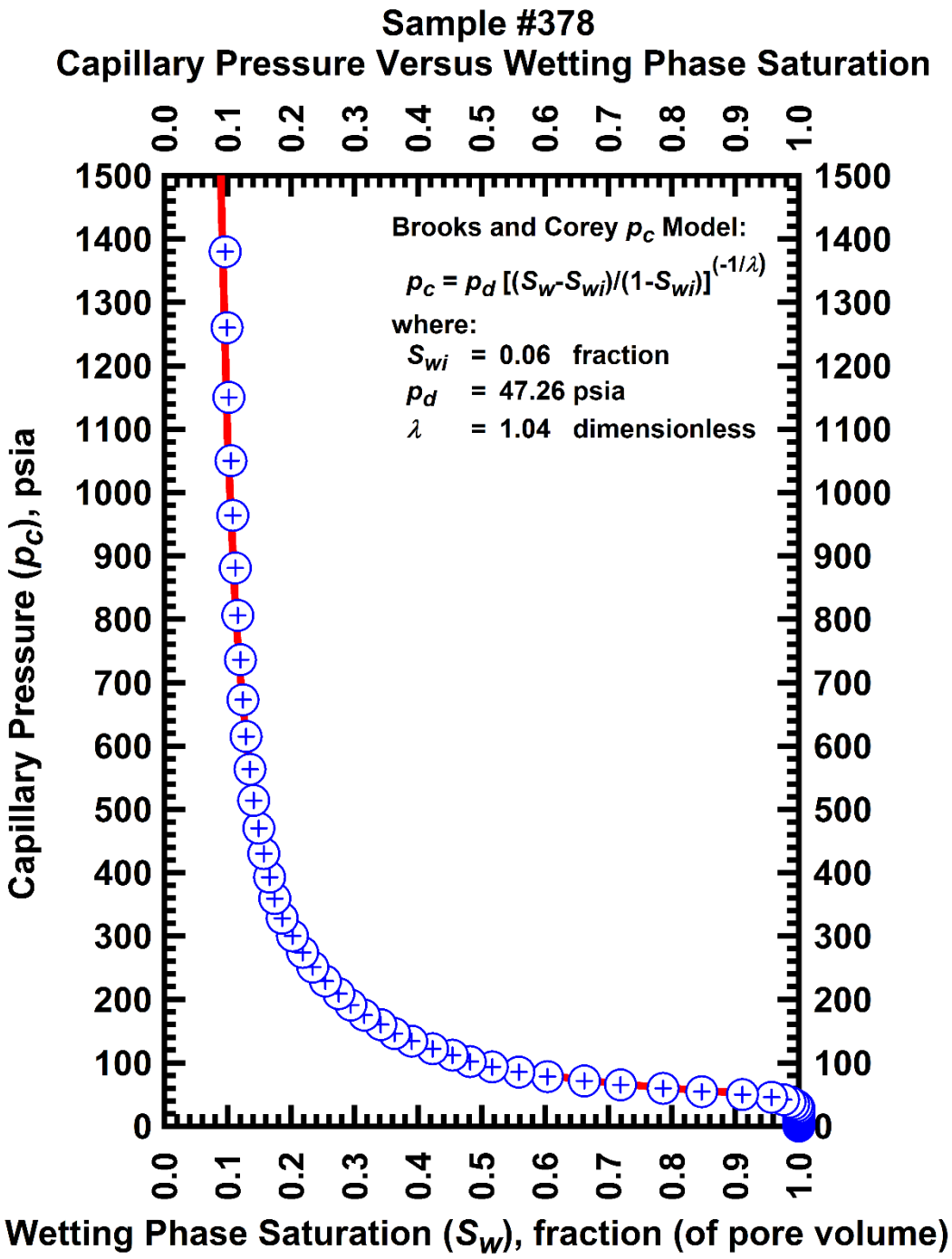

Figure G-13 — Plot of capillary pressure (p_c) vs. wetting phase saturation (S_w) — Sample #378.

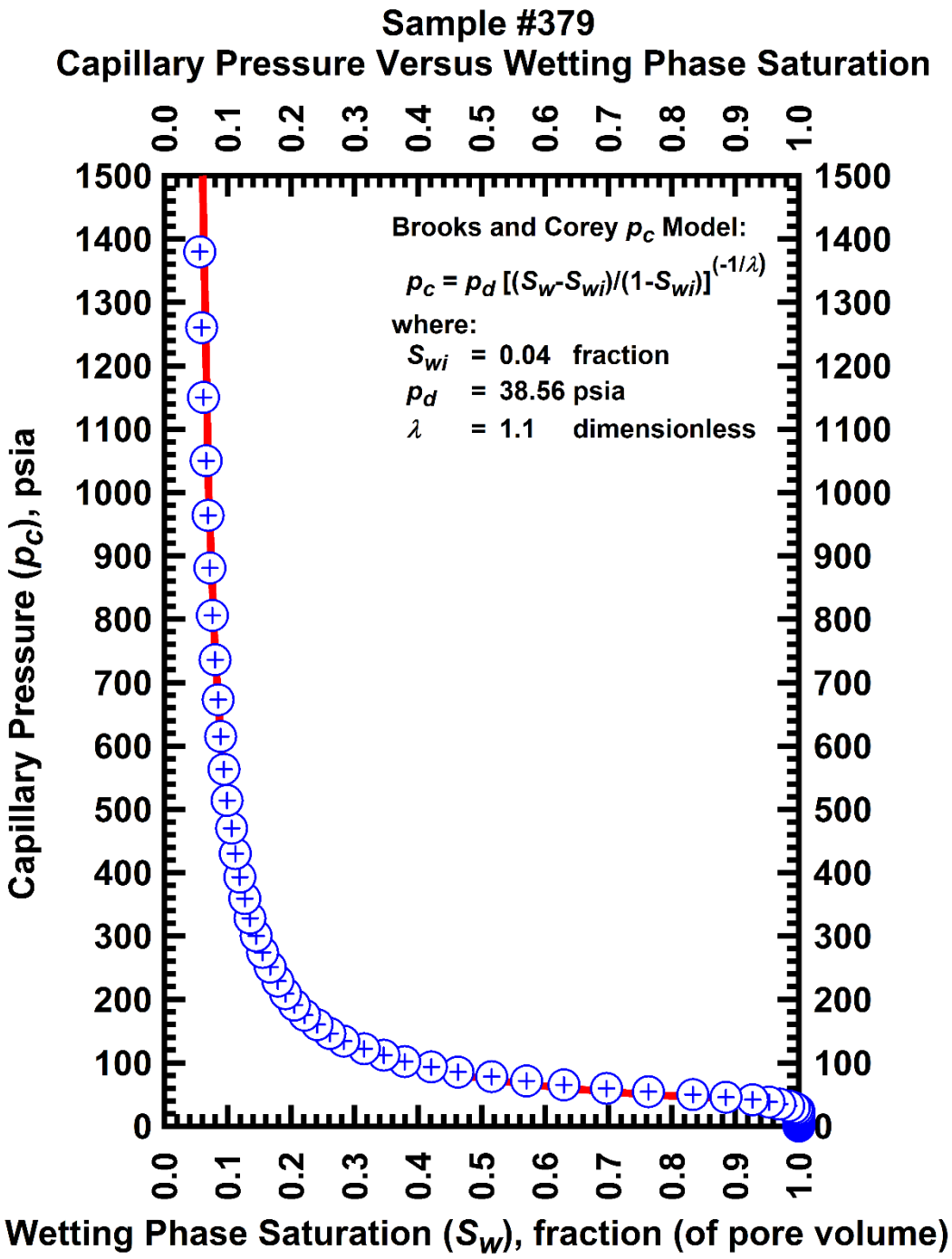

Figure G-14 — Plot of capillary pressure (p_c) vs. wetting phase saturation (S_w) — Sample #379.

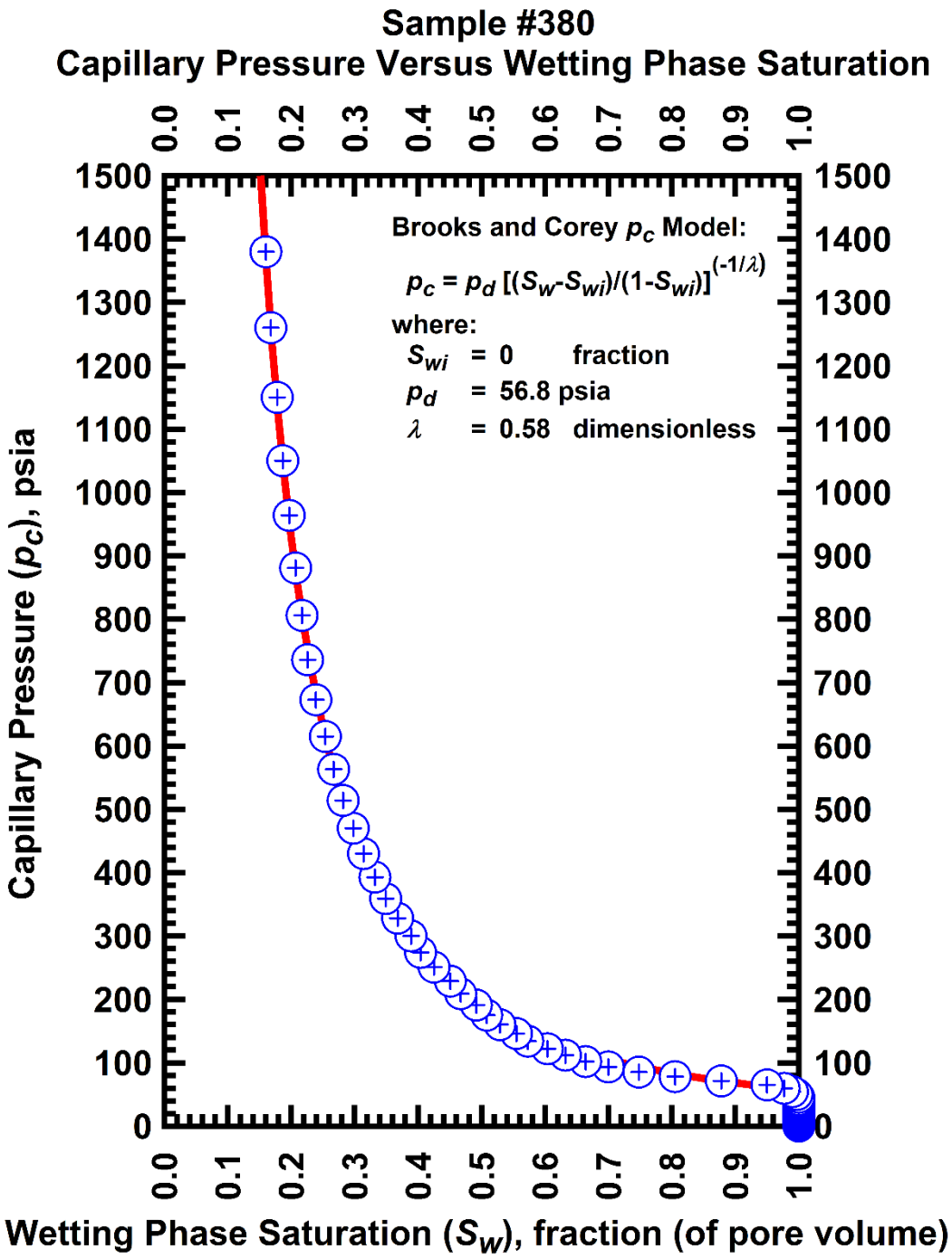

Figure G-15 — Plot of capillary pressure (p_c) vs. wetting phase saturation (S_w) — Sample #380.

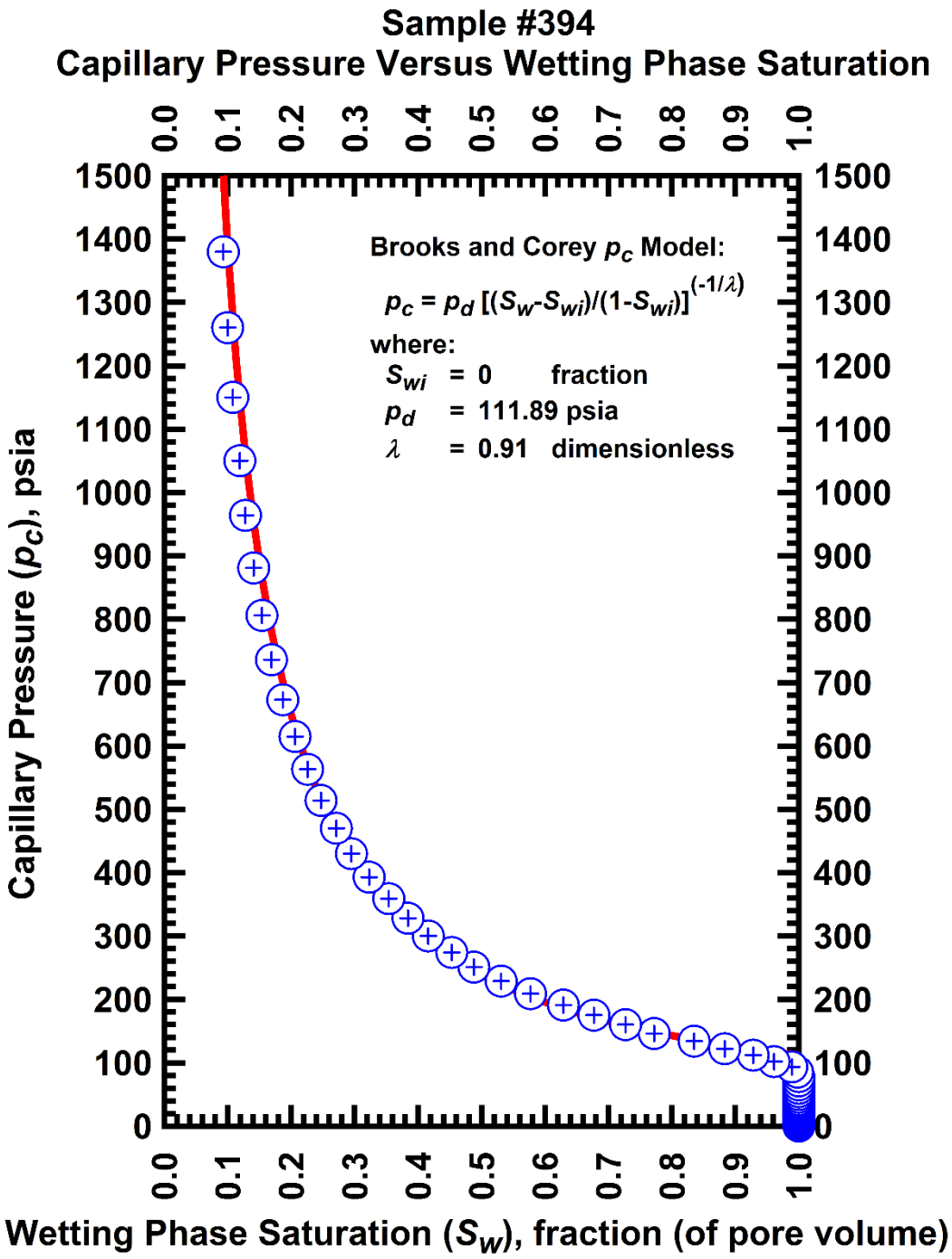

Figure G-16 — Plot of capillary pressure (p_c) vs. wetting phase saturation (S_w) — Sample #394.

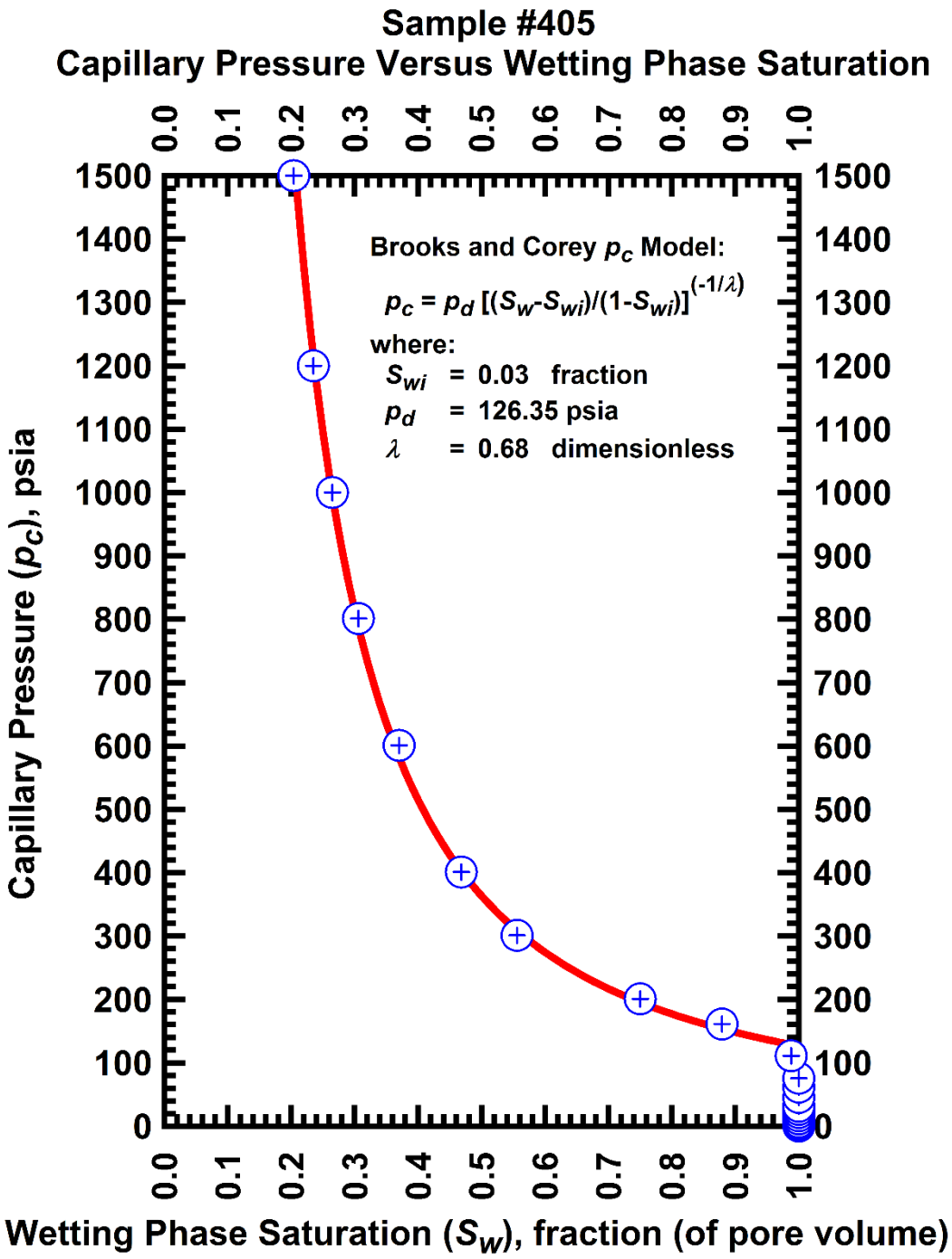

Figure G-17 — Plot of capillary pressure (p_c) vs. wetting phase saturation (S_w) — Sample #405.

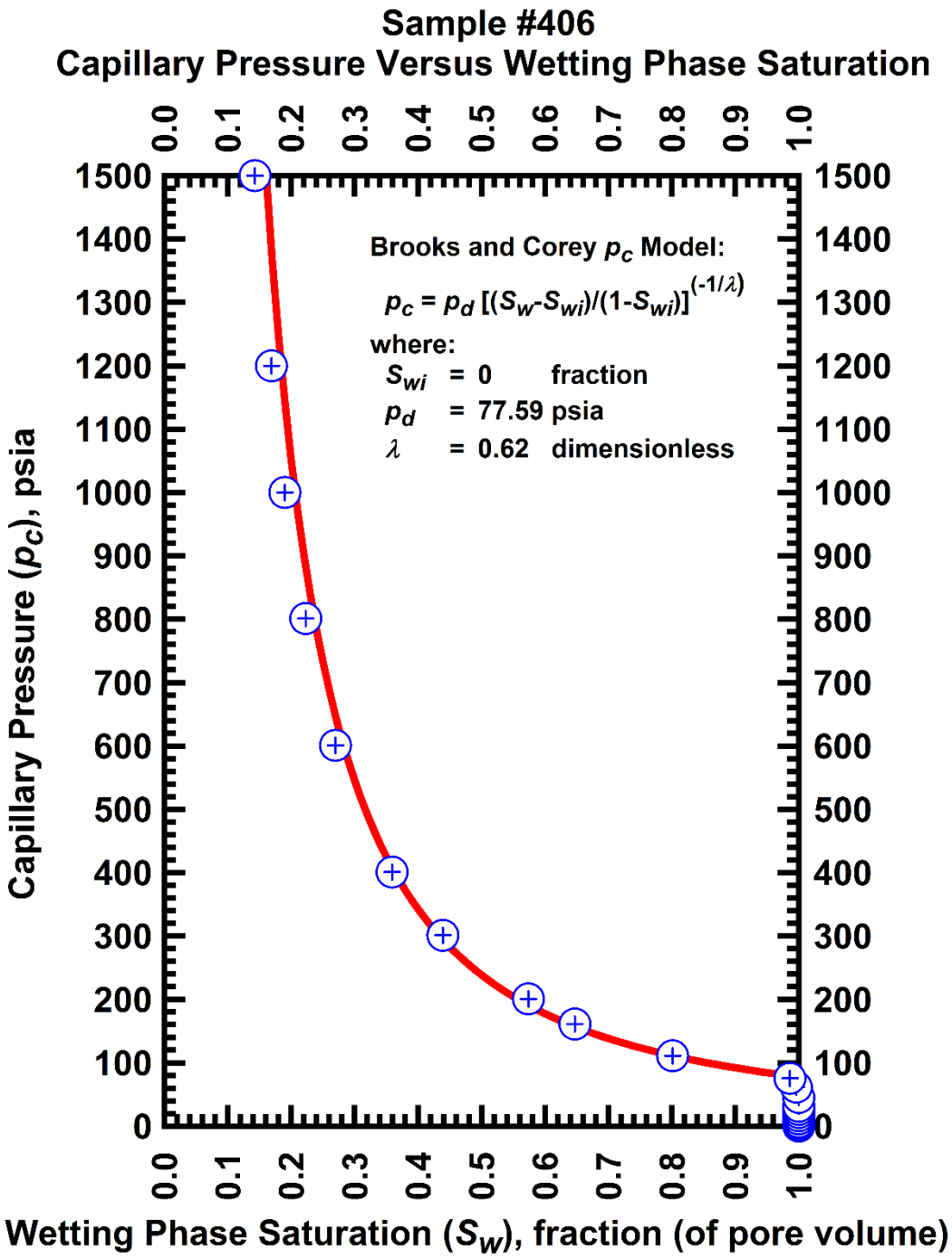

Figure G-18 — Plot of capillary pressure (p_c) vs. wetting phase saturation (S_w) — Sample #406.

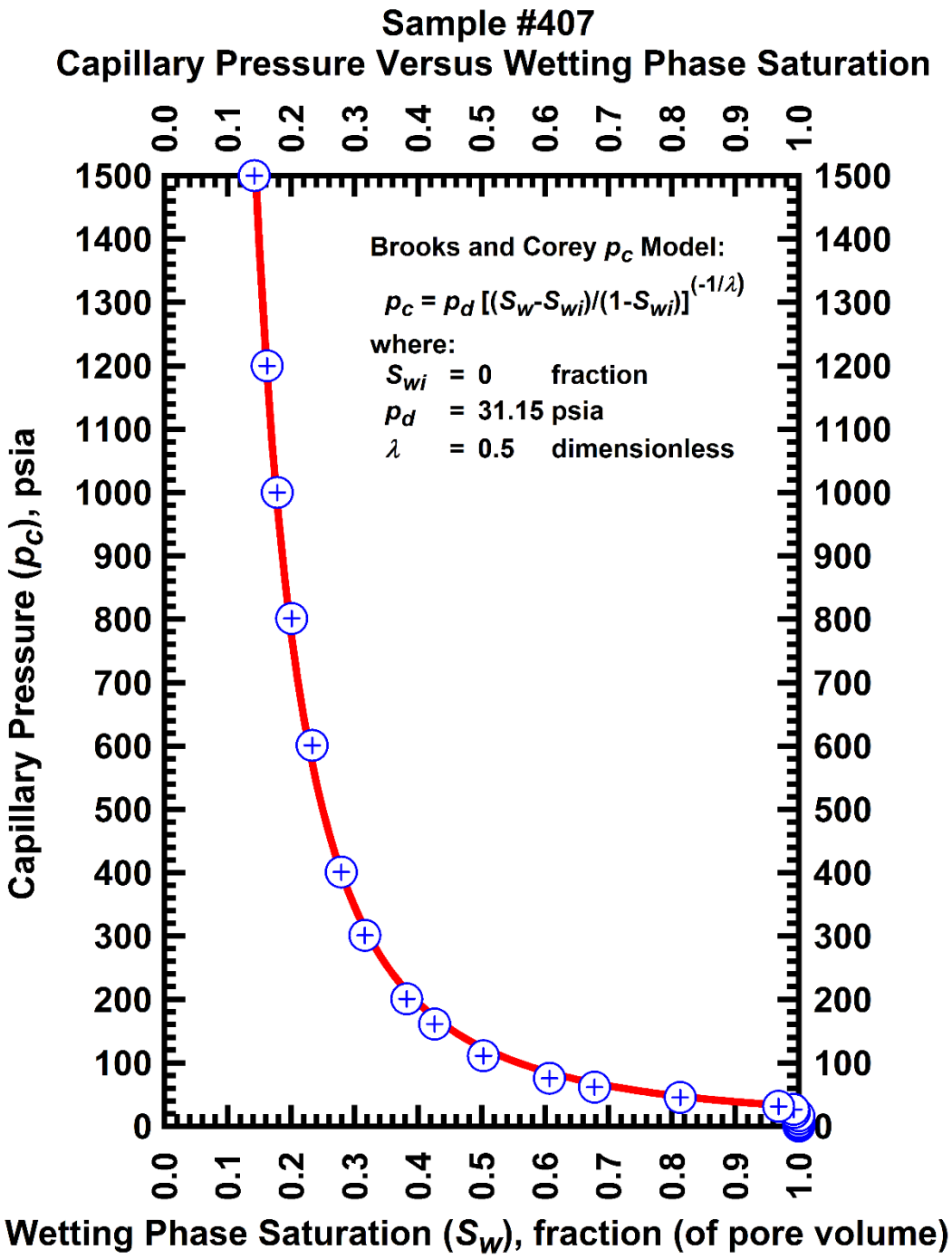

Figure G-19 — Plot of capillary pressure (p_c) vs. wetting phase saturation (S_w) — Sample #407.

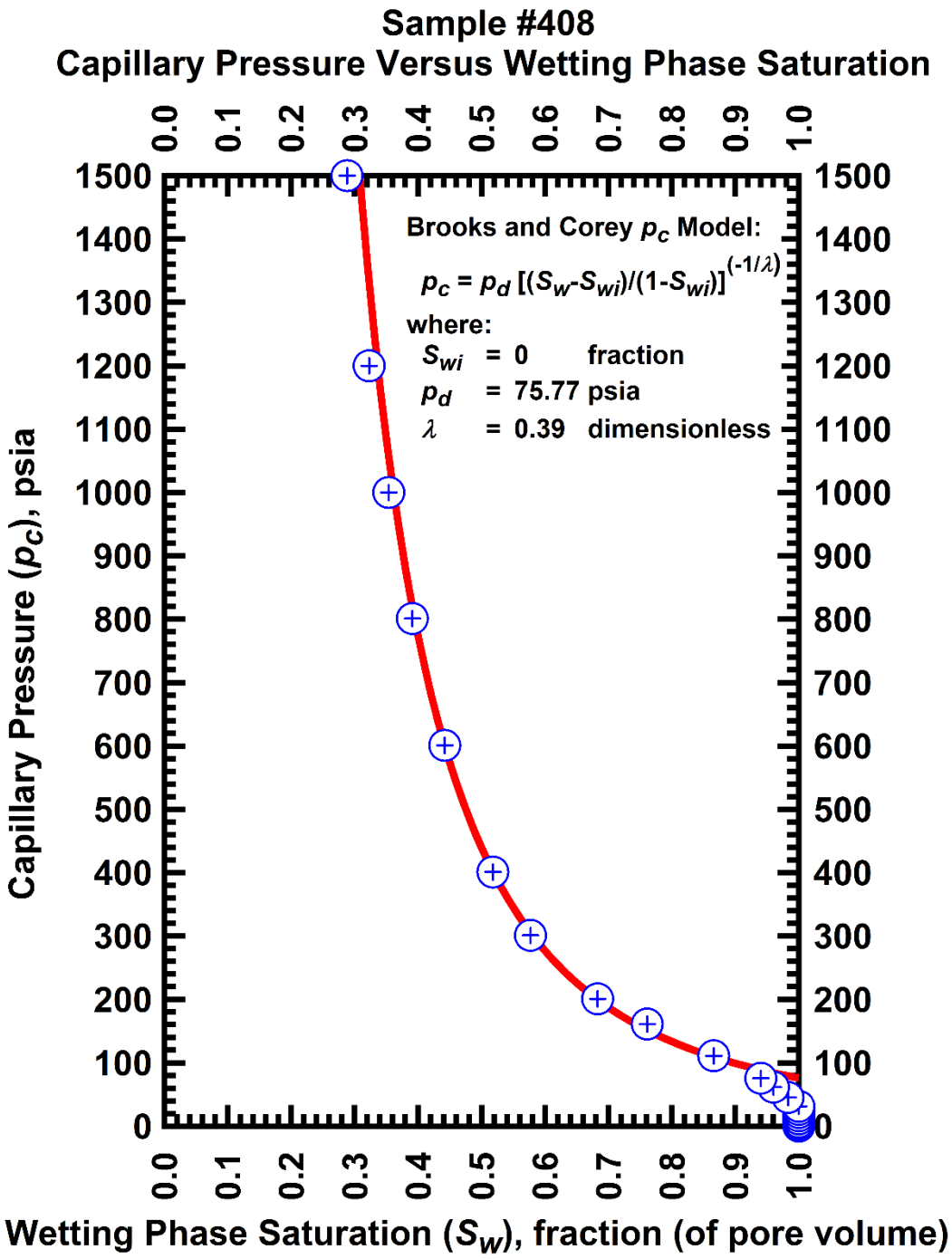

Figure G-20 — Plot of capillary pressure (p_c) vs. wetting phase saturation (S_w) — Sample #408.

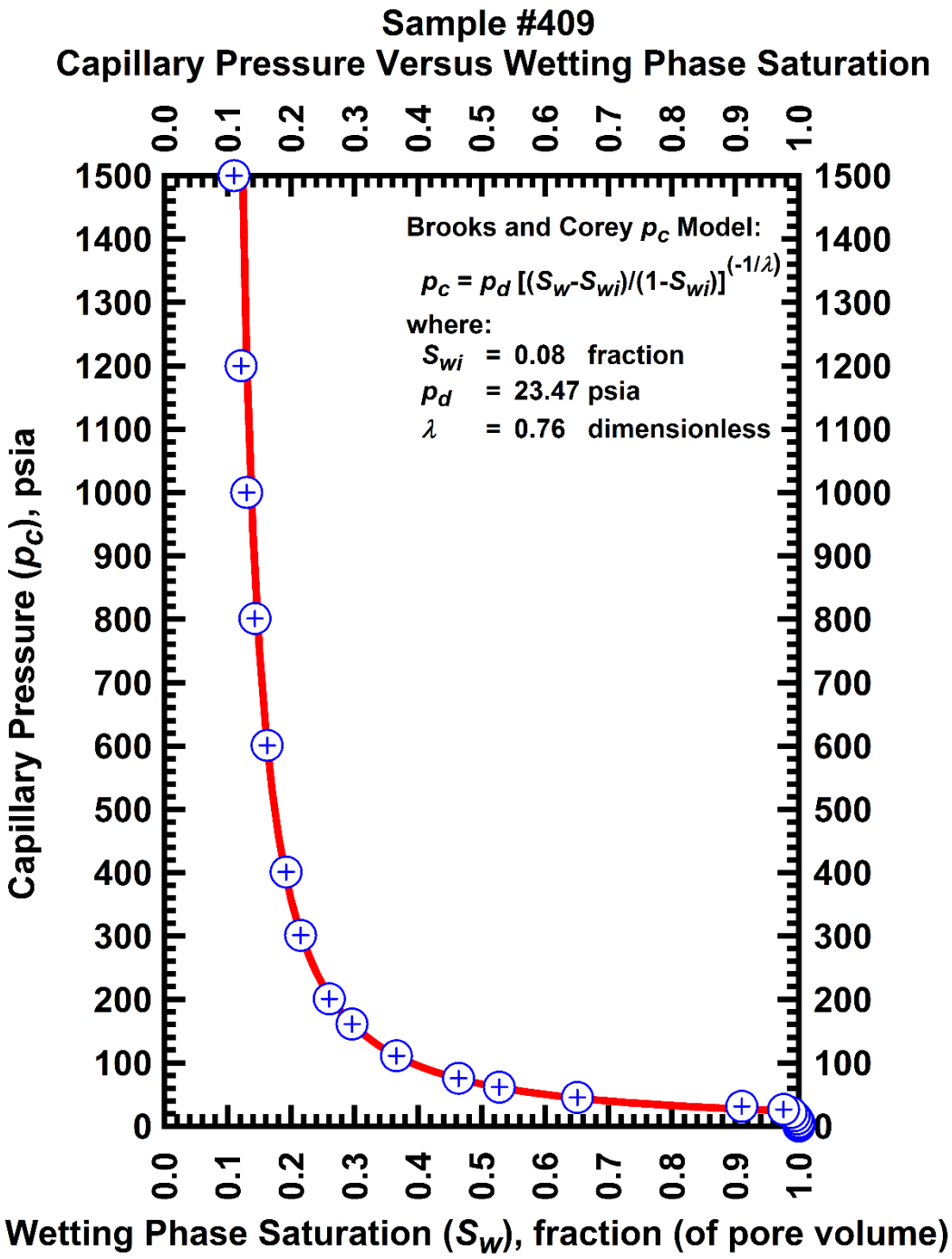

Figure G-21 — Plot of capillary pressure (p_c) vs. wetting phase saturation (S_w) — Sample #409.

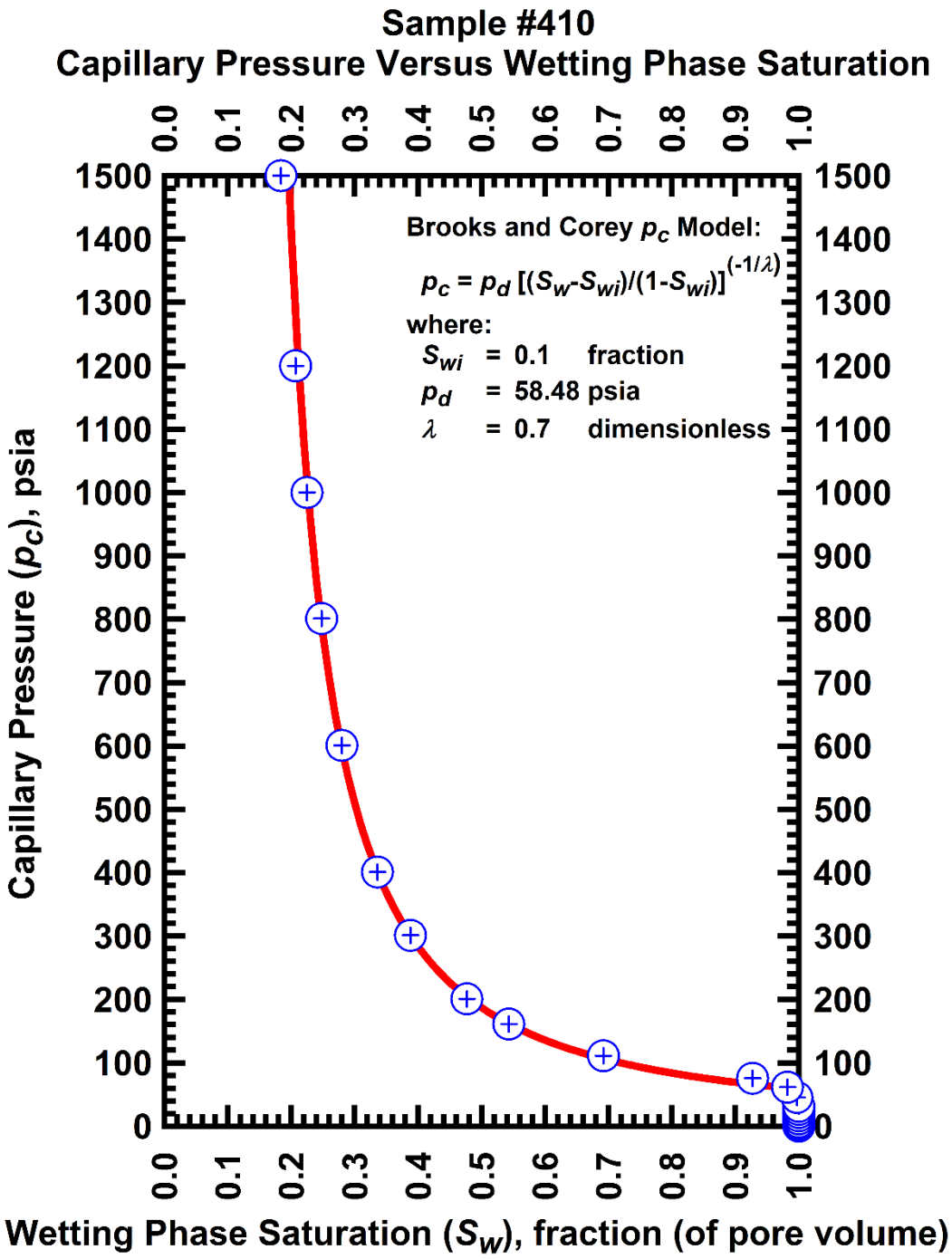

Figure G-22 — Plot of capillary pressure (p_c) vs. wetting phase saturation (S_w) — Sample #410.

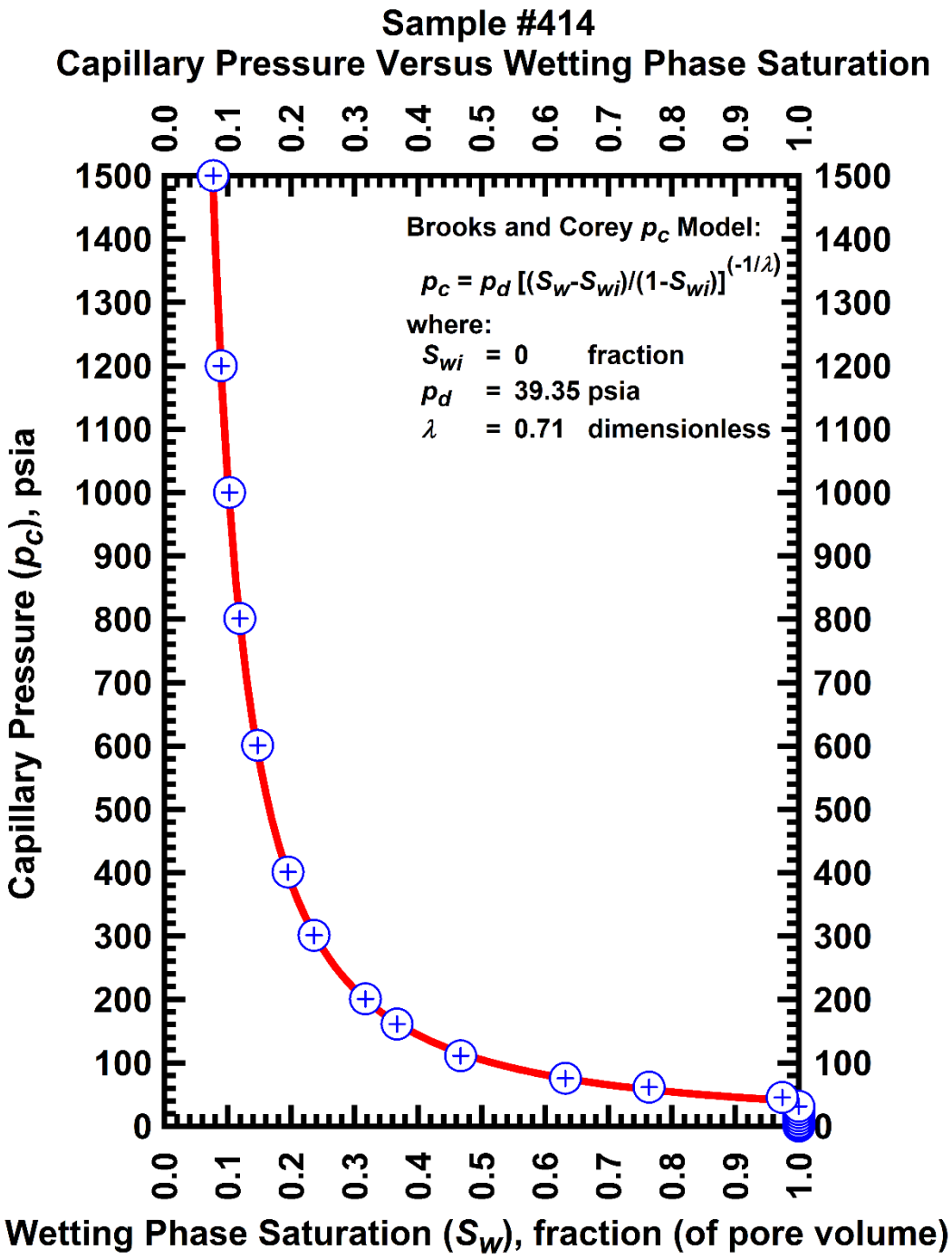

Figure G-23 — Plot of capillary pressure (p_c) vs. wetting phase saturation (S_w) — Sample #414.

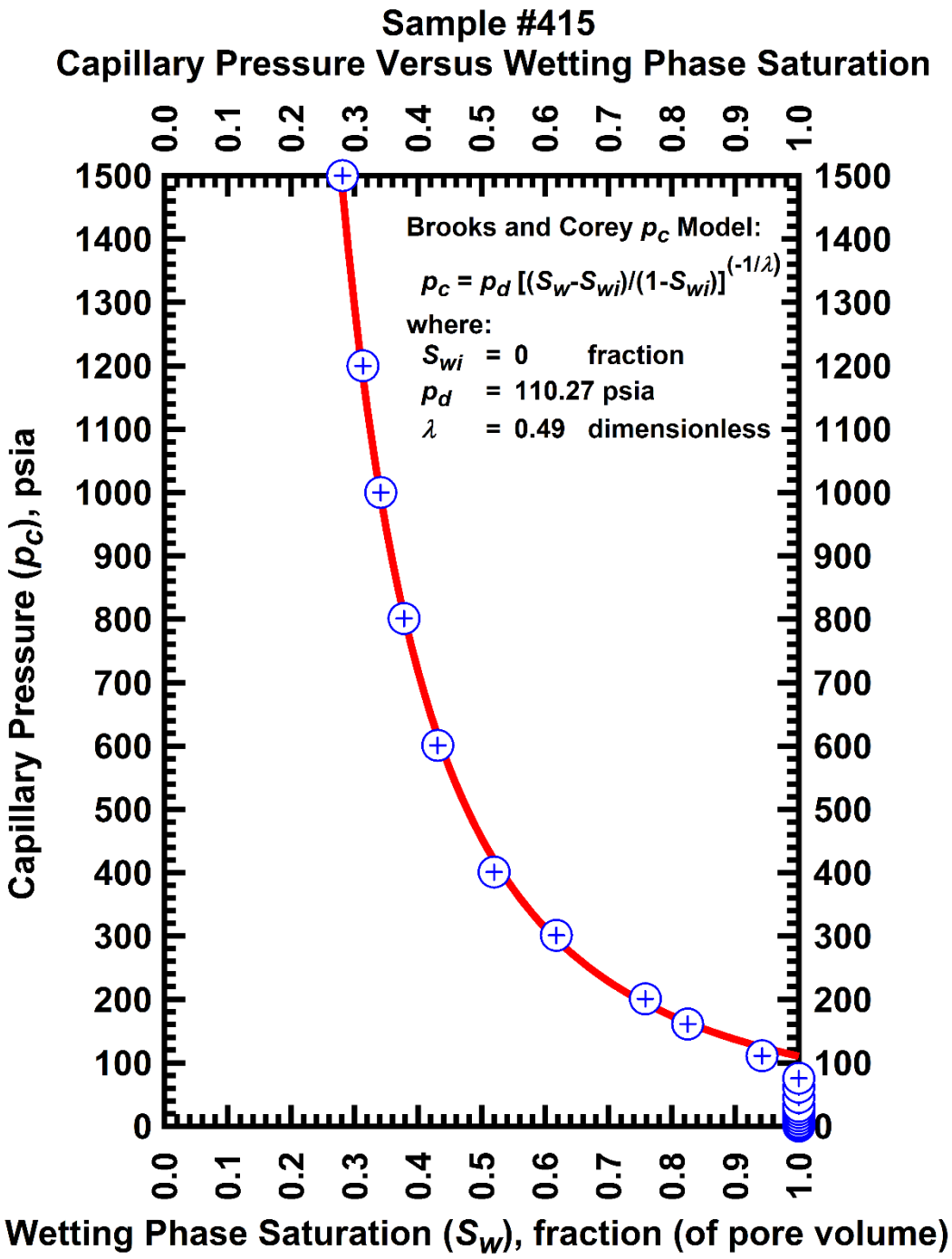

Figure G-24 — Plot of capillary pressure (p_c) vs. wetting phase saturation (S_w) — Sample #415.

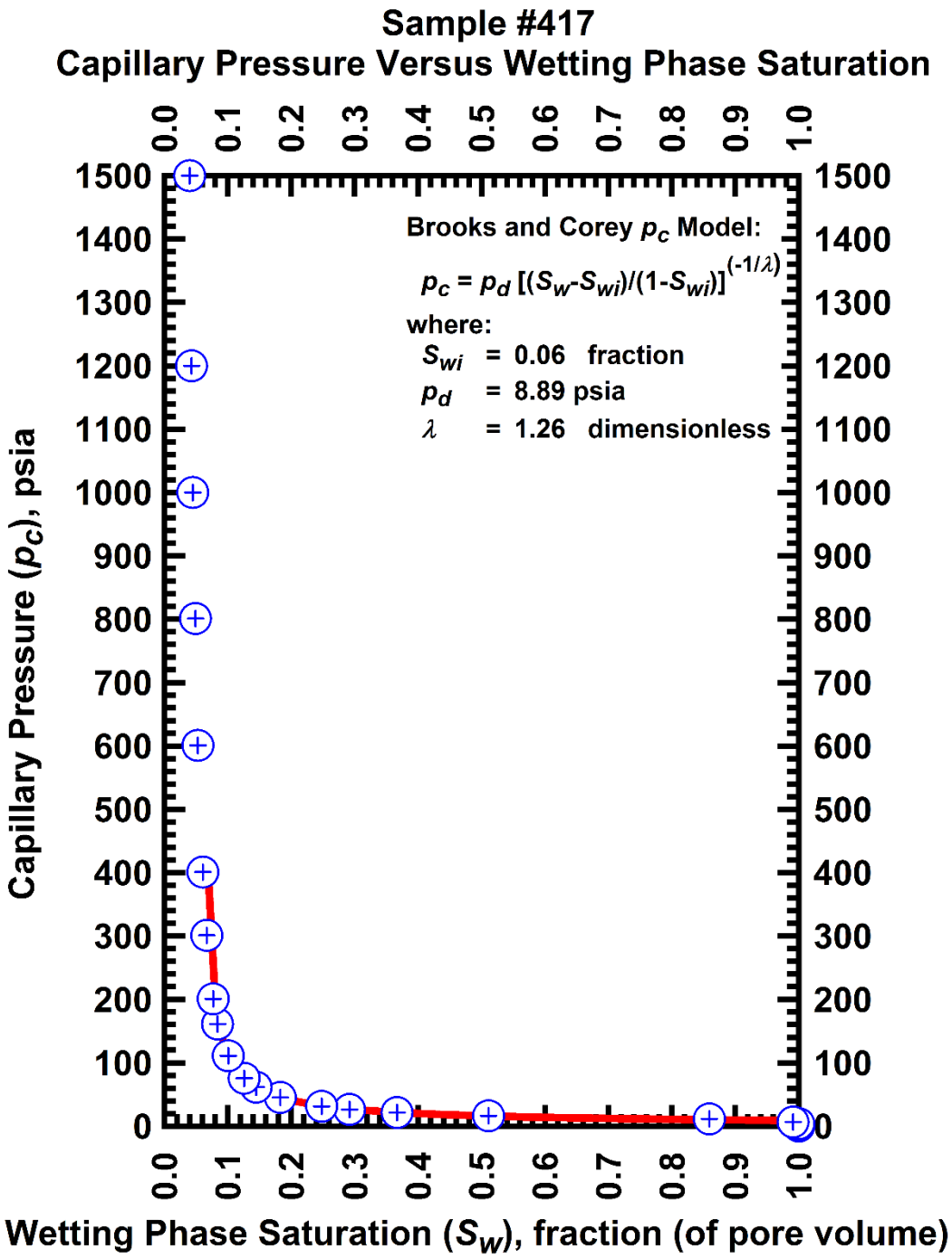

Figure G-25 — Plot of capillary pressure (p_c) vs. wetting phase saturation (S_w) — Sample #417.

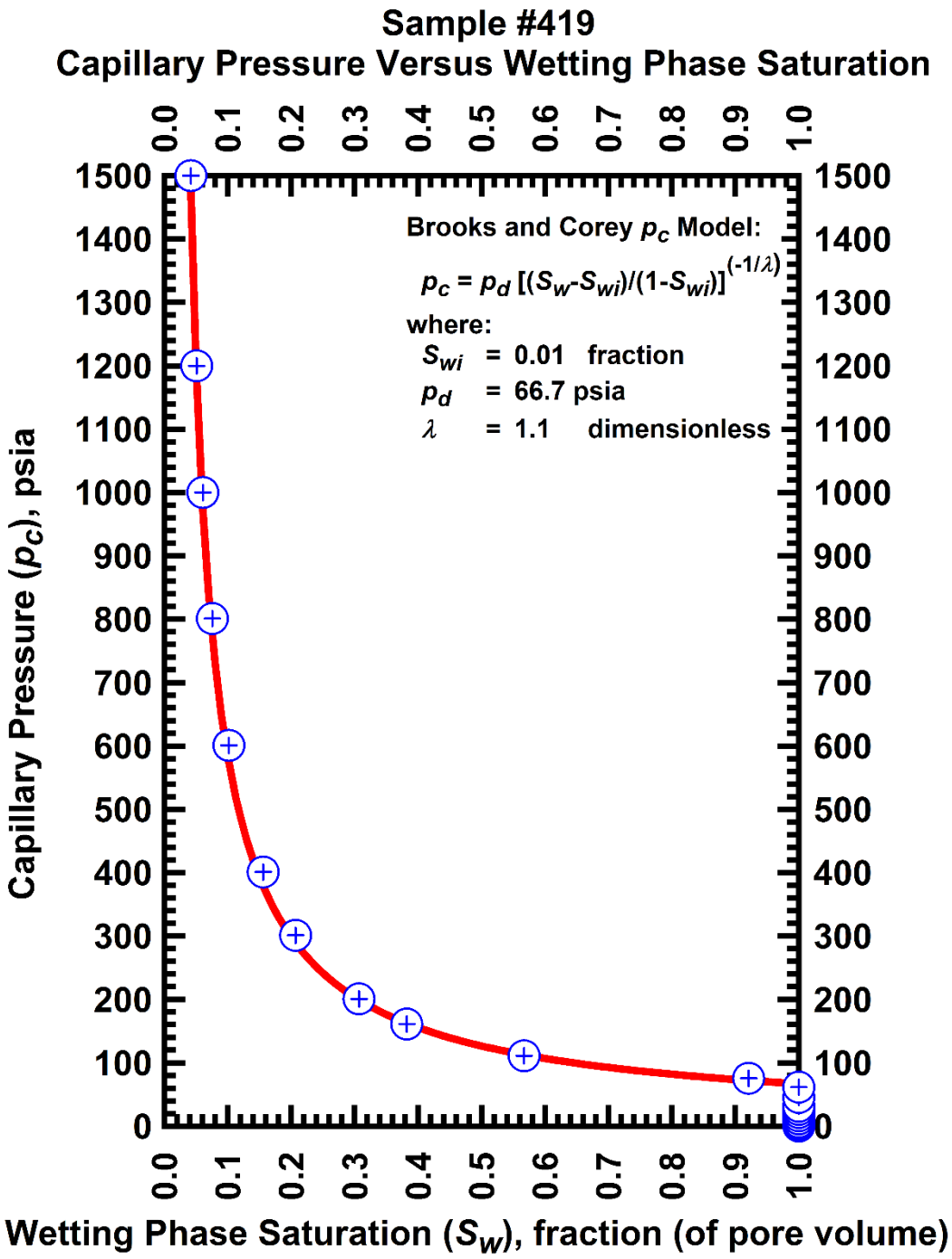

Figure G-26 — Plot of capillary pressure (p_c) vs. wetting phase saturation (S_w) — Sample #419.

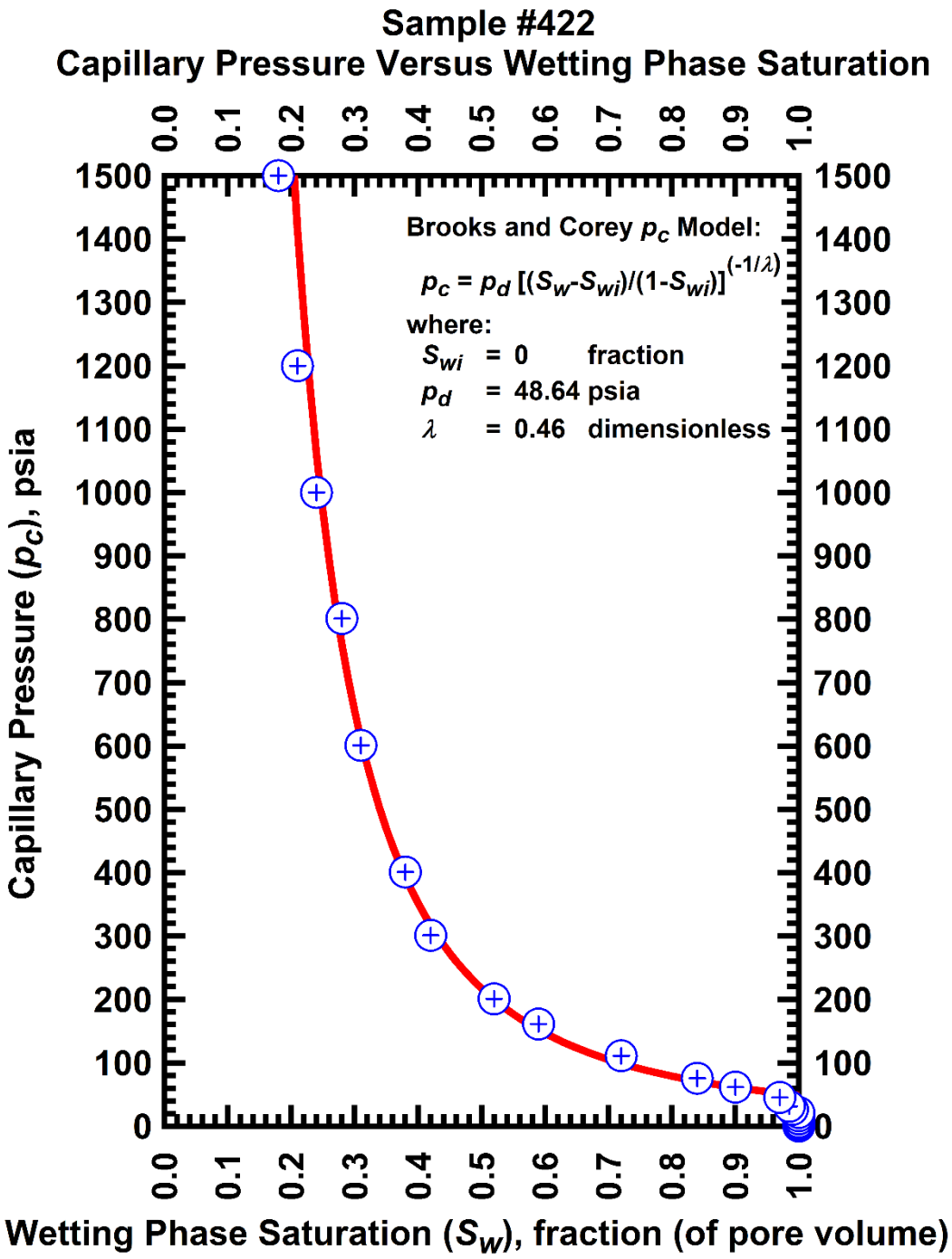

Figure G-27 — Plot of capillary pressure (p_c) vs. wetting phase saturation (S_w) — Sample #422.

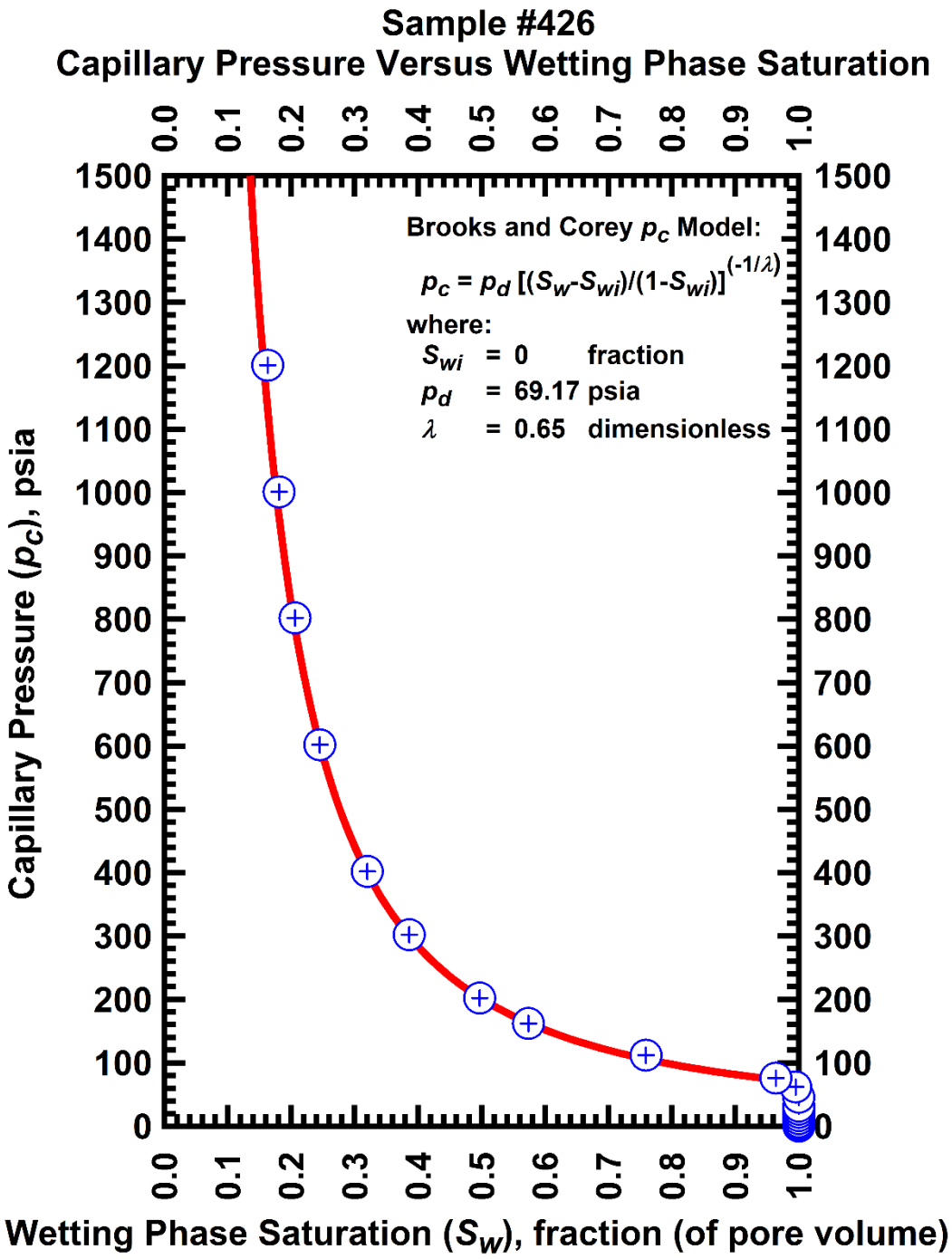

Figure G-28 — Plot of capillary pressure (p_c) vs. wetting phase saturation (S_w) — Sample #426.

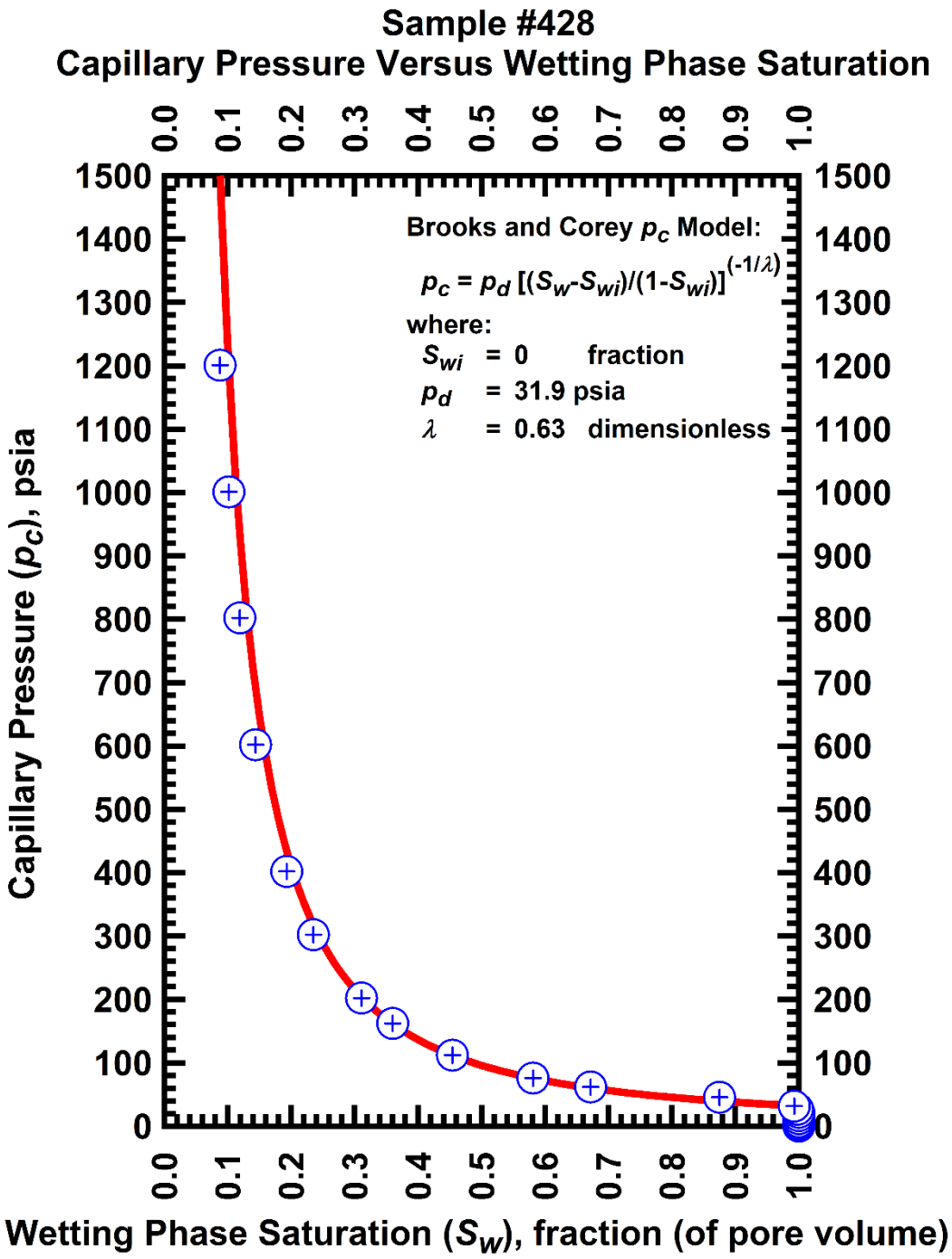

Figure G-29 — Plot of capillary pressure (p_c) vs. wetting phase saturation (S_w) — Sample #428.

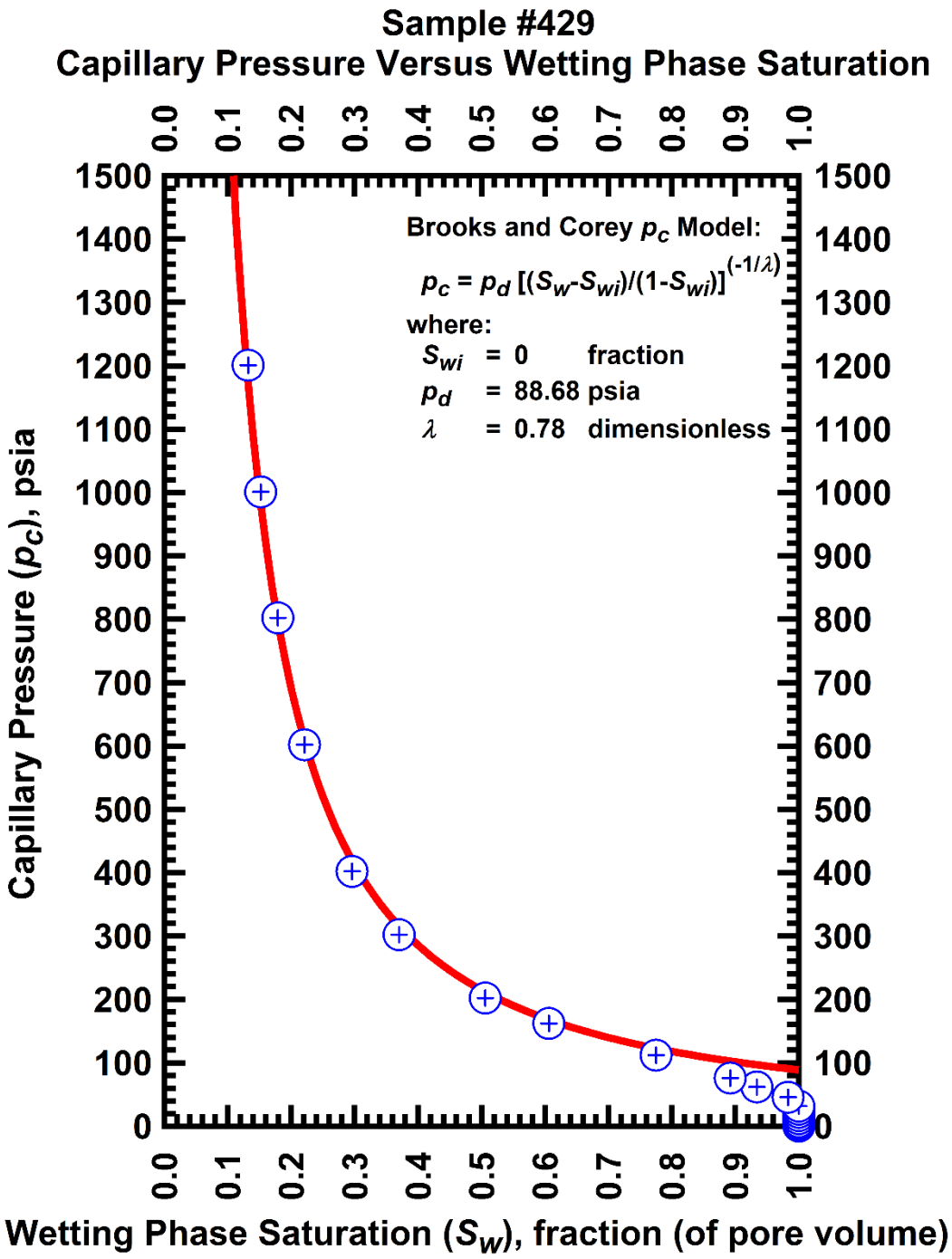

Figure G-30 — Plot of capillary pressure (p_c) vs. wetting phase saturation (S_w) — Sample #429.

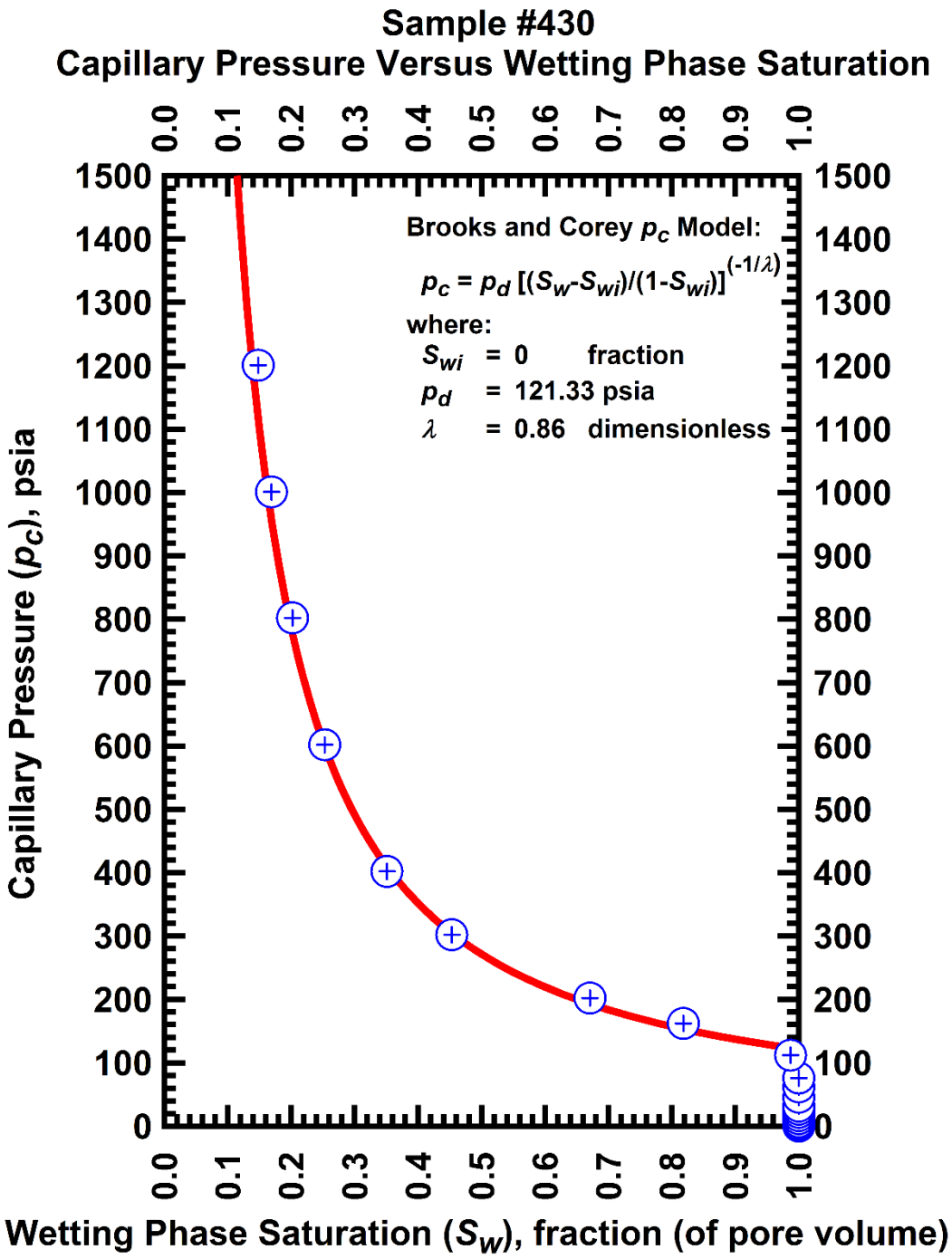

Figure G-31 — Plot of capillary pressure (p_c) vs. wetting phase saturation (S_w) — Sample #430.

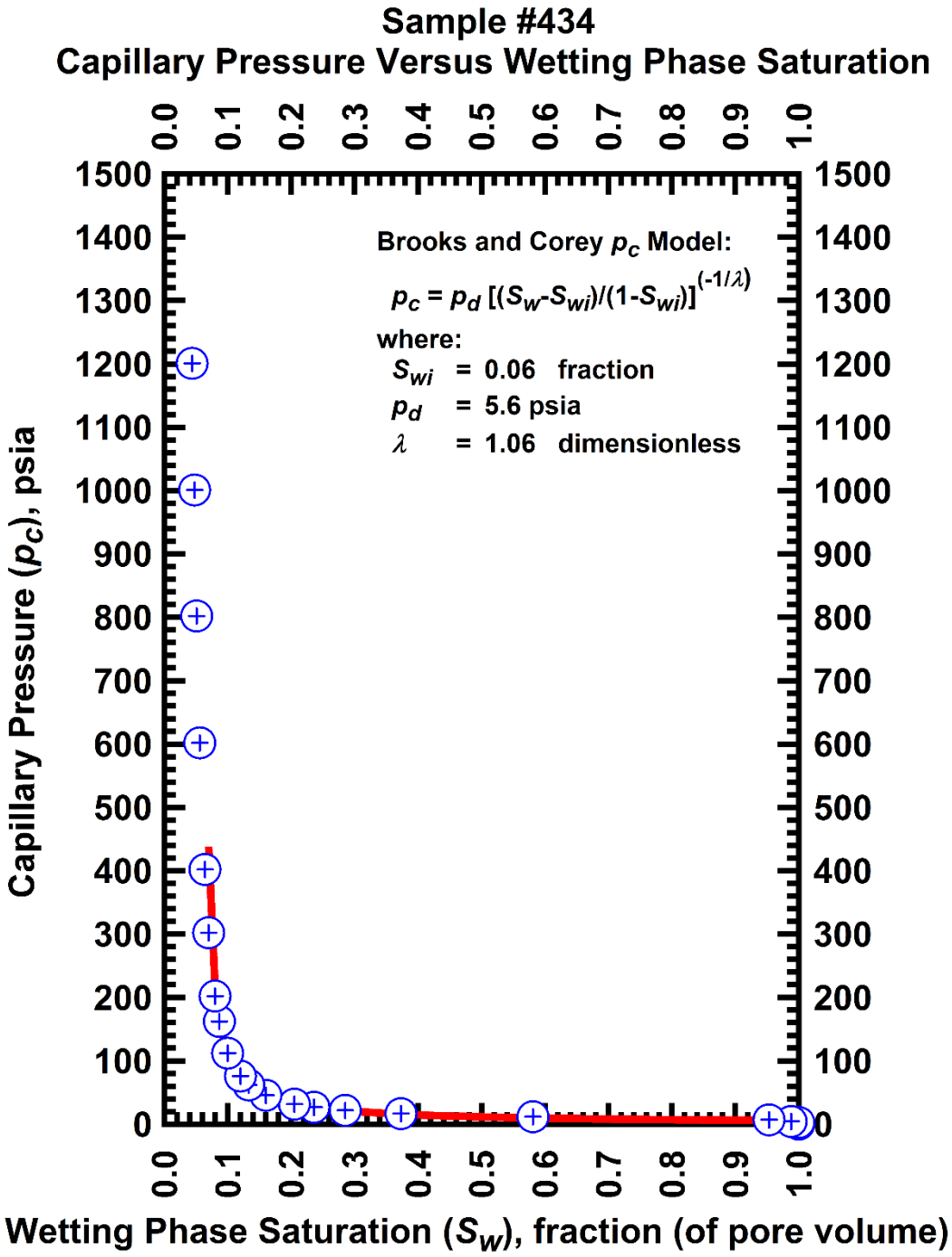

Figure G-32 — Plot of capillary pressure (p_c) vs. wetting phase saturation (S_w) — Sample #434.

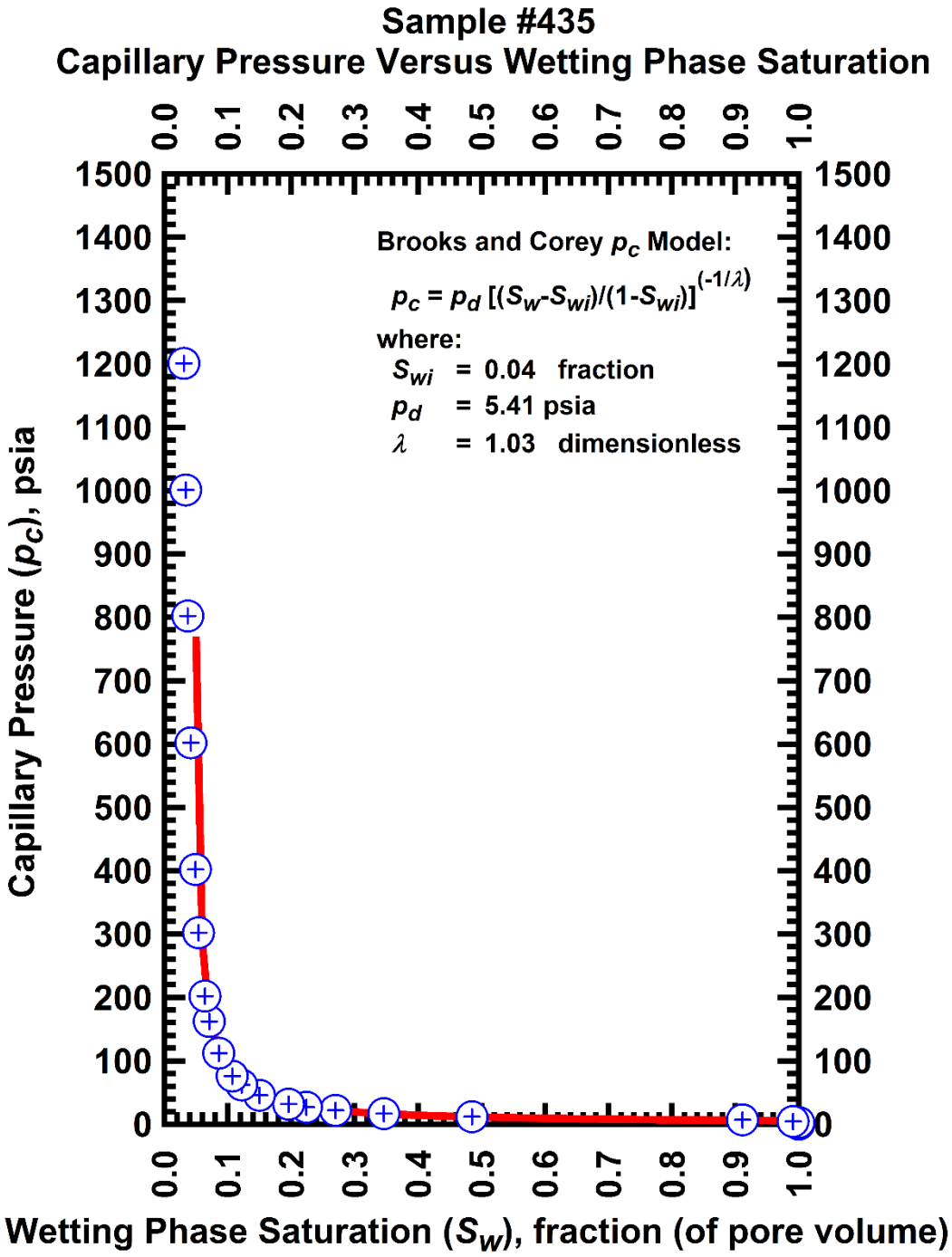

Figure G-33 — Plot of capillary pressure (p_c) vs. wetting phase saturation (S_w) — Sample #435.

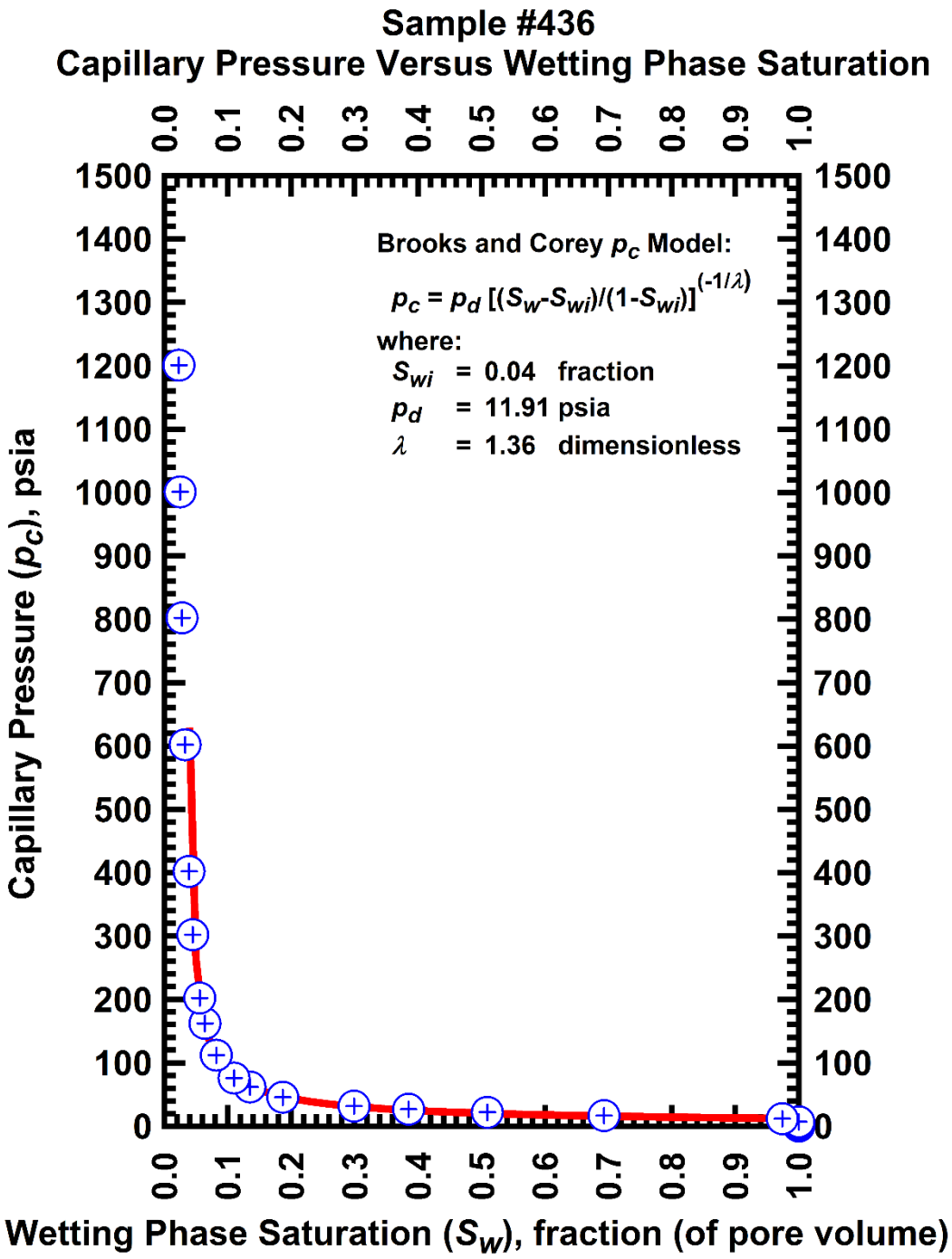

Figure G-34 — Plot of capillary pressure (p_c) vs. wetting phase saturation (S_w) — Sample #436.

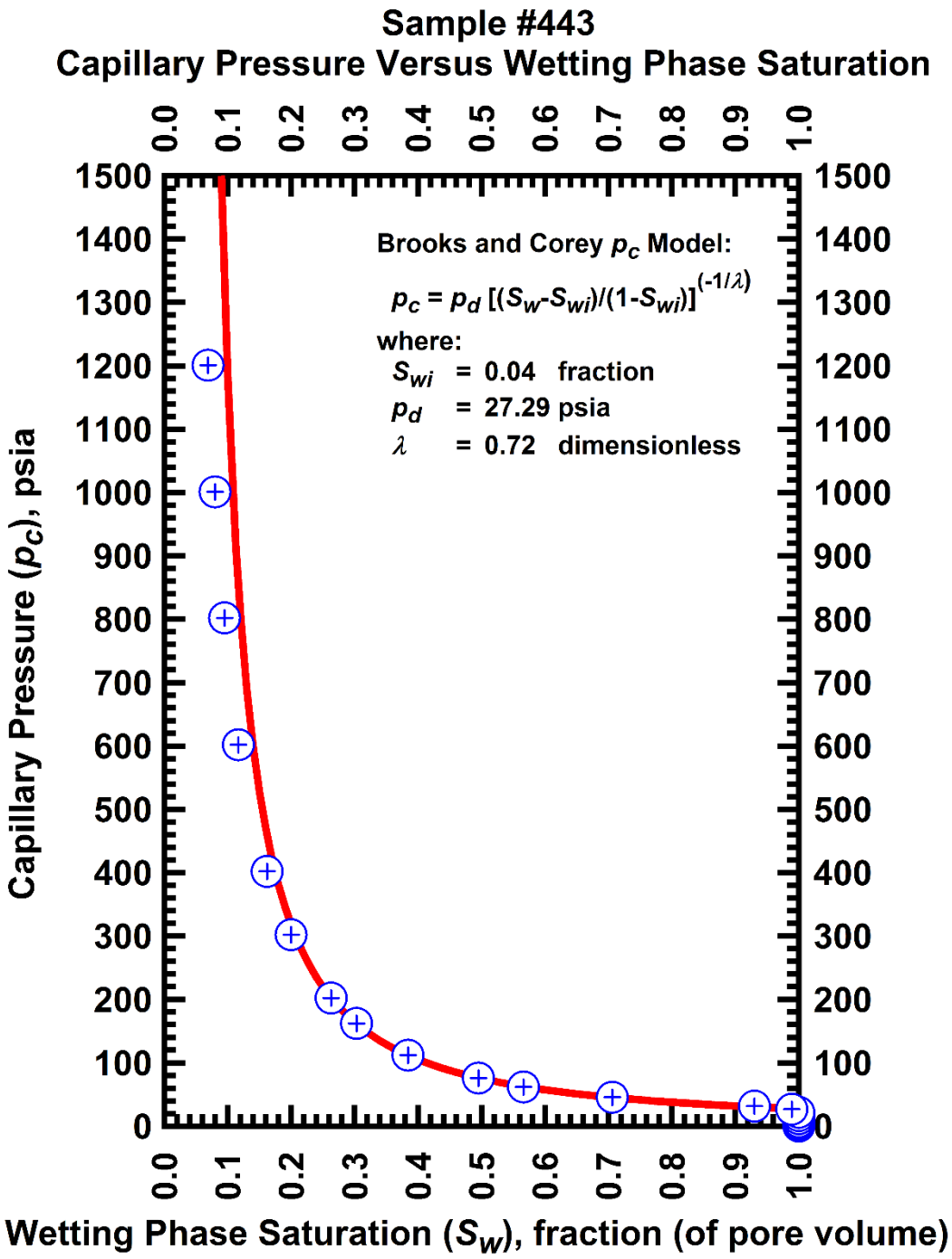

Figure G-35 — Plot of capillary pressure (p_c) vs. wetting phase saturation (S_w) — Sample #443.

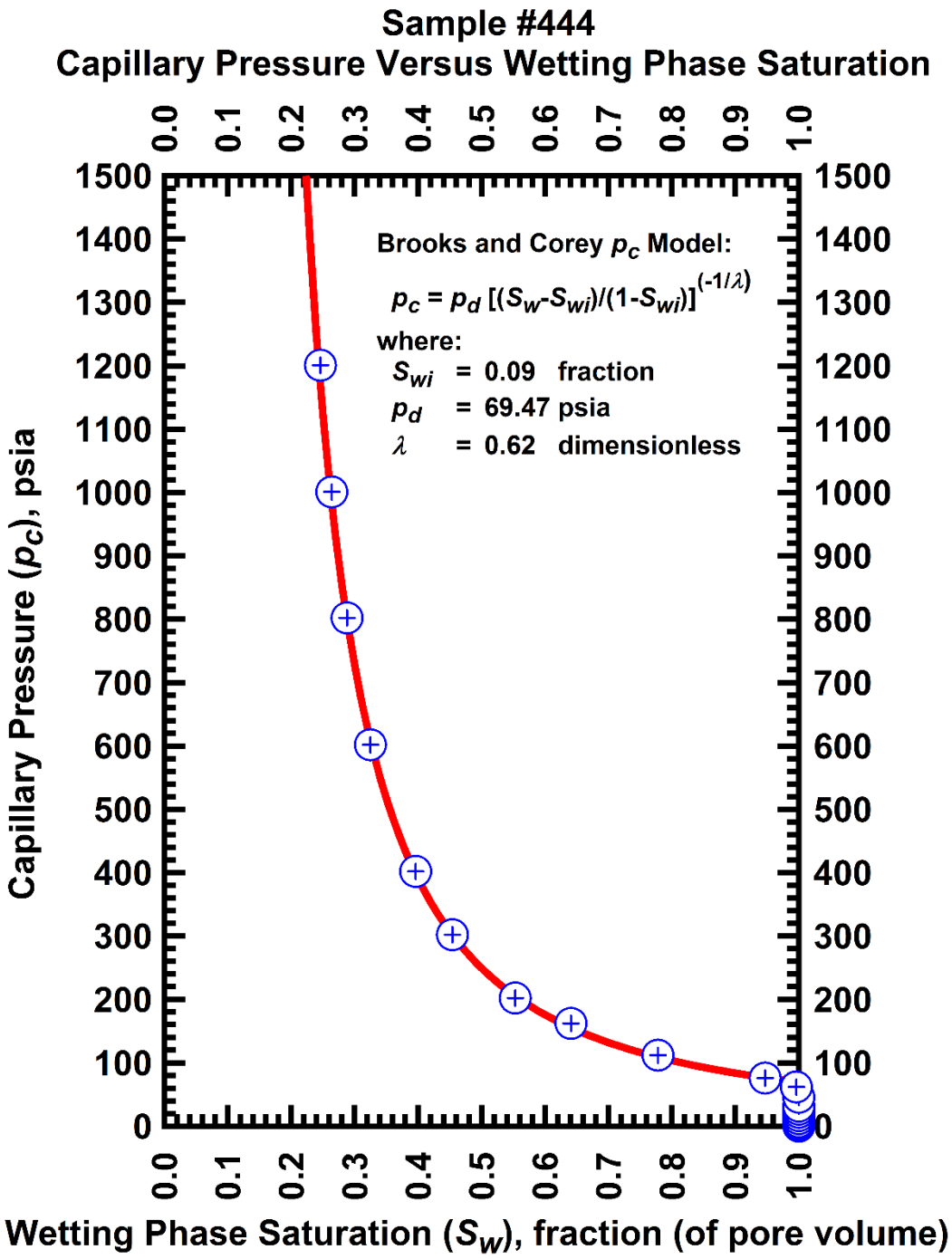

Figure G-36 — Plot of capillary pressure (p_c) vs. wetting phase saturation (S_w) — Sample #444.

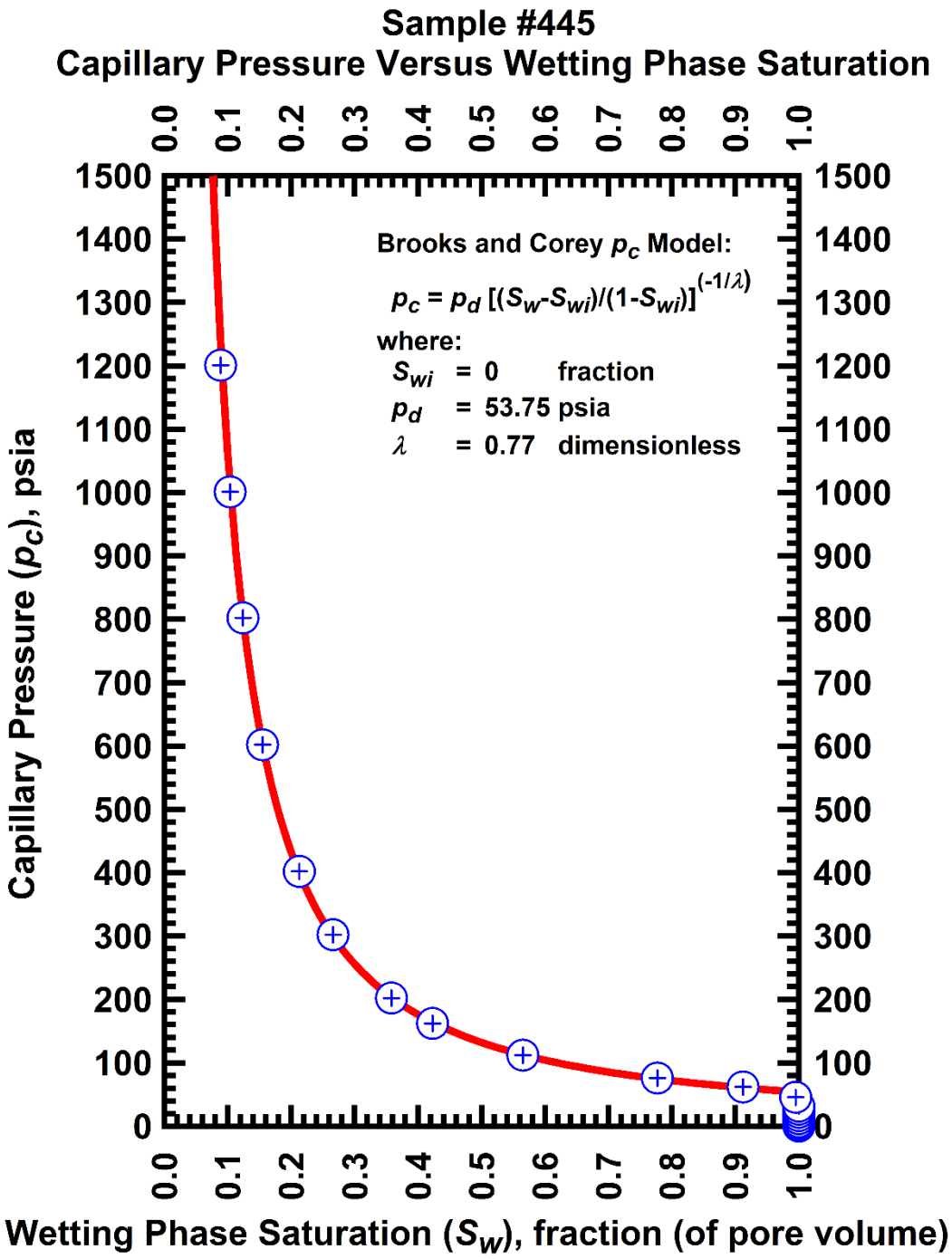

Figure G-37 — Plot of capillary pressure (p_c) vs. wetting phase saturation (S_w) — Sample #445.

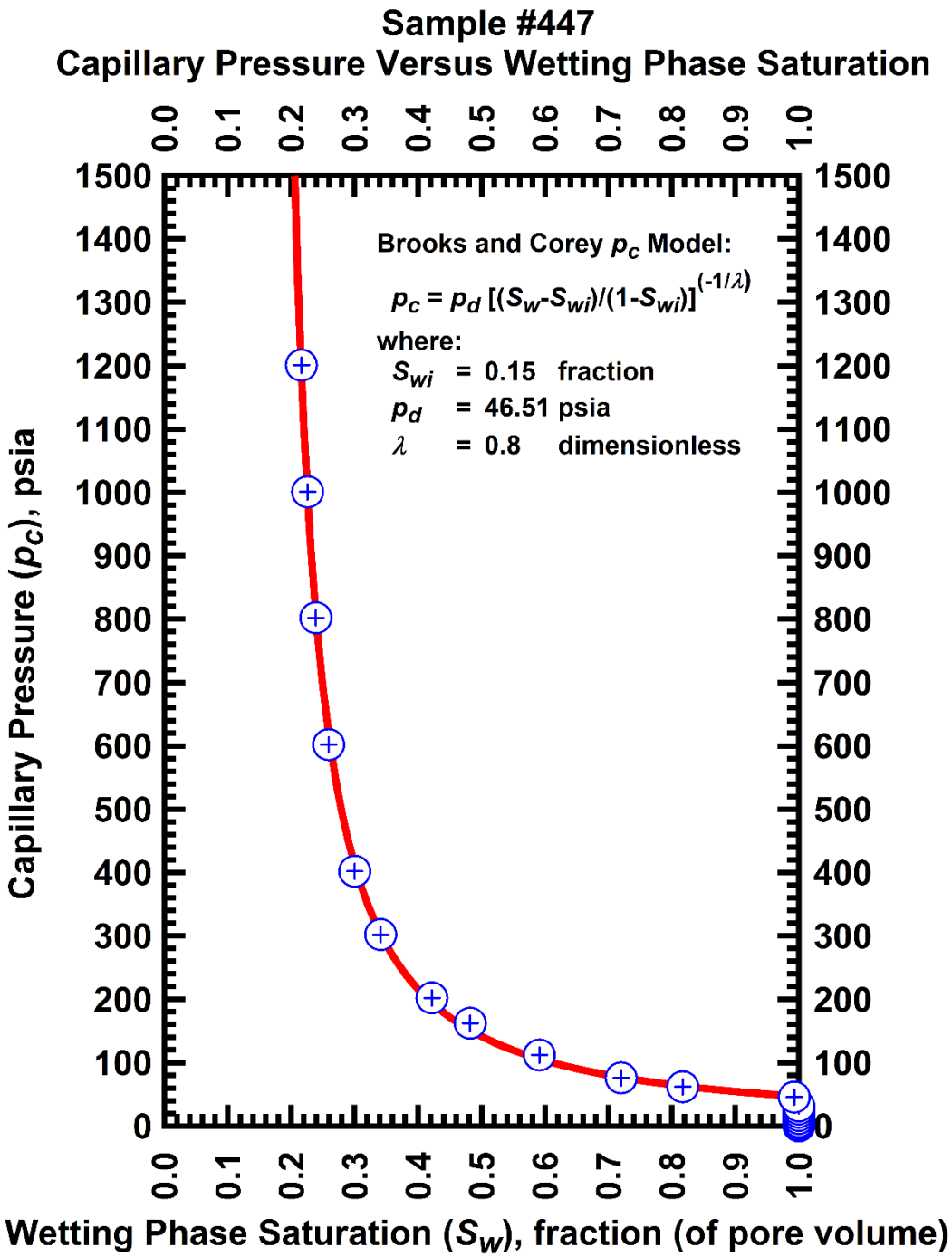

Figure G-38 — Plot of capillary pressure (p_c) vs. wetting phase saturation (S_w) — Sample #447.

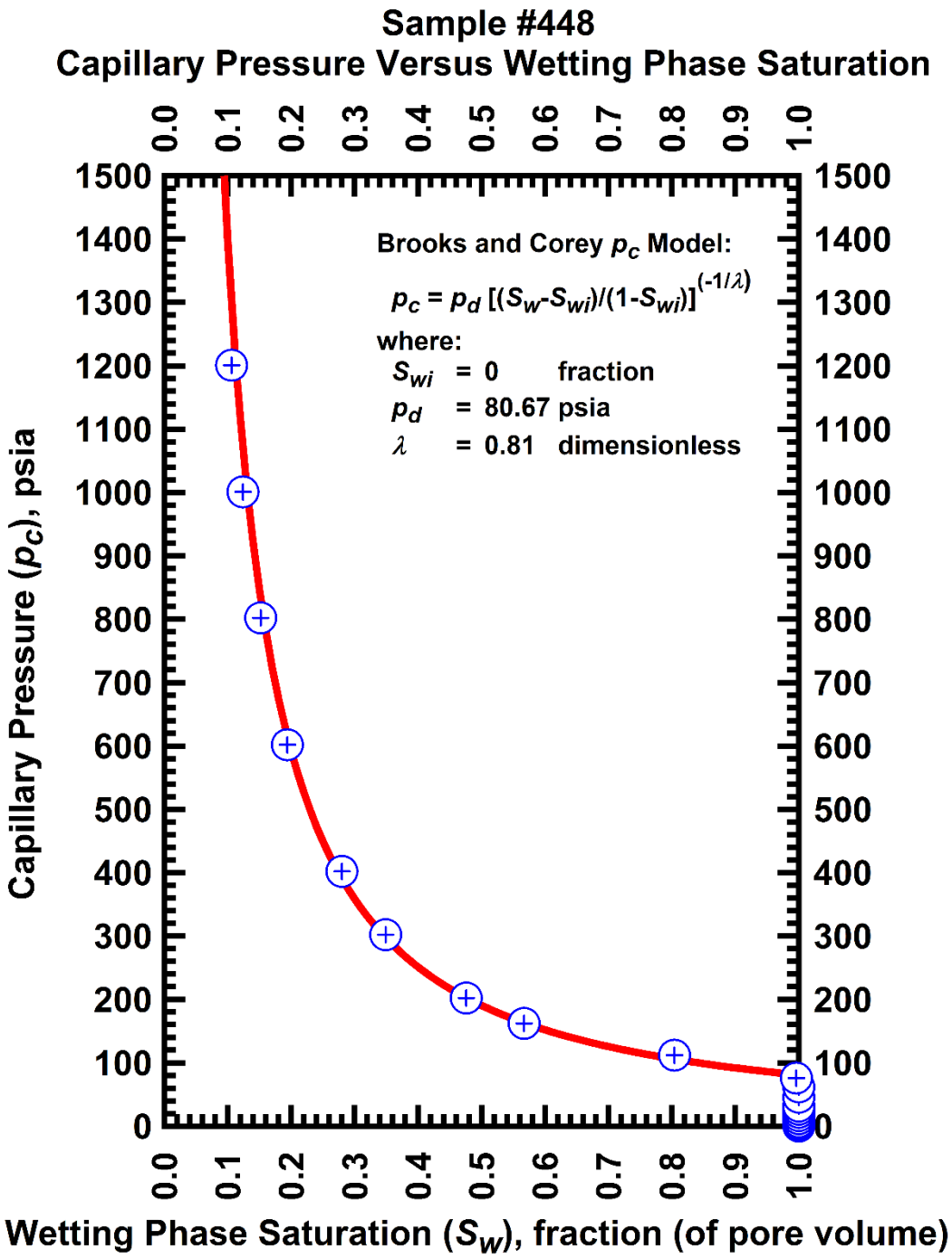

Figure G-39 — Plot of capillary pressure (p_c) vs. wetting phase saturation (S_w) — Sample #448.

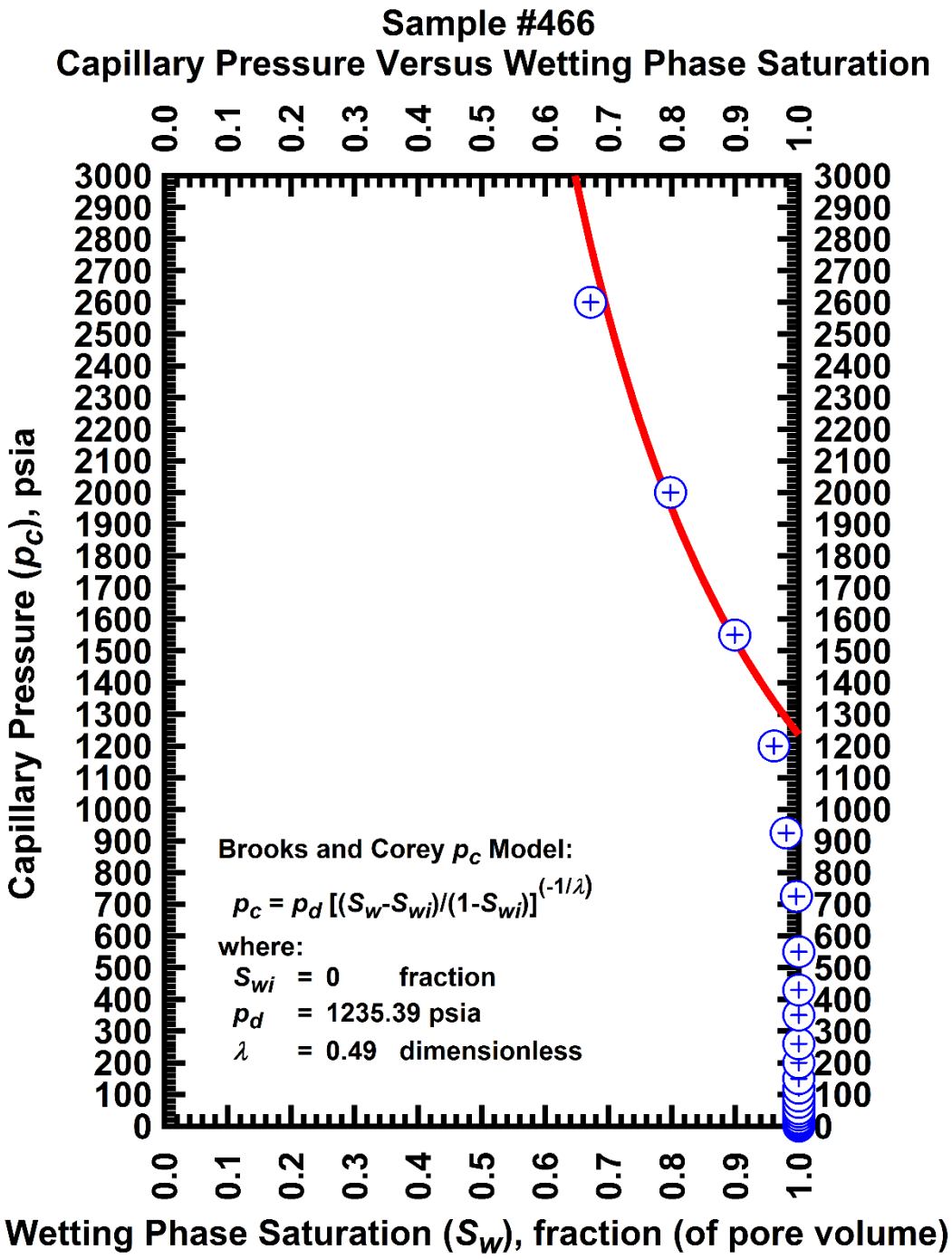

Figure G-40 — Plot of capillary pressure (p_c) vs. wetting phase saturation (S_w) — Sample #466.

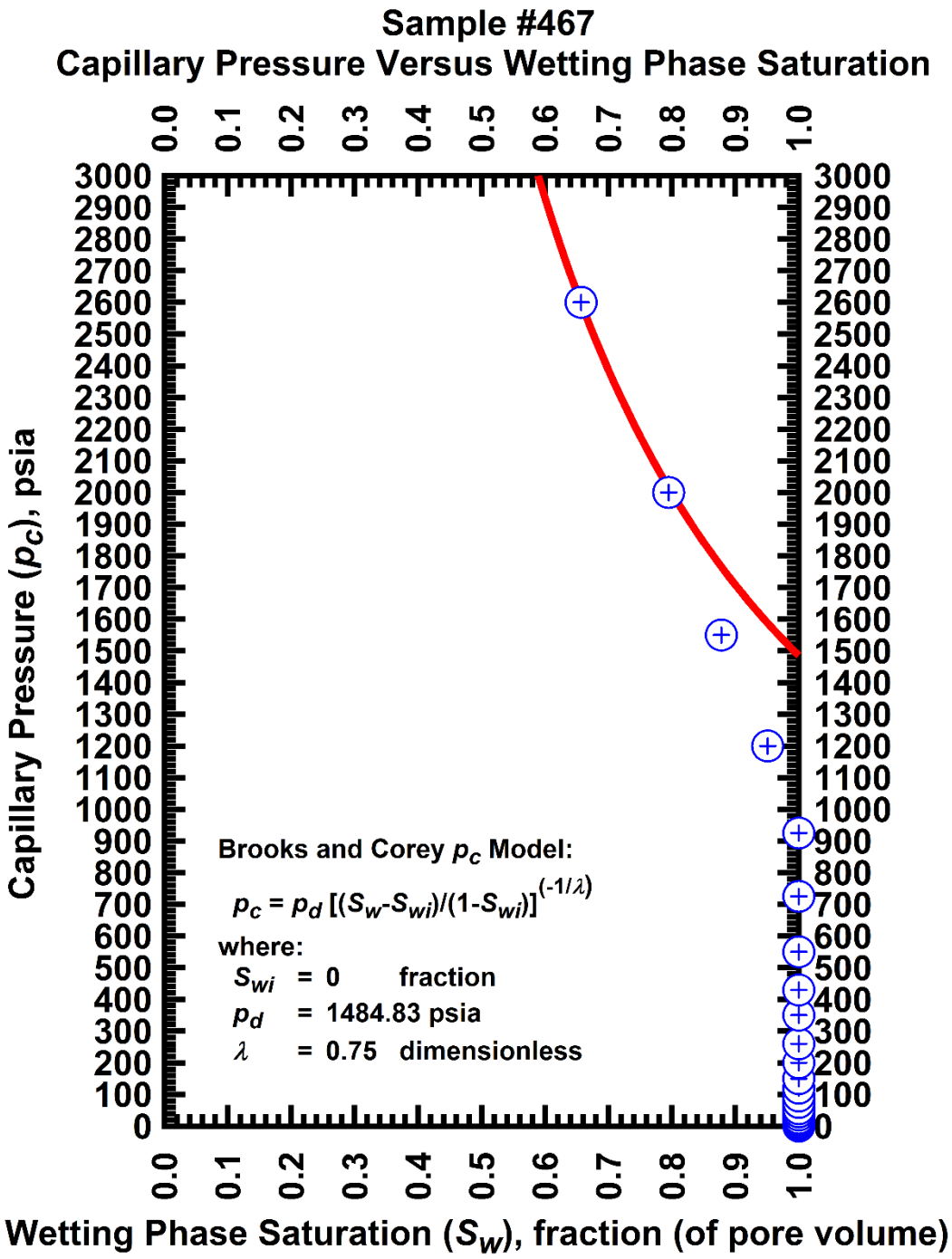

Figure G-41 — Plot of capillary pressure (p_c) vs. wetting phase saturation (S_w) — Sample #467.

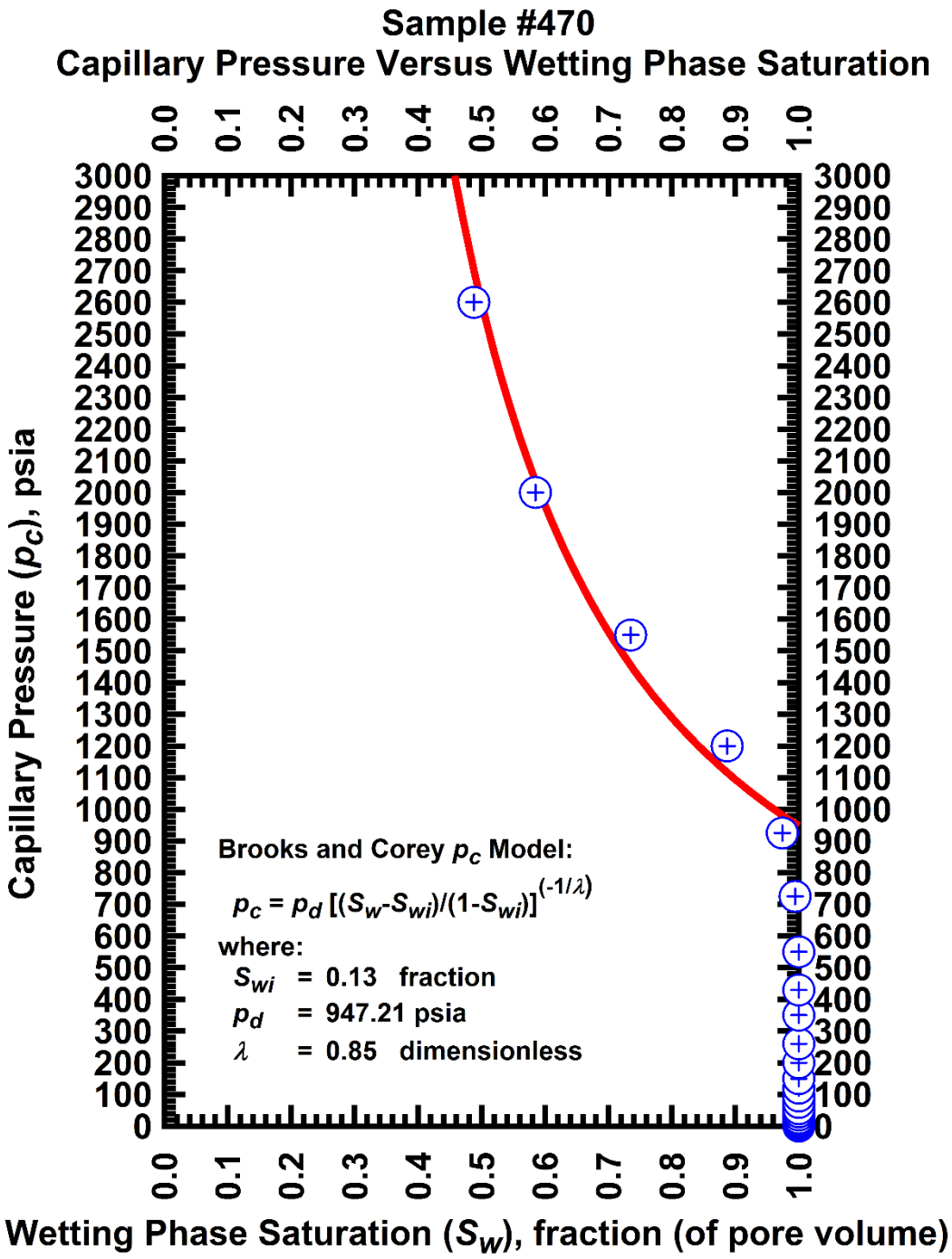

Figure G-42 — Plot of capillary pressure (p_c) vs. wetting phase saturation (S_w) — Sample #470.

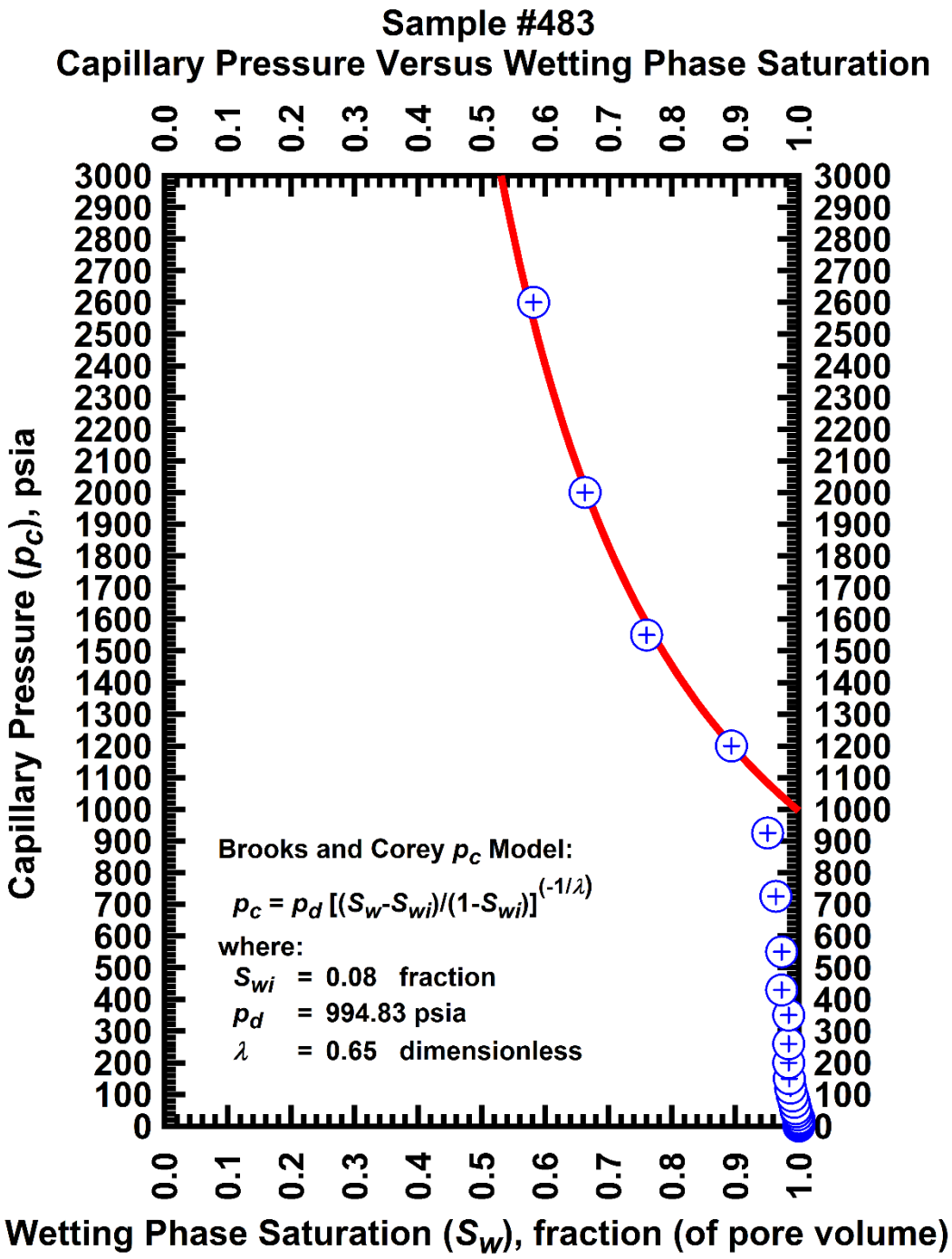

Figure G-43 — Plot of capillary pressure (p_c) vs. wetting phase saturation (S_w) — Sample #483.

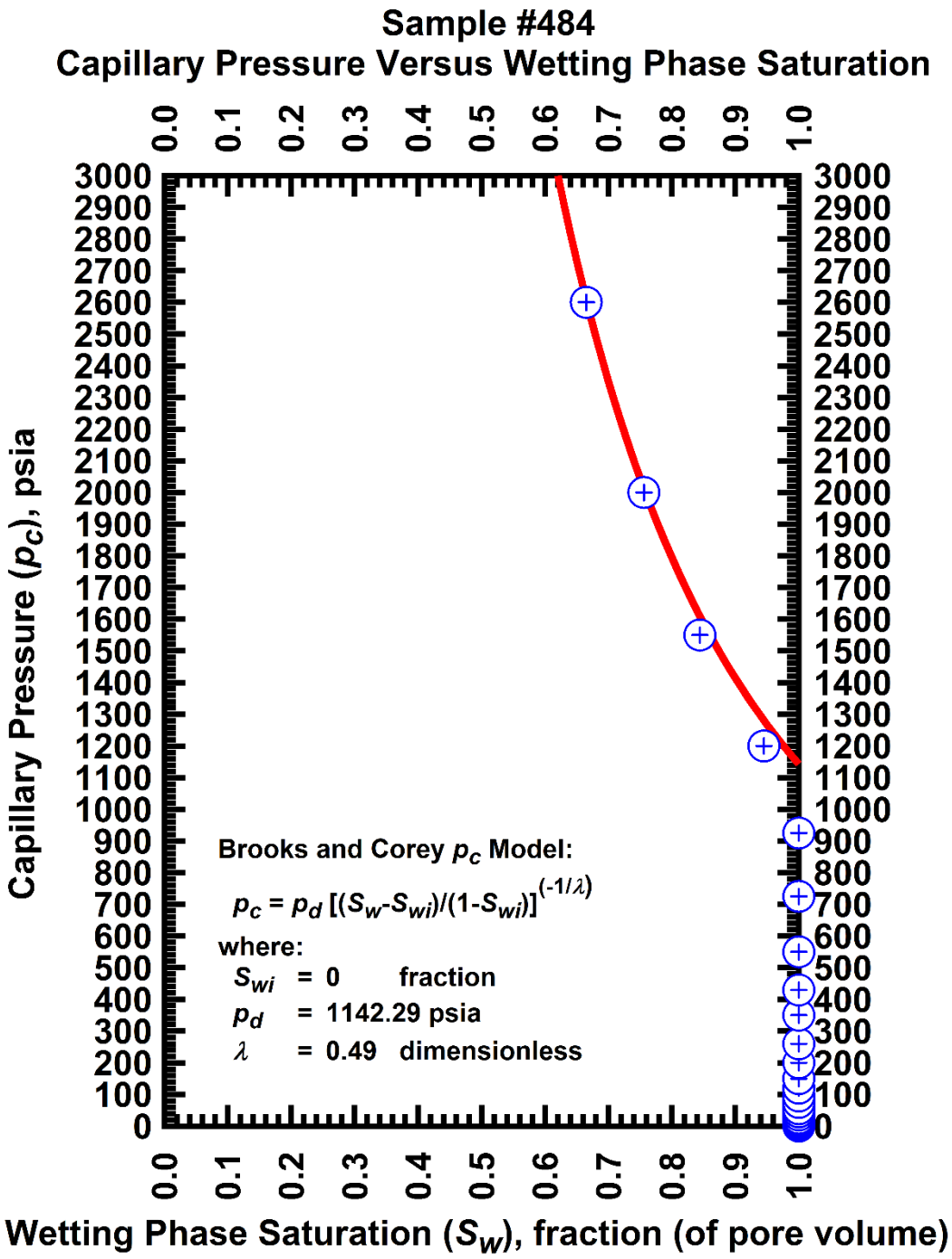

Figure G-44 — Plot of capillary pressure (p_c) vs. wetting phase saturation (S_w) — Sample #484.

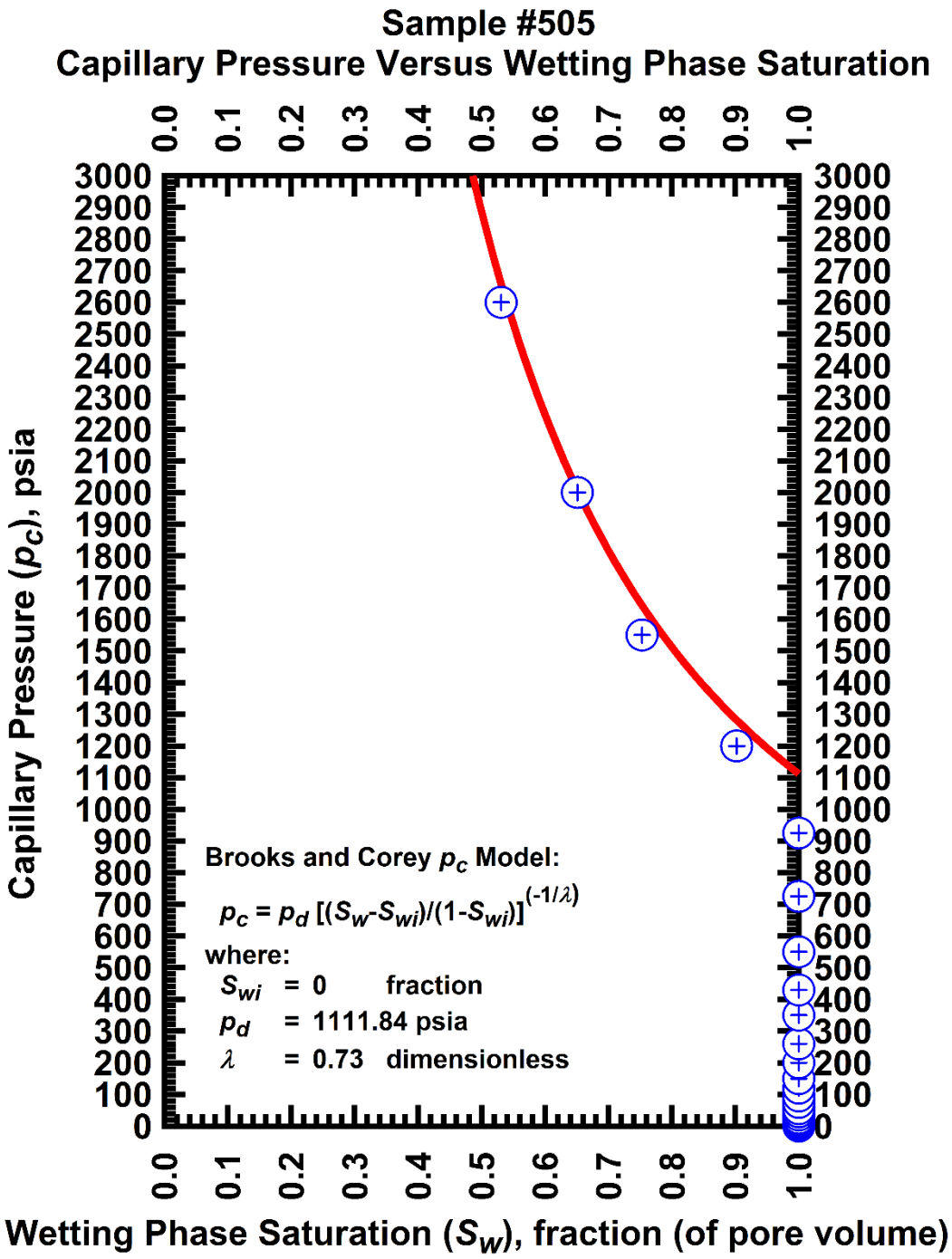

Figure G-45 — Plot of capillary pressure (p_c) vs. wetting phase saturation (S_w) — Sample #505.

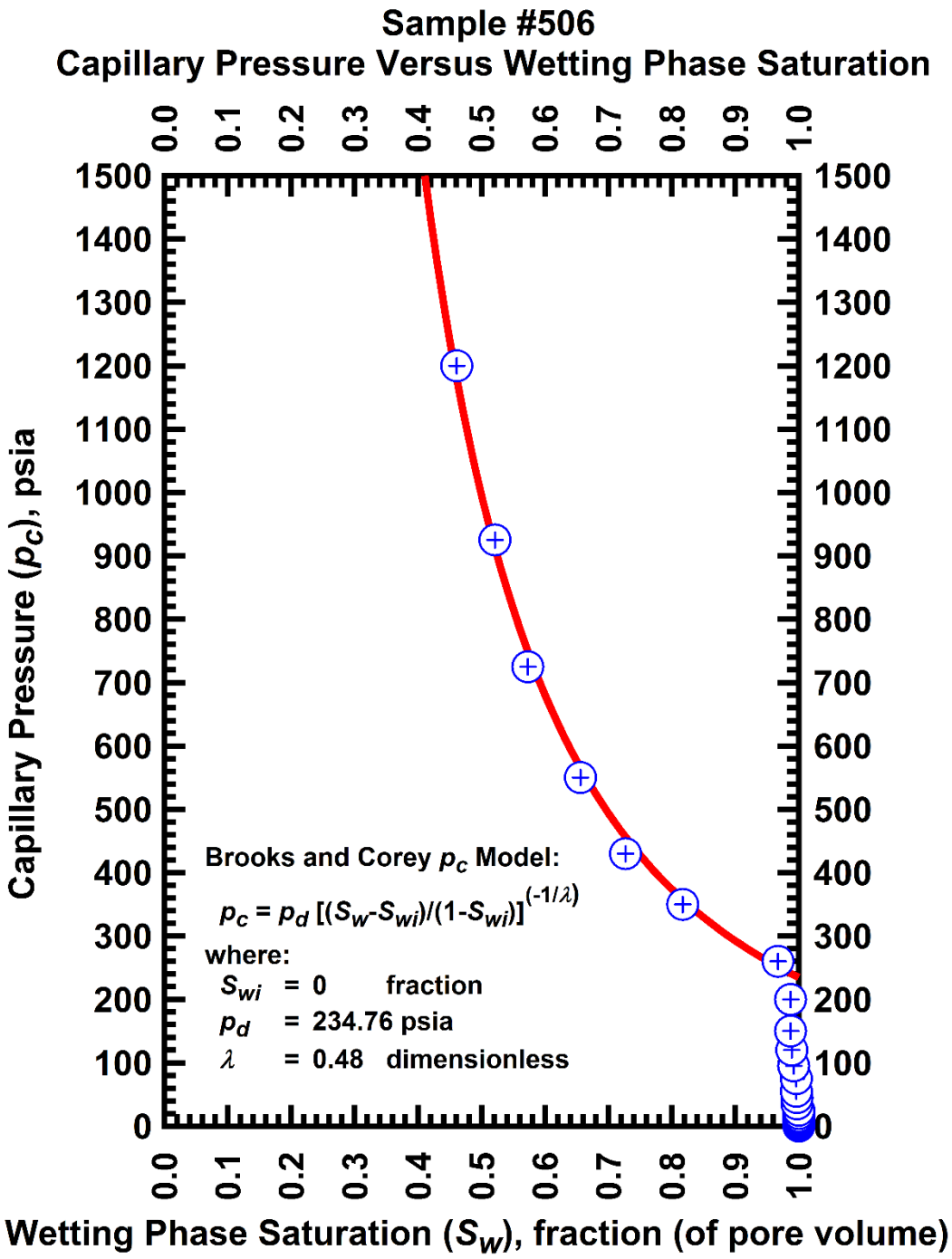

Figure G-46 — Plot of capillary pressure (p_c) vs. wetting phase saturation (S_w) — Sample #506.

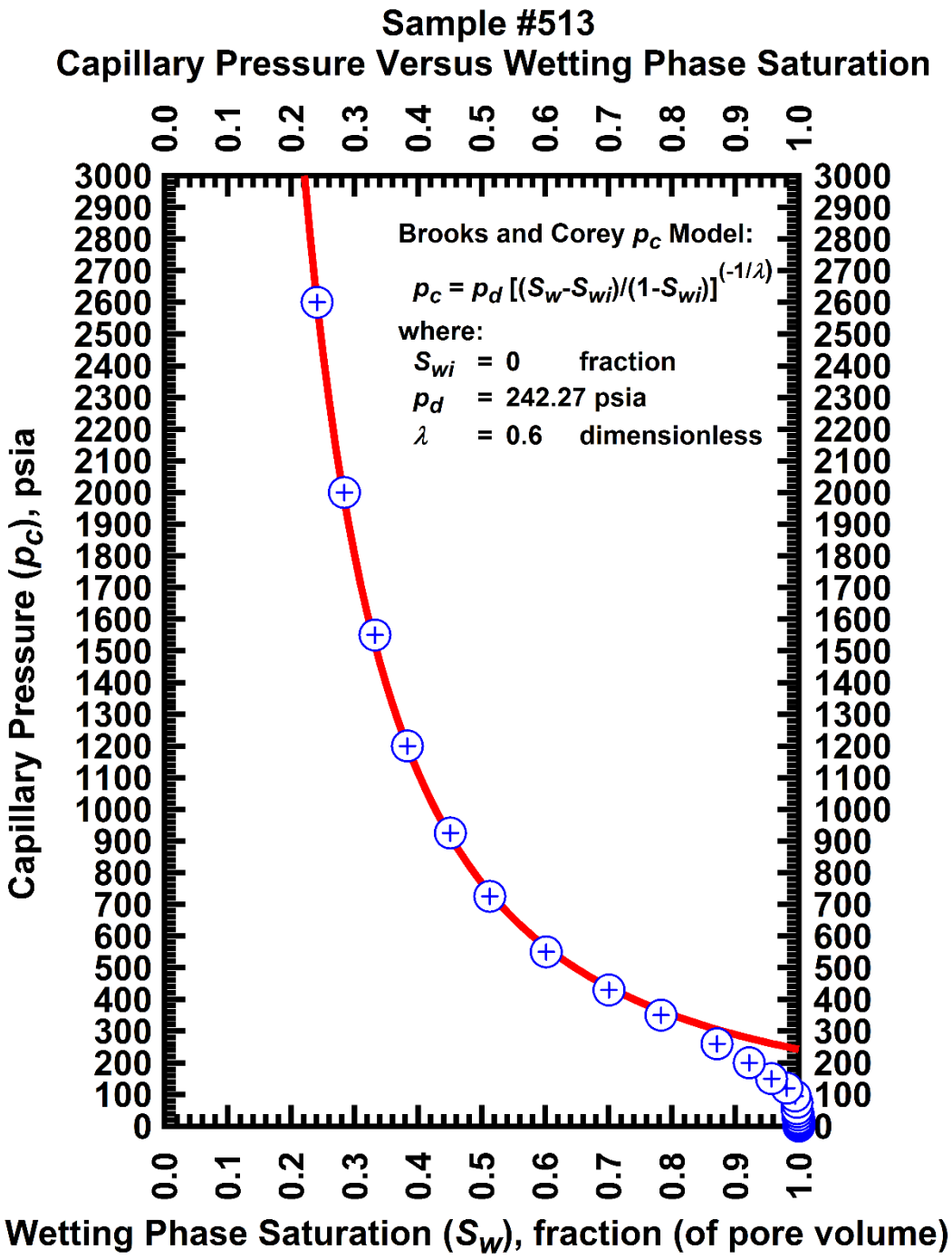

Figure G-47 — Plot of capillary pressure (p_c) vs. wetting phase saturation (S_w) — Sample #513.

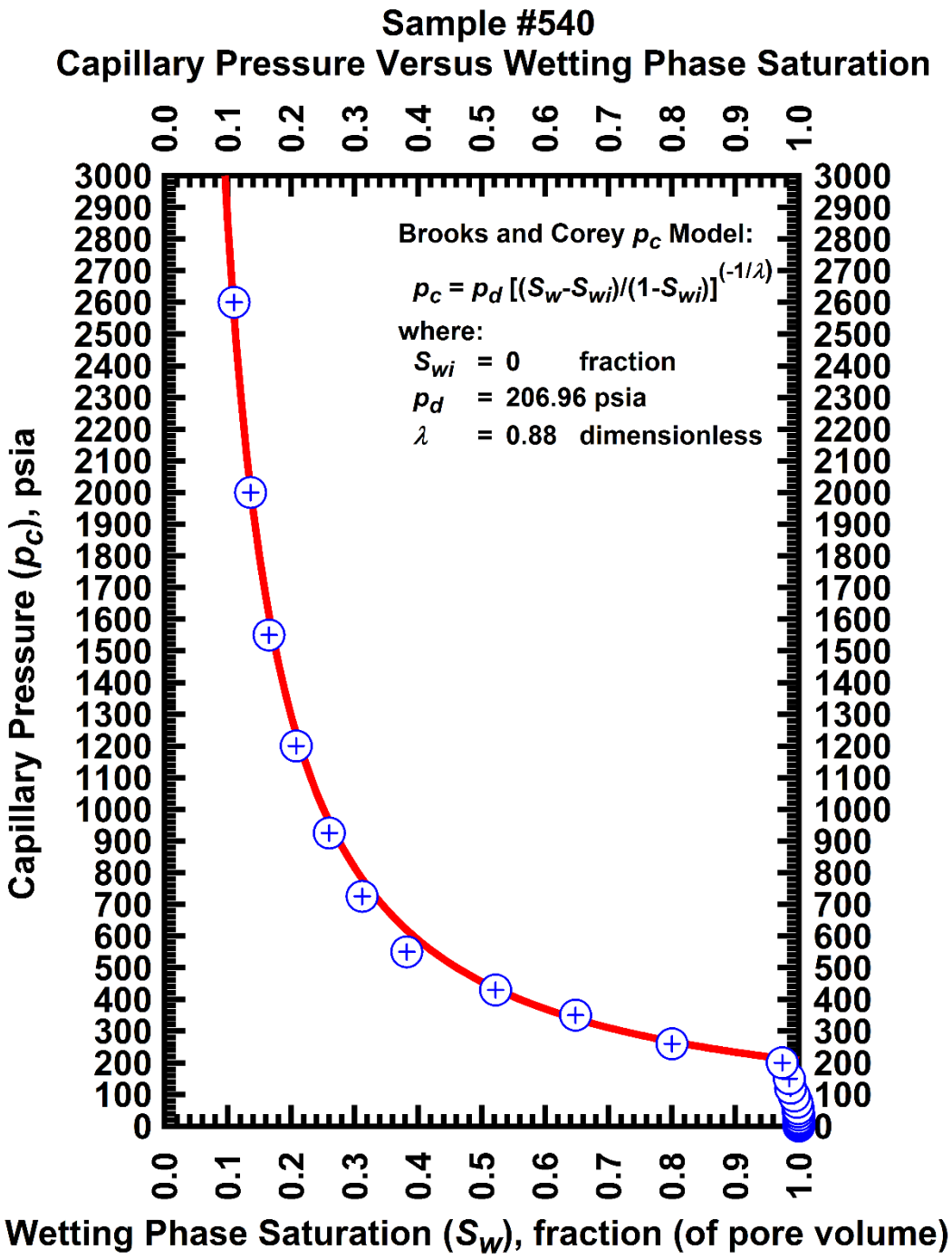

Figure G-48 — Plot of capillary pressure (p_c) vs. wetting phase saturation (S_w) — Sample #540.

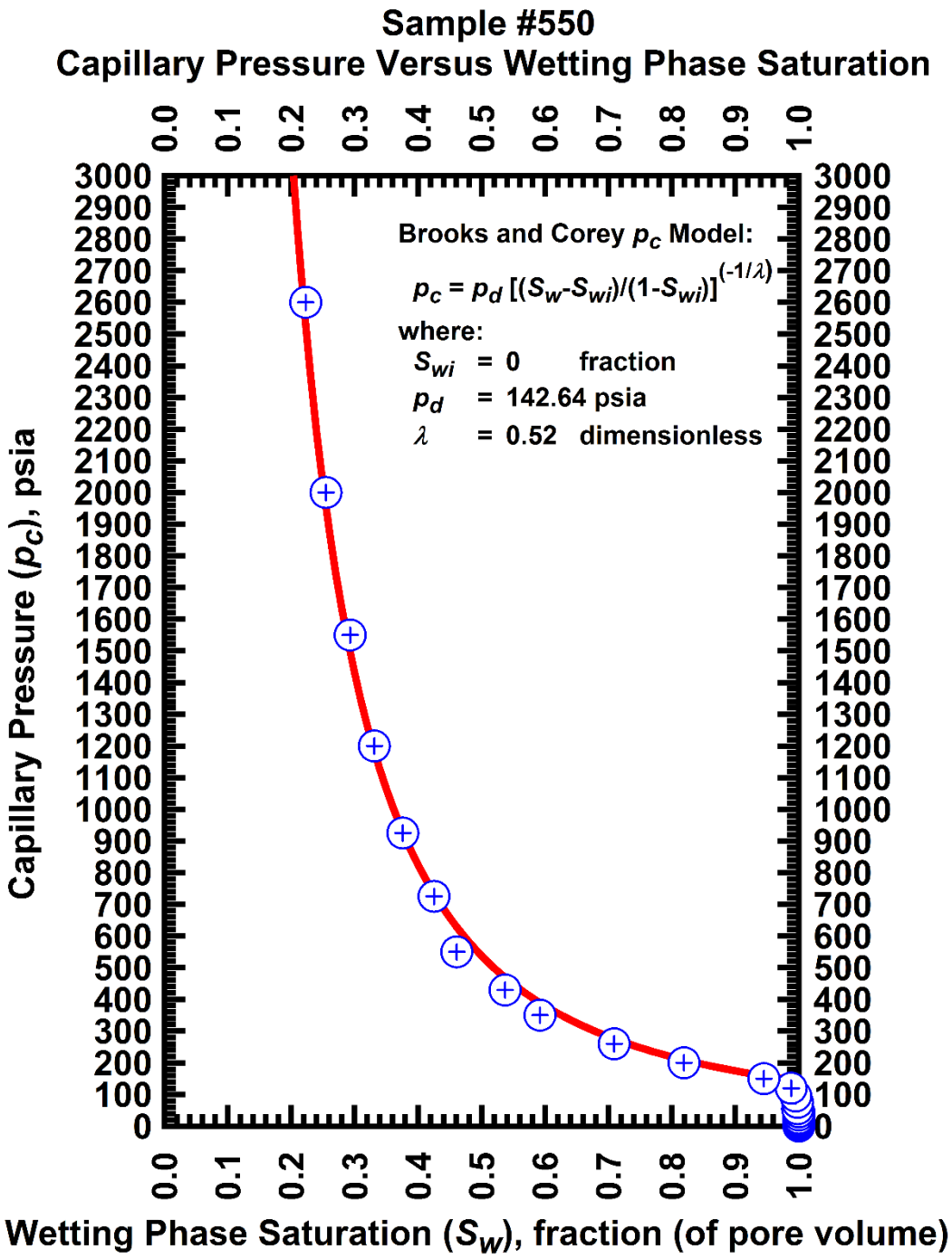

Figure G-49 — Plot of capillary pressure (p_c) vs. wetting phase saturation (S_w) — Sample #550.

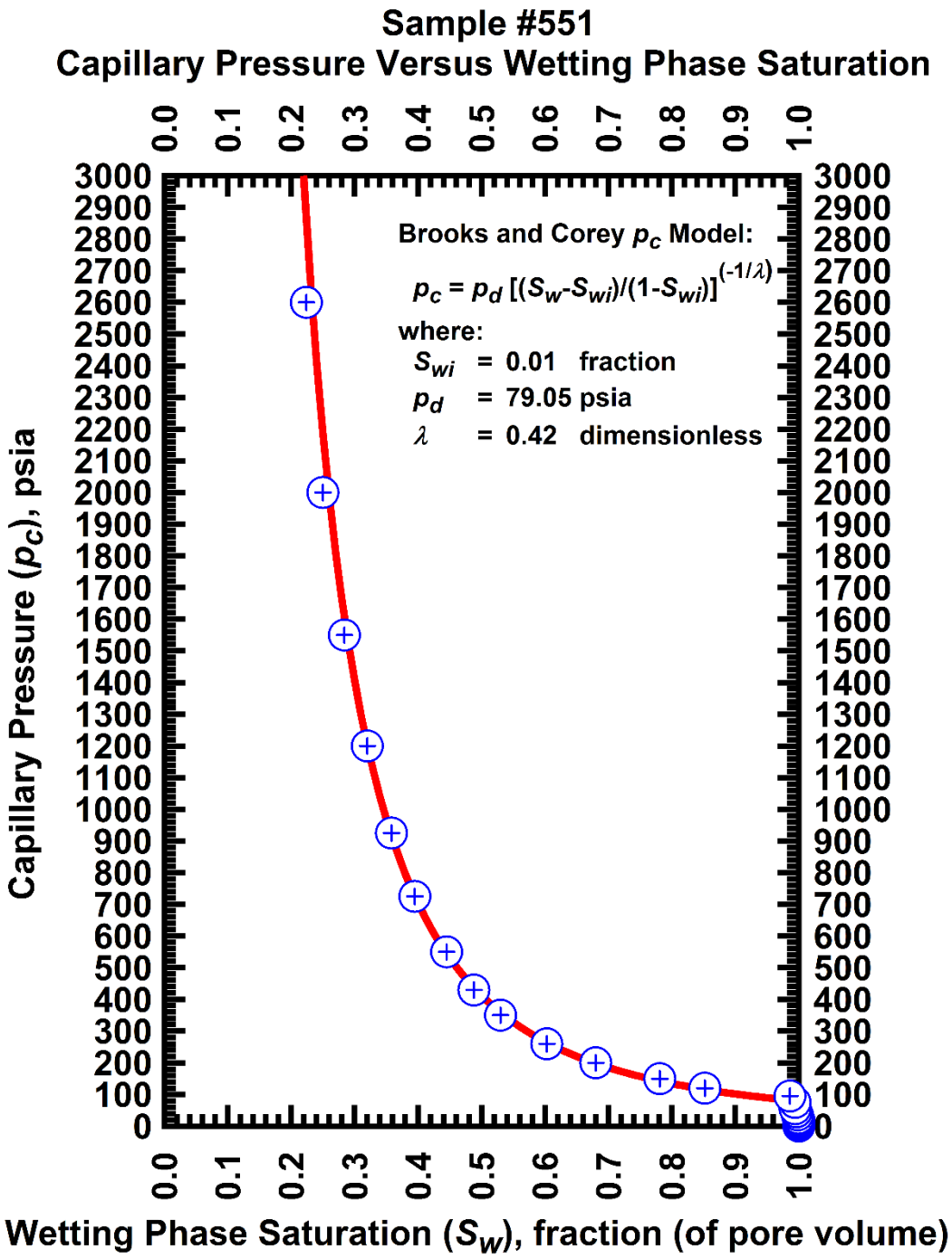

Figure G-50 — Plot of capillary pressure (p_c) vs. wetting phase saturation (S_w) — Sample #551.

APPENDIX H

LIBRARY OF CAPILLARY PRESSURE VERSUS WETTING PHASE SATURATION PLOTS — LOGARITHMIC CAPILLARY PRESSURE FORMAT

This Appendix presents the calibration of the capillary displacement pressure (p_d), irreducible wetting phase saturation (S_{wi}), and the index of pore-size distribution (λ) on a sample-by-sample basis using the Brooks-Corey $p_c(S_w)$ model. In this Appendix, we provide example plots of capillary pressure (p_c) vs. wetting phase saturation (S_w) – logarithmic capillary pressure format of 50 (fifty) samples used in this study.

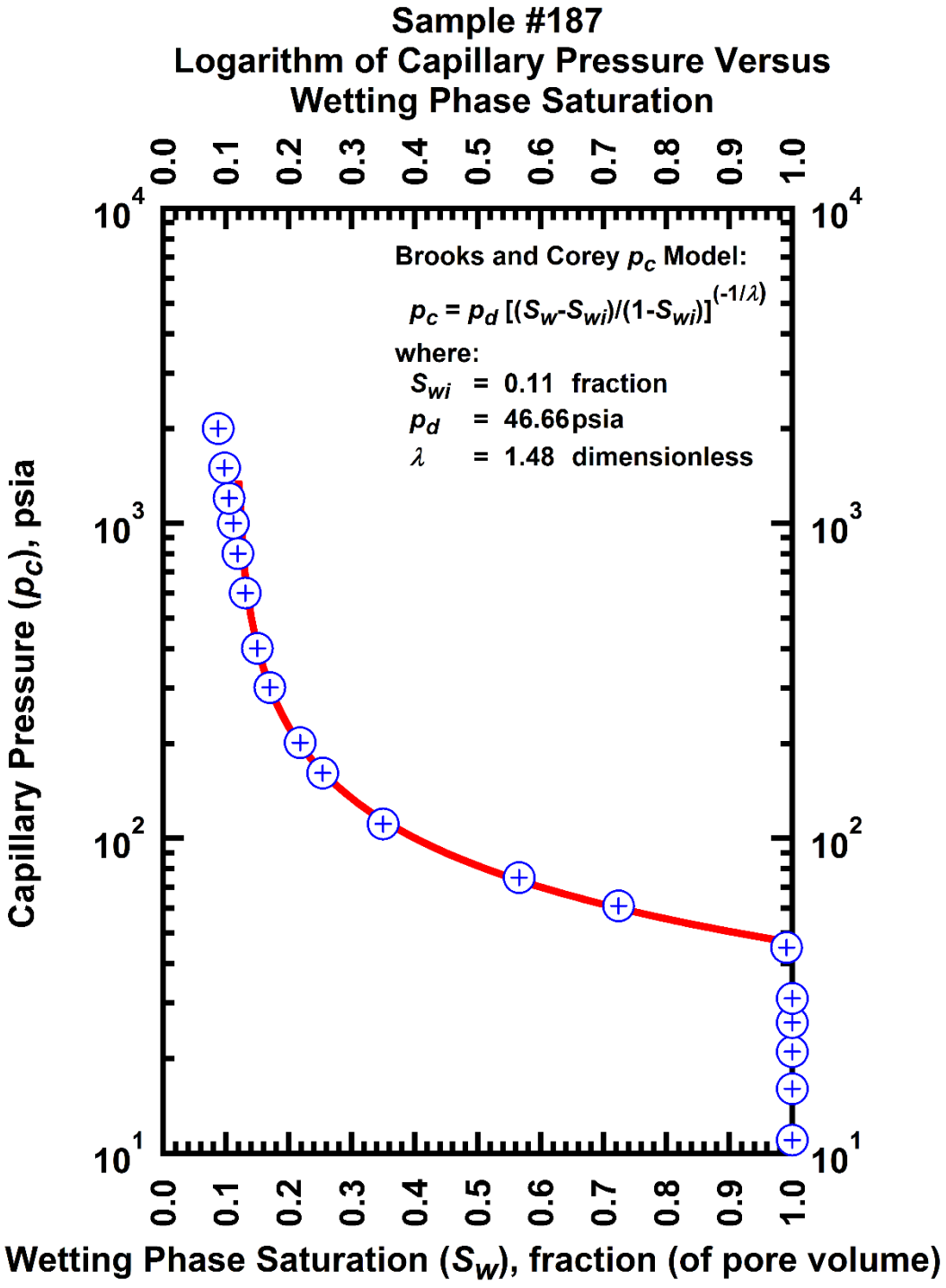

Figure H-1 — Plot of logarithm of capillary pressure vs. wetting phase saturation — Sample #187.

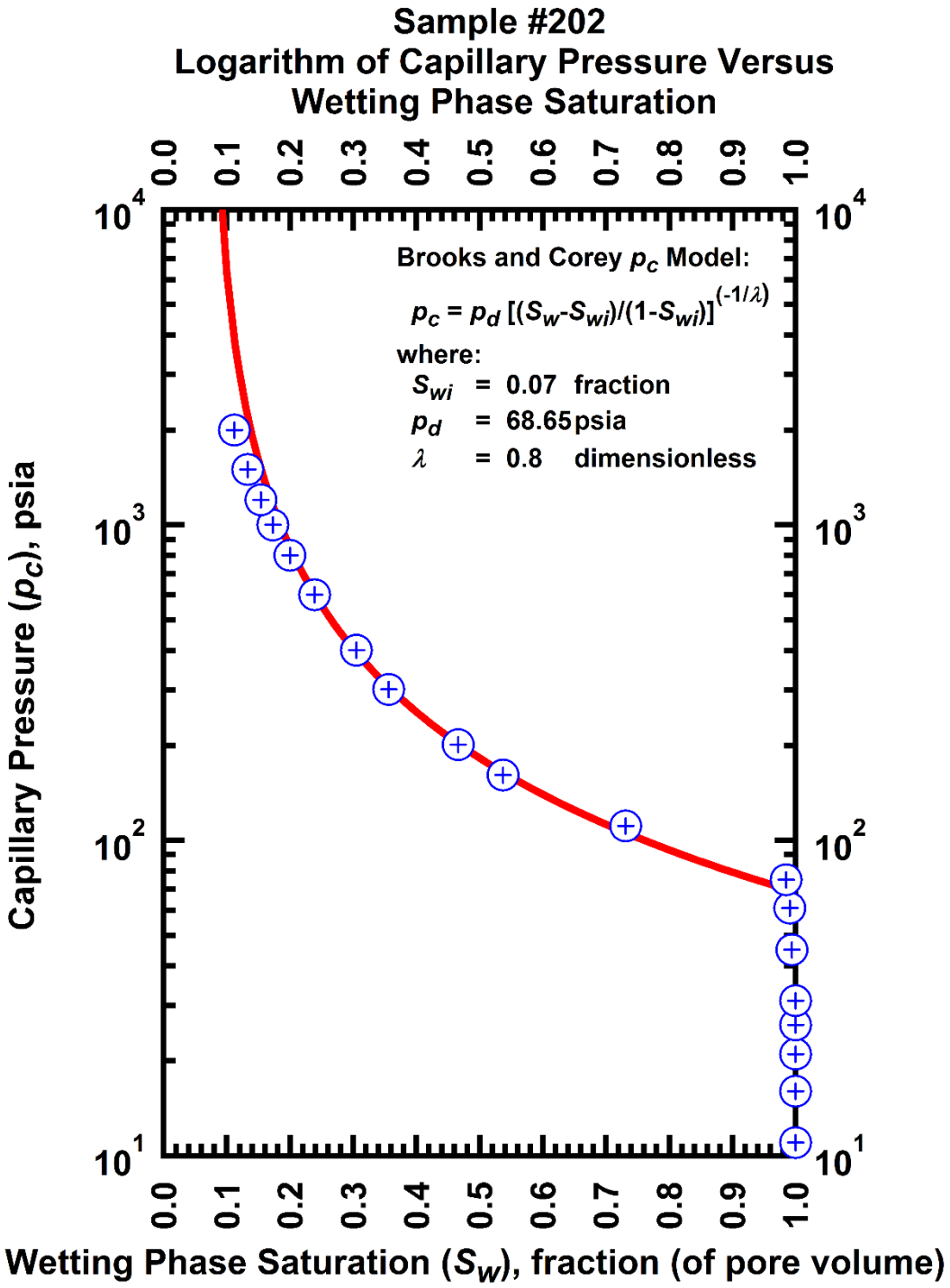

Figure H-2 — Plot of logarithm of capillary pressure vs. wetting phase saturation — Sample #202.

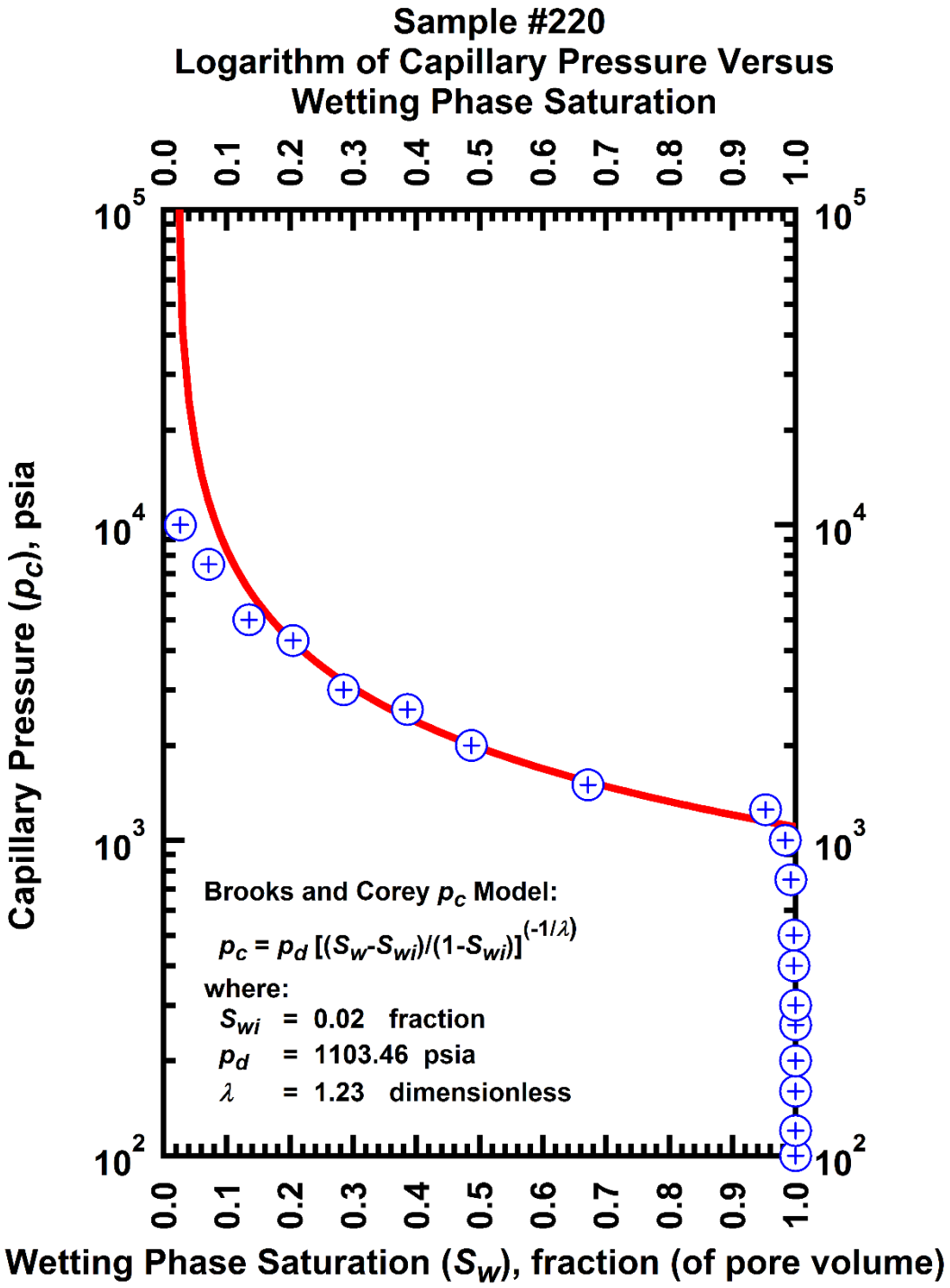

Figure H-3 — Plot of logarithm of capillary pressure vs. wetting phase saturation — Sample #220.

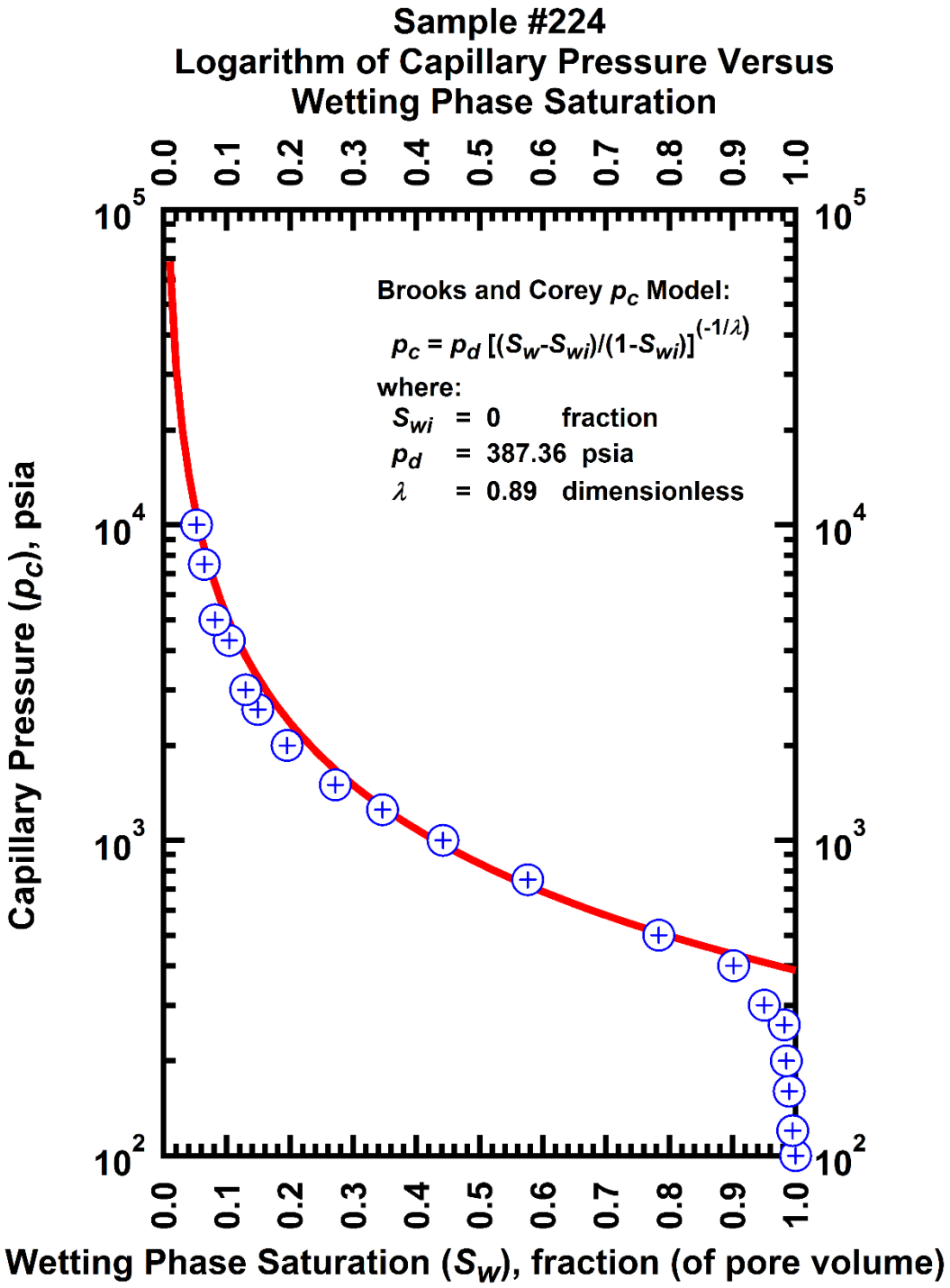

Figure H-4 — Plot of logarithm of capillary pressure vs. wetting phase saturation — Sample #224.

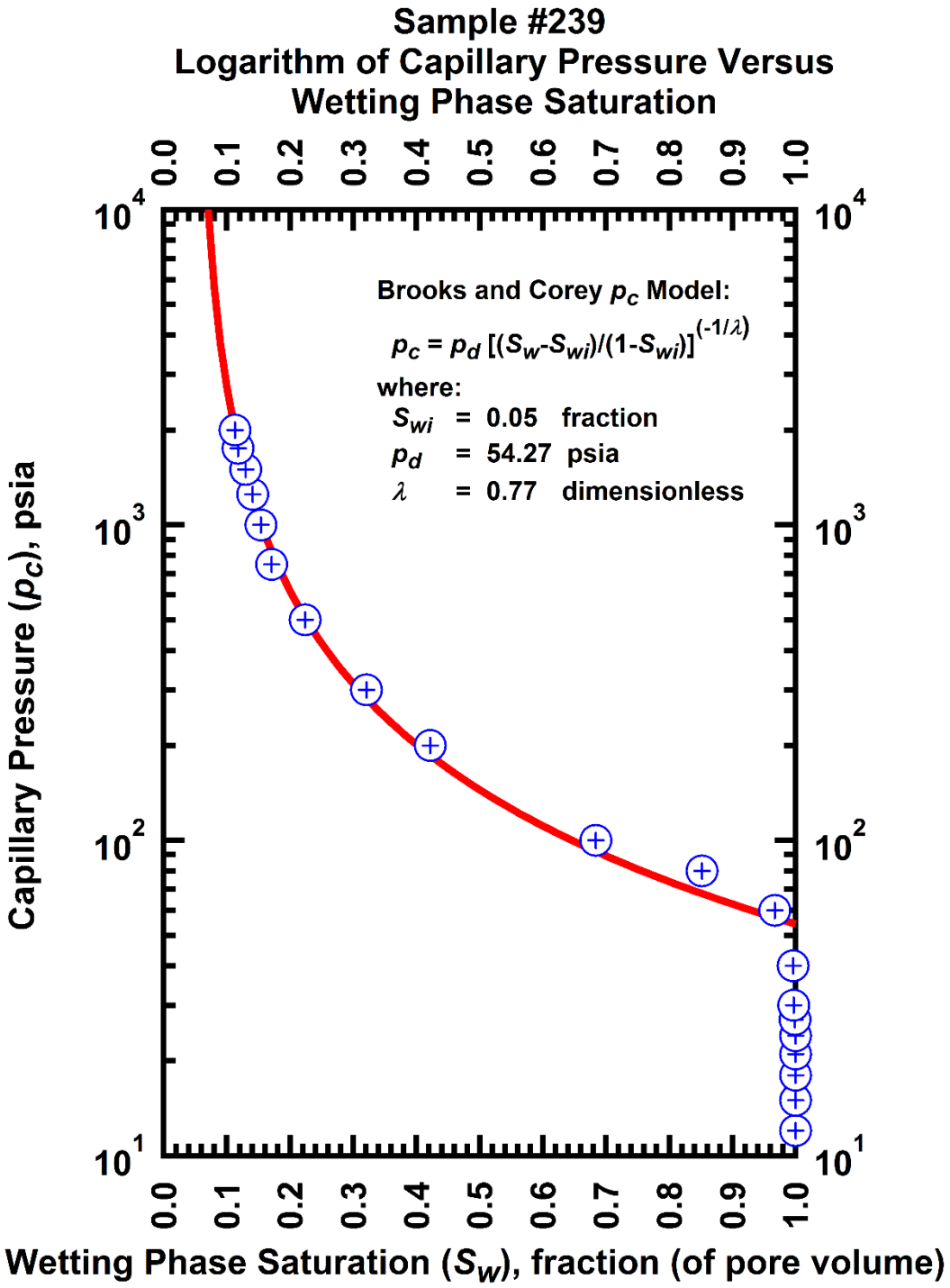

Figure H-5 — Plot of logarithm of capillary pressure vs. wetting phase saturation — Sample #239.

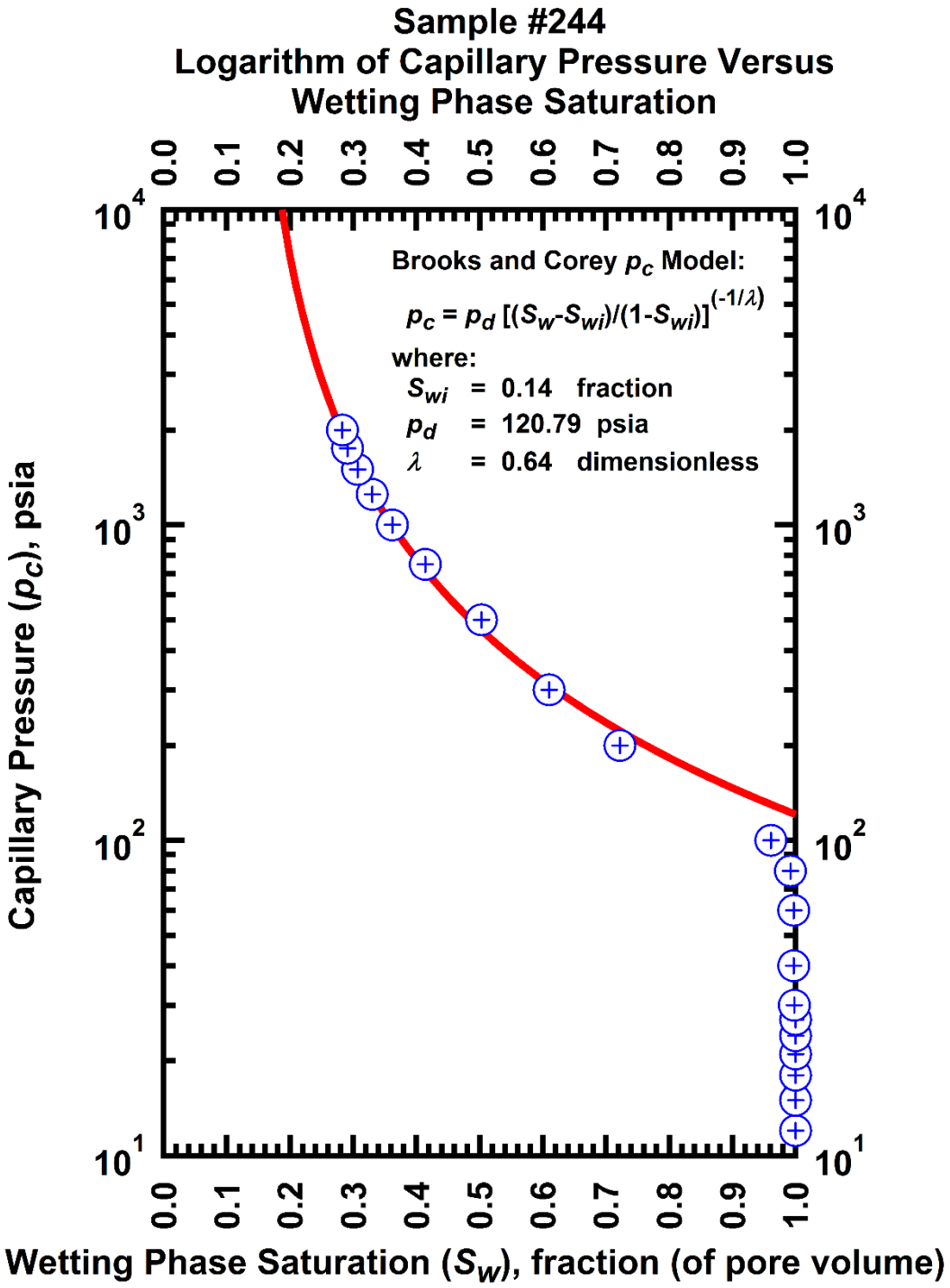

Figure H-6 — Plot of logarithm of capillary pressure vs. wetting phase saturation — Sample #244.

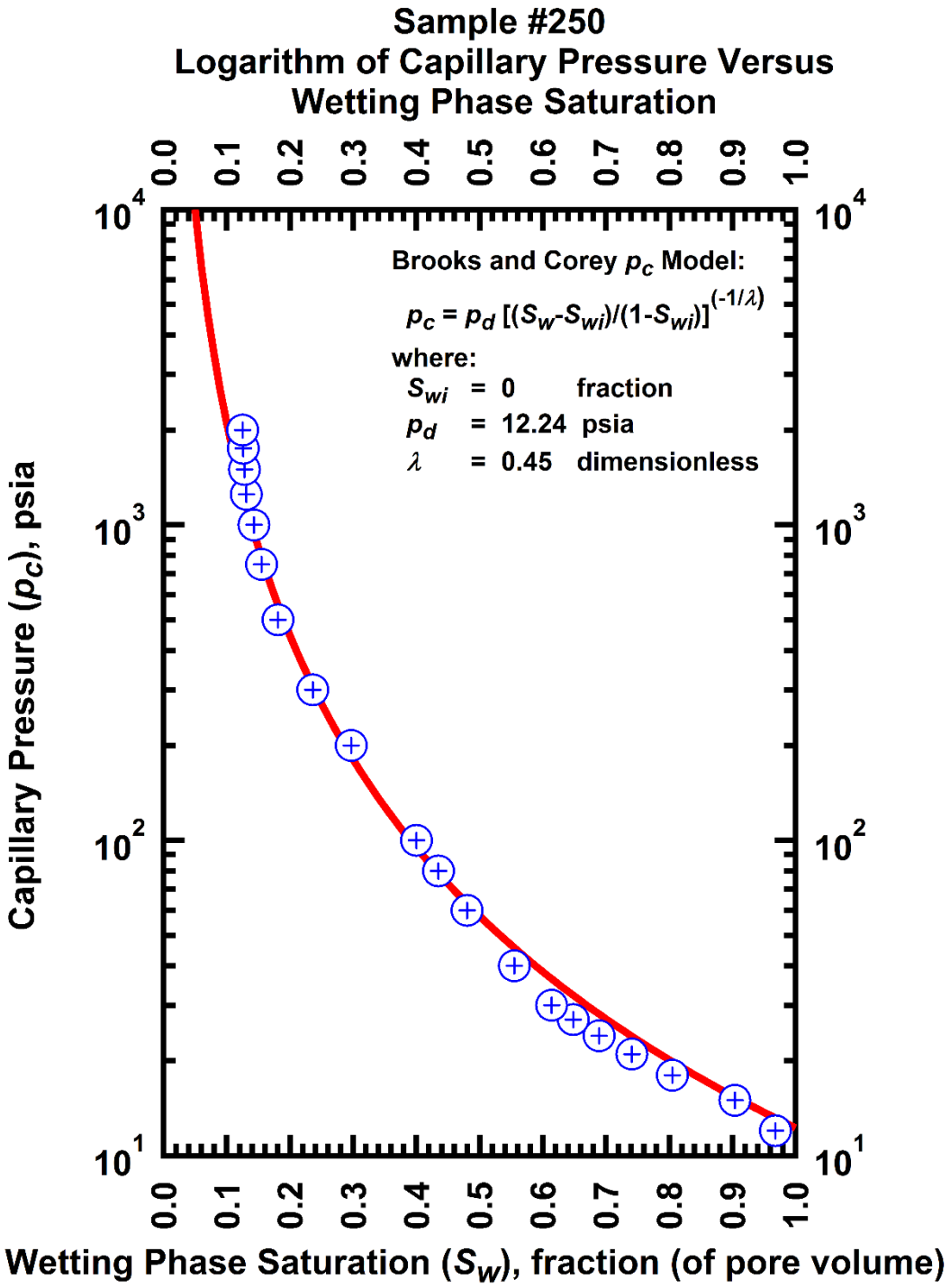

Figure H-7 — Plot of logarithm of capillary pressure vs. wetting phase saturation — Sample #250.

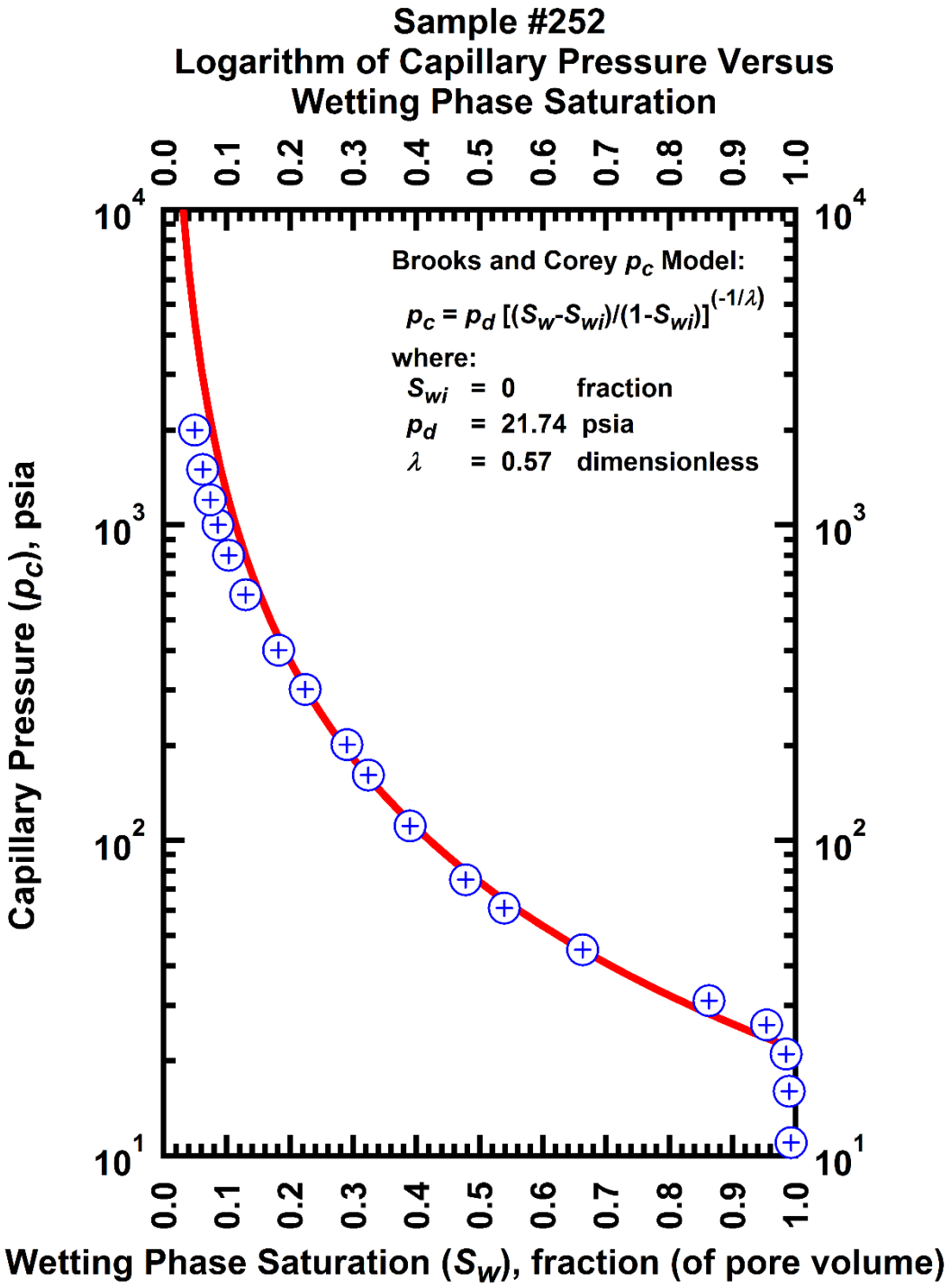

Figure H-8 — Plot of logarithm of capillary pressure vs. wetting phase saturation — Sample #252.

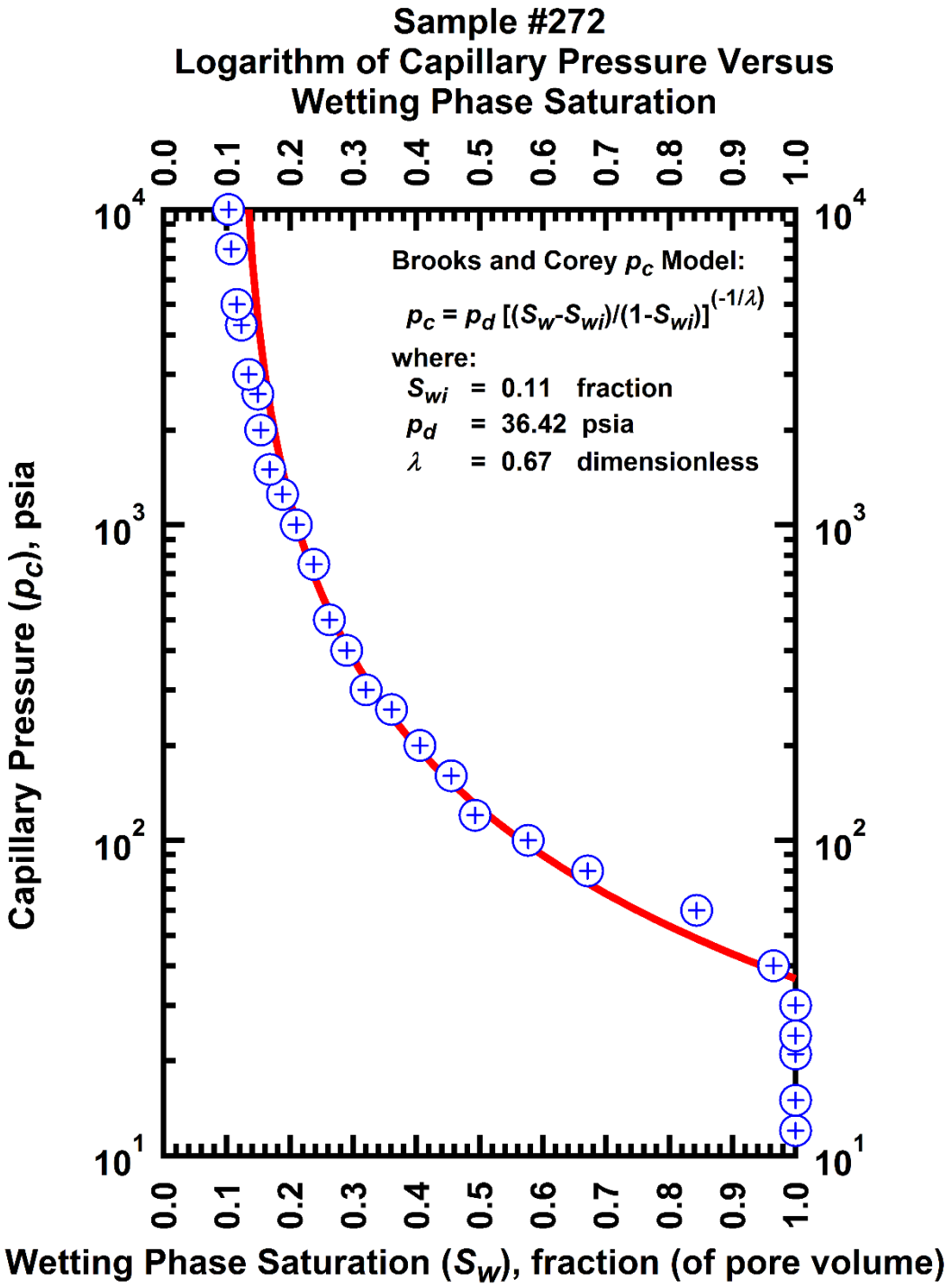

Figure H-9 — Plot of logarithm of capillary pressure vs. wetting phase saturation — Sample #272.

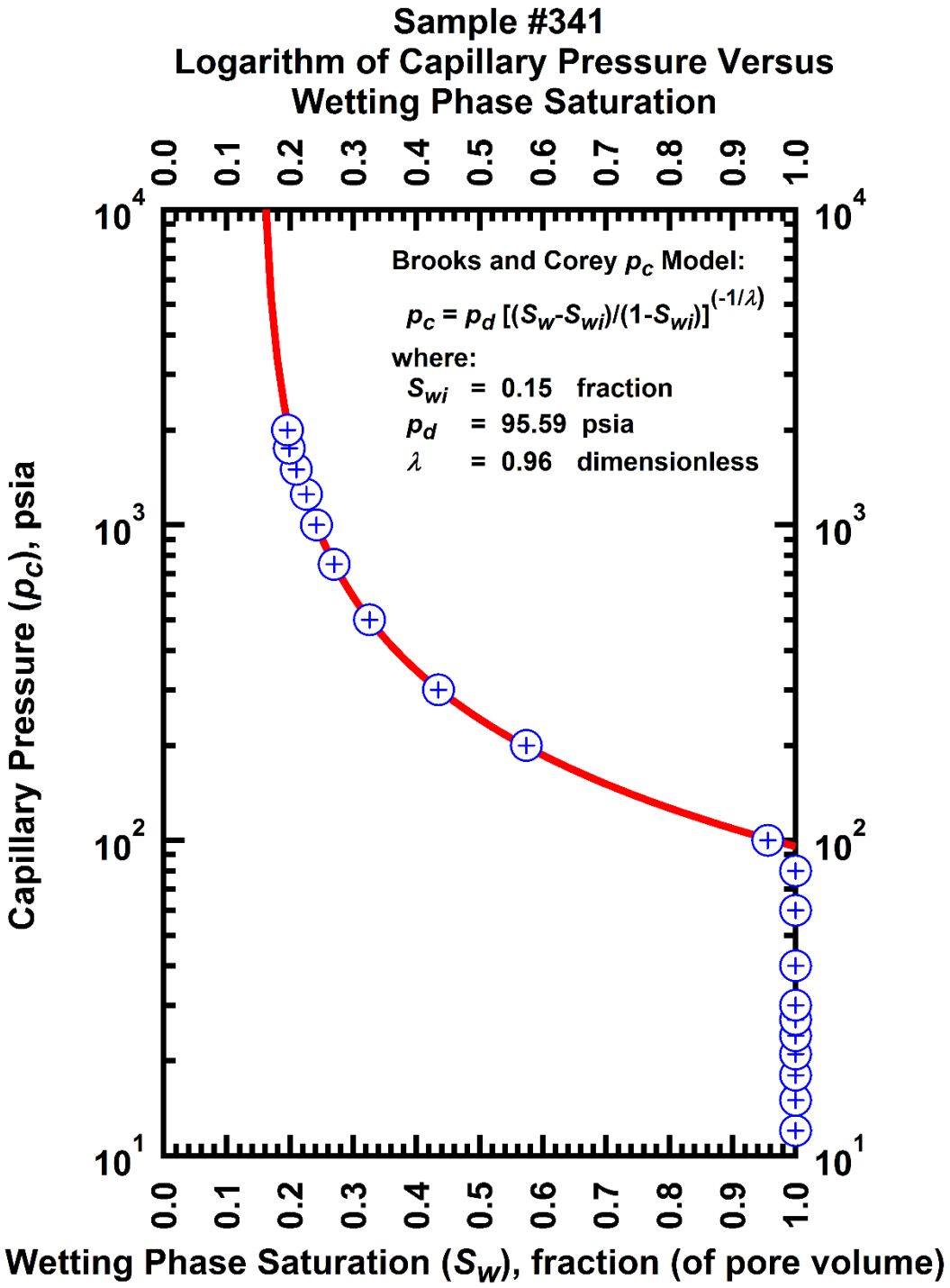

Figure H-10 — Plot of logarithm of capillary pressure vs. wetting phase saturation — Sample #341.

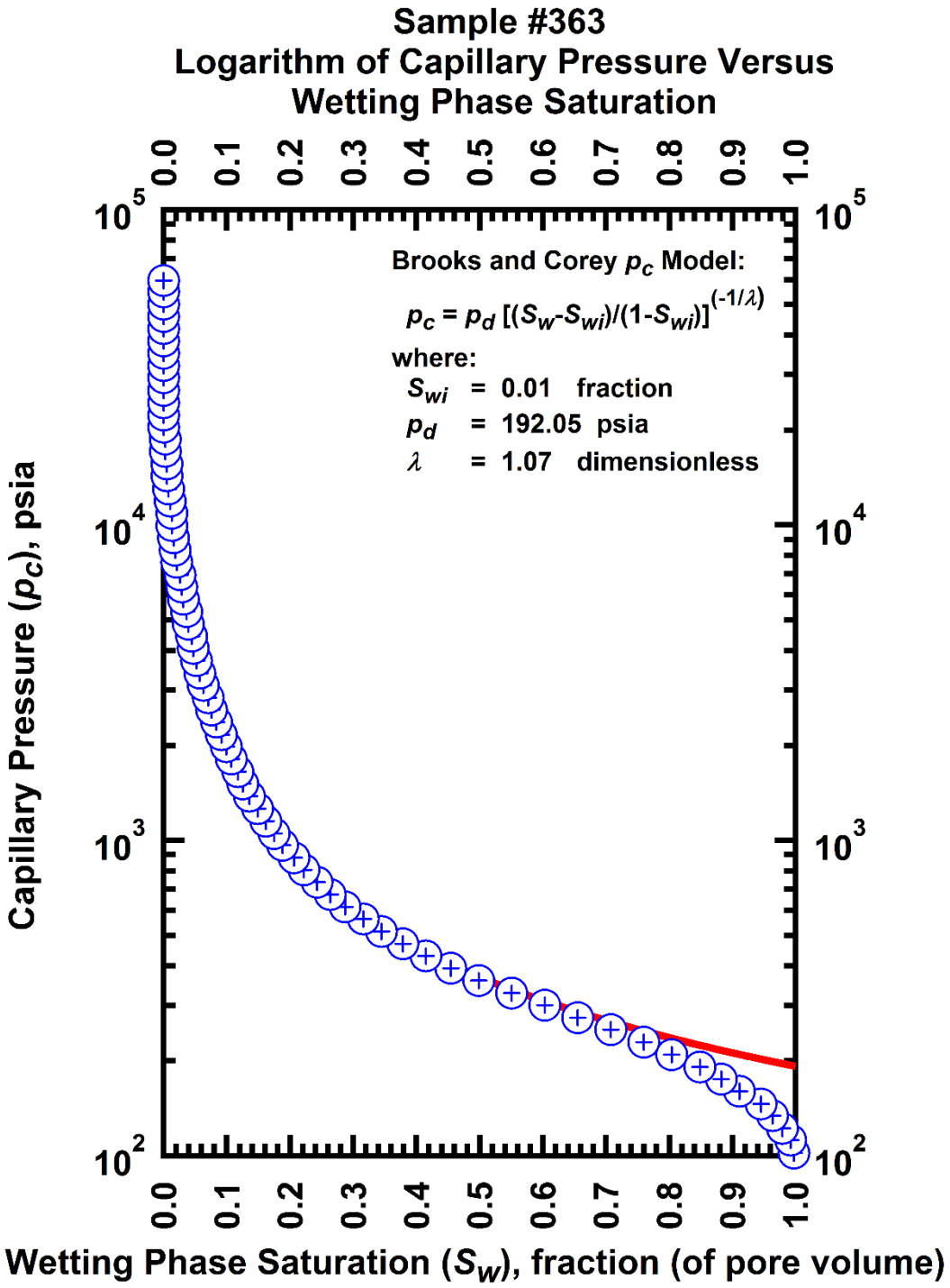

Figure H-11 — Plot of logarithm of capillary pressure vs. wetting phase saturation — Sample #363.

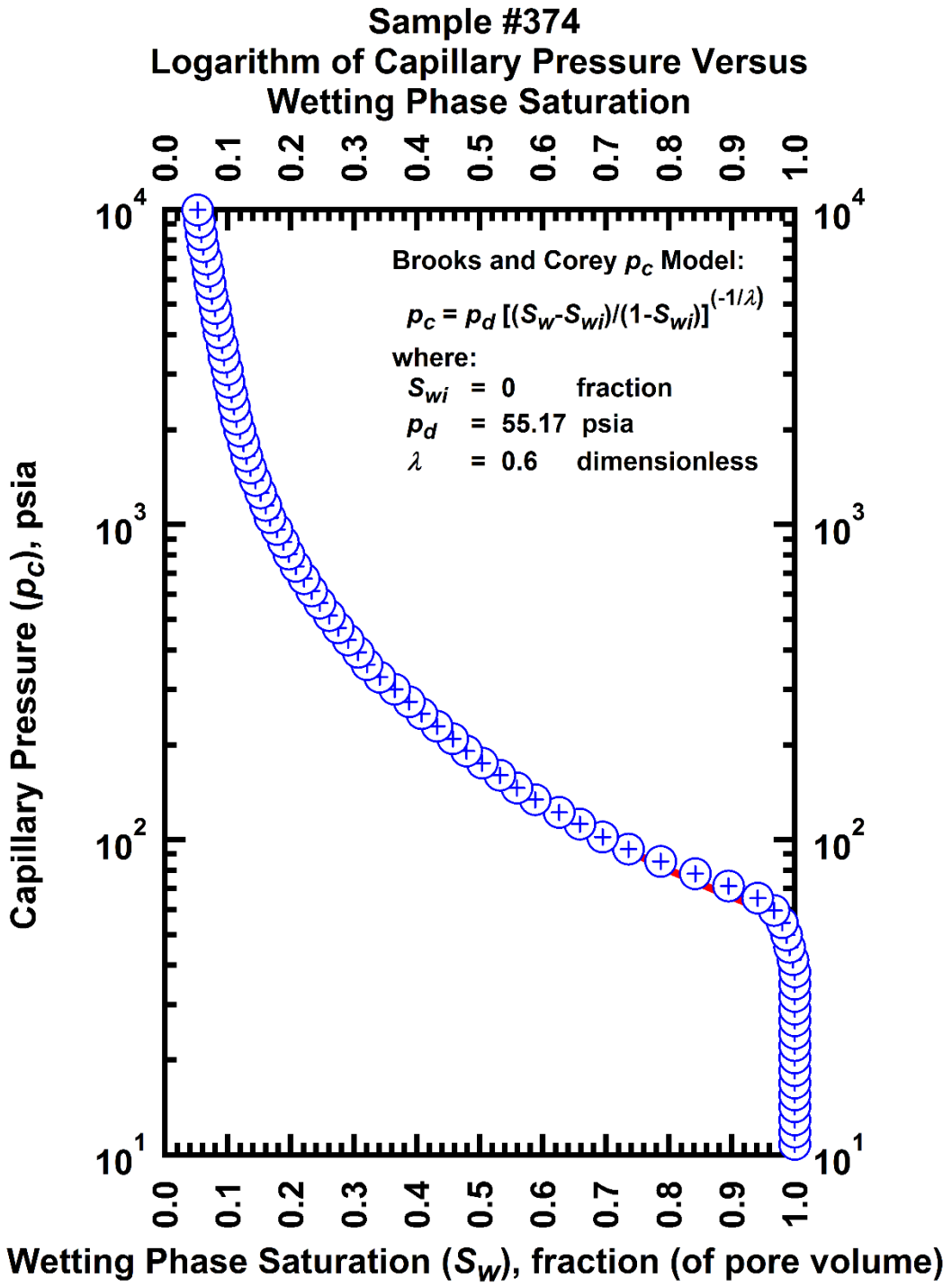

Figure H-12 — Plot of logarithm of capillary pressure vs. wetting phase saturation — Sample #374.

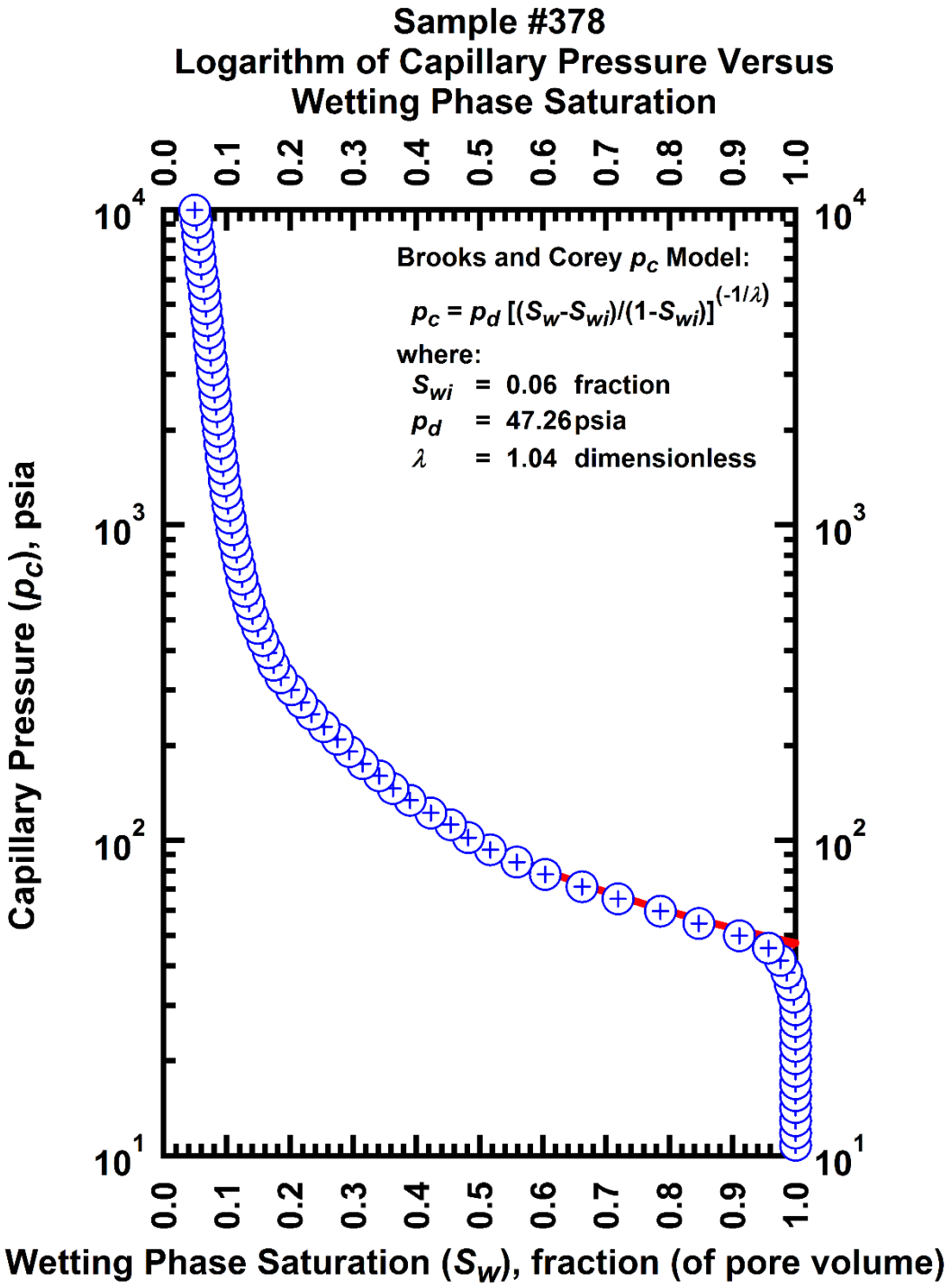

Figure H-13 — Plot of logarithm of capillary pressure vs. wetting phase saturation — Sample #378.

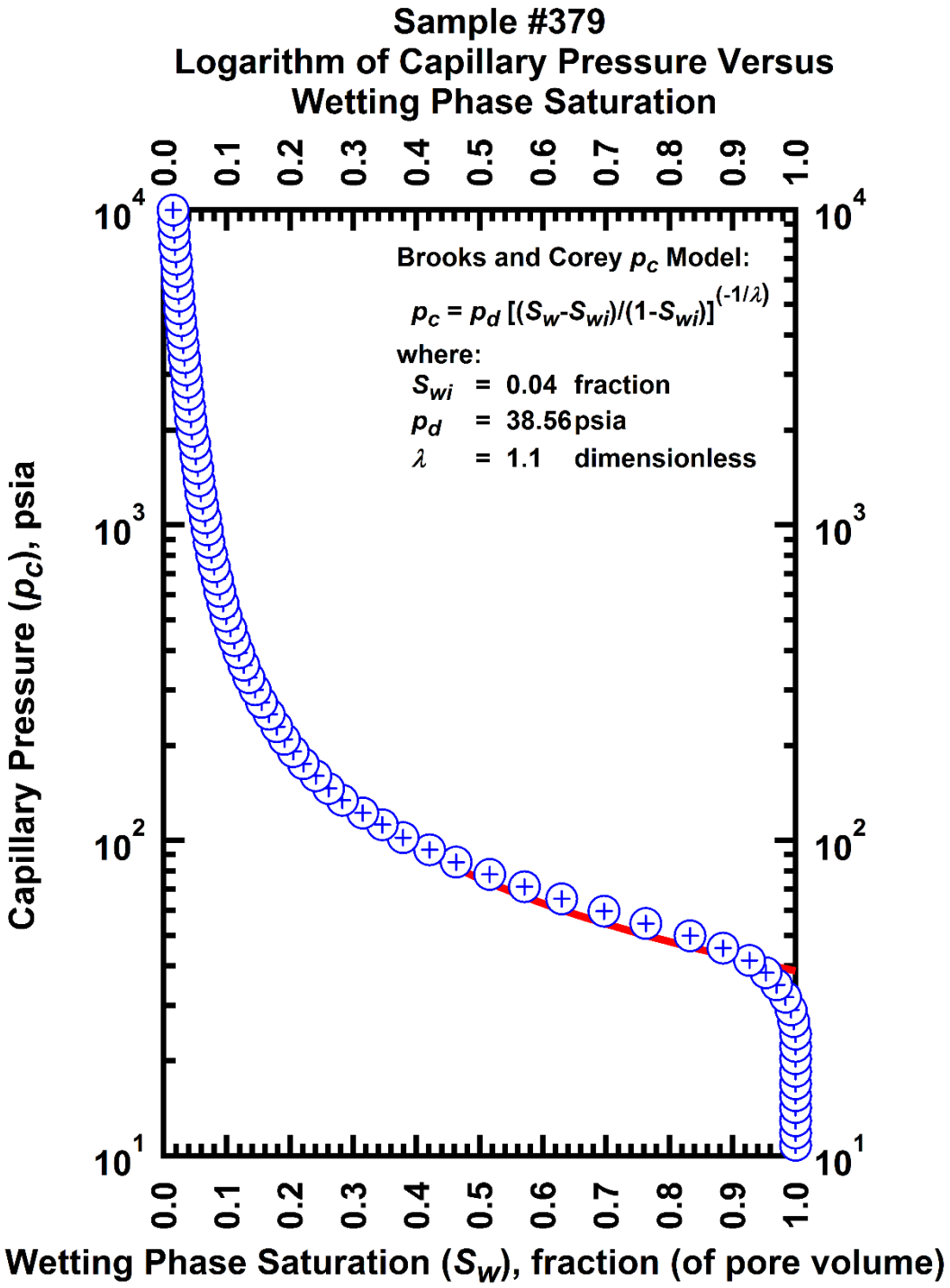

Figure H-14 — Plot of logarithm of capillary pressure vs. wetting phase saturation — Sample #379.

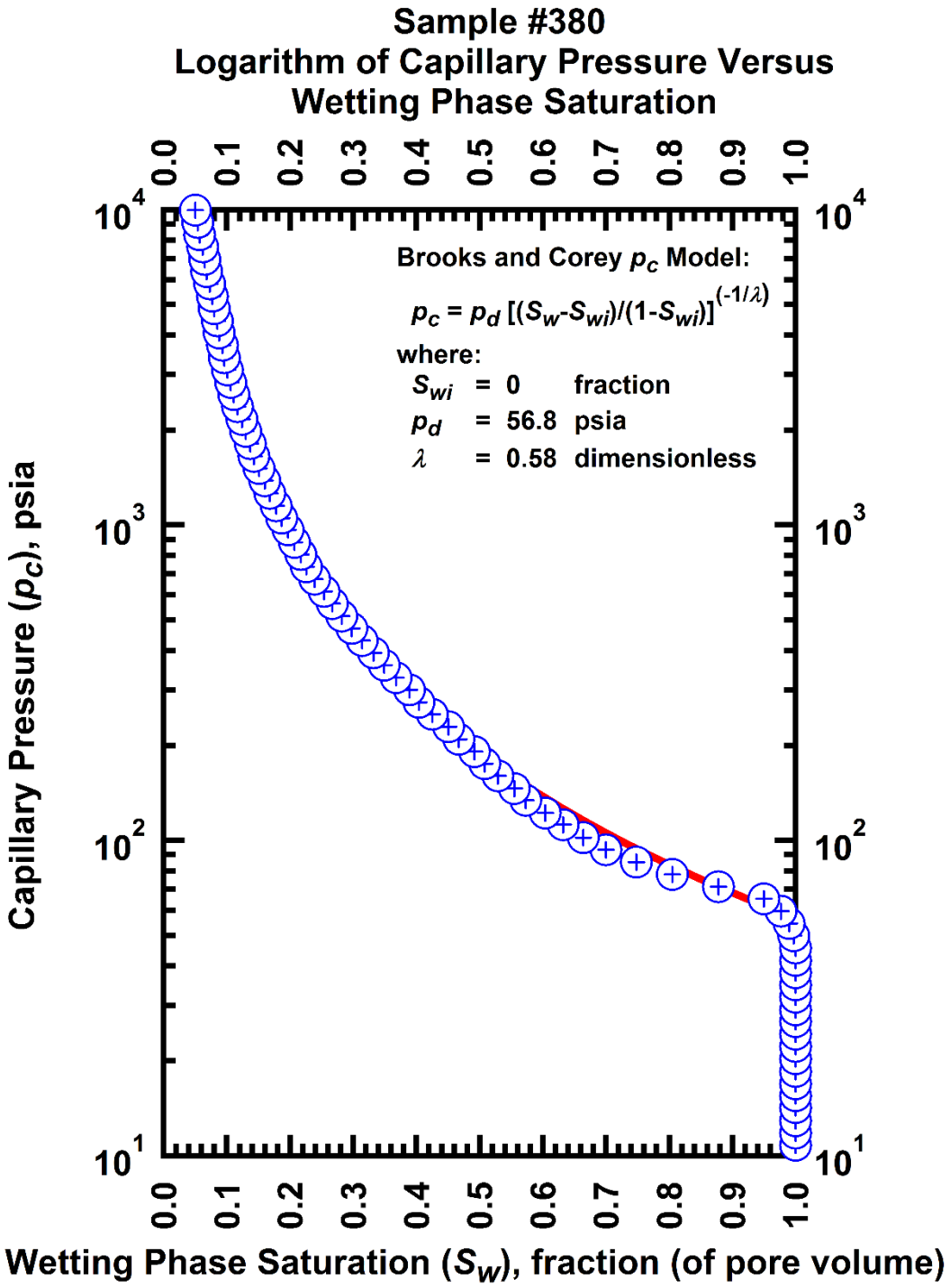

Figure H-15 — Plot of logarithm of capillary pressure vs. wetting phase saturation — Sample #380.

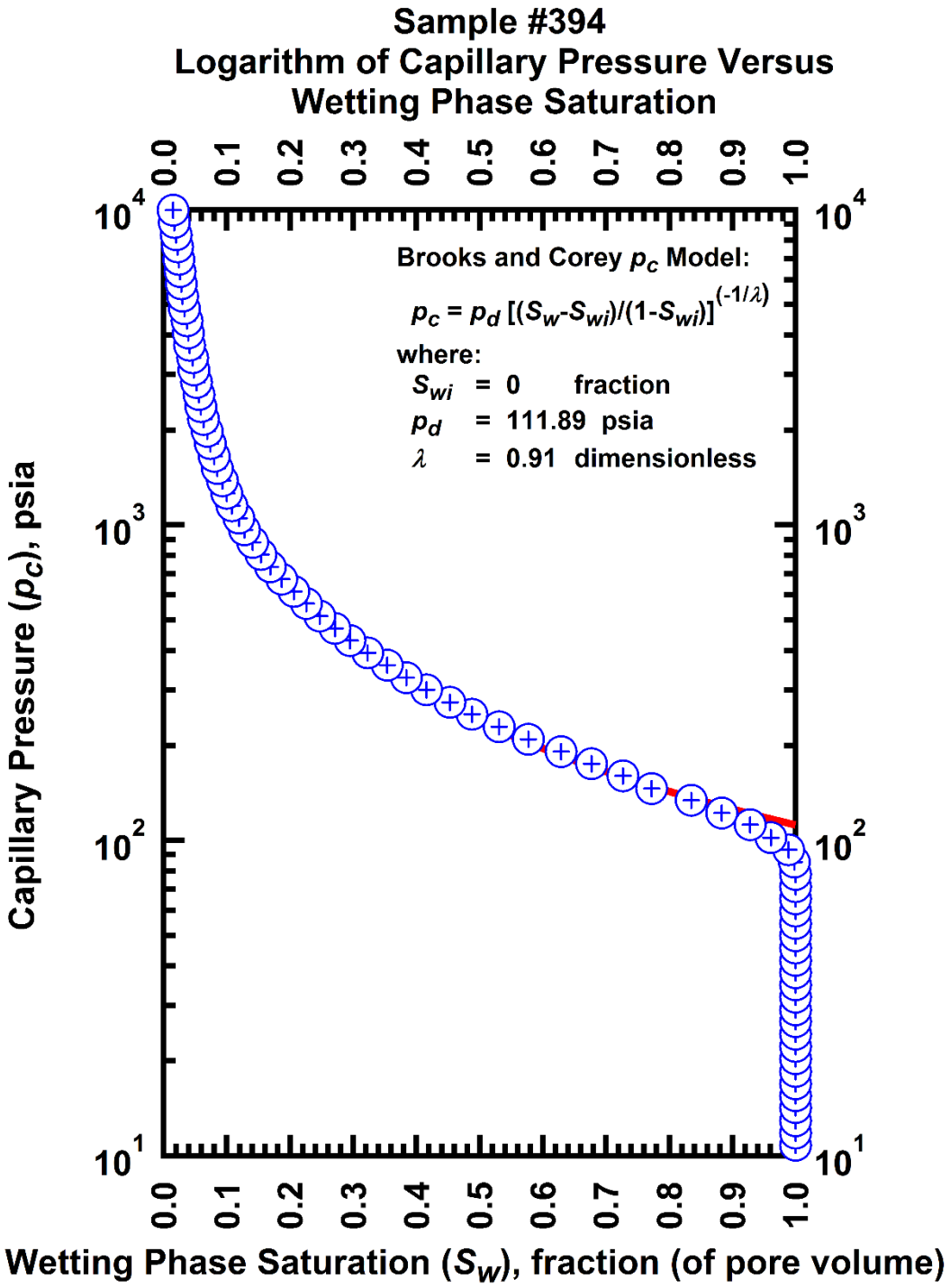

Figure H-16 — Plot of logarithm of capillary pressure vs. wetting phase saturation — Sample #394.

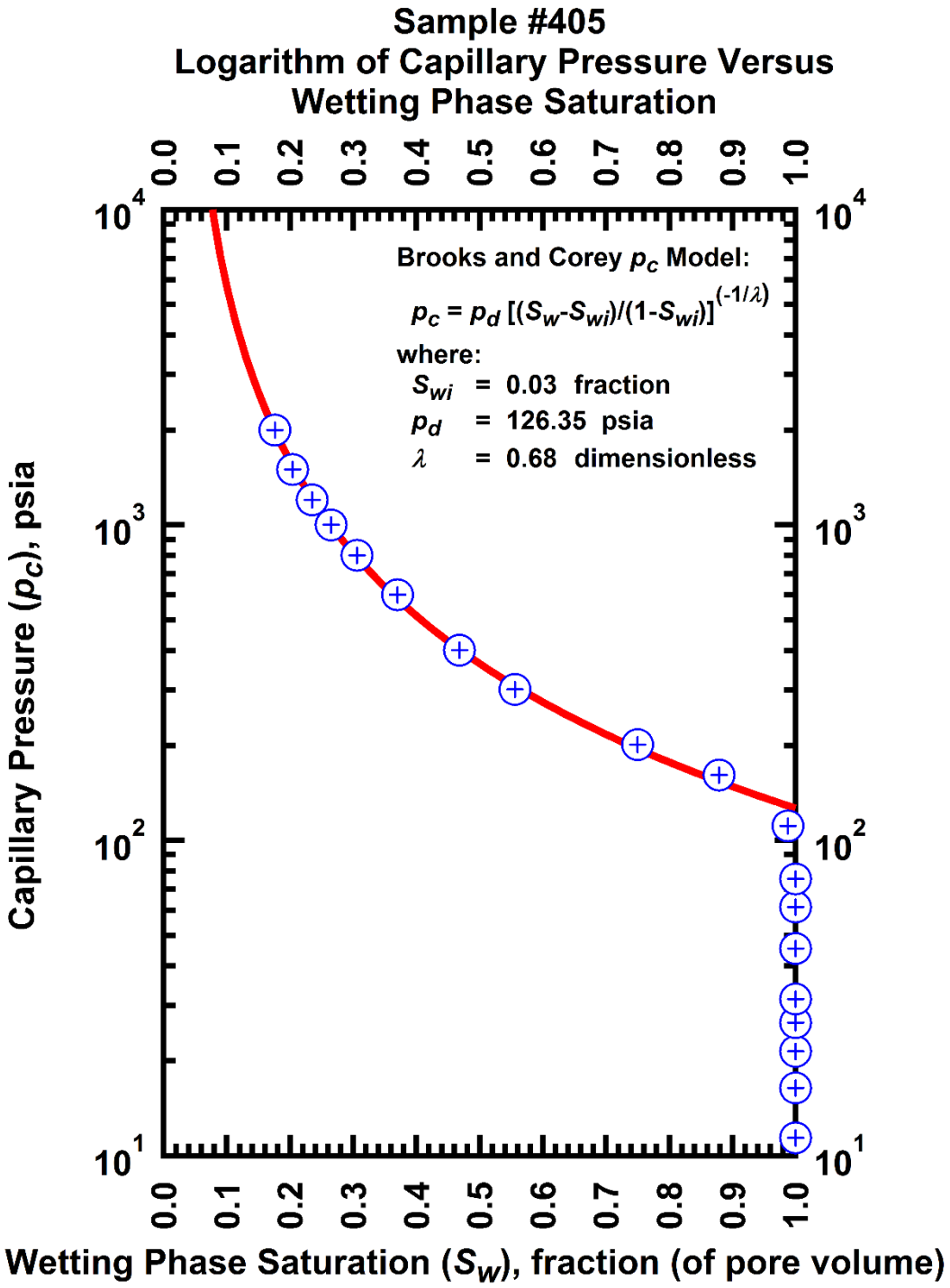

Figure H-17 — Plot of logarithm of capillary pressure vs. wetting phase saturation — Sample #405.

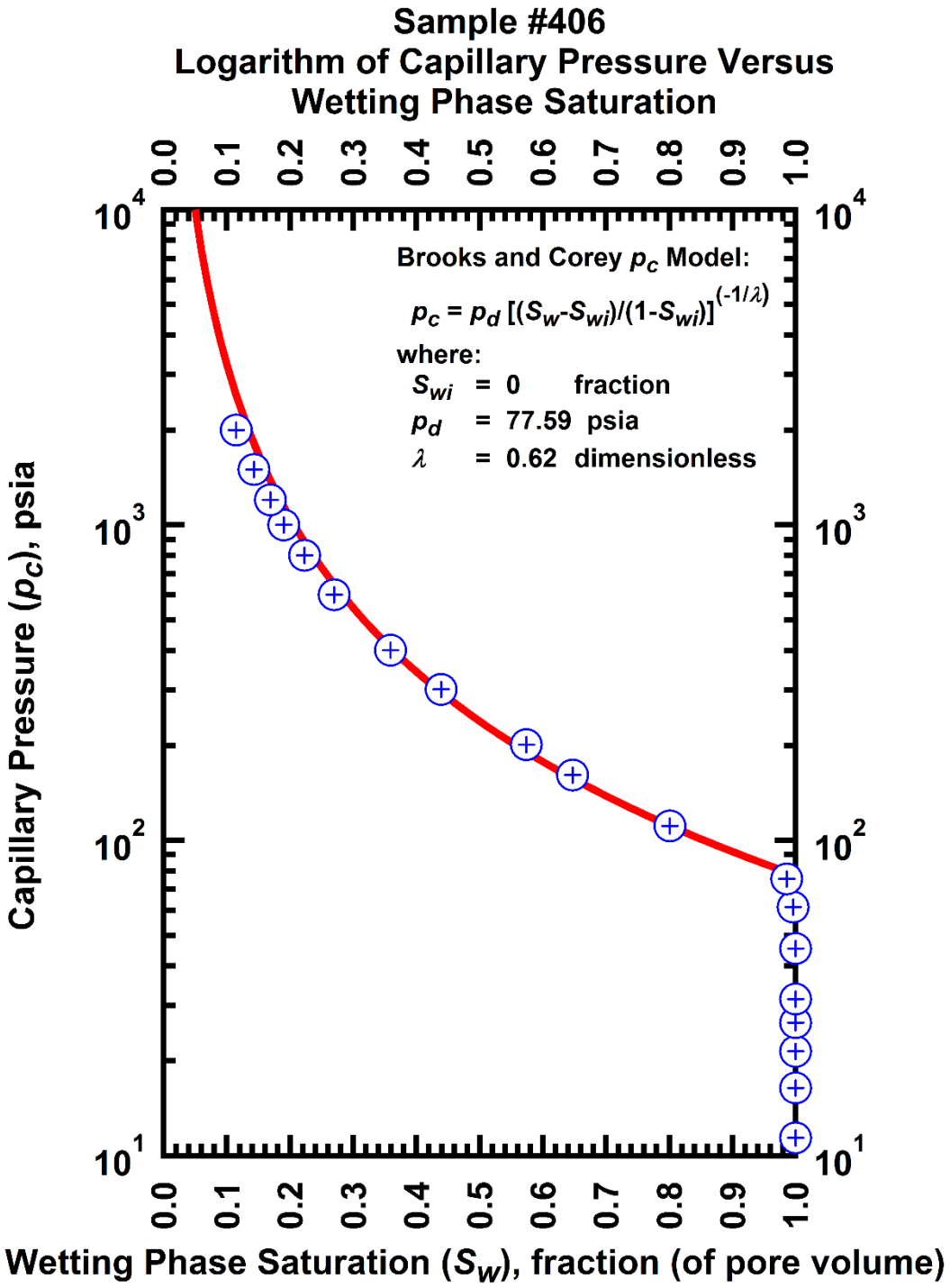

Figure H-18 — Plot of logarithm of capillary pressure vs. wetting phase saturation — Sample #406.

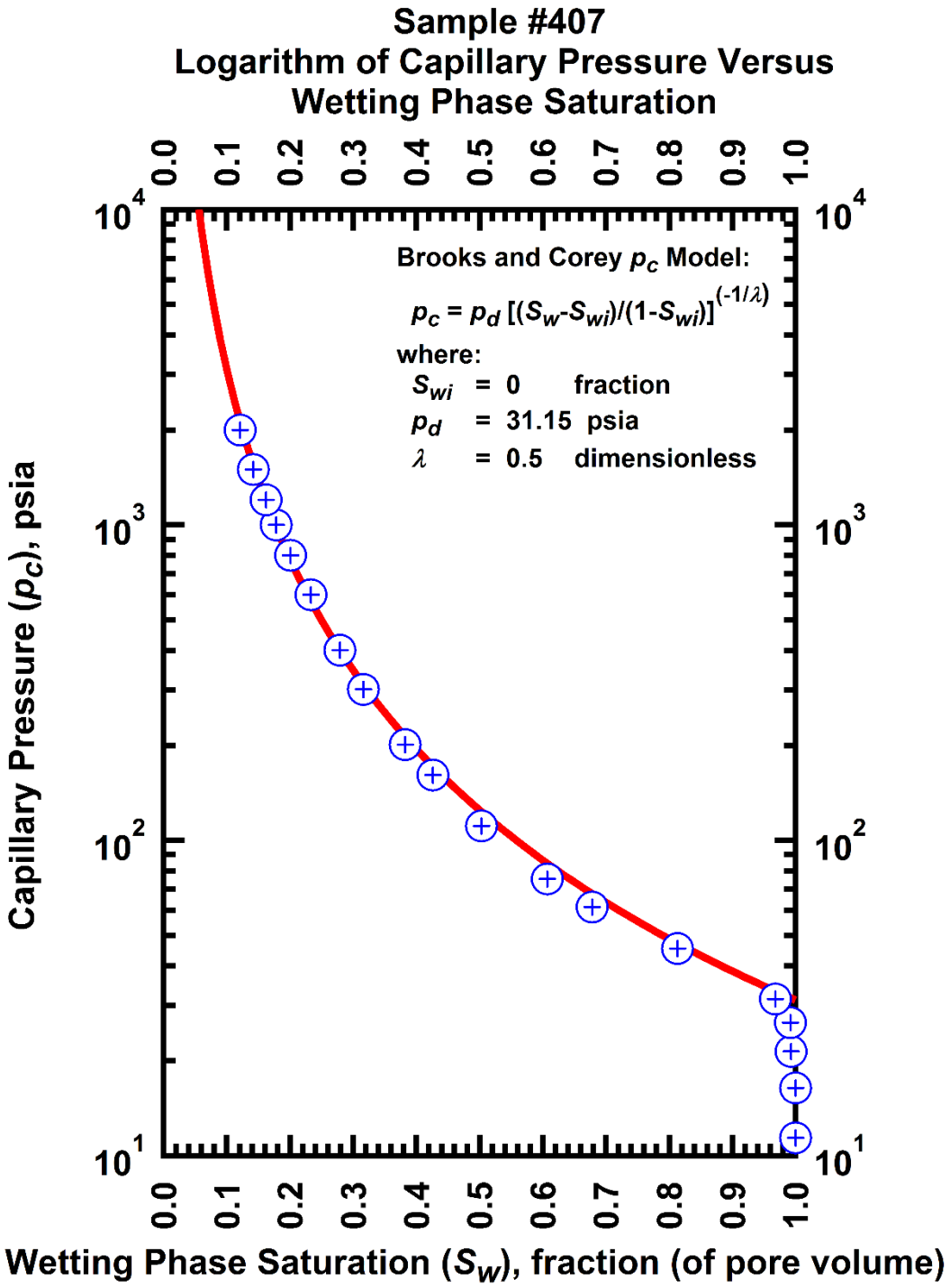

Figure H-19 — Plot of logarithm of capillary pressure vs. wetting phase saturation — Sample #407.

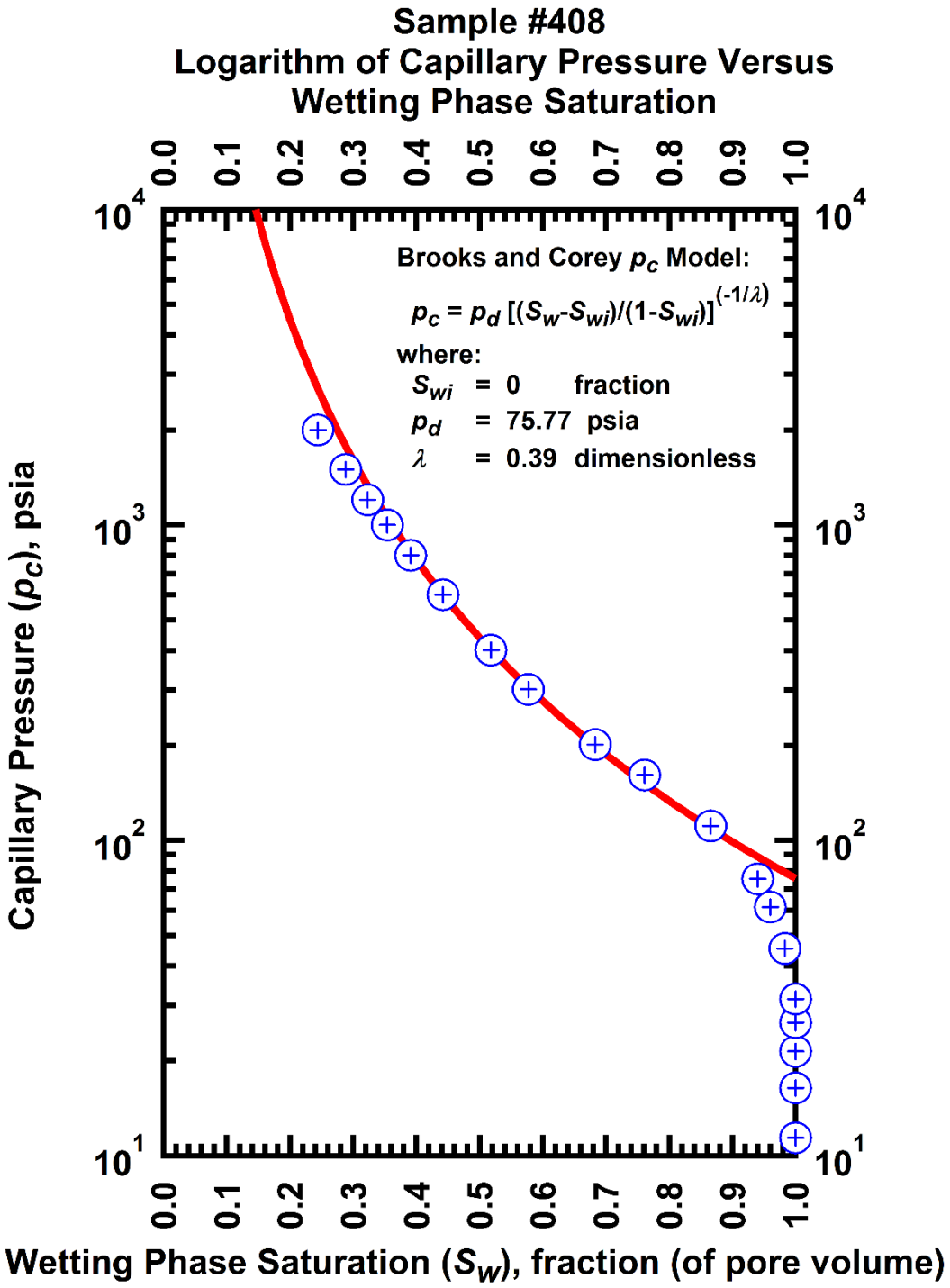

Figure H-20 — Plot of logarithm of capillary pressure vs. wetting phase saturation — Sample #408.

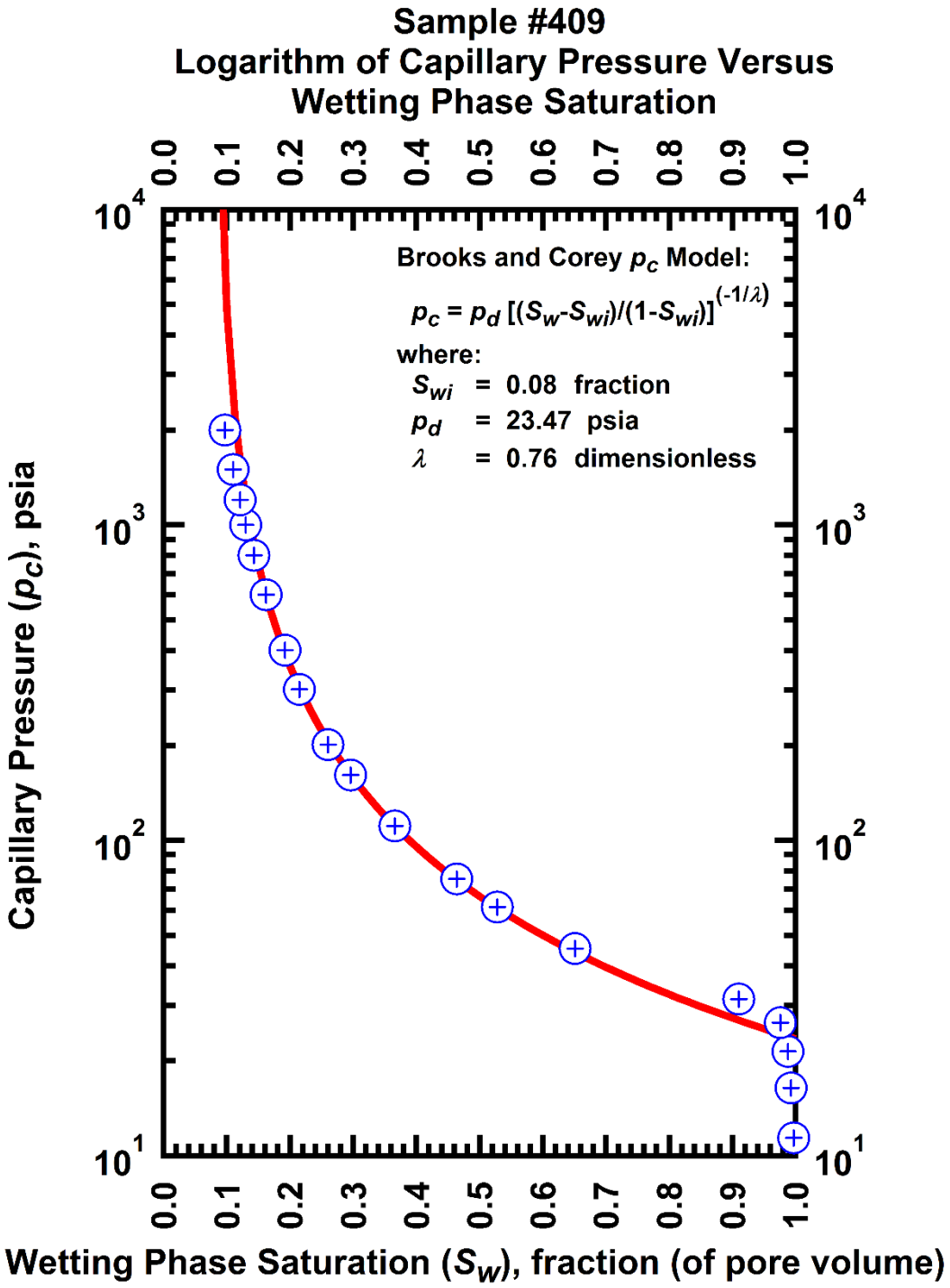

Figure H-21 — Plot of logarithm of capillary pressure vs. wetting phase saturation — Sample #409.

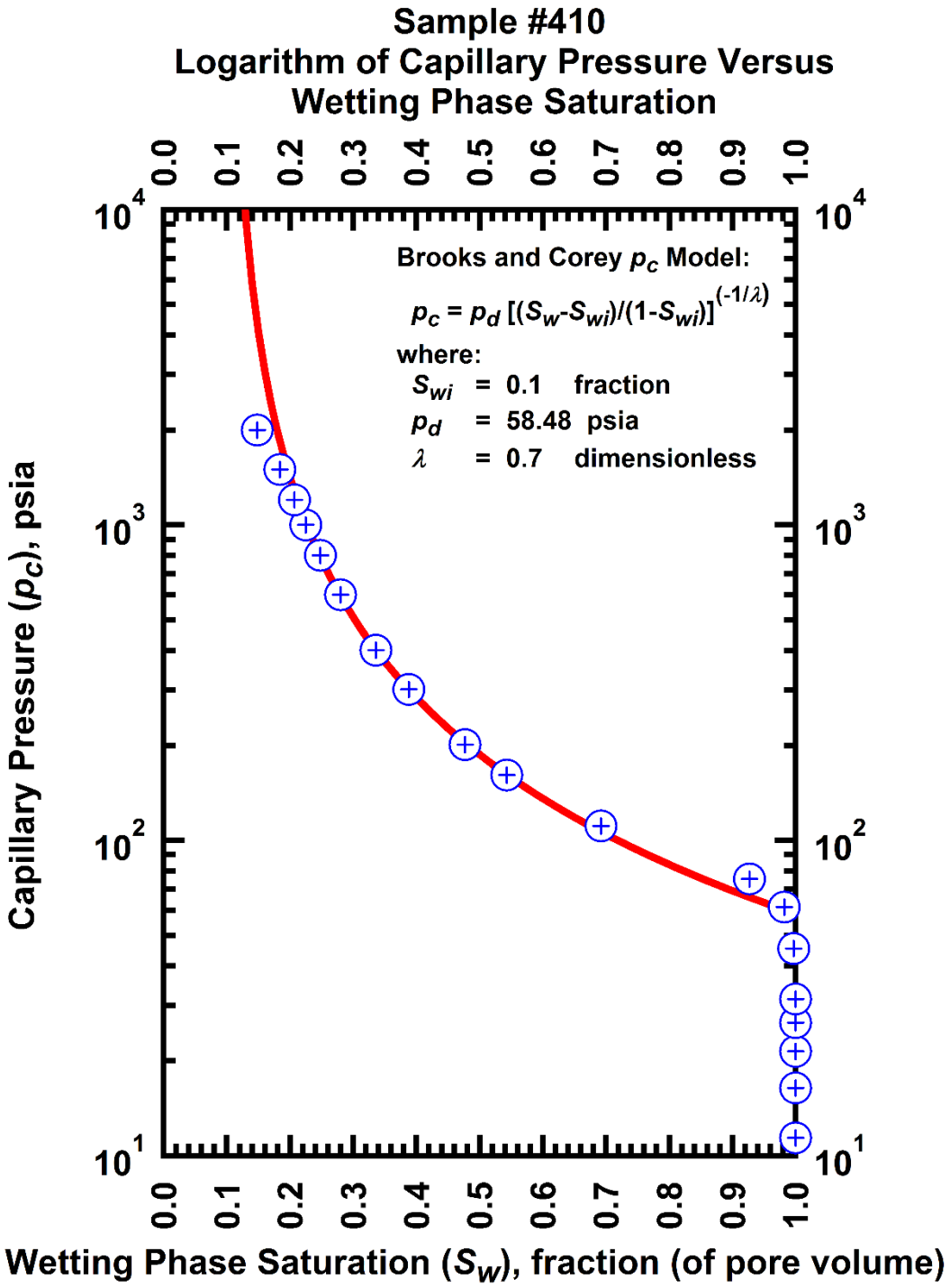

Figure H-22 — Plot of logarithm of capillary pressure vs. wetting phase saturation — Sample #410.

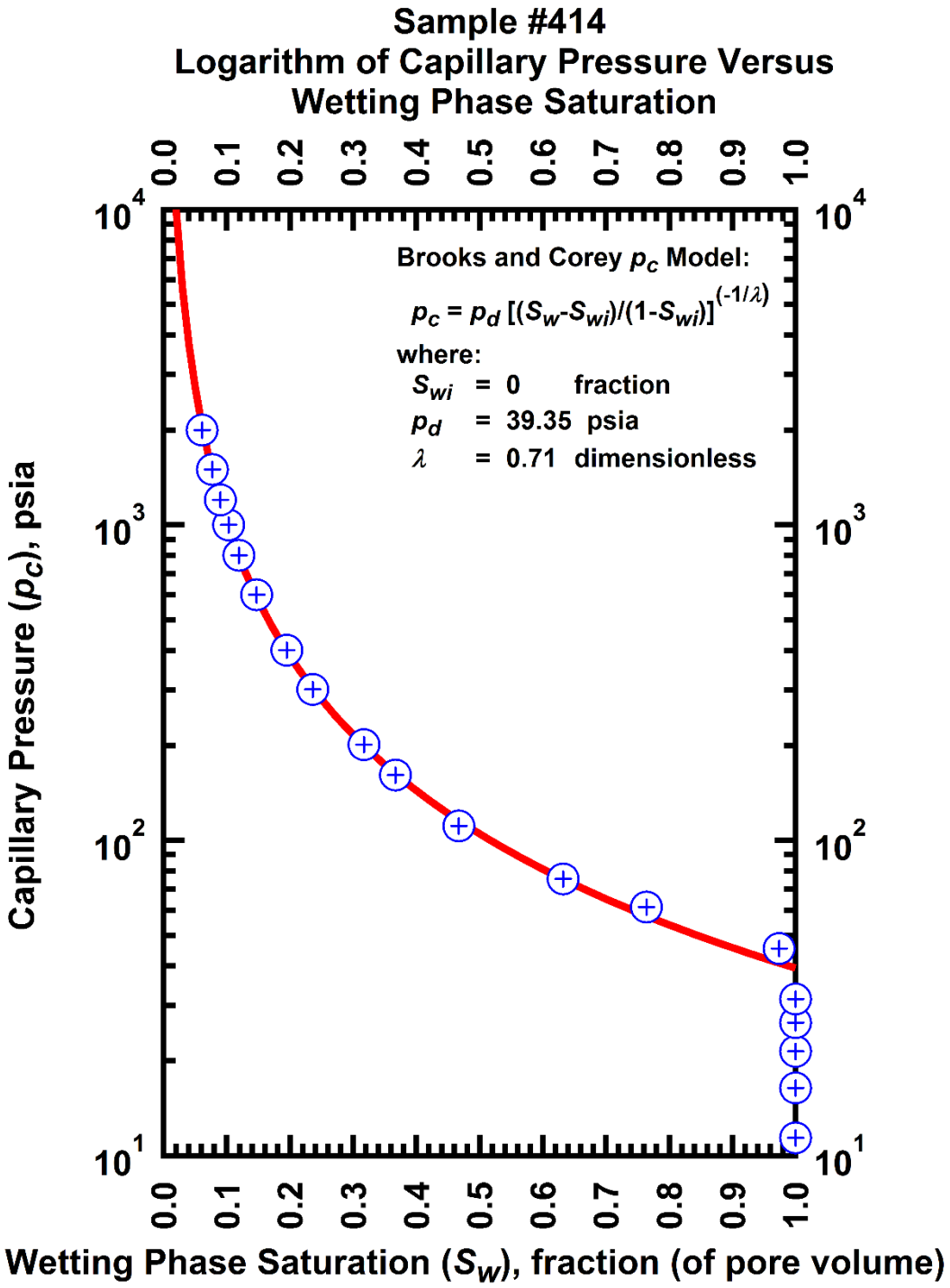

Figure H-23 — Plot of logarithm of capillary pressure vs. wetting phase saturation — Sample #414.

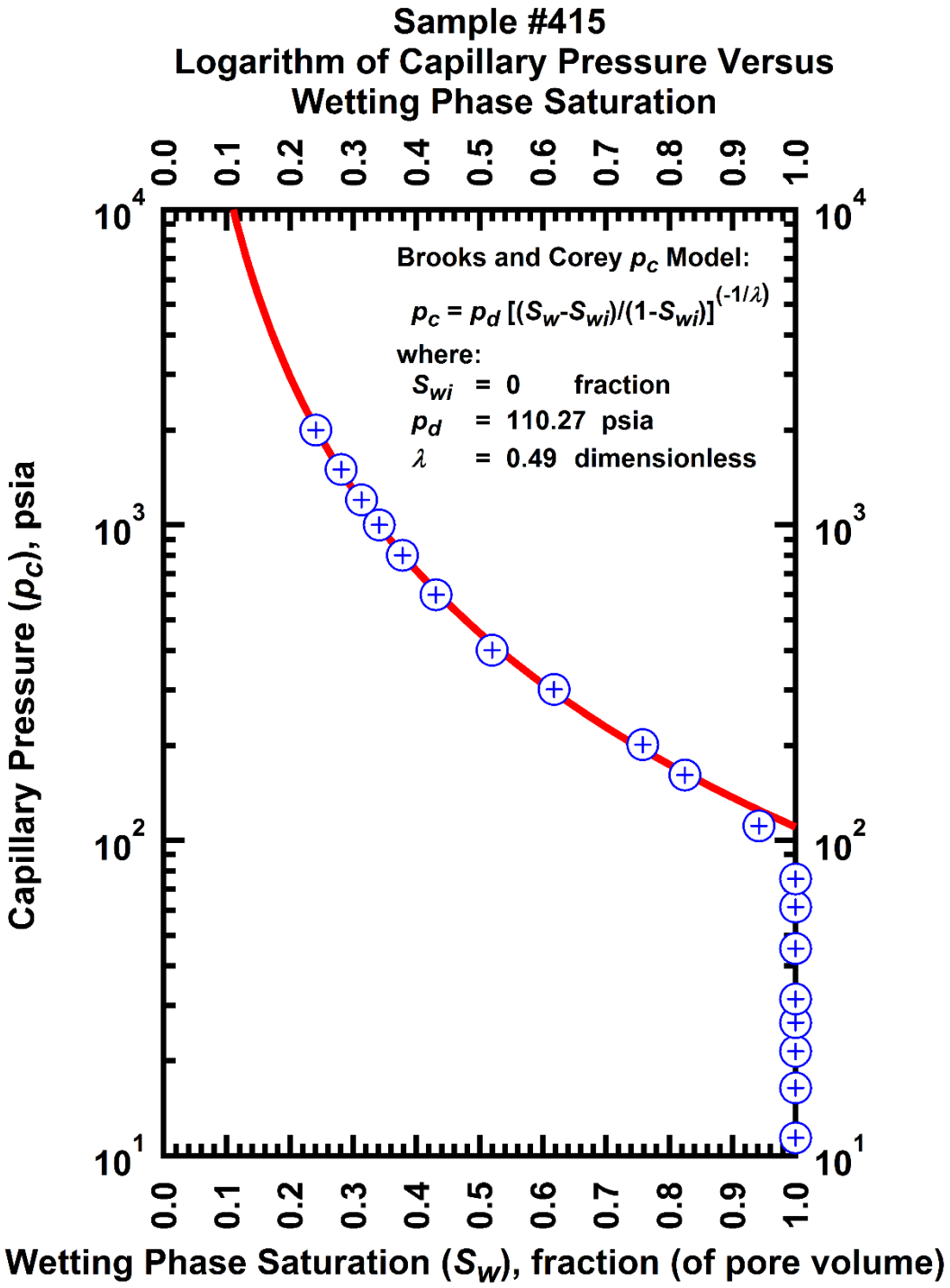

Figure H-24 — Plot of logarithm of capillary pressure vs. wetting phase saturation — Sample #415.

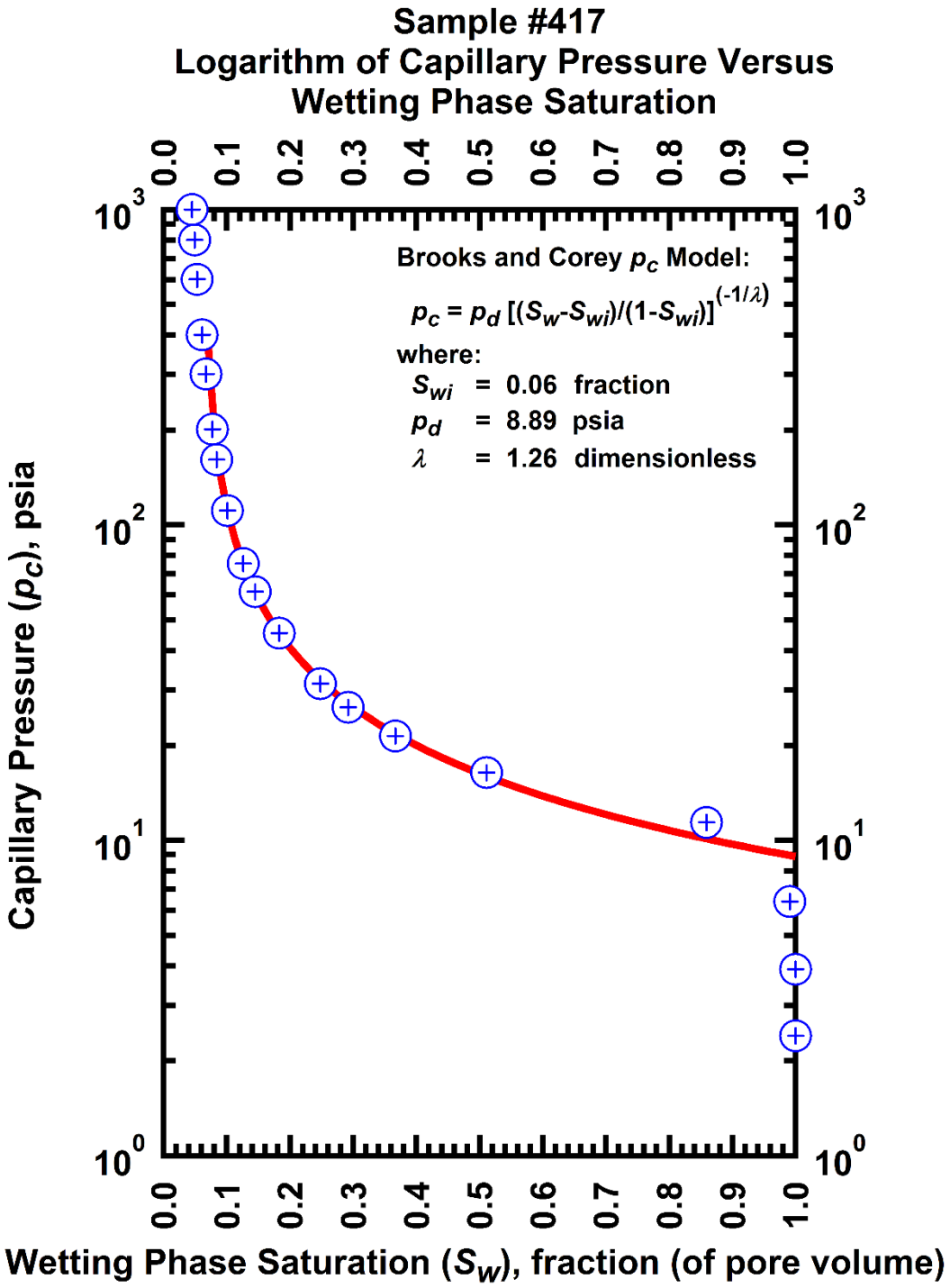

Figure H-25 — Plot of logarithm of capillary pressure vs. wetting phase saturation — Sample #417.

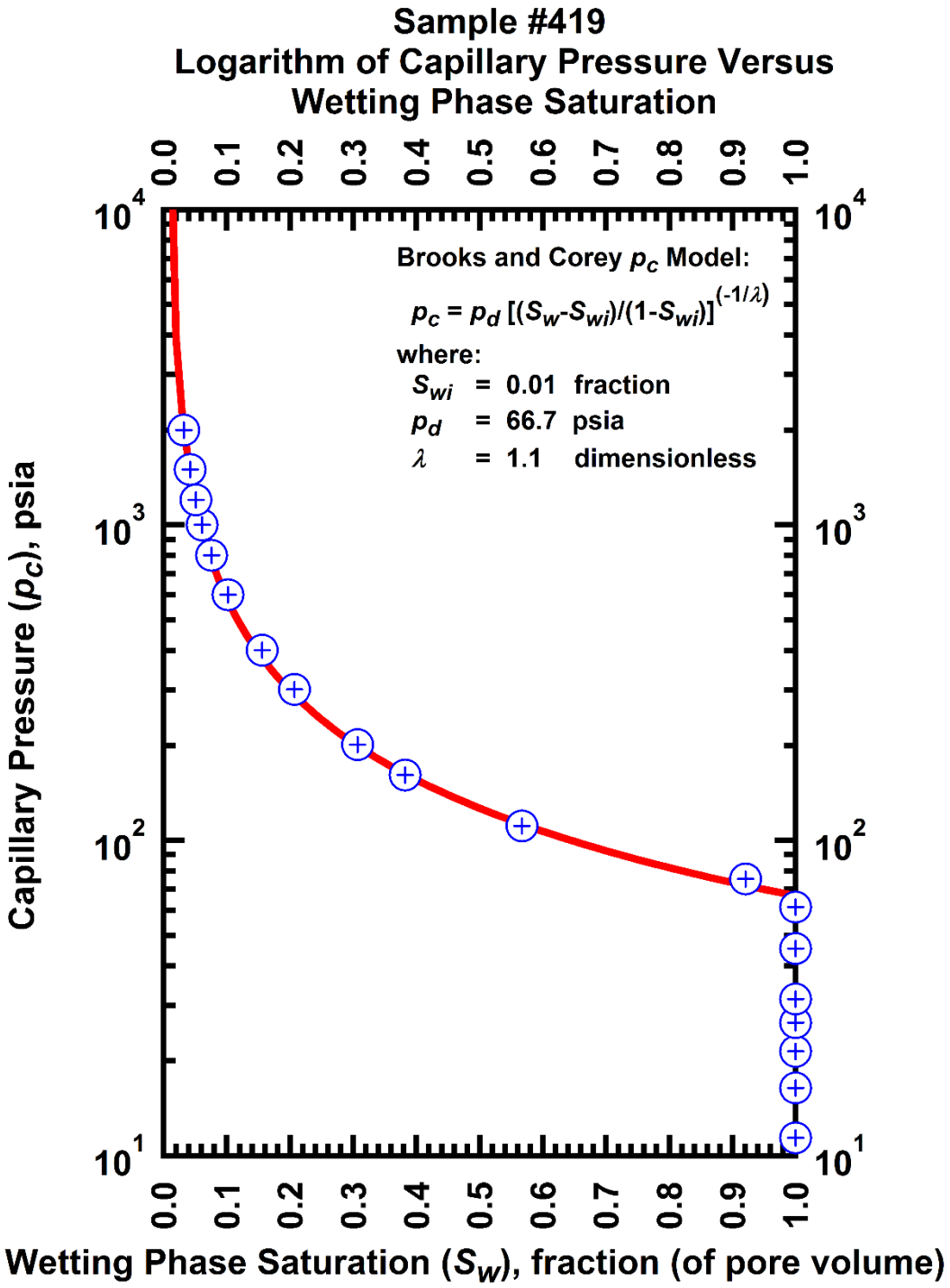

Figure H-26 — Plot of logarithm of capillary pressure vs. wetting phase saturation — Sample #419.

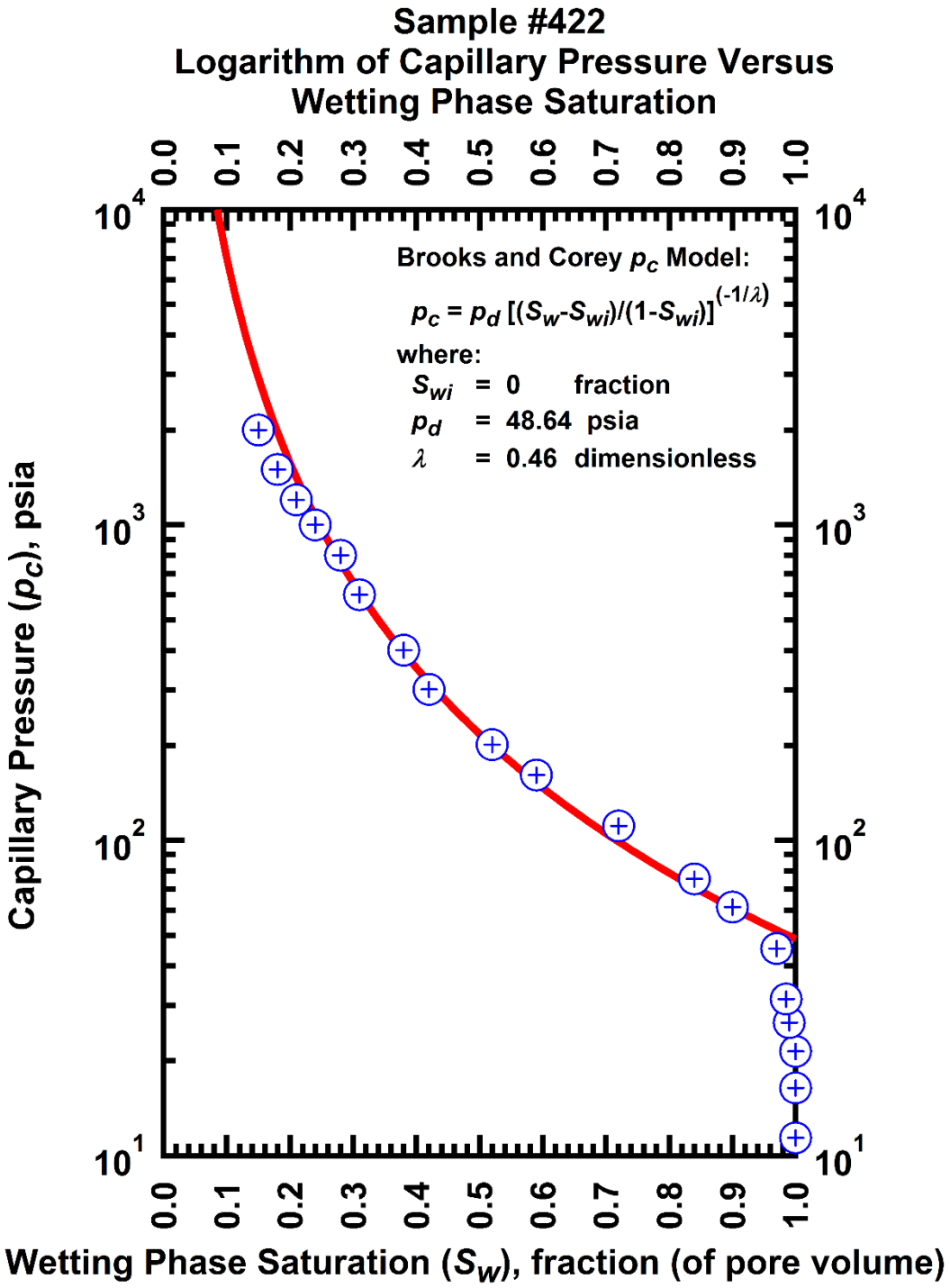

Figure H-27 — Plot of logarithm of capillary pressure vs. wetting phase saturation — Sample #422.

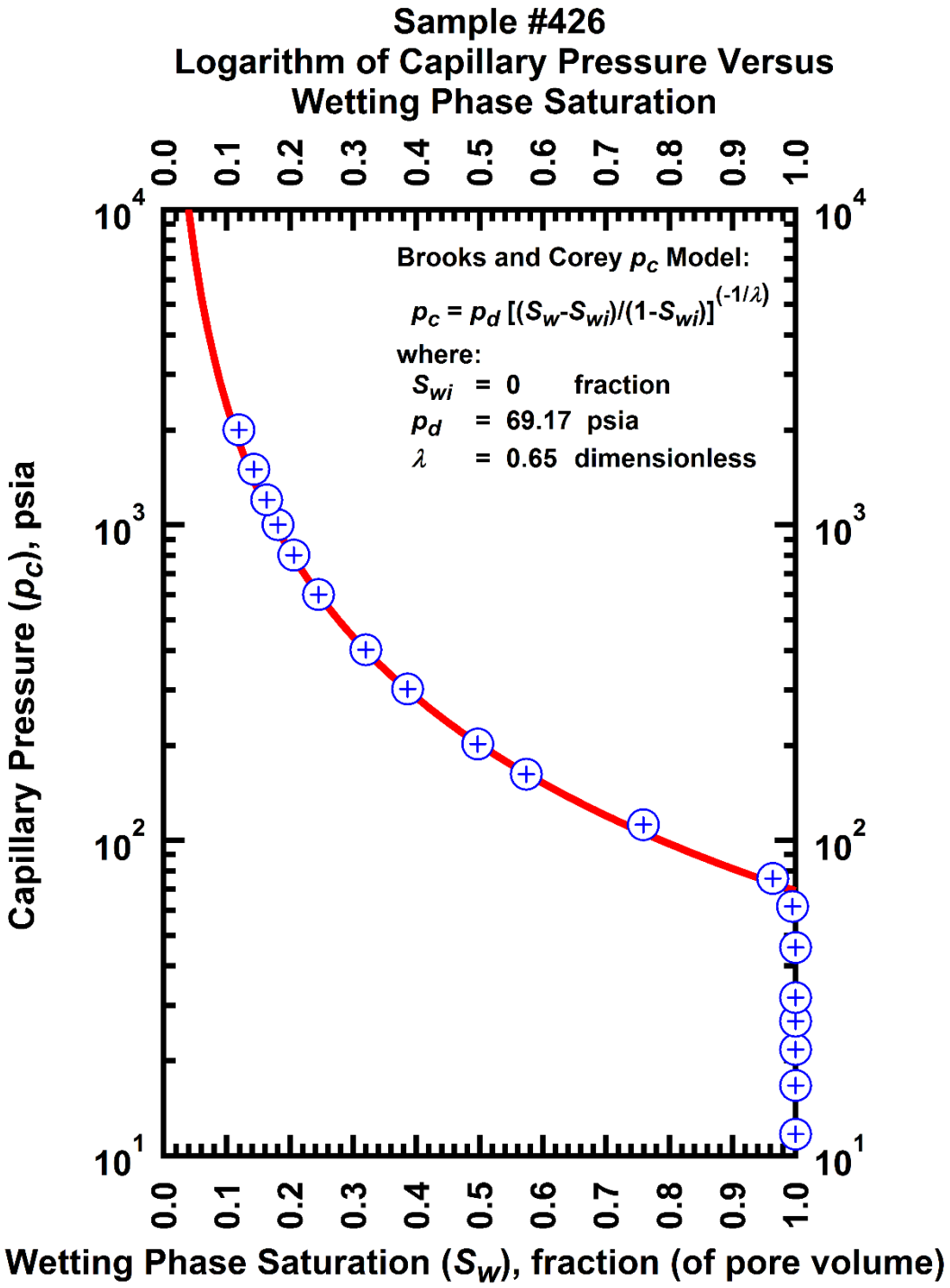

Figure H-28 — Plot of logarithm of capillary pressure vs. wetting phase saturation — Sample #426.

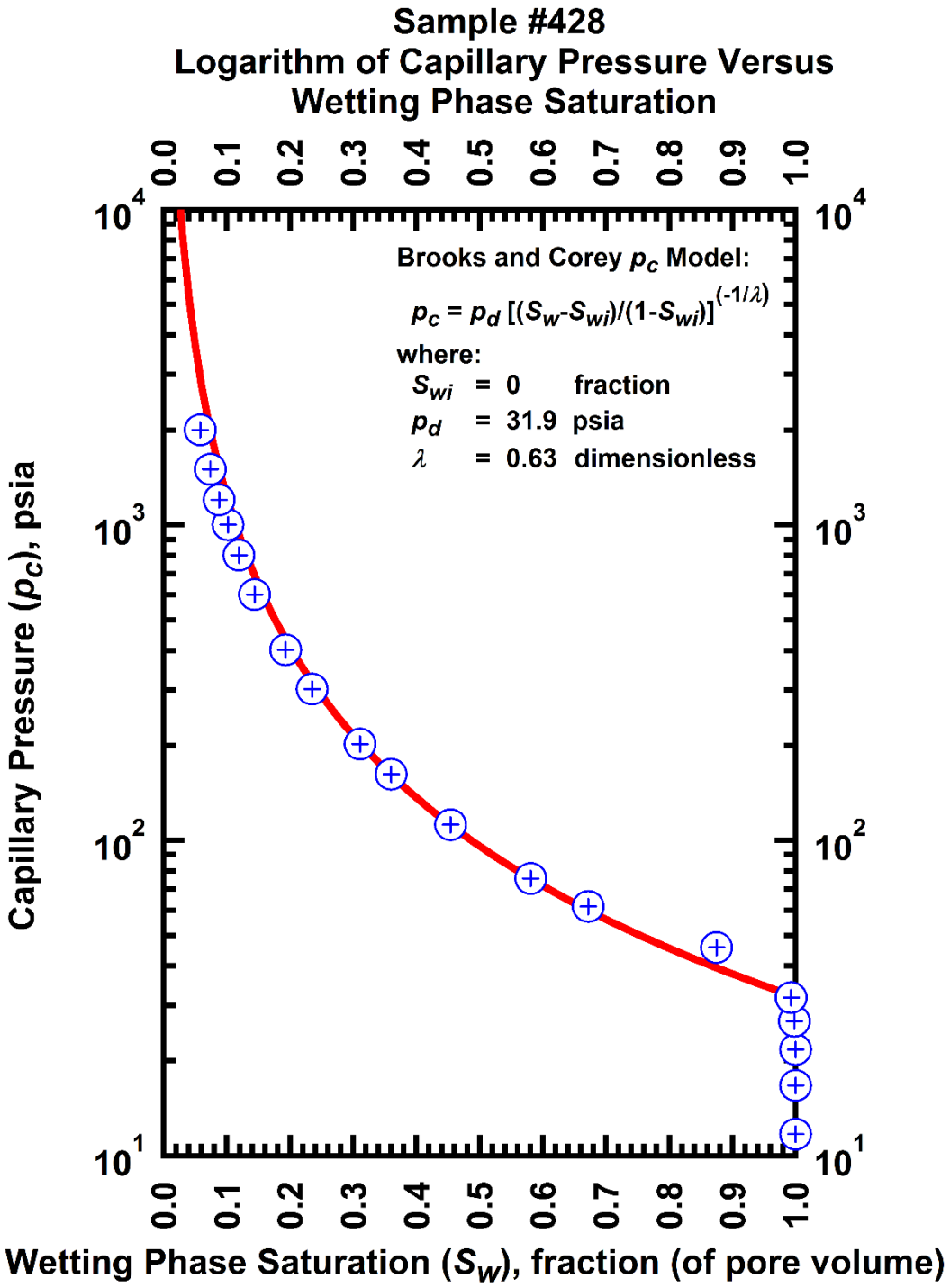

Figure H-29 — Plot of logarithm of capillary pressure vs. wetting phase saturation — Sample #428.

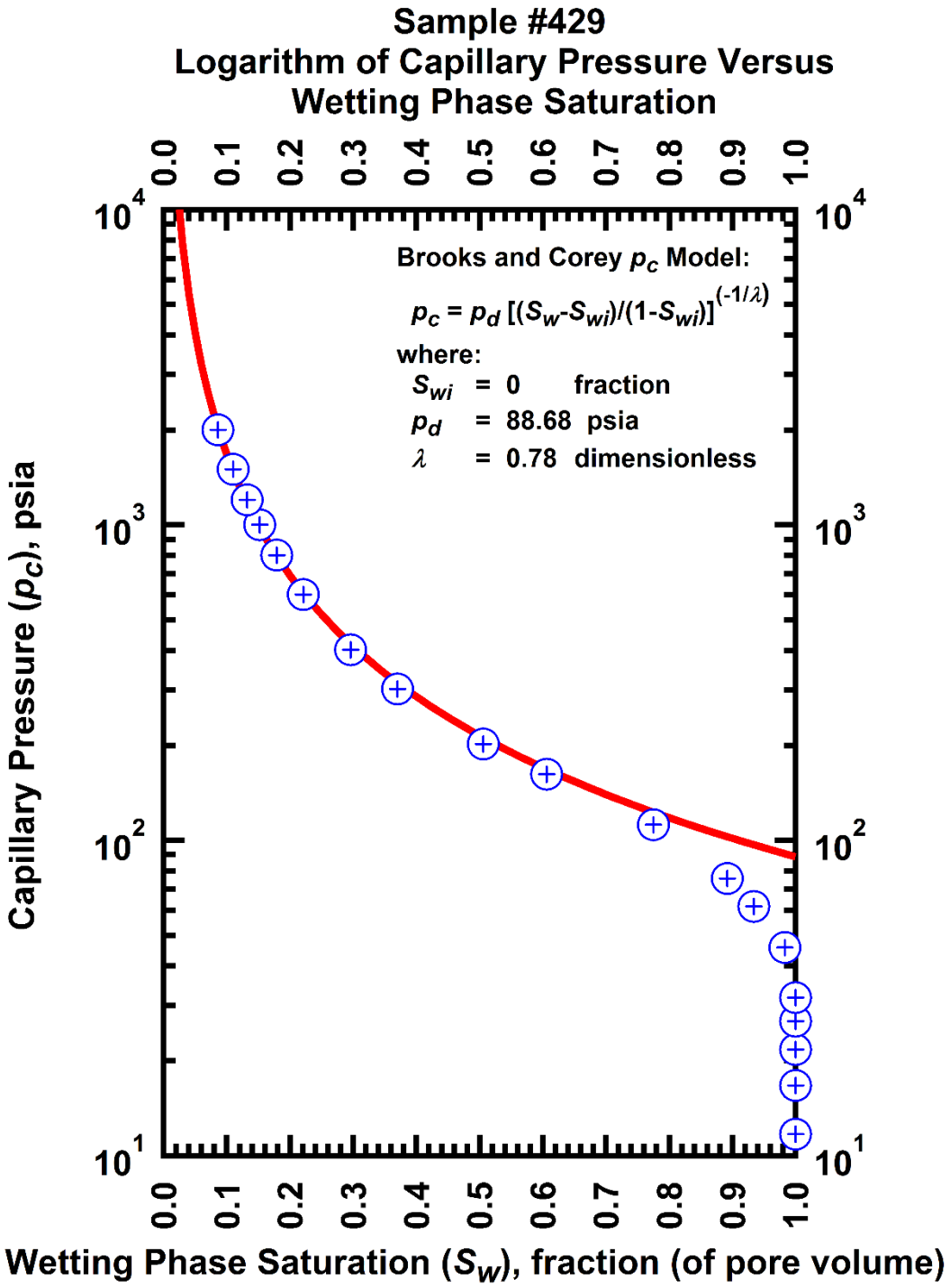

Figure H-30 — Plot of logarithm of capillary pressure vs. wetting phase saturation — Sample #429.

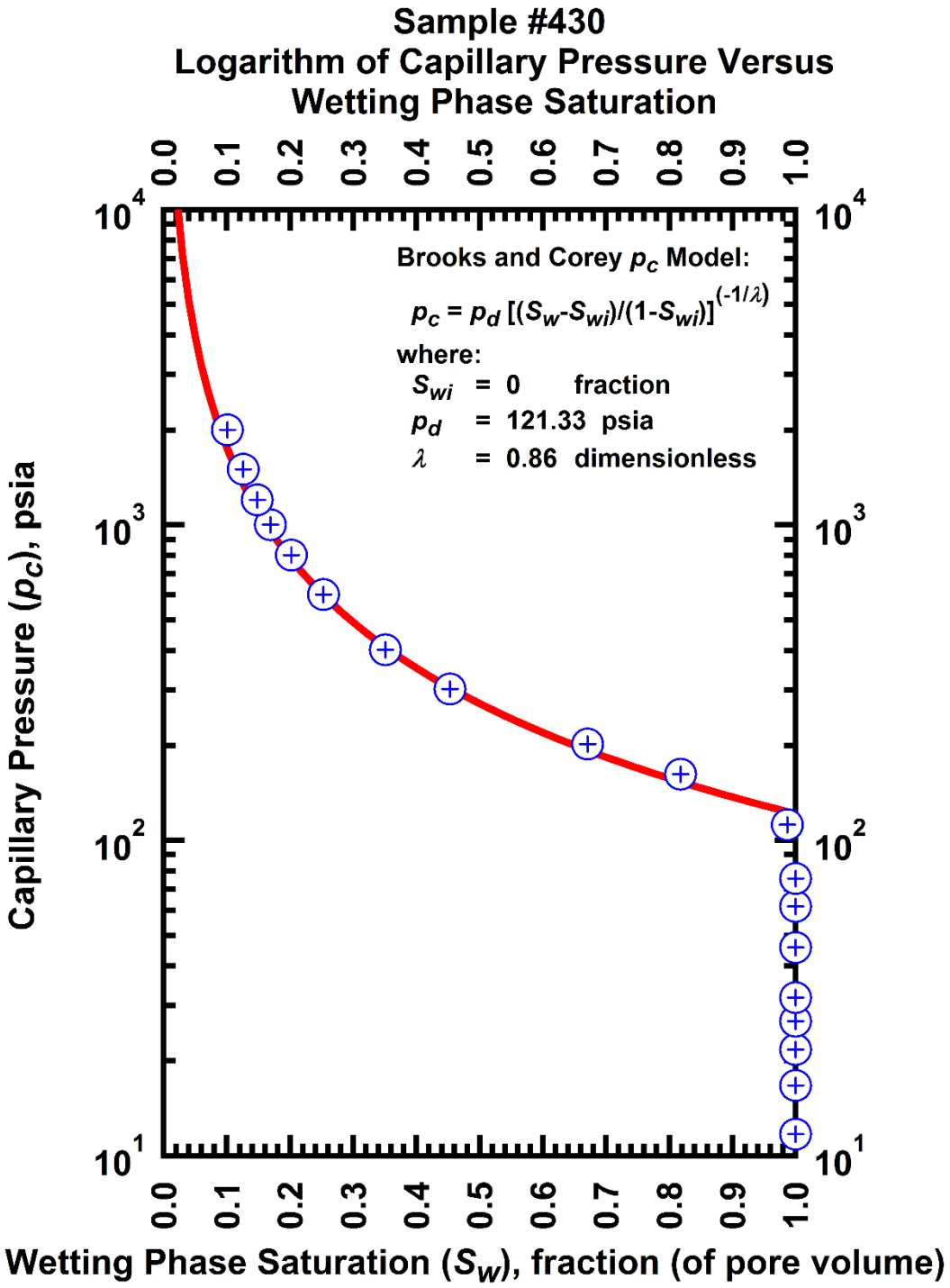

Figure H-31 — Plot of logarithm of capillary pressure vs. wetting phase saturation — Sample #430.

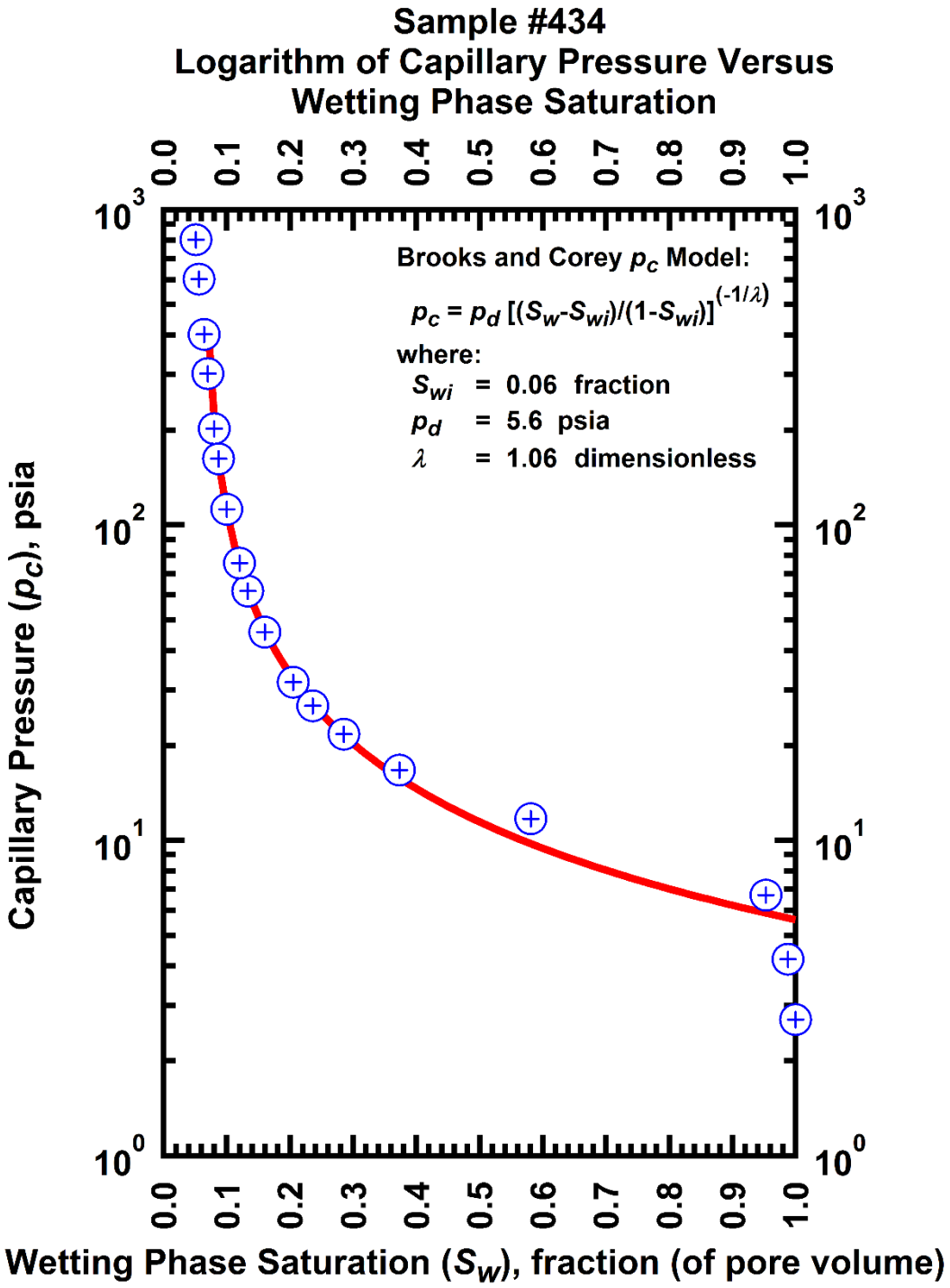

Figure H-32 — Plot of logarithm of capillary pressure vs. wetting phase saturation — Sample #434.

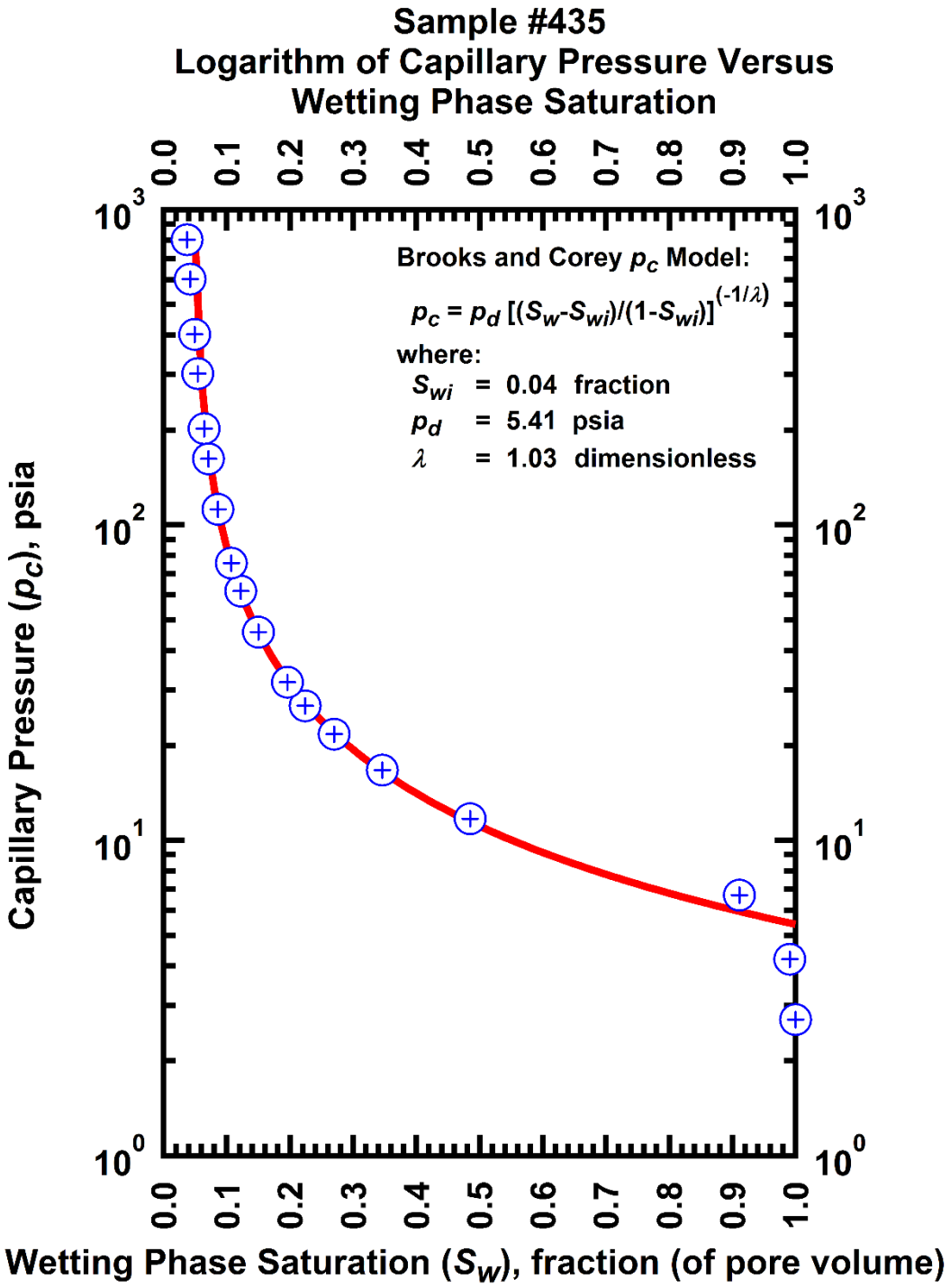

Figure H-33 — Plot of logarithm of capillary pressure vs. wetting phase saturation — Sample #435.

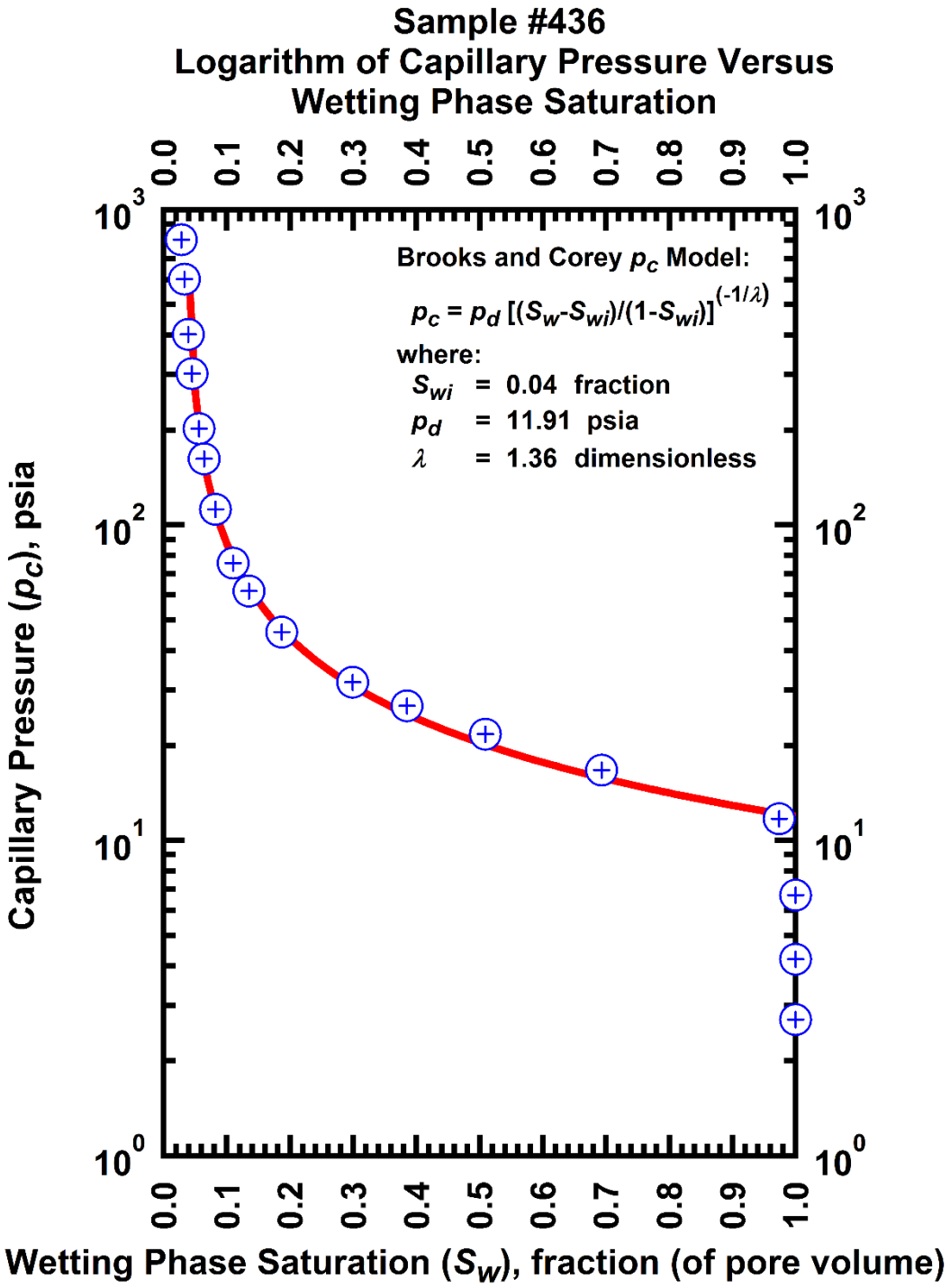

Figure H-34 — Plot of logarithm of capillary pressure vs. wetting phase saturation — Sample #436.

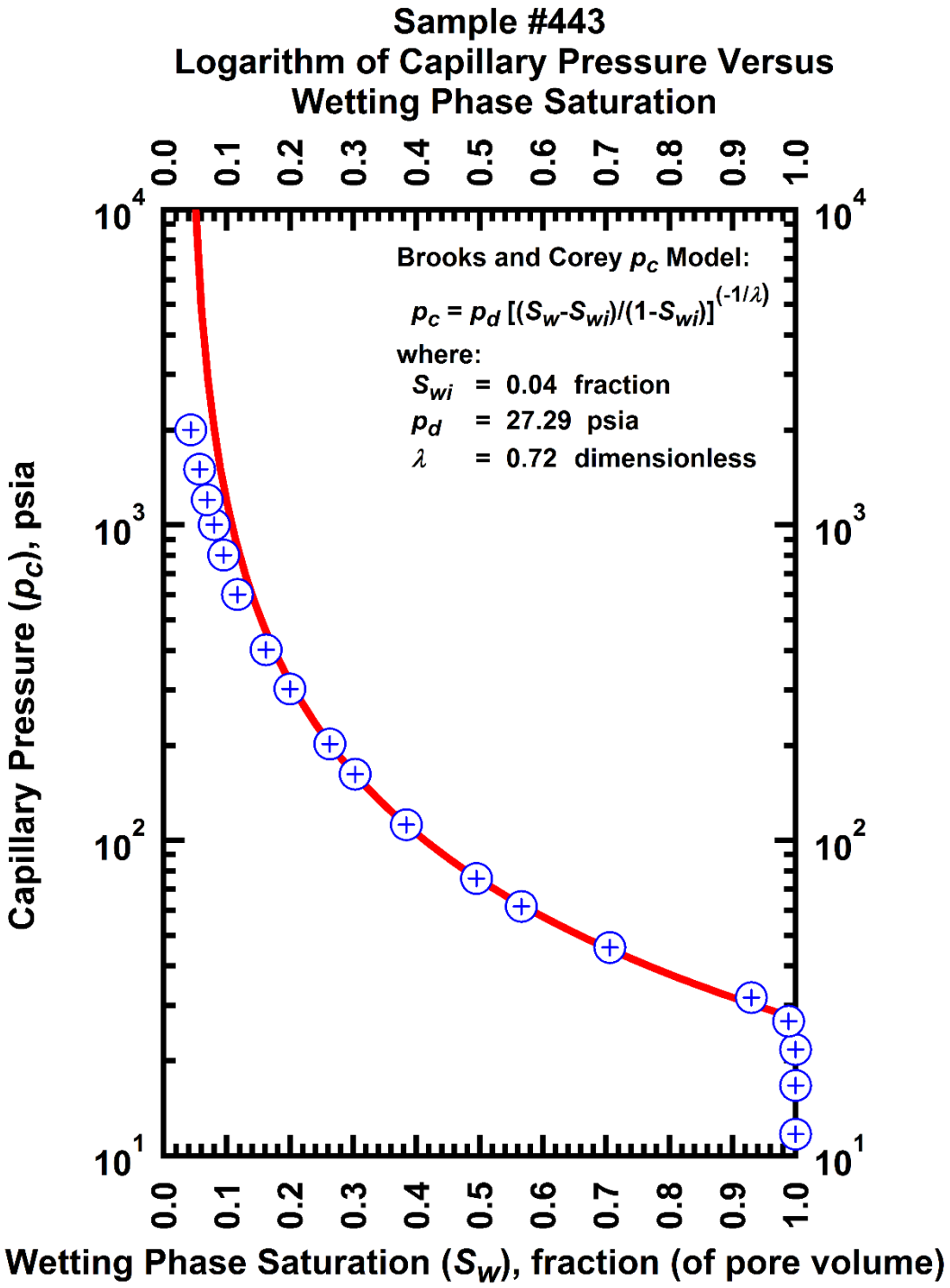

Figure H-35 — Plot of logarithm of capillary pressure vs. wetting phase saturation — Sample #443.

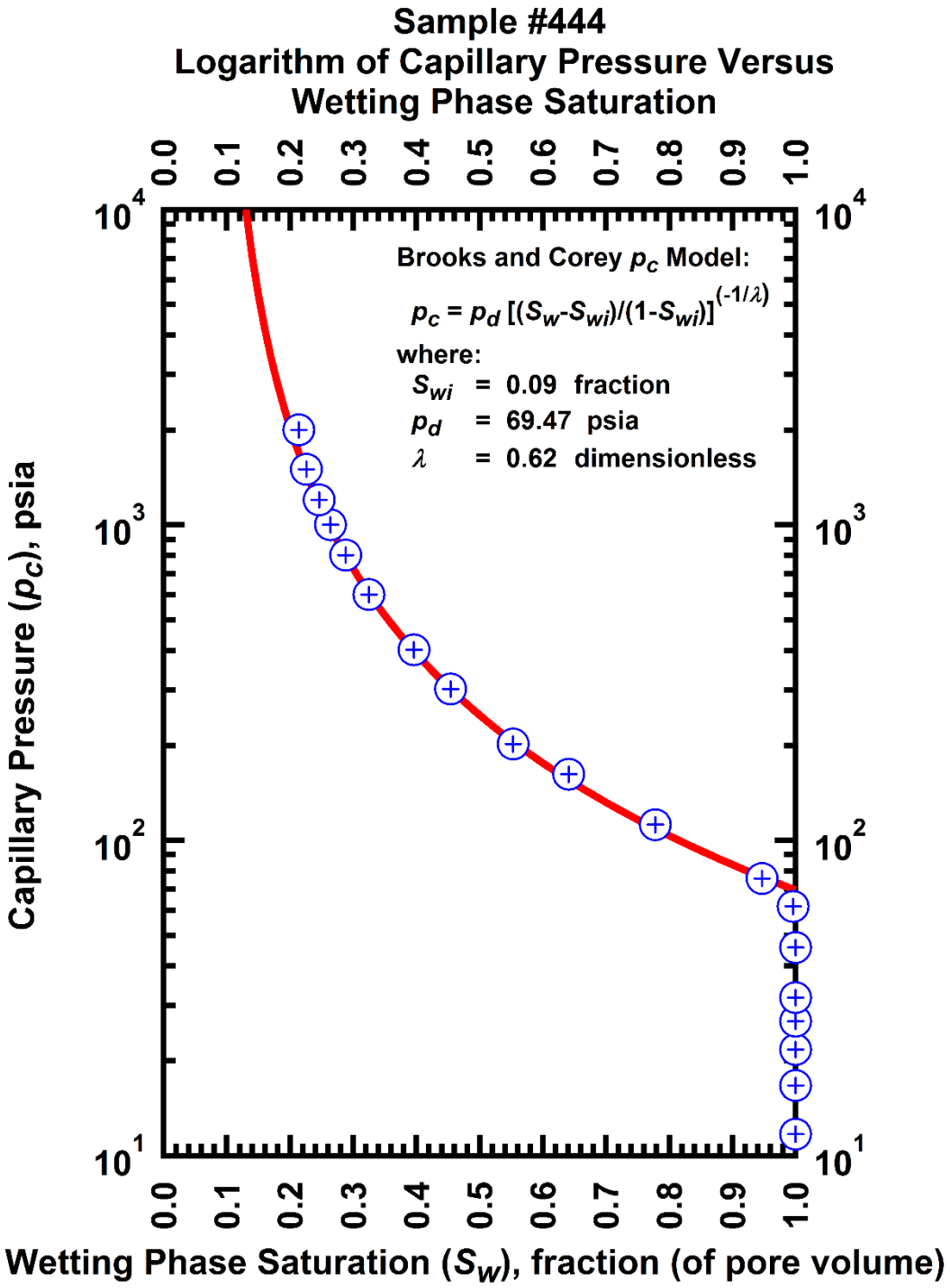

Figure H-36 — Plot of logarithm of capillary pressure vs. wetting phase saturation — Sample #444.

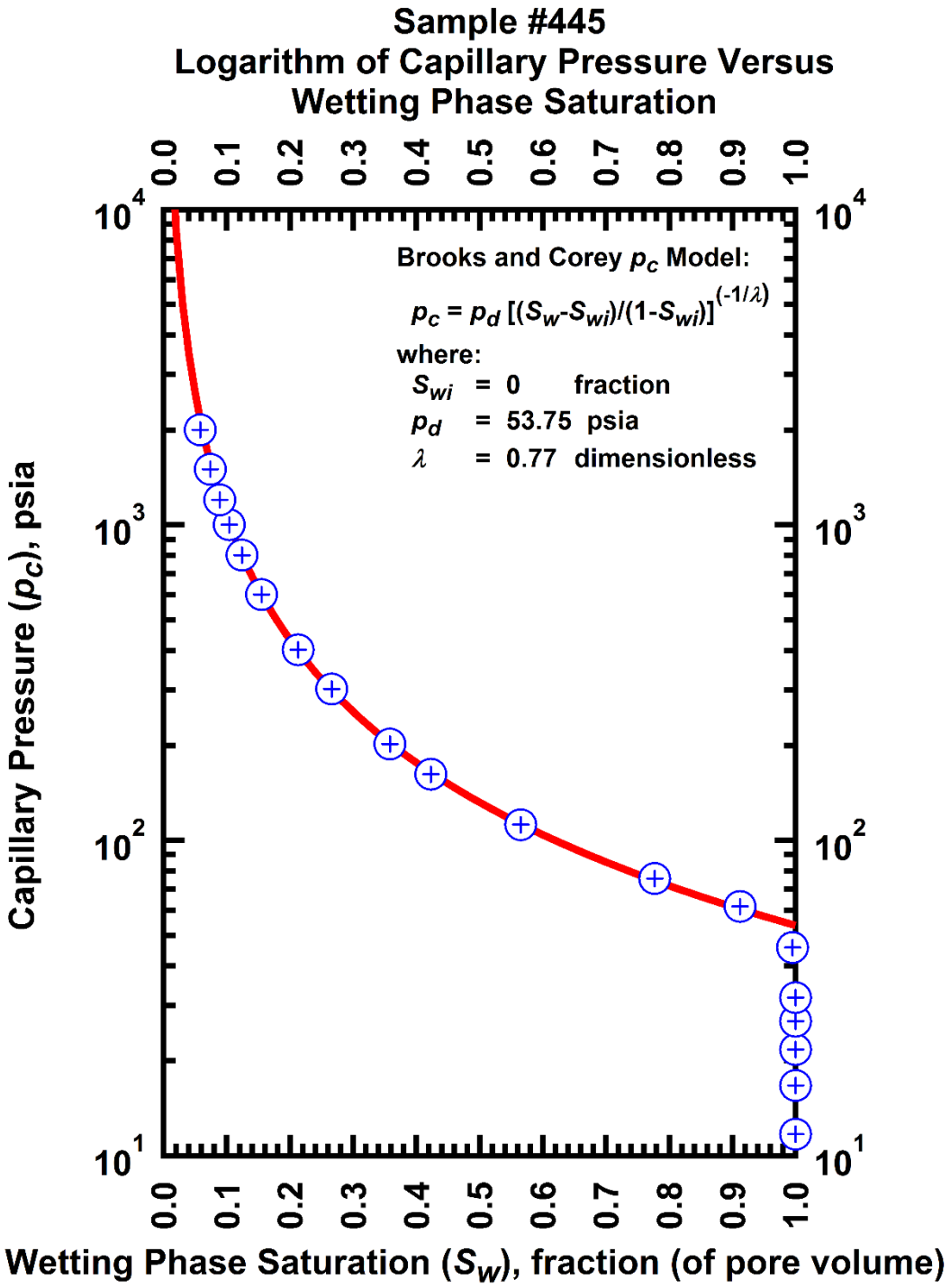

Figure H-37 — Plot of logarithm of capillary pressure vs. wetting phase saturation — Sample #445.

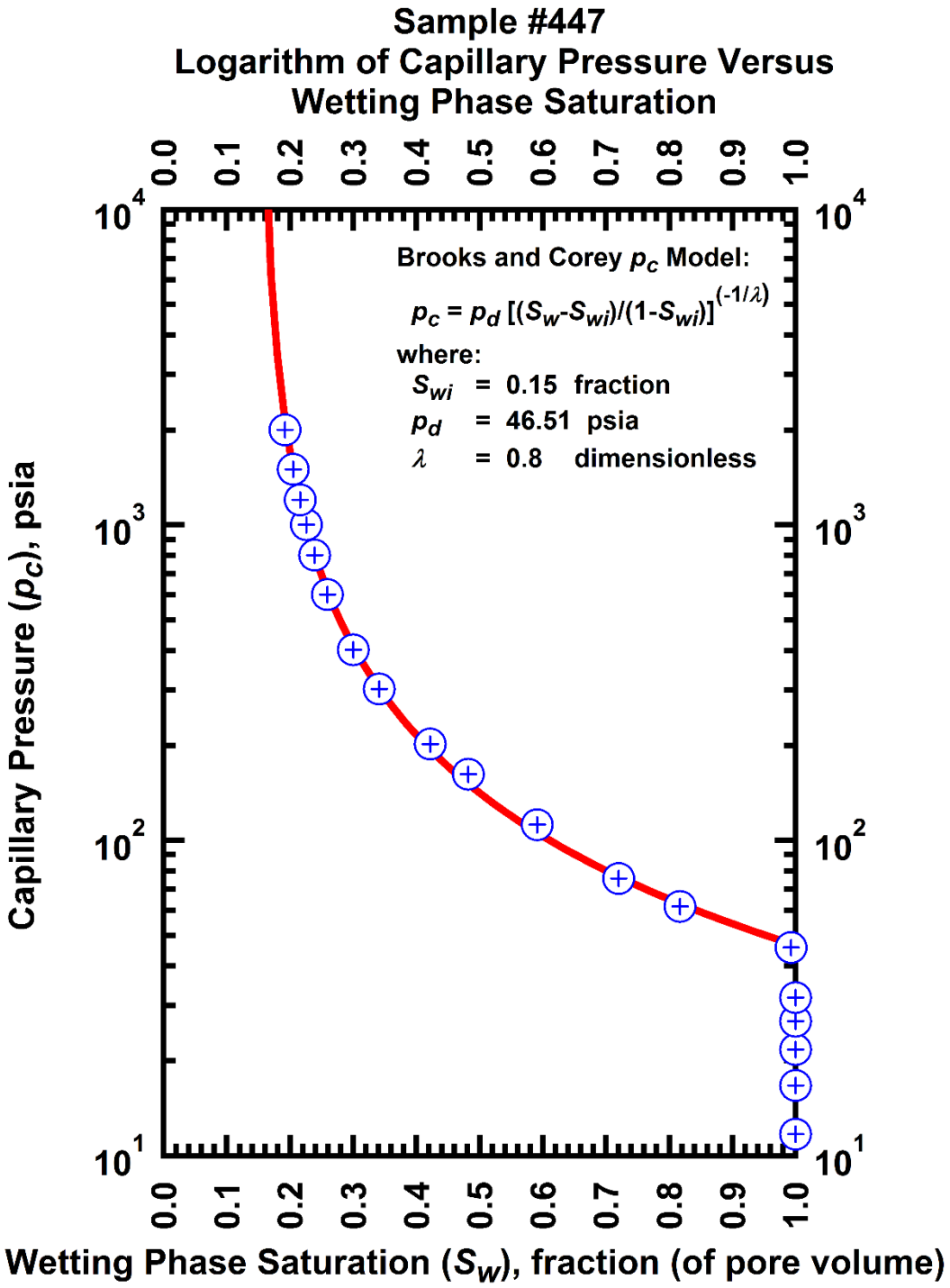

Figure H-38 — Plot of logarithm of capillary pressure vs. wetting phase saturation — Sample #447.

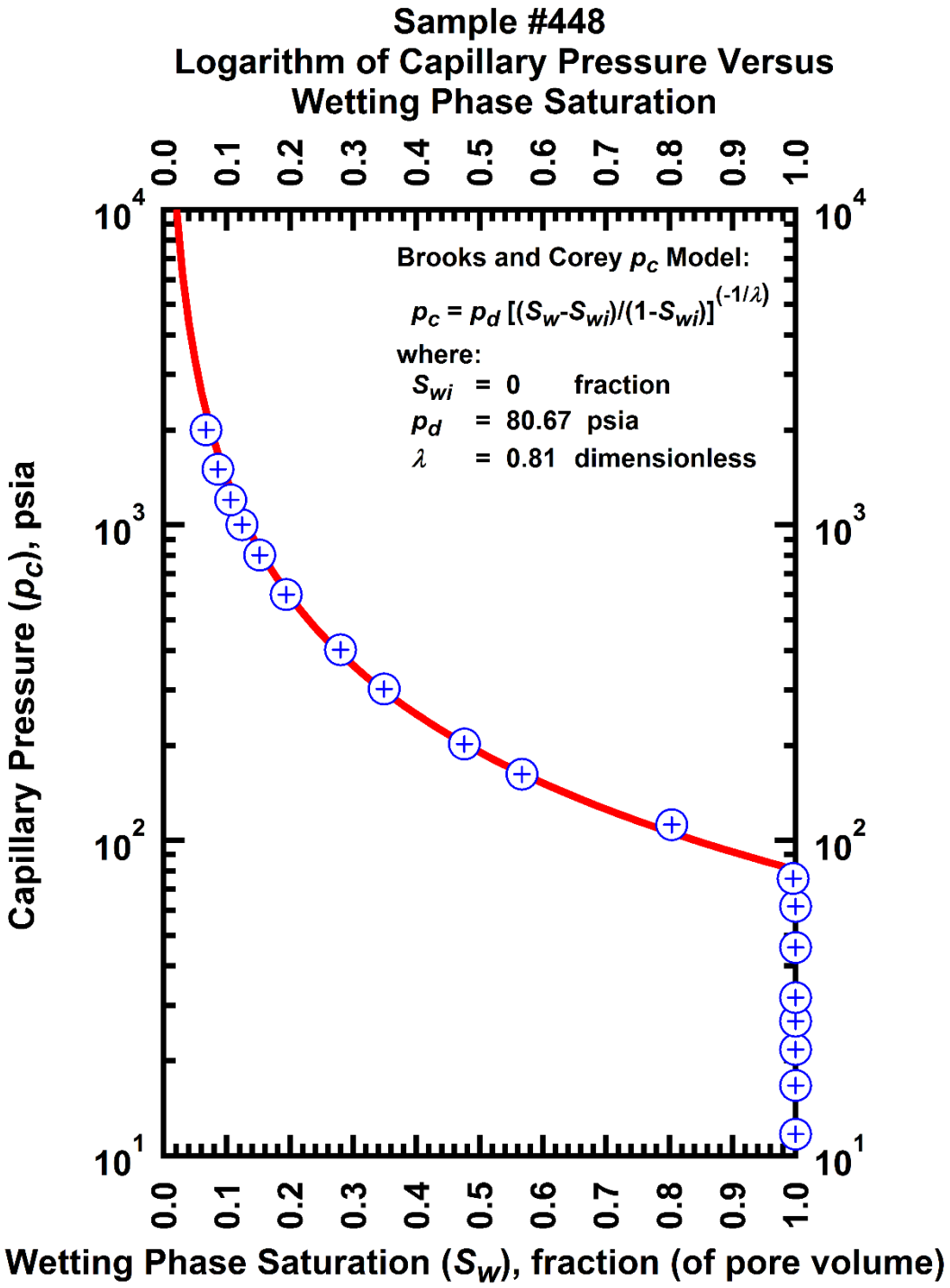

Figure H-39 — Plot of logarithm of capillary pressure vs. wetting phase saturation — Sample #448.

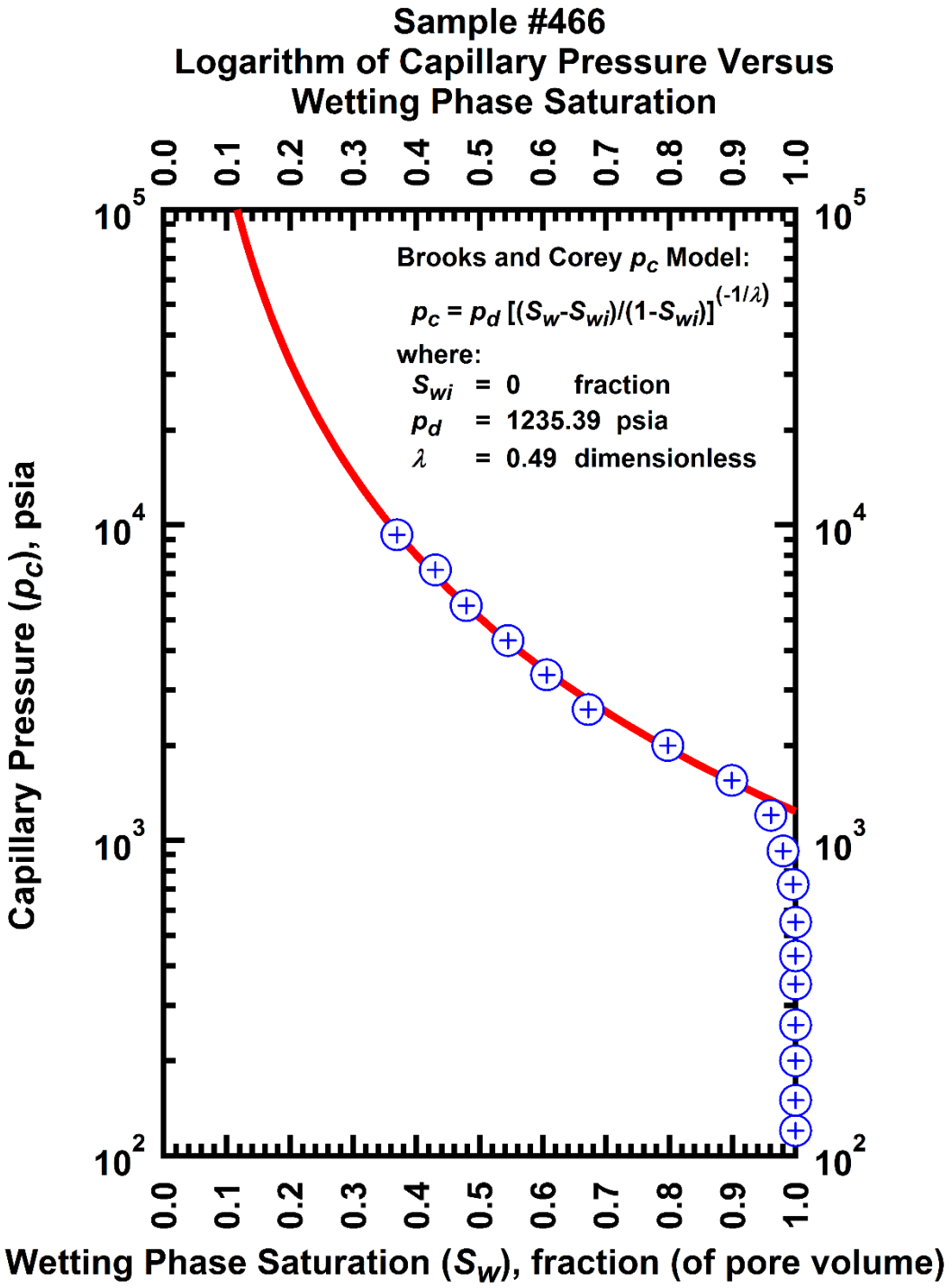

Figure H-40 — Plot of logarithm of capillary pressure vs. wetting phase saturation — Sample #466.

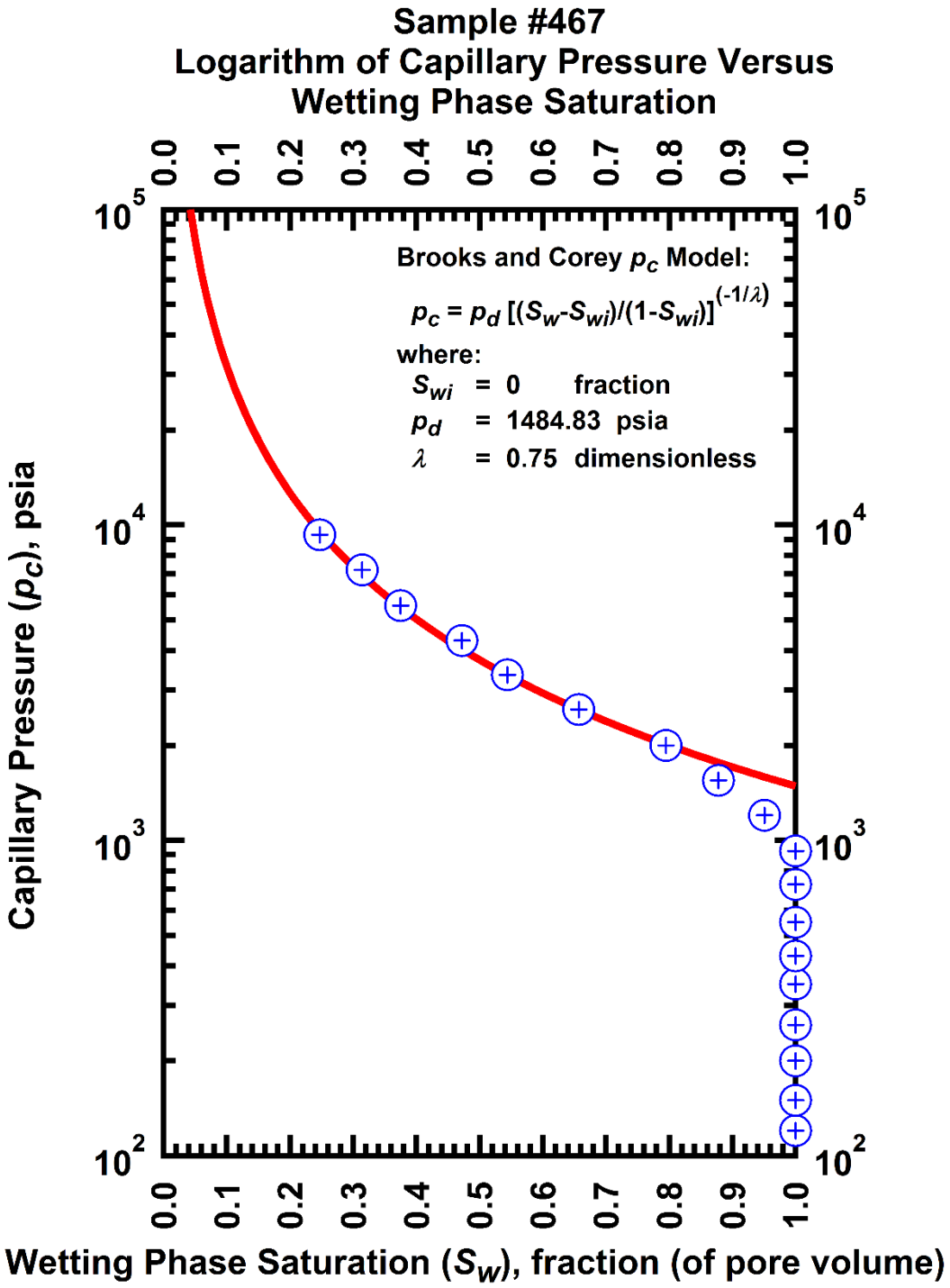

Figure H-41 — Plot of logarithm of capillary pressure vs. wetting phase saturation — Sample #467.

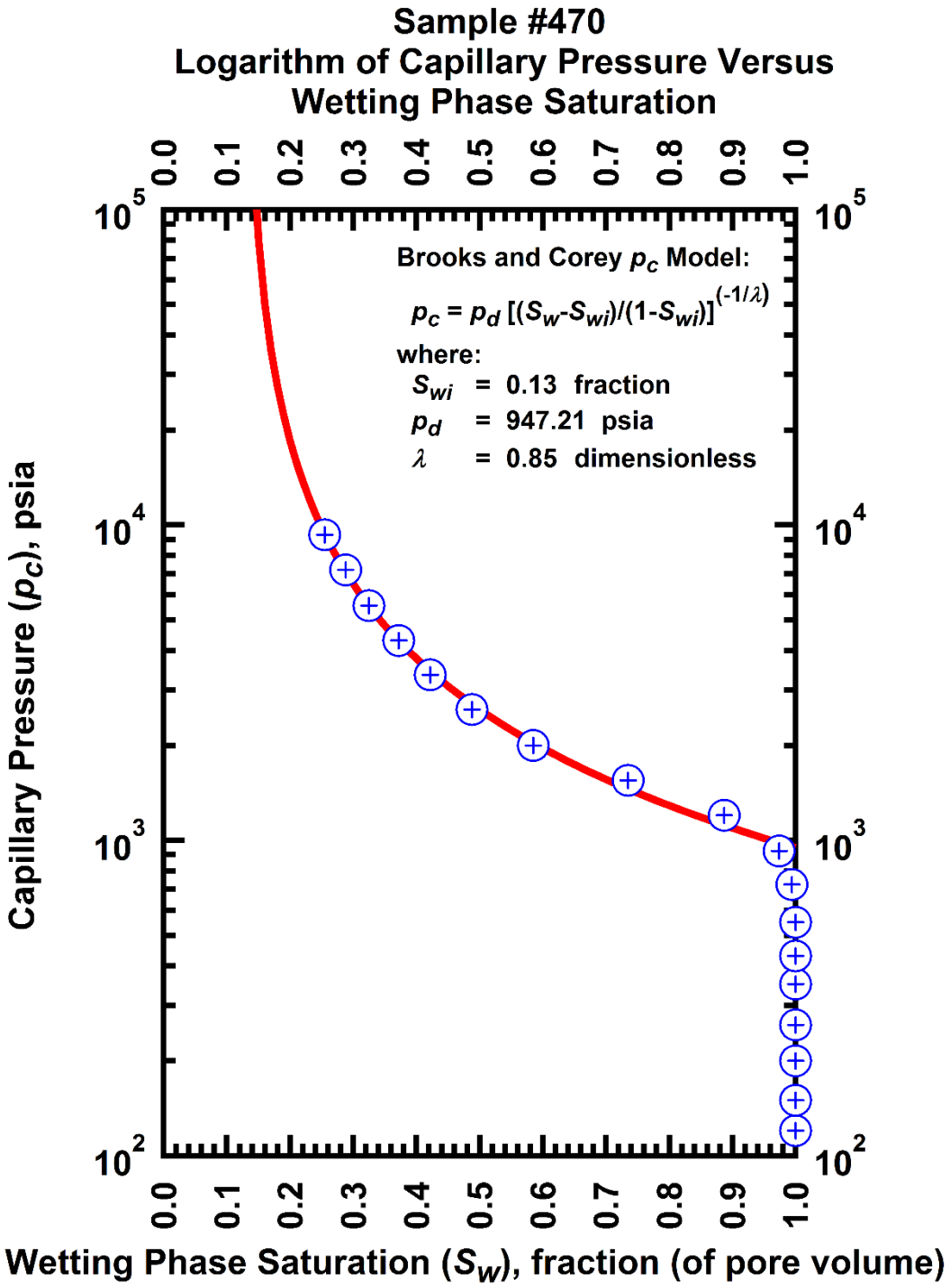

Figure H-42 — Plot of logarithm of capillary pressure vs. wetting phase saturation — Sample #470.

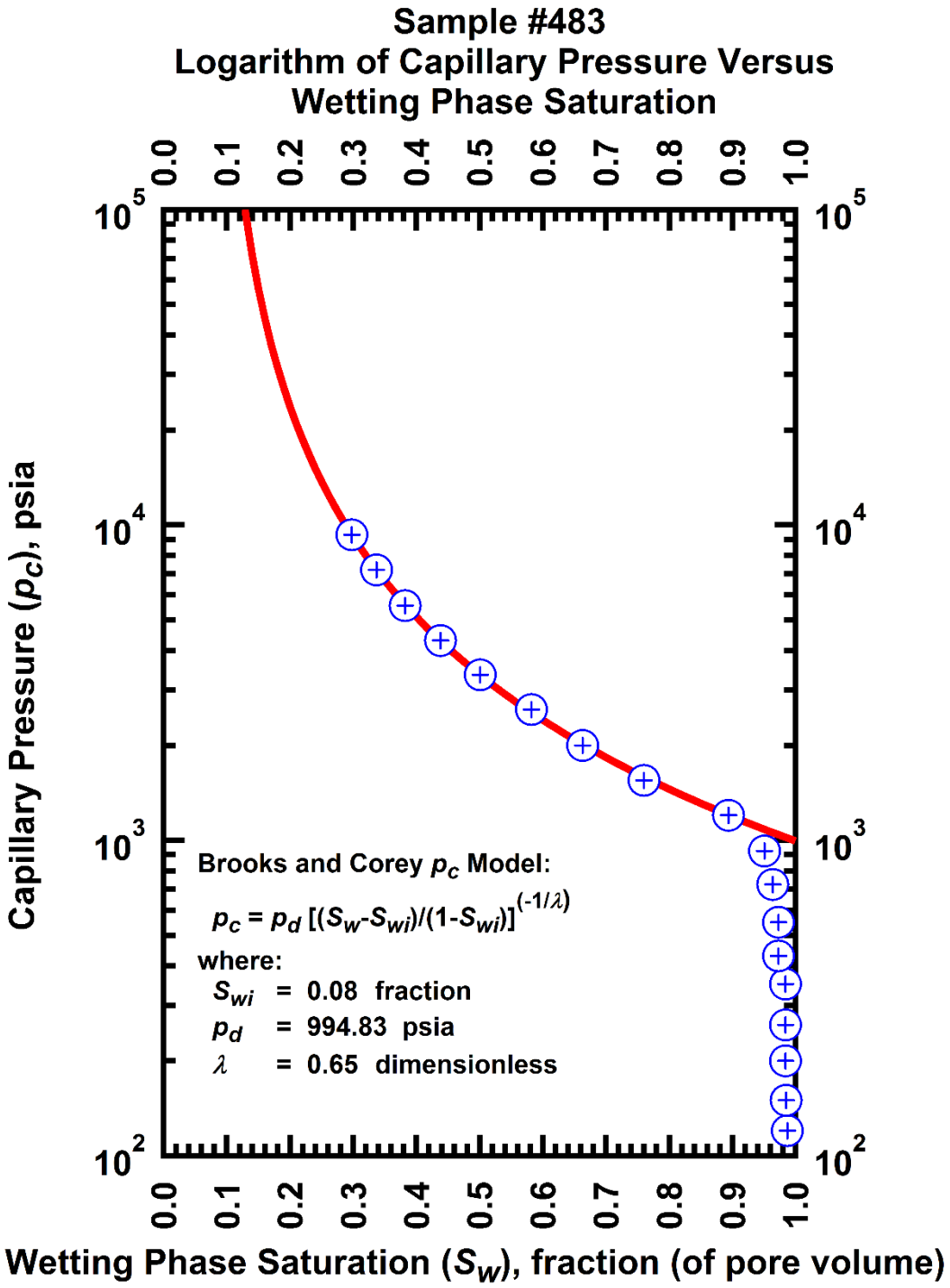

Figure H-43 — Plot of logarithm of capillary pressure vs. wetting phase saturation — Sample #483.

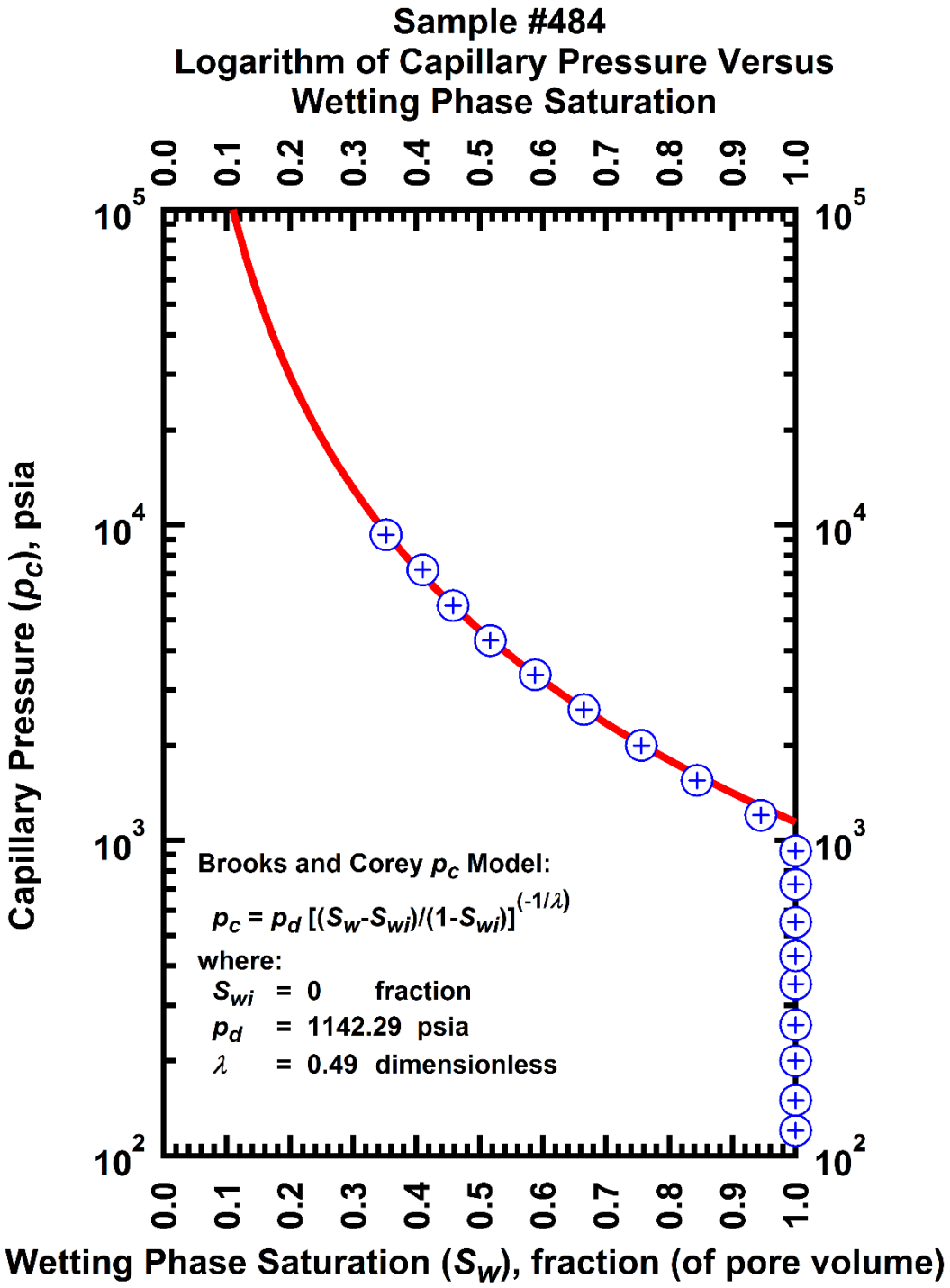

Figure H-44 — Plot of logarithm of capillary pressure vs. wetting phase saturation — Sample #484.

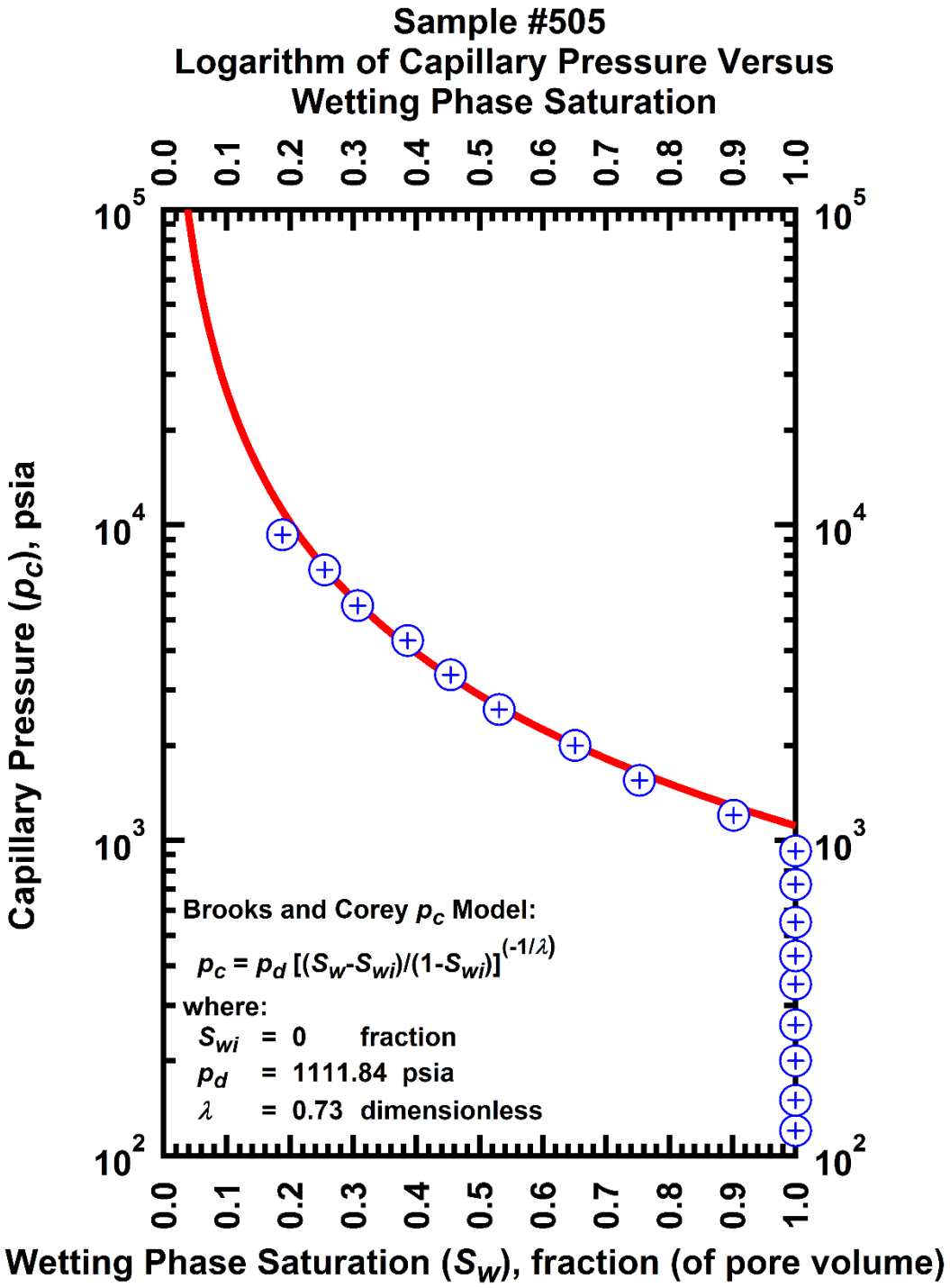

Figure H-45 — Plot of logarithm of capillary pressure vs. wetting phase saturation — Sample #505.

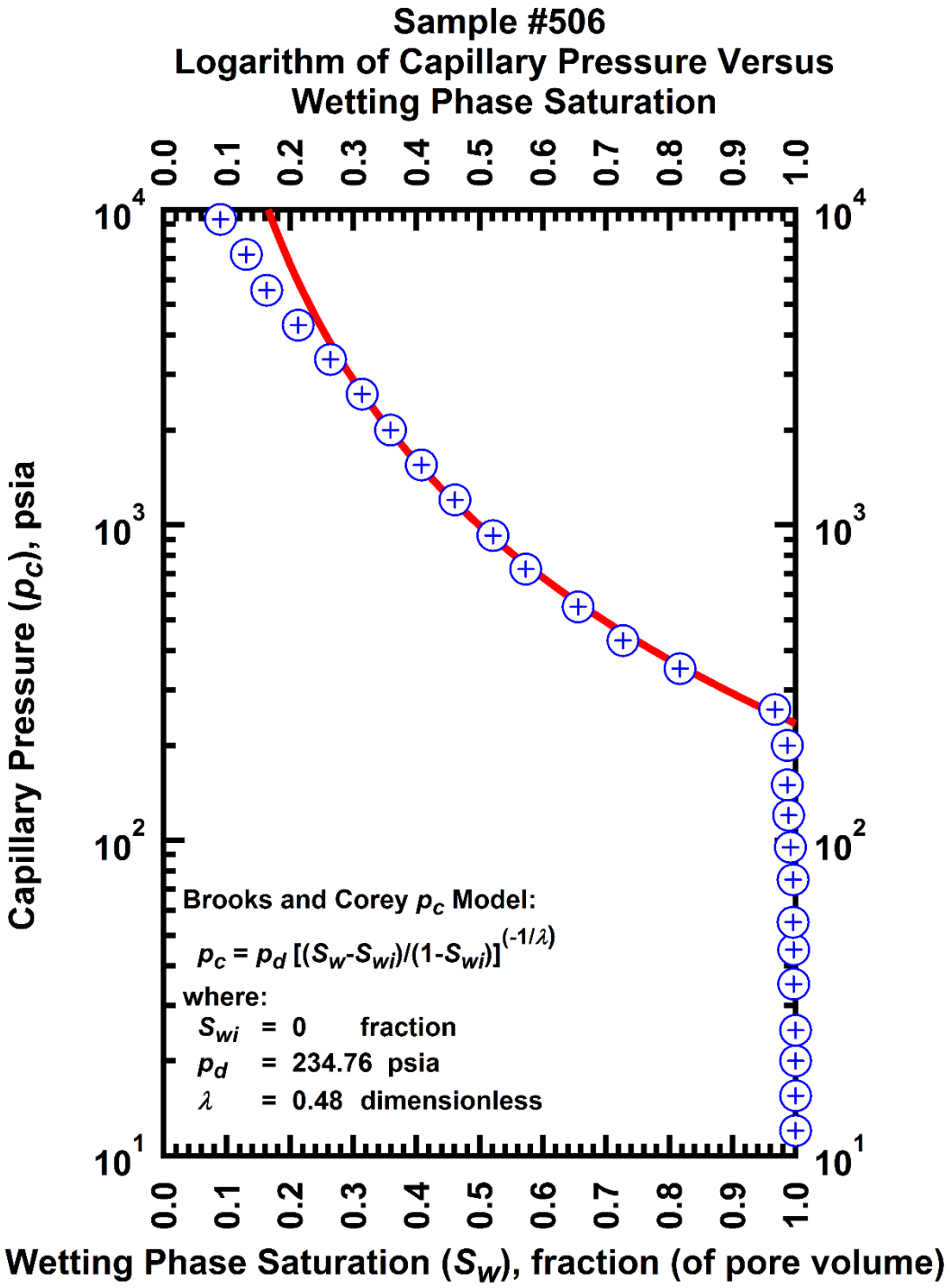

Figure H-46 — Plot of logarithm of capillary pressure vs. wetting phase saturation — Sample #506.

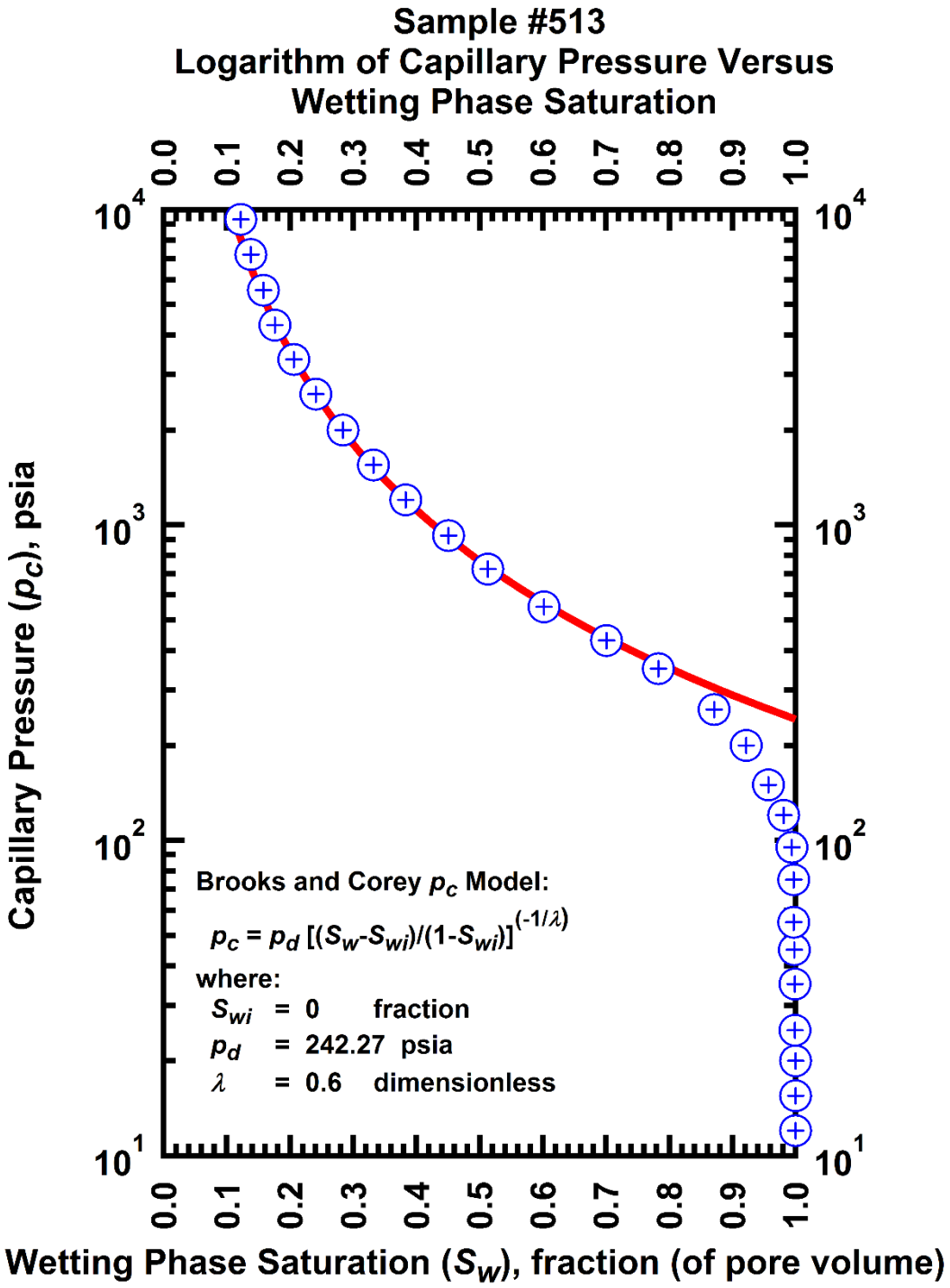

Figure H-47 — Plot of logarithm of capillary pressure vs. wetting phase saturation — Sample #513.

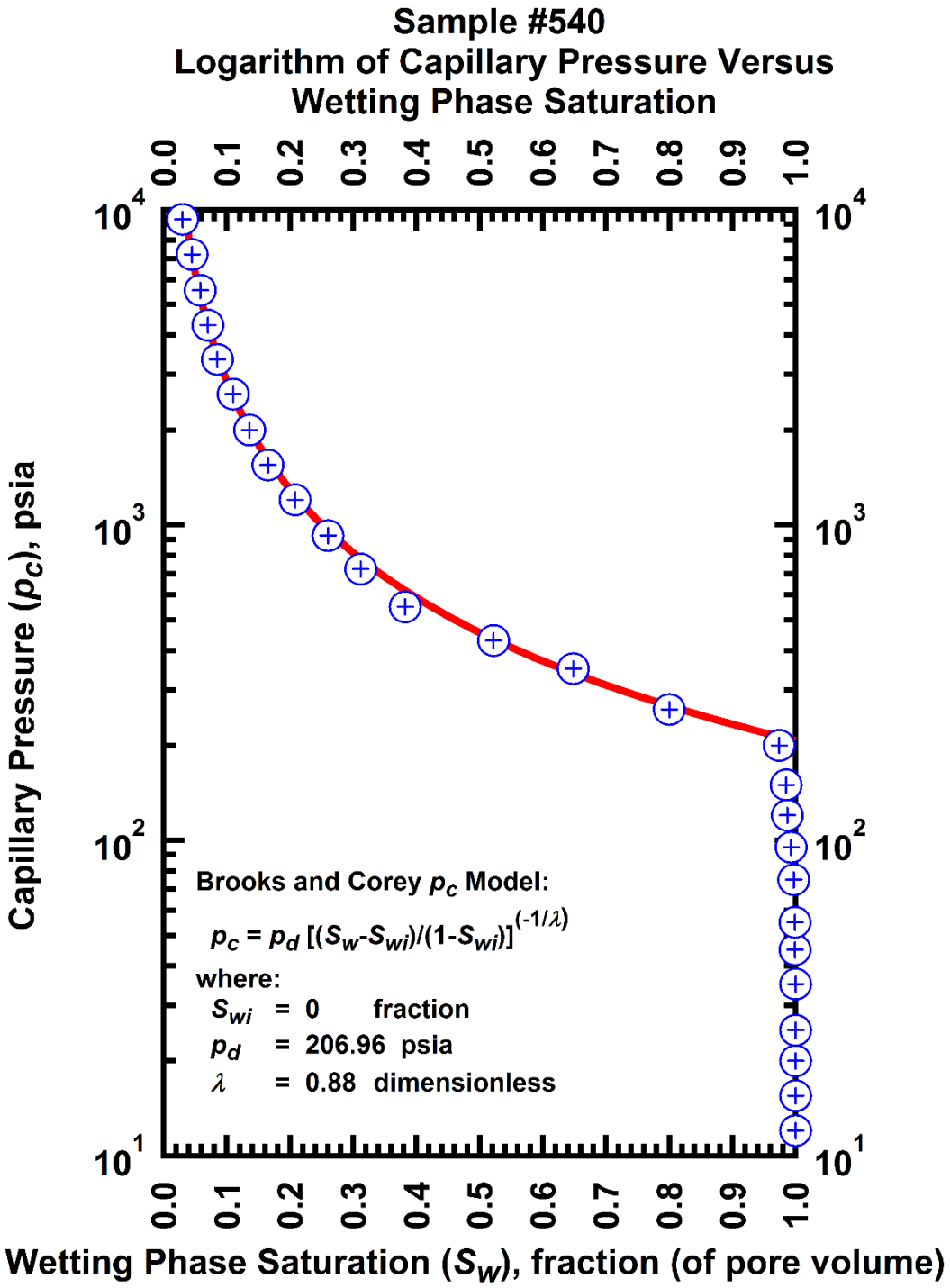

Figure H-48 — Plot of logarithm of capillary pressure vs. wetting phase saturation — Sample #540.

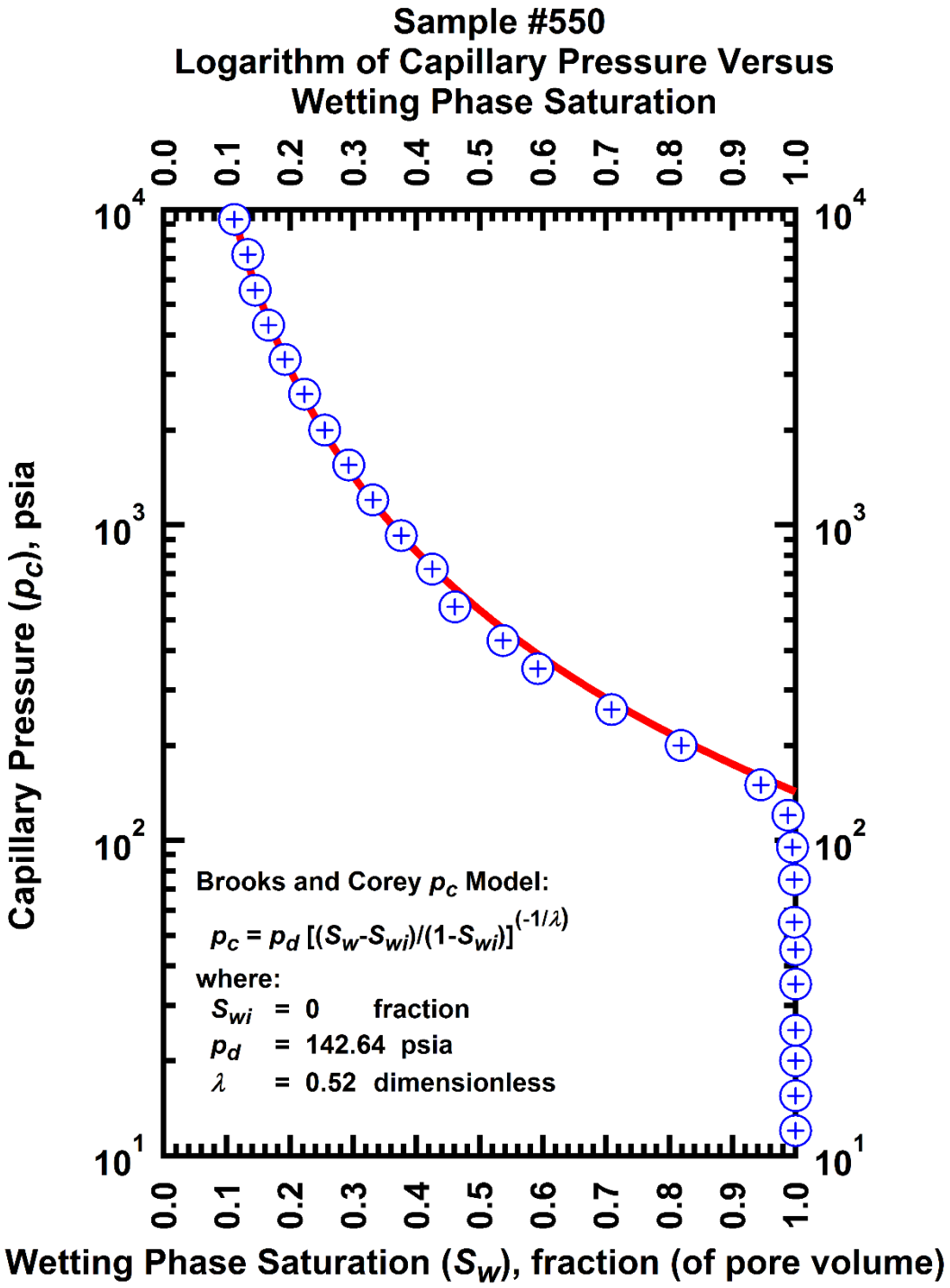

Figure H-49 — Plot of logarithm of capillary pressure vs. wetting phase saturation — Sample #550.

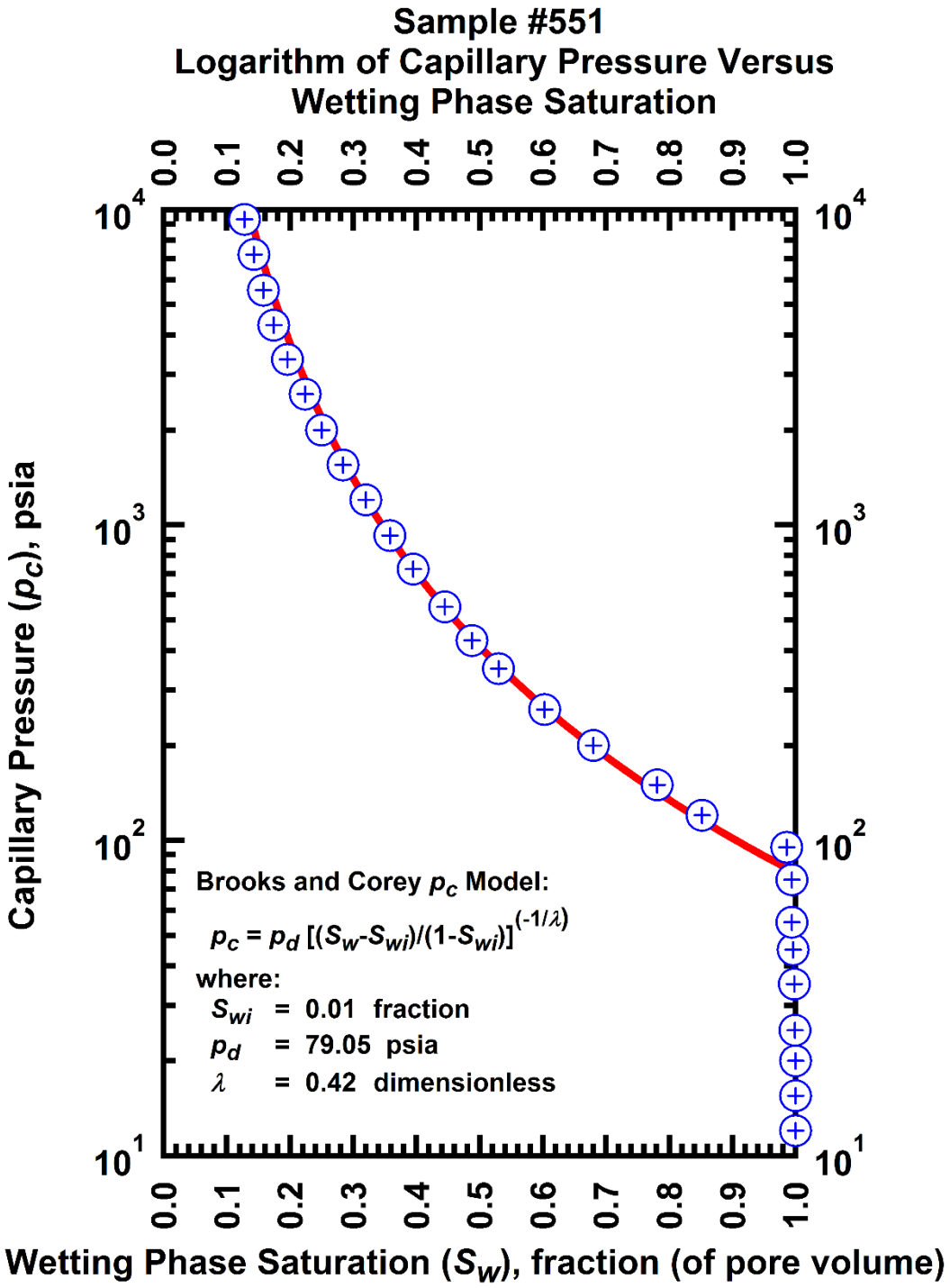

Figure H-50 — Plot of logarithm of capillary pressure vs. wetting phase saturation — Sample #551.

APPENDIX I

LIBRARY OF CAPILLARY PRESSURE VERSUS NORMALIZED WETTING PHASE SATURATION PLOTS — LOGARITHMIC CAPILLARY PRESSURE FORMAT

This Appendix presents the calibration of the capillary displacement pressure (p_d), irreducible wetting phase saturation (S_{wi}), and the index of pore-size distribution (λ) on a sample-by-sample basis using the Brooks-Corey $p_c(S_w)$ model. In this Appendix, we provide example plots of capillary pressure (p_c) vs. normalized wetting phase saturation (S_w^*) – logarithmic capillary pressure format of 50 (fifty) samples used in this study.

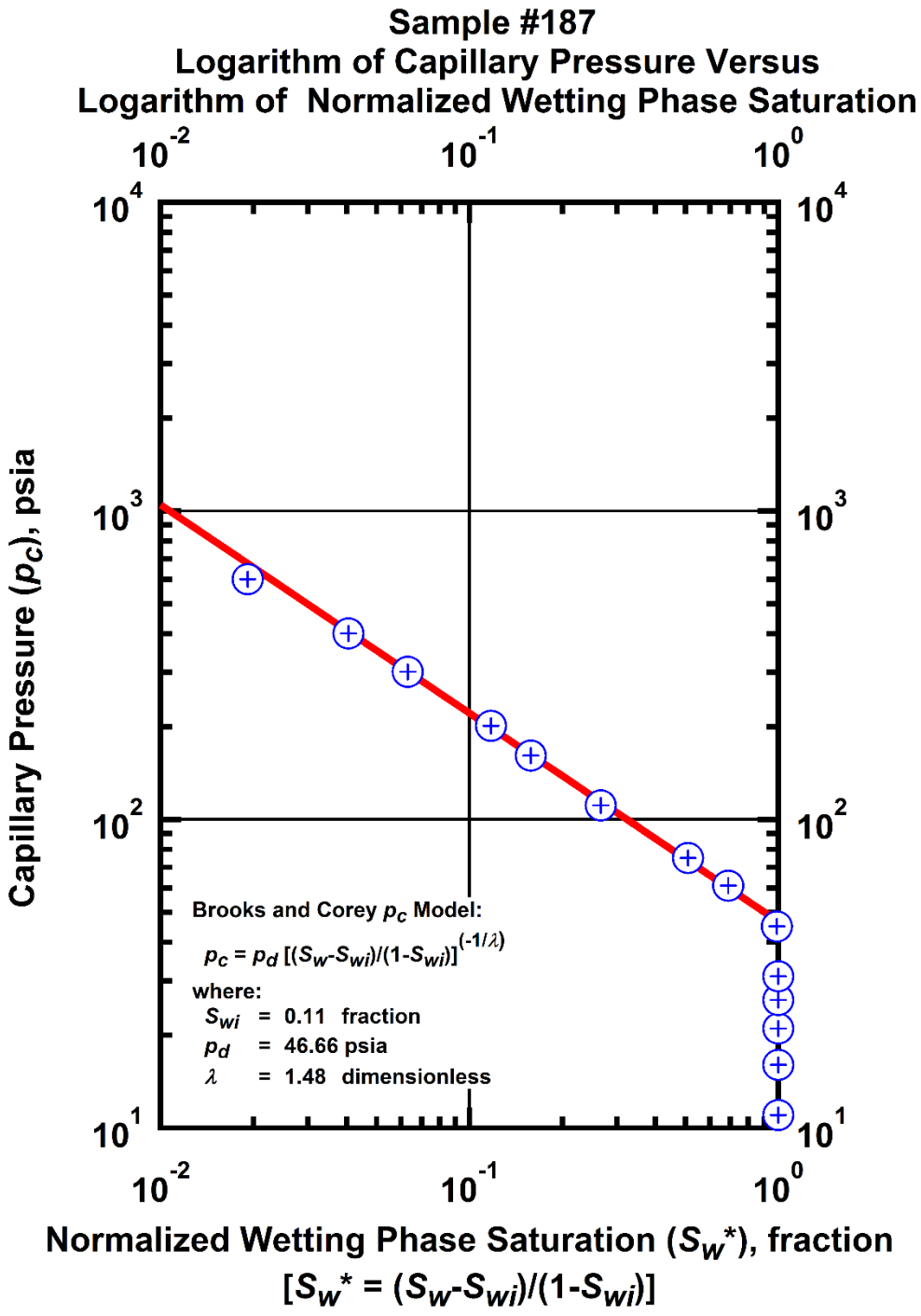

Figure I-1 — Plot of logarithm of capillary pressure vs. logarithm of normalized wetting phase saturation — Sample #187.

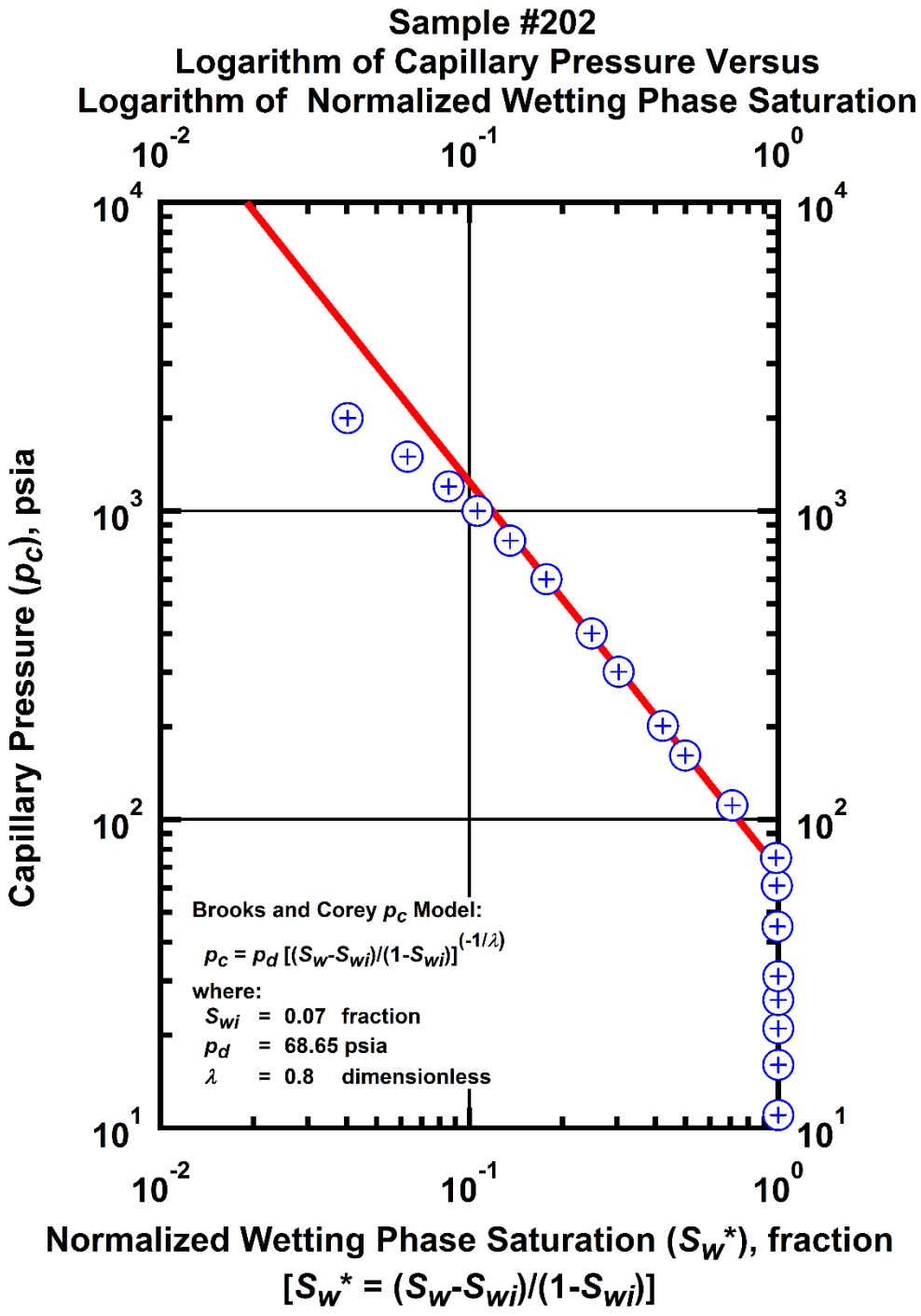

Figure I-2 — Plot of logarithm of capillary pressure vs. logarithm of normalized wetting phase saturation — Sample #202.

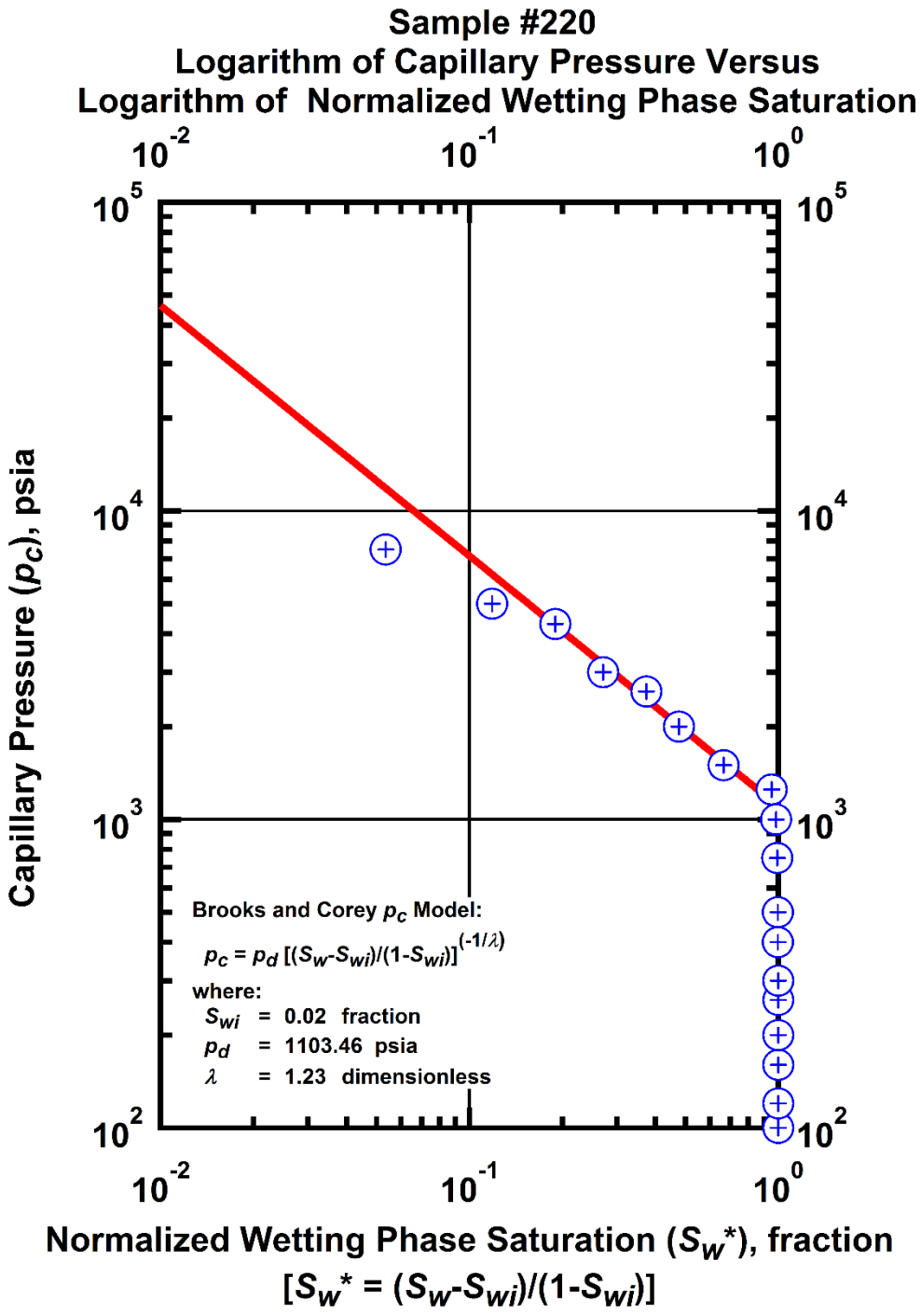

Figure I-3 — Plot of logarithm of capillary pressure vs. logarithm of normalized wetting phase saturation — Sample #220.

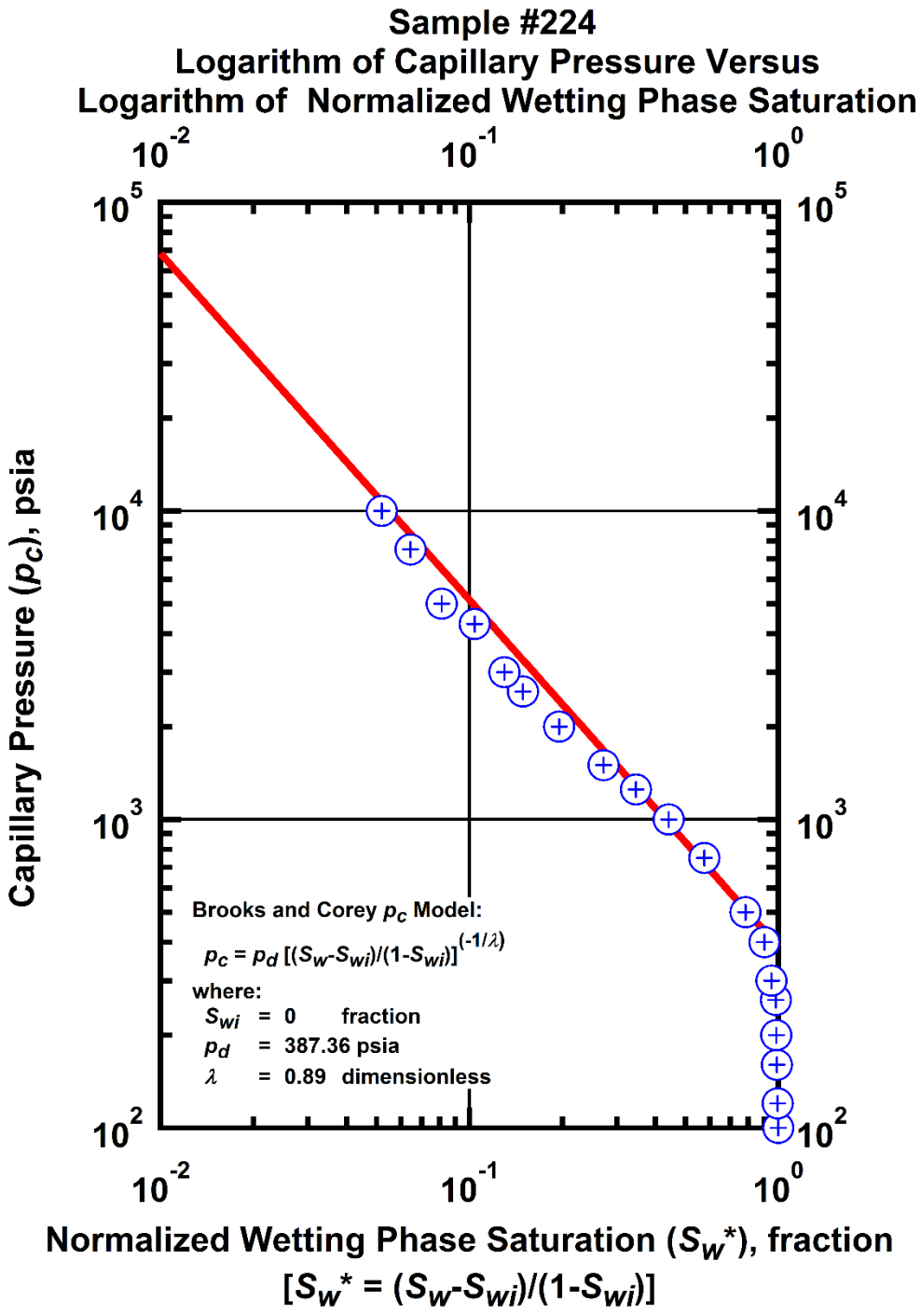

Figure I-4 — Plot of logarithm of capillary pressure vs. logarithm of normalized wetting phase saturation — Sample #224.

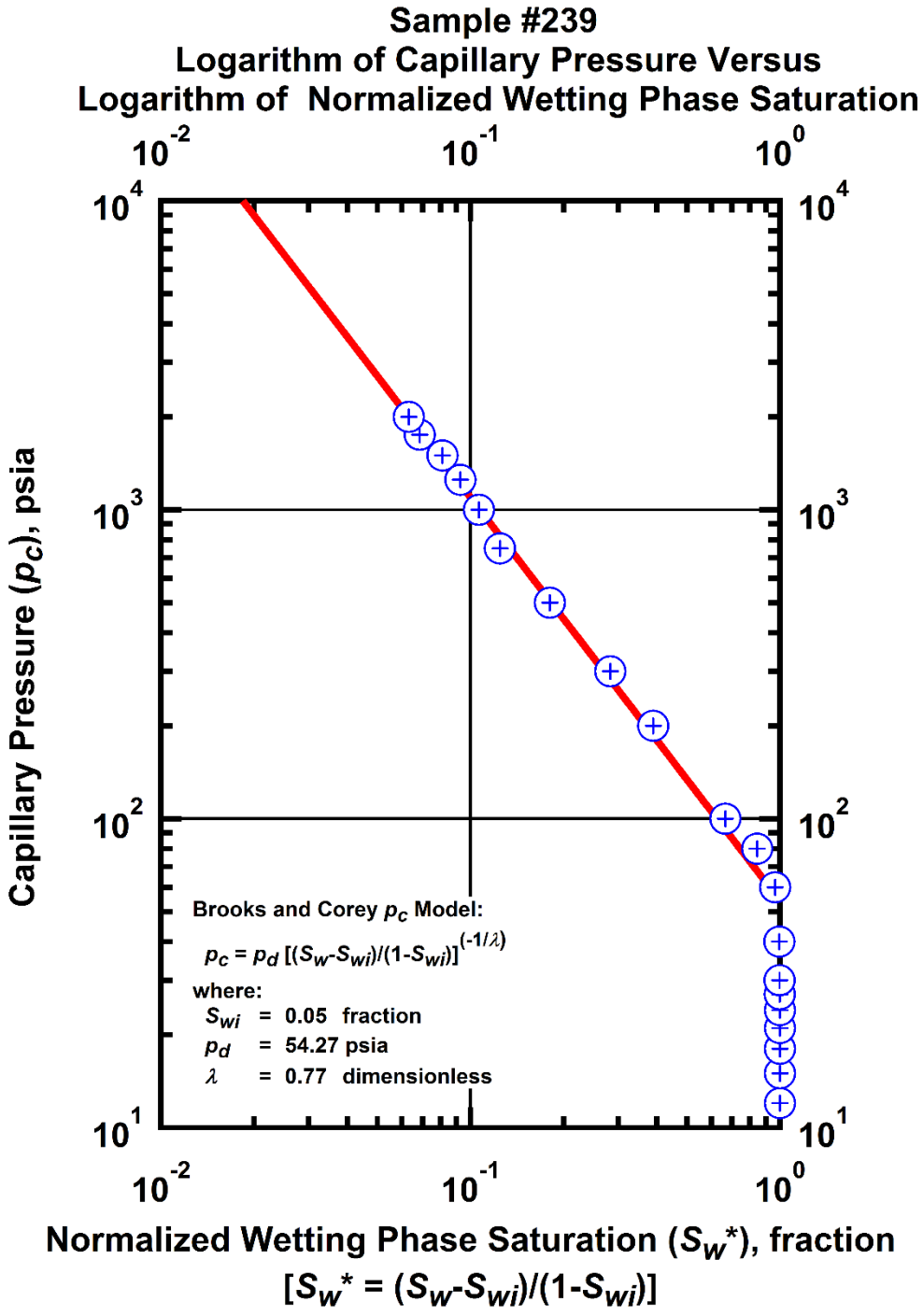

Figure I-5 — Plot of logarithm of capillary pressure vs. logarithm of normalized wetting phase saturation — Sample #239.

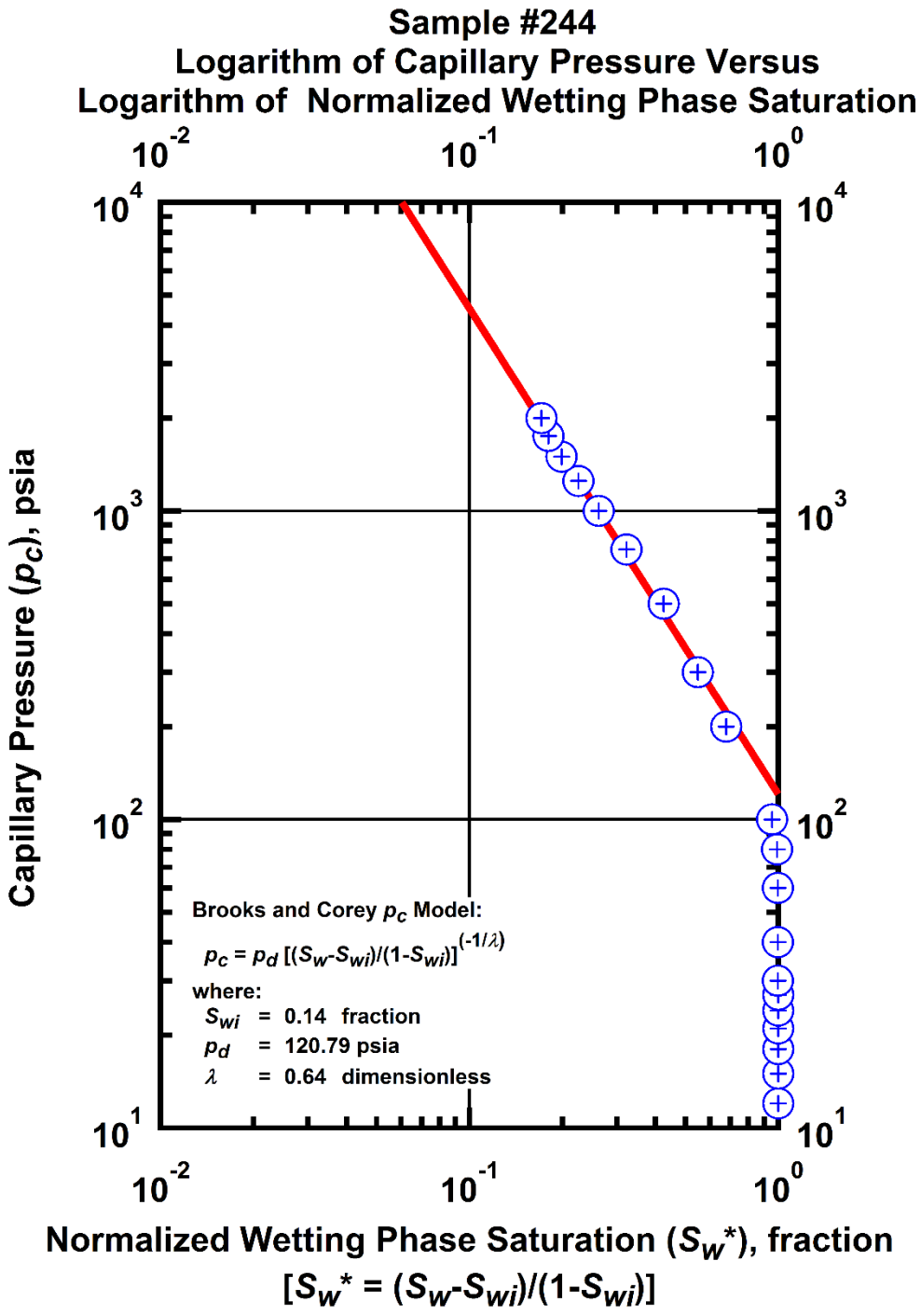

Figure I-6 — Plot of logarithm of capillary pressure vs. logarithm of normalized wetting phase saturation — Sample #244.

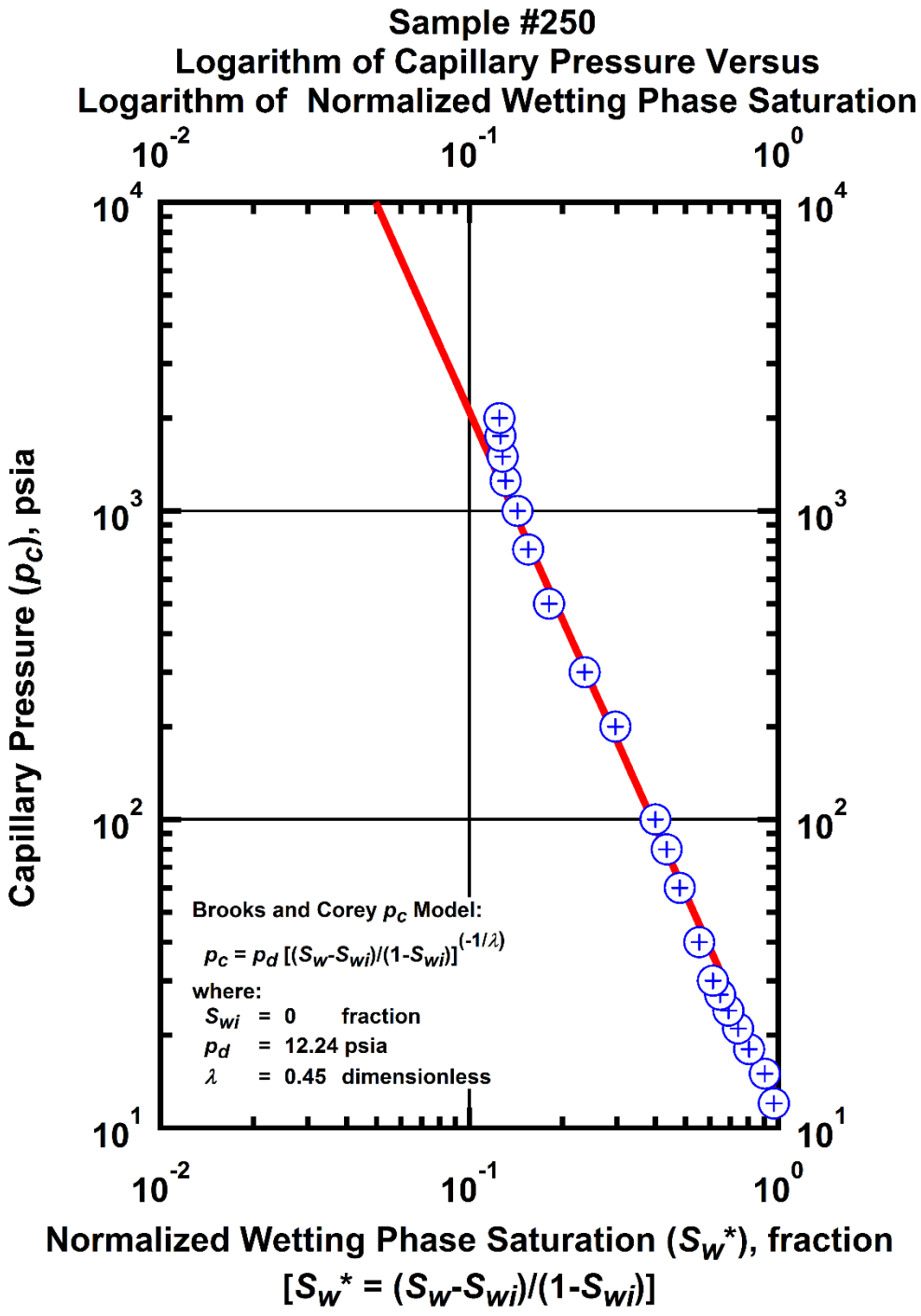

Figure I-7 — Plot of logarithm of capillary pressure vs. logarithm of normalized wetting phase saturation — Sample #250.

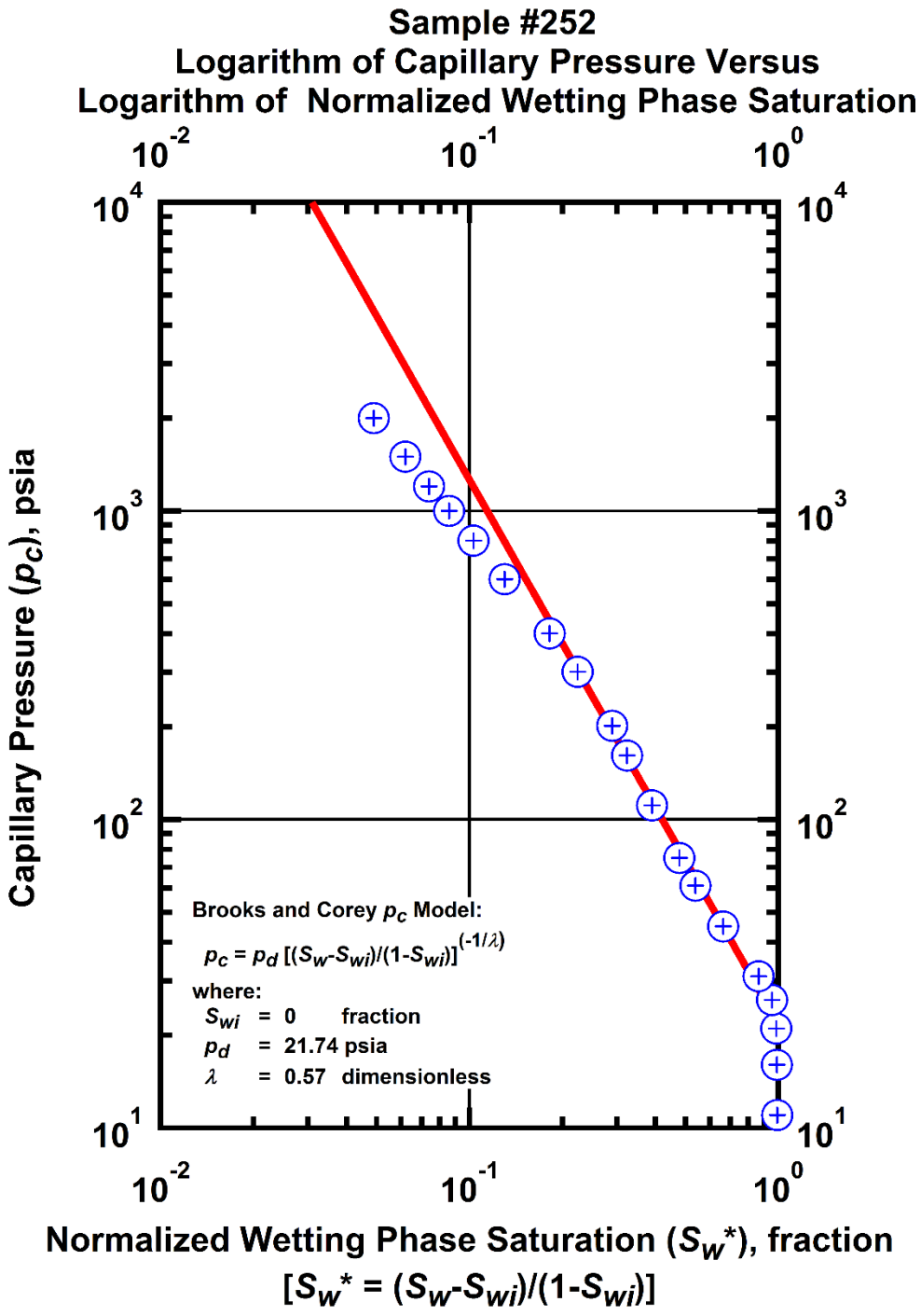

Figure I-8 — Plot of logarithm of capillary pressure vs. logarithm of normalized wetting phase saturation — Sample #252.

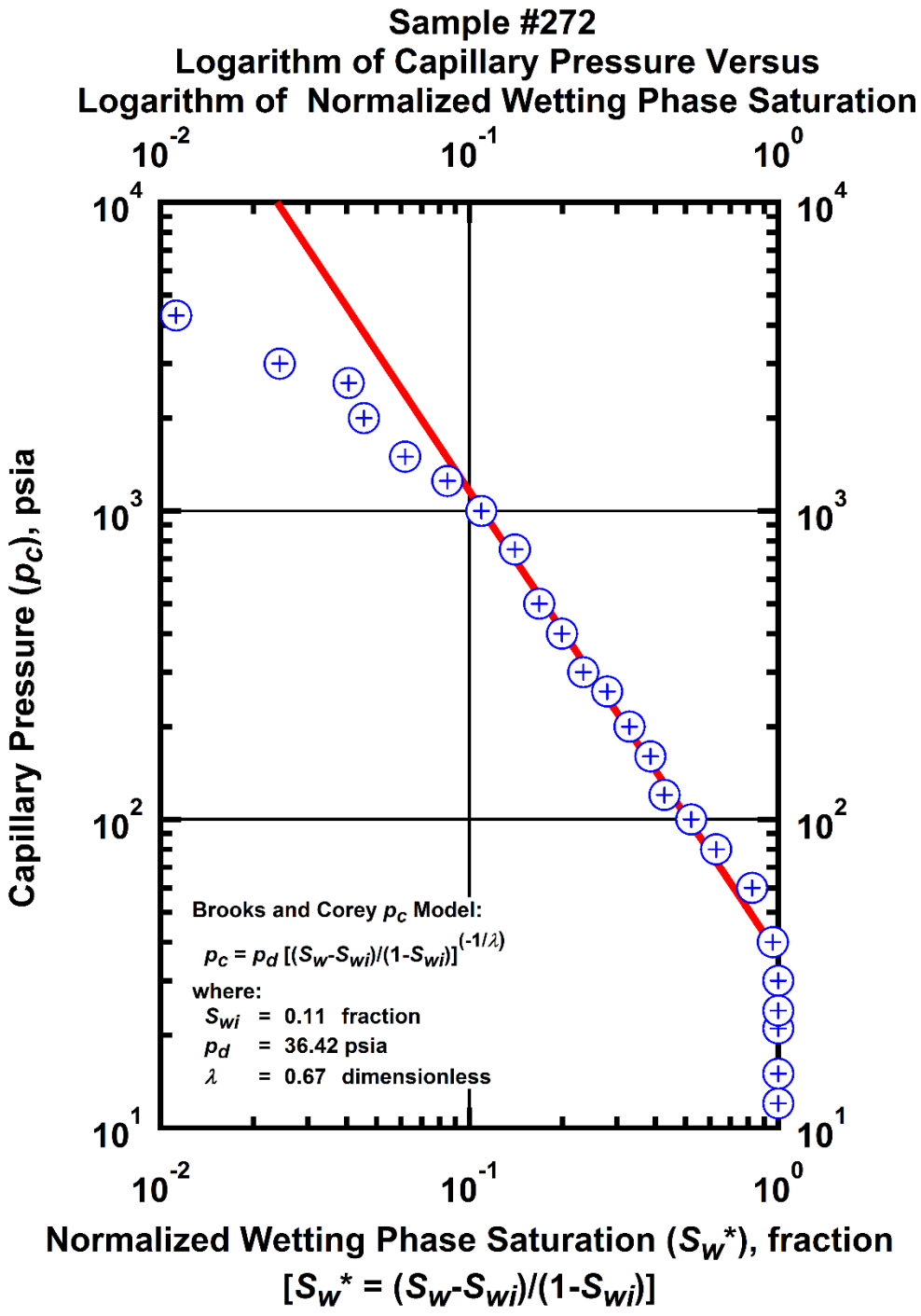

Figure I-9 — Plot of logarithm of capillary pressure vs. logarithm of normalized wetting phase saturation — Sample #272.

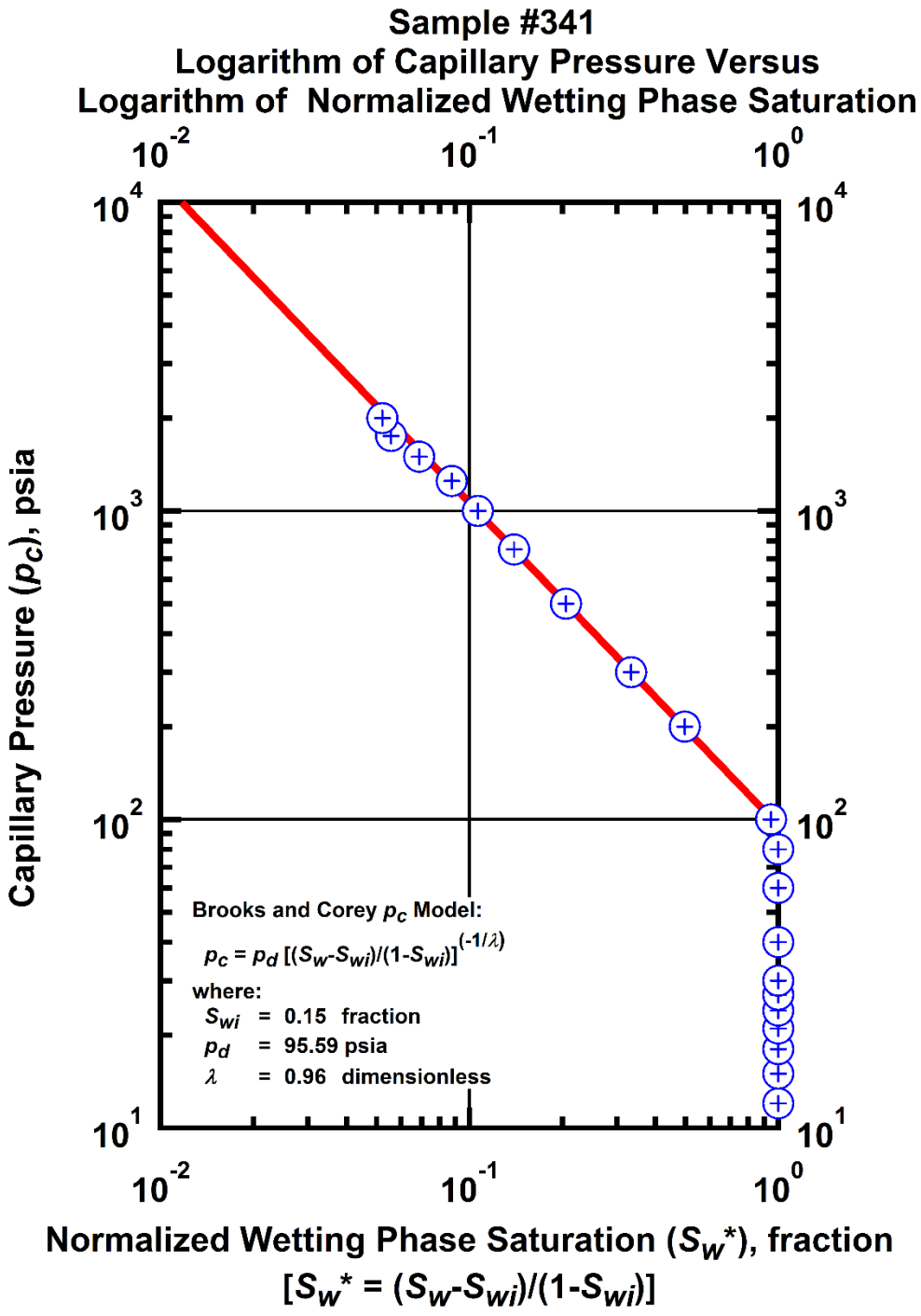

Figure I-10 — Plot of logarithm of capillary pressure vs. logarithm of normalized wetting phase saturation — Sample #341.

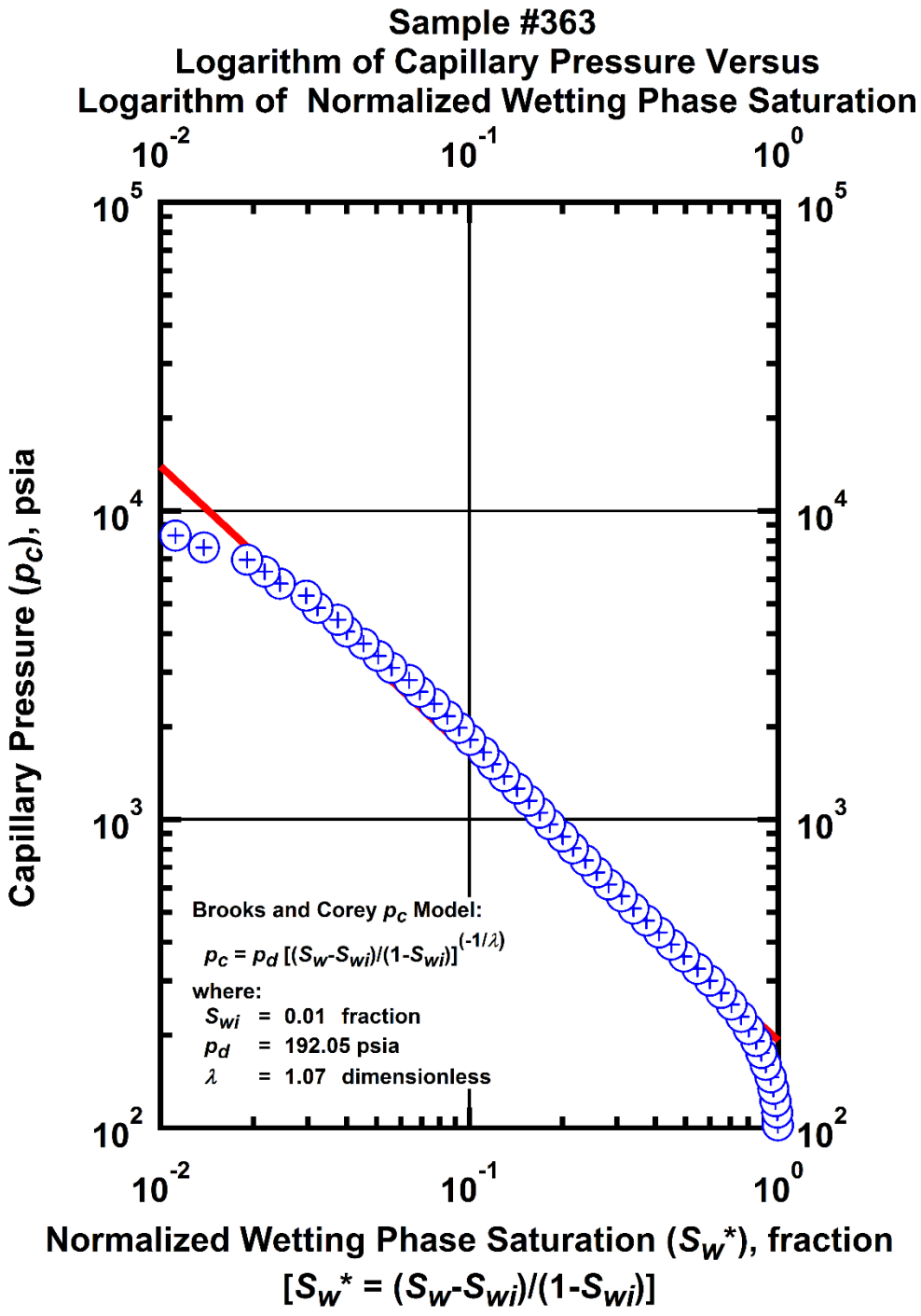

Figure I-11 — Plot of logarithm of capillary pressure vs. logarithm of normalized wetting phase saturation — Sample #363.

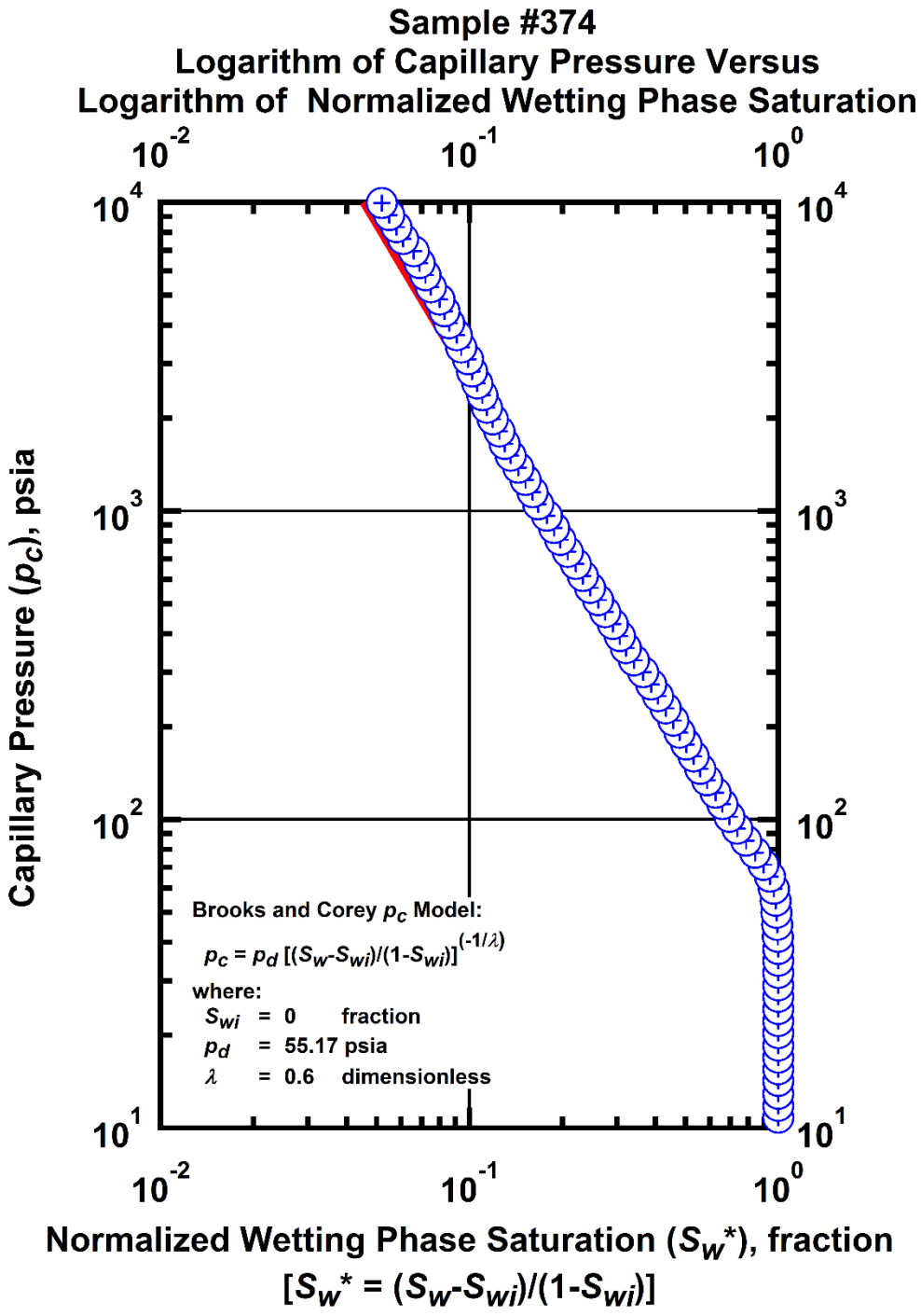

Figure I-12 — Plot of logarithm of capillary pressure vs. logarithm of normalized wetting phase saturation — Sample #374.

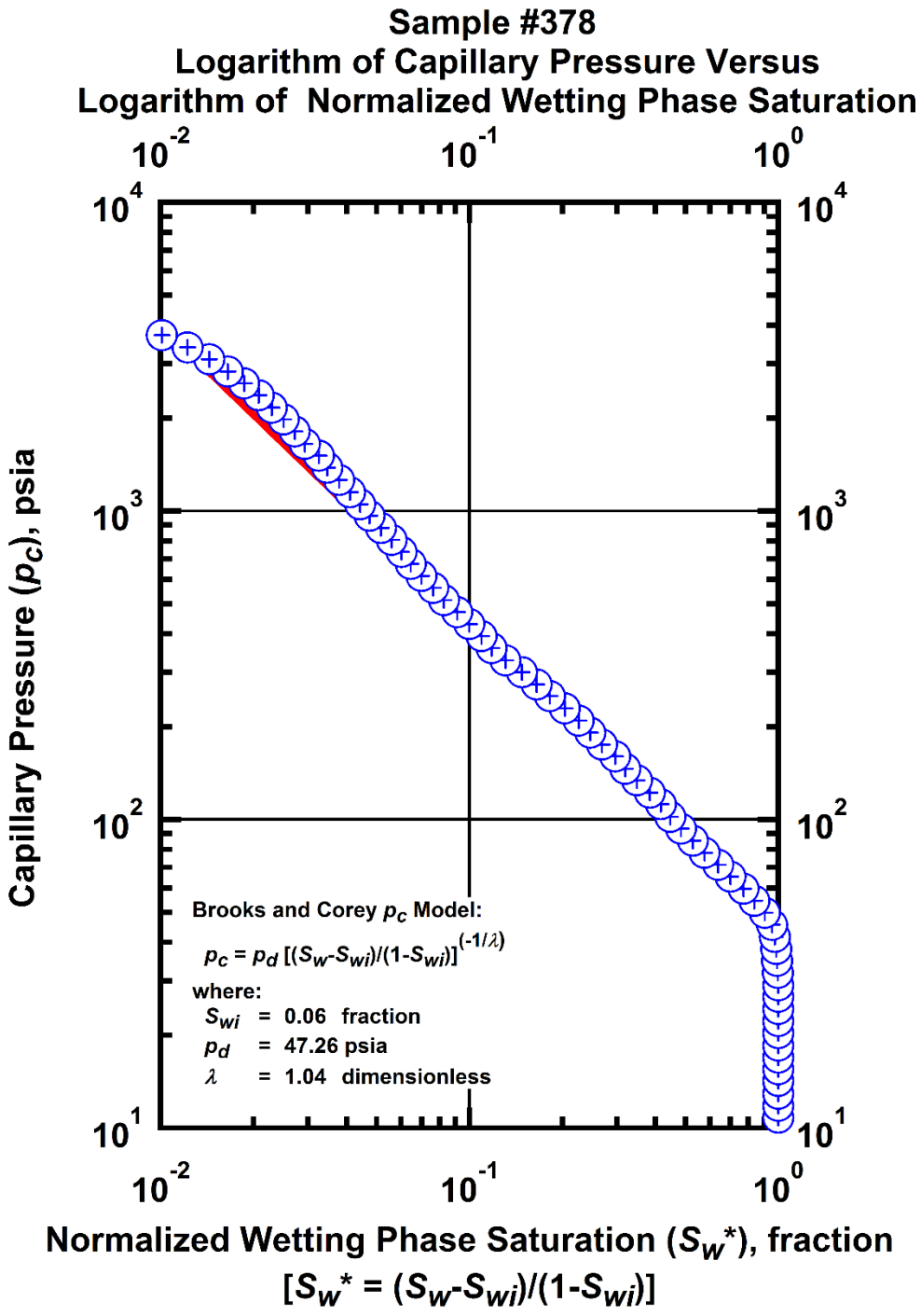

Figure I-13 — Plot of logarithm of capillary pressure vs. logarithm of normalized wetting phase saturation — Sample #378.

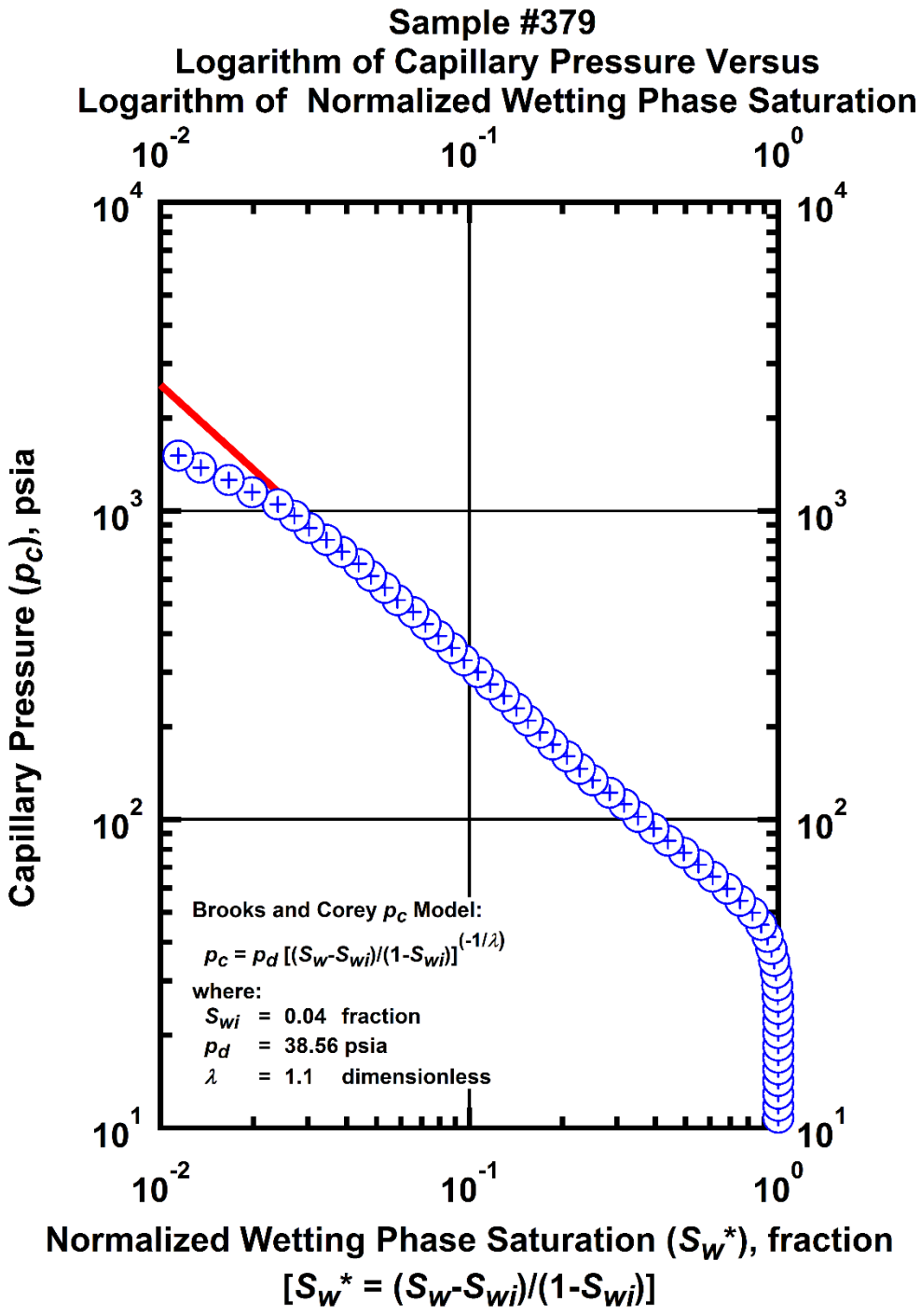

Figure I-14 — Plot of logarithm of capillary pressure vs. logarithm of normalized wetting phase saturation — Sample #379.

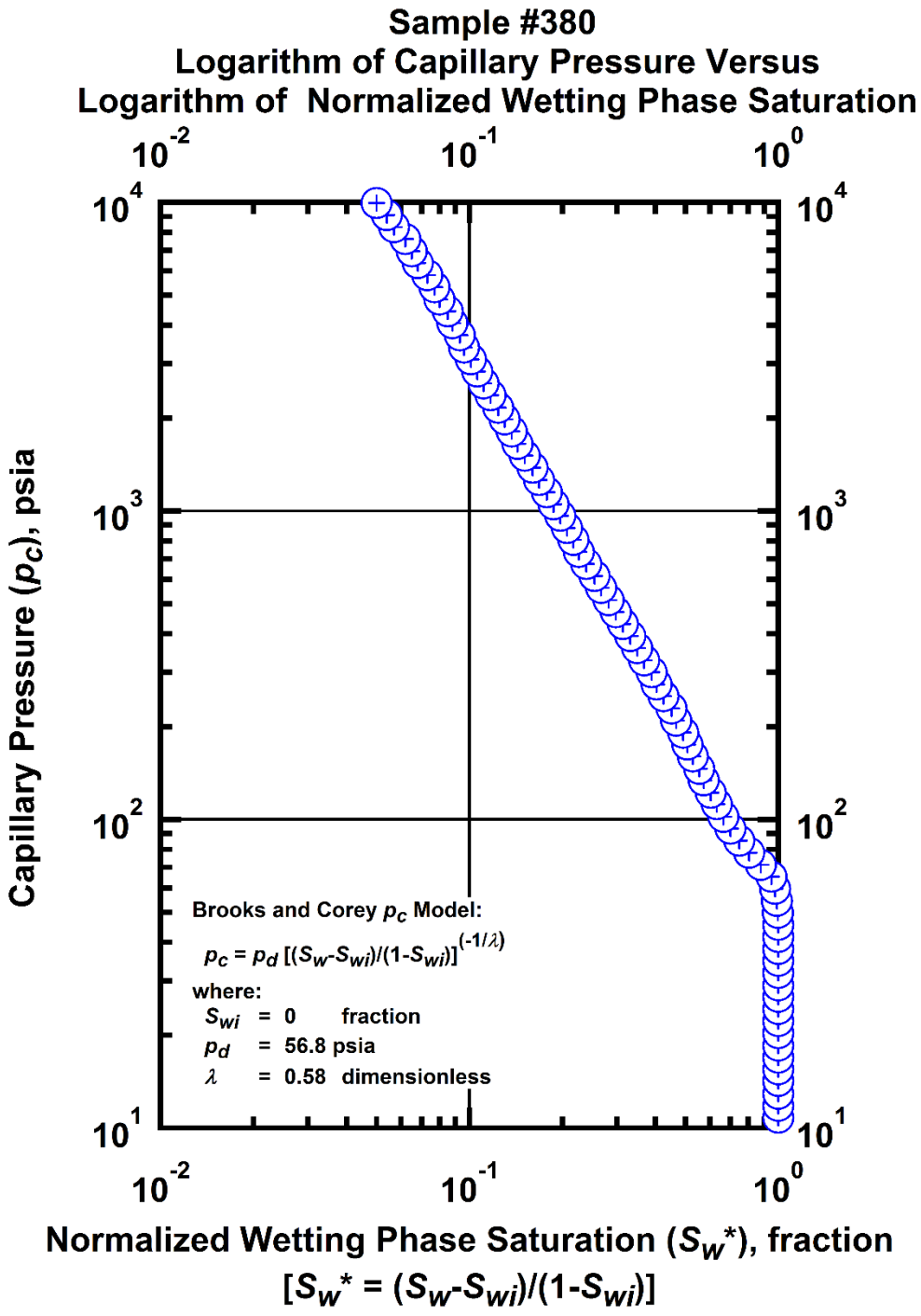

Figure I-15 — Plot of logarithm of capillary pressure vs. logarithm of normalized wetting phase saturation — Sample #380.

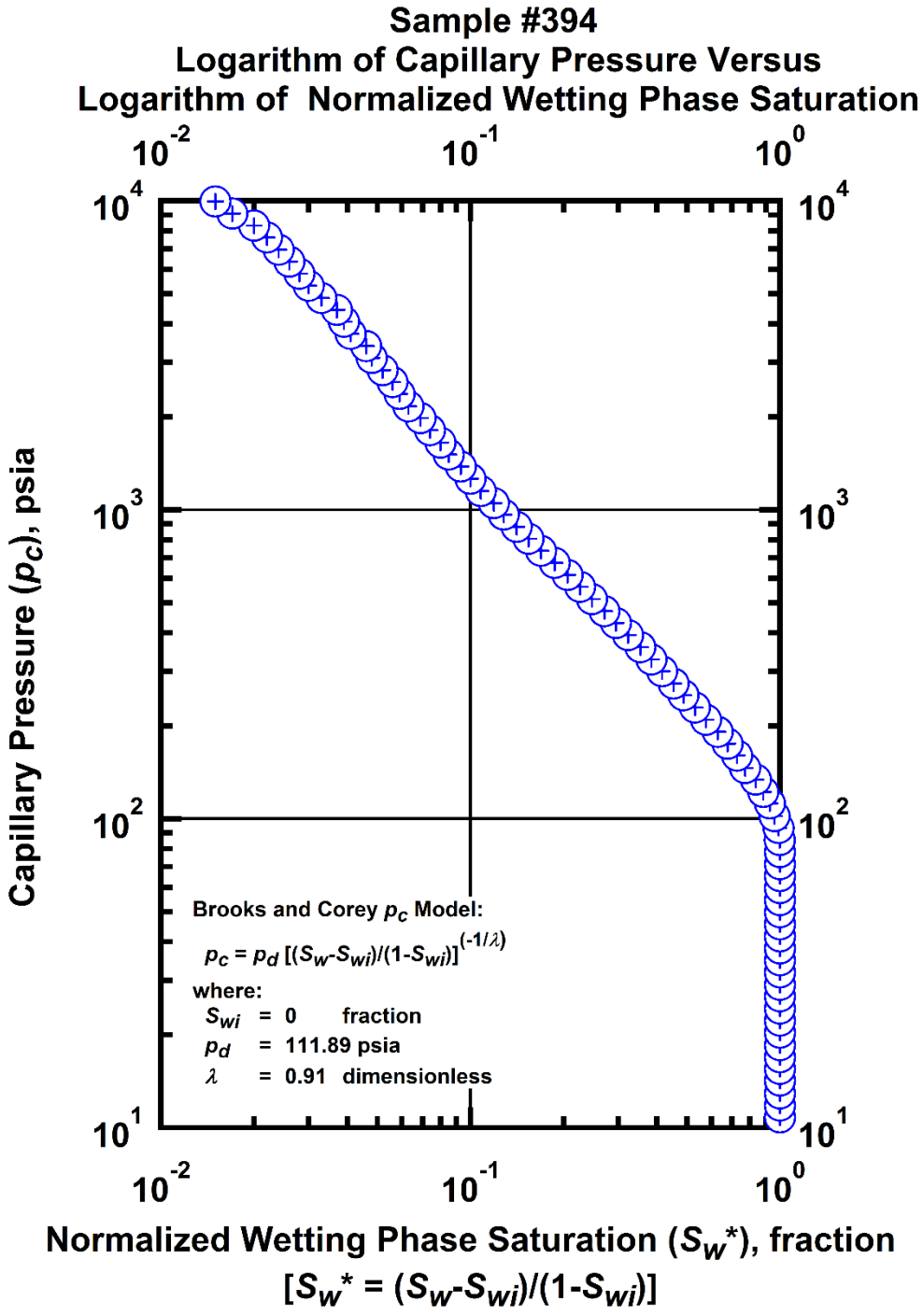

Figure I-16 — Plot of logarithm of capillary pressure vs. logarithm of normalized wetting phase saturation — Sample #394.

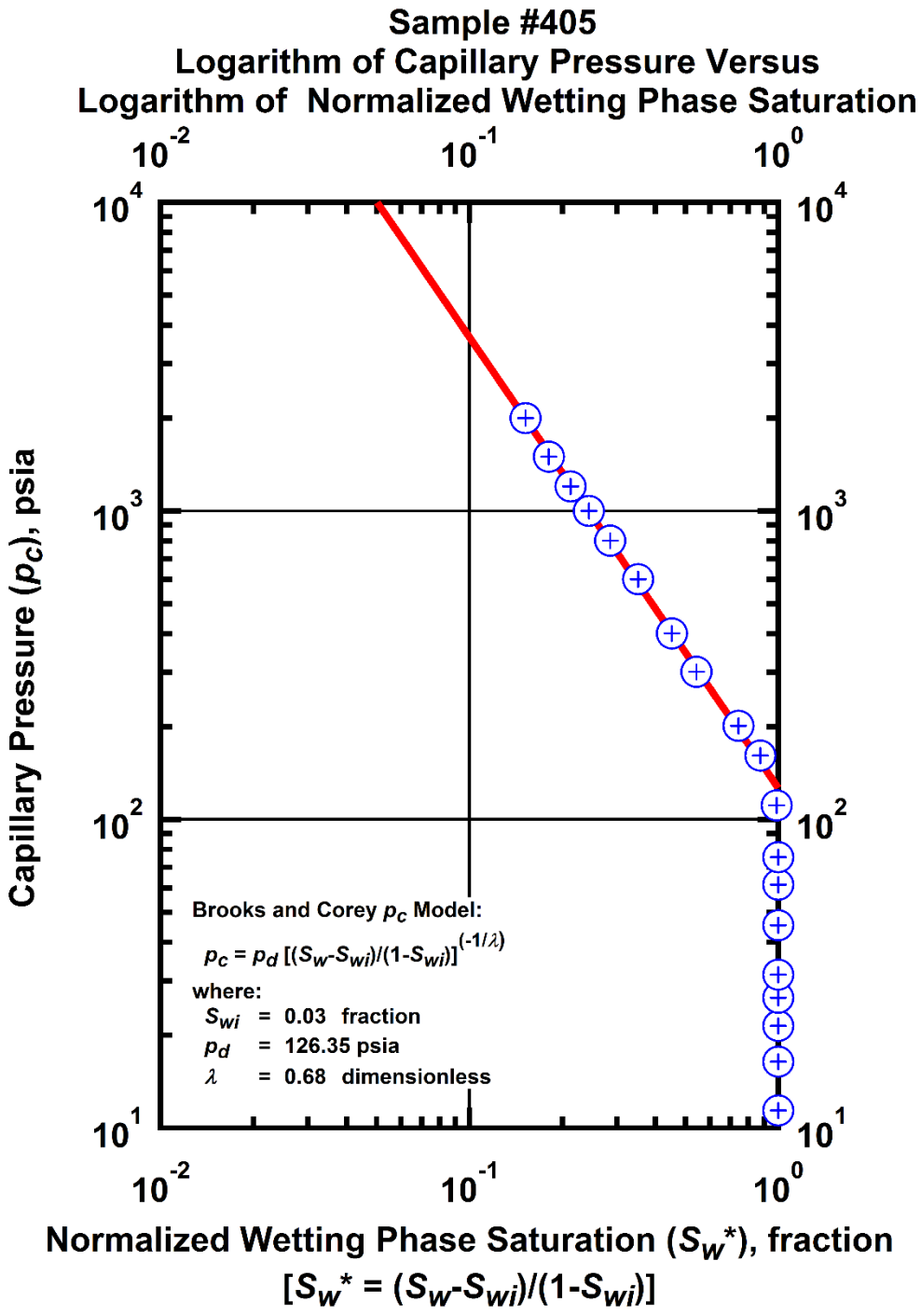

Figure I-17 — Plot of logarithm of capillary pressure vs. logarithm of normalized wetting phase saturation — Sample #405.

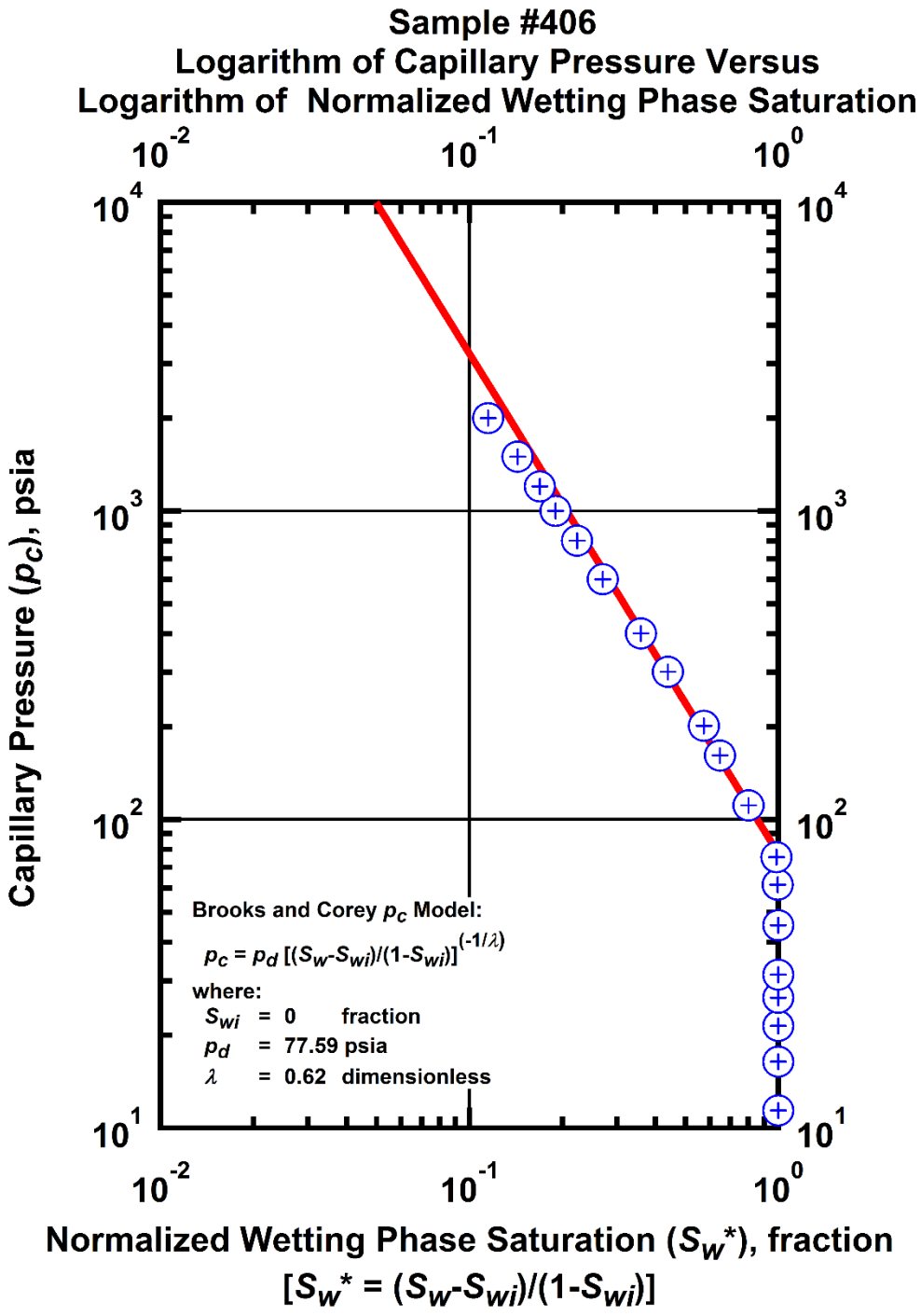

Figure I-18 — Plot of logarithm of capillary pressure vs. logarithm of normalized wetting phase saturation — Sample #406.

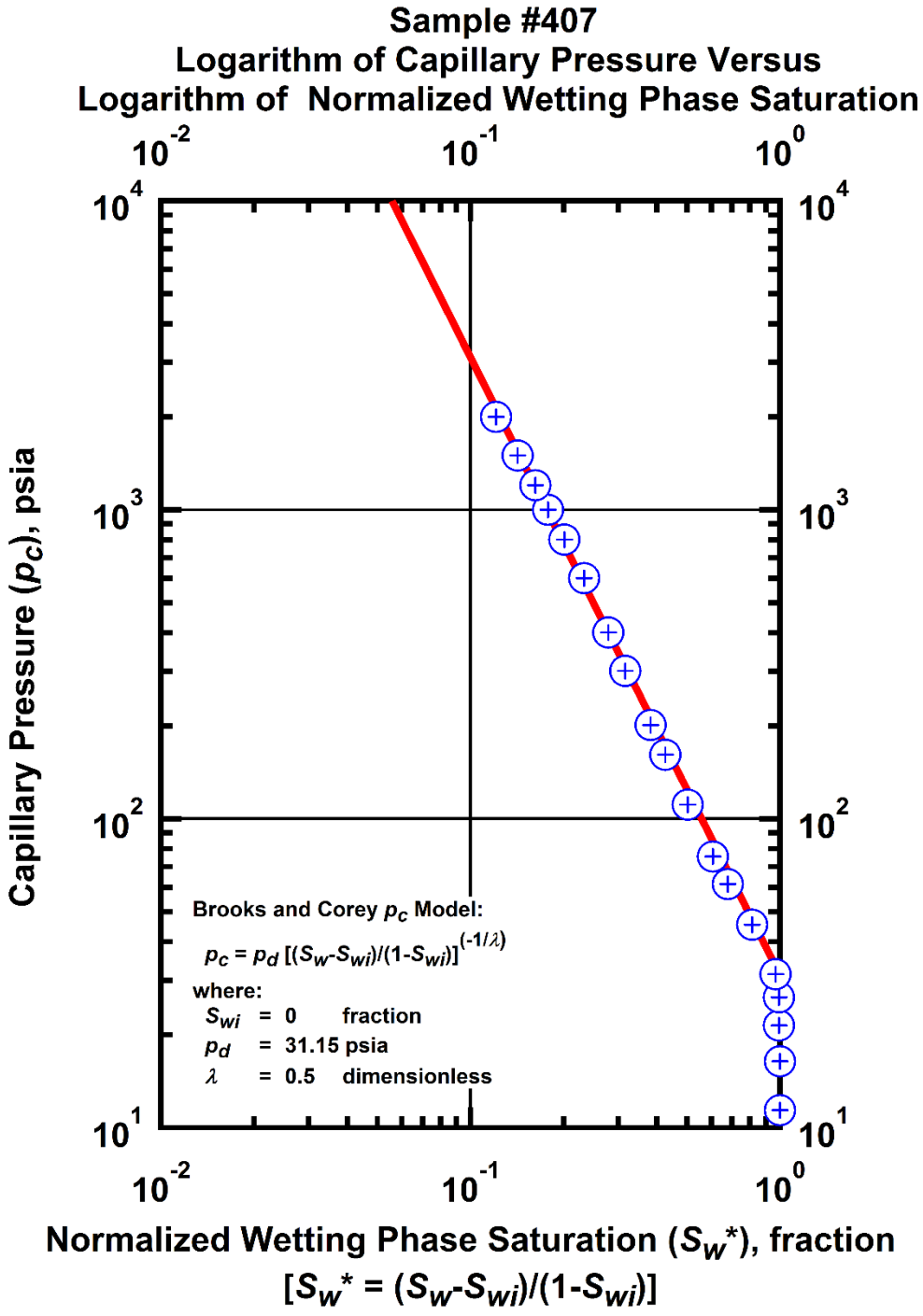

Figure I-19 — Plot of logarithm of capillary pressure vs. logarithm of normalized wetting phase saturation — Sample #407.

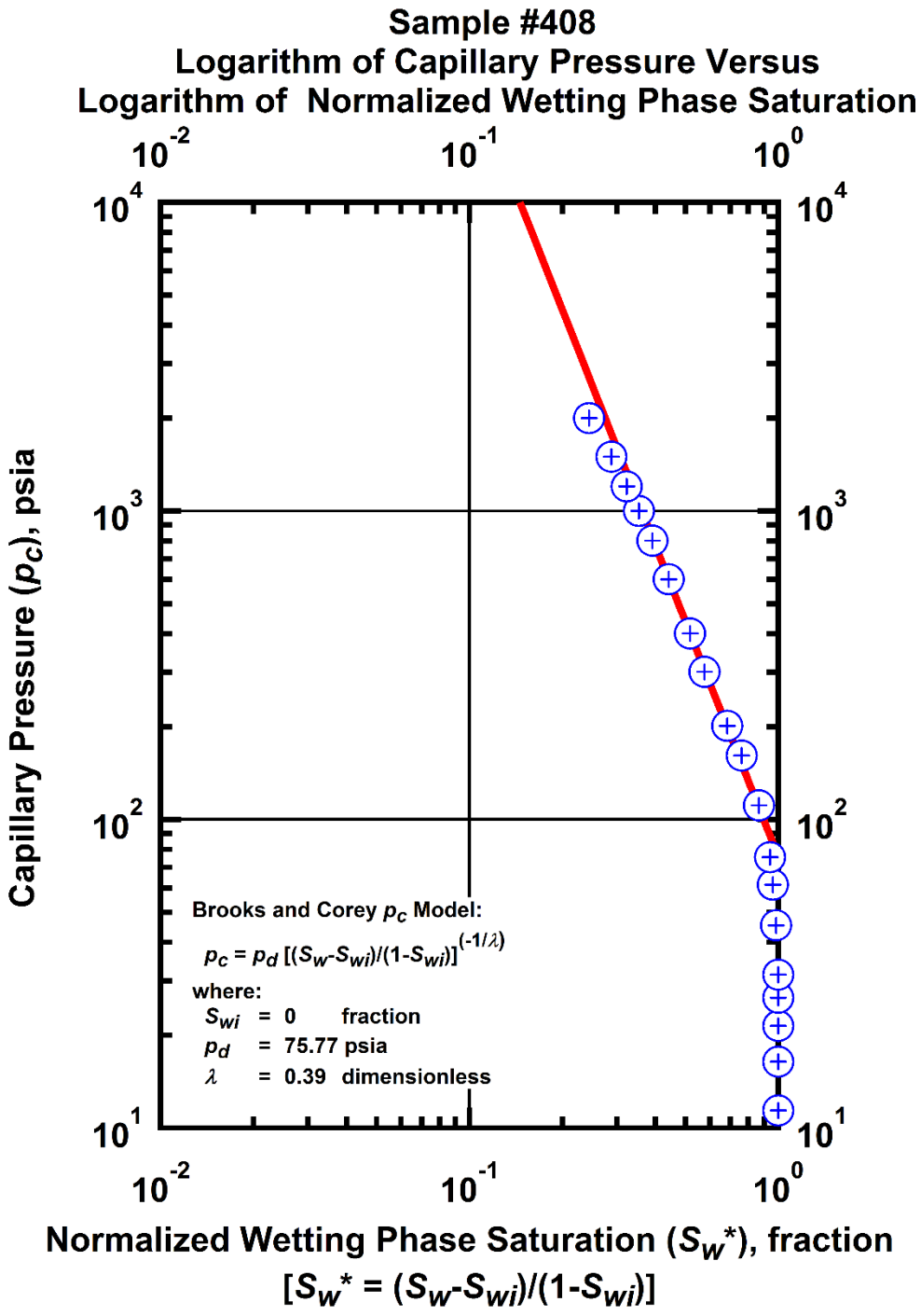

Figure I-20 — Plot of logarithm of capillary pressure vs. logarithm of normalized wetting phase saturation — Sample #408.

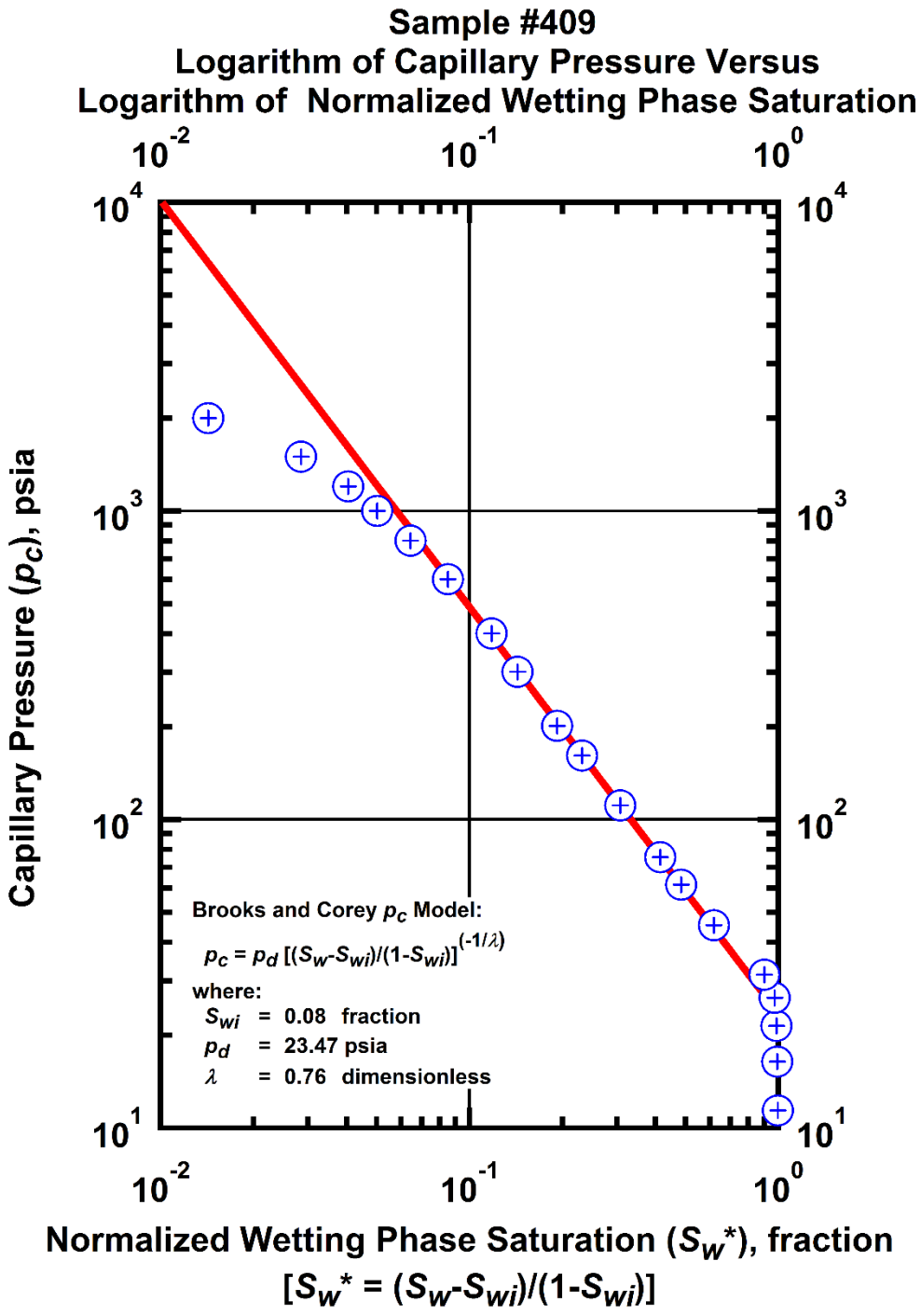

Figure I-21 — Plot of logarithm of capillary pressure vs. logarithm of normalized wetting phase saturation — Sample #409.

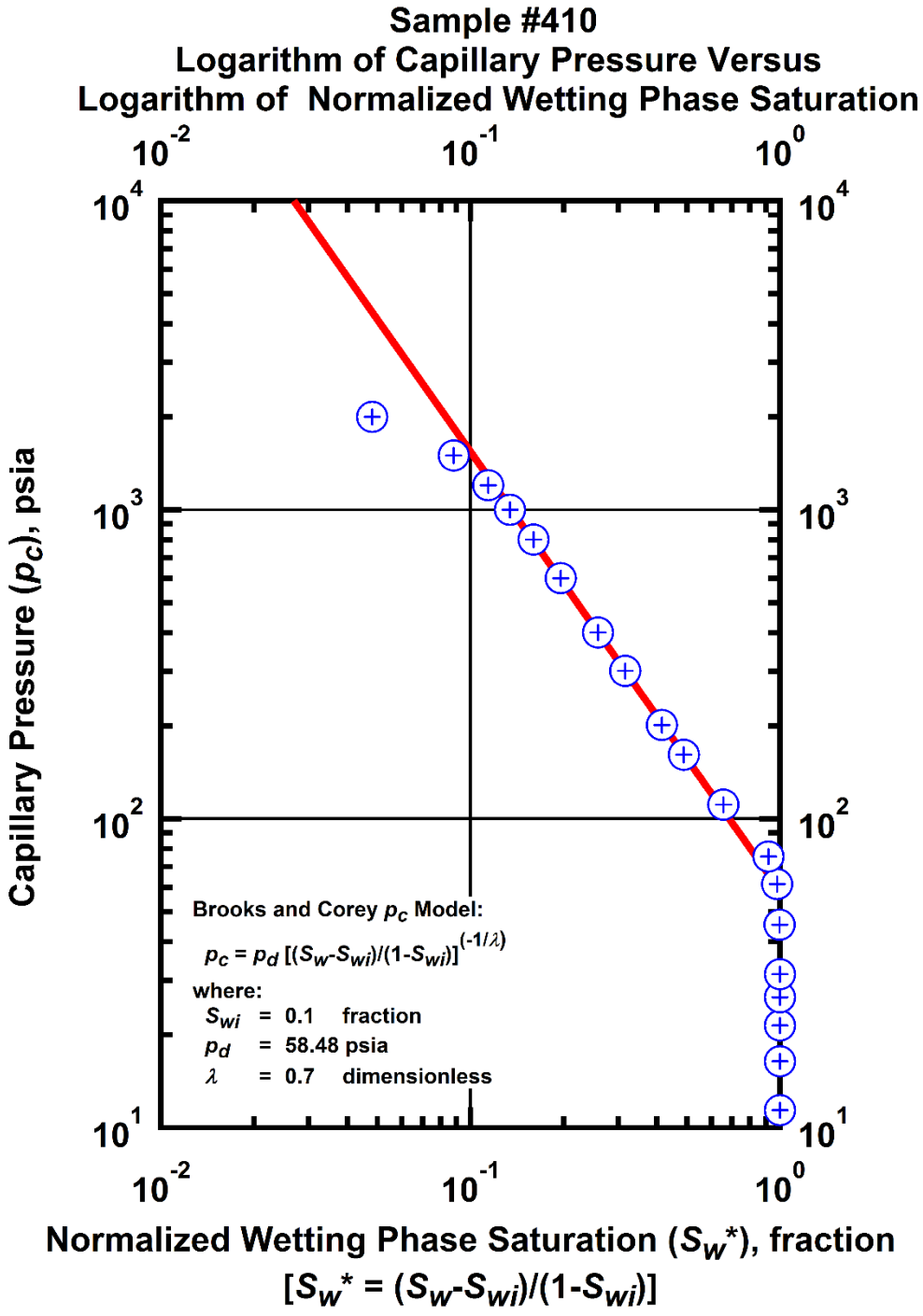

Figure I-22 — Plot of logarithm of capillary pressure vs. logarithm of normalized wetting phase saturation — Sample #410.

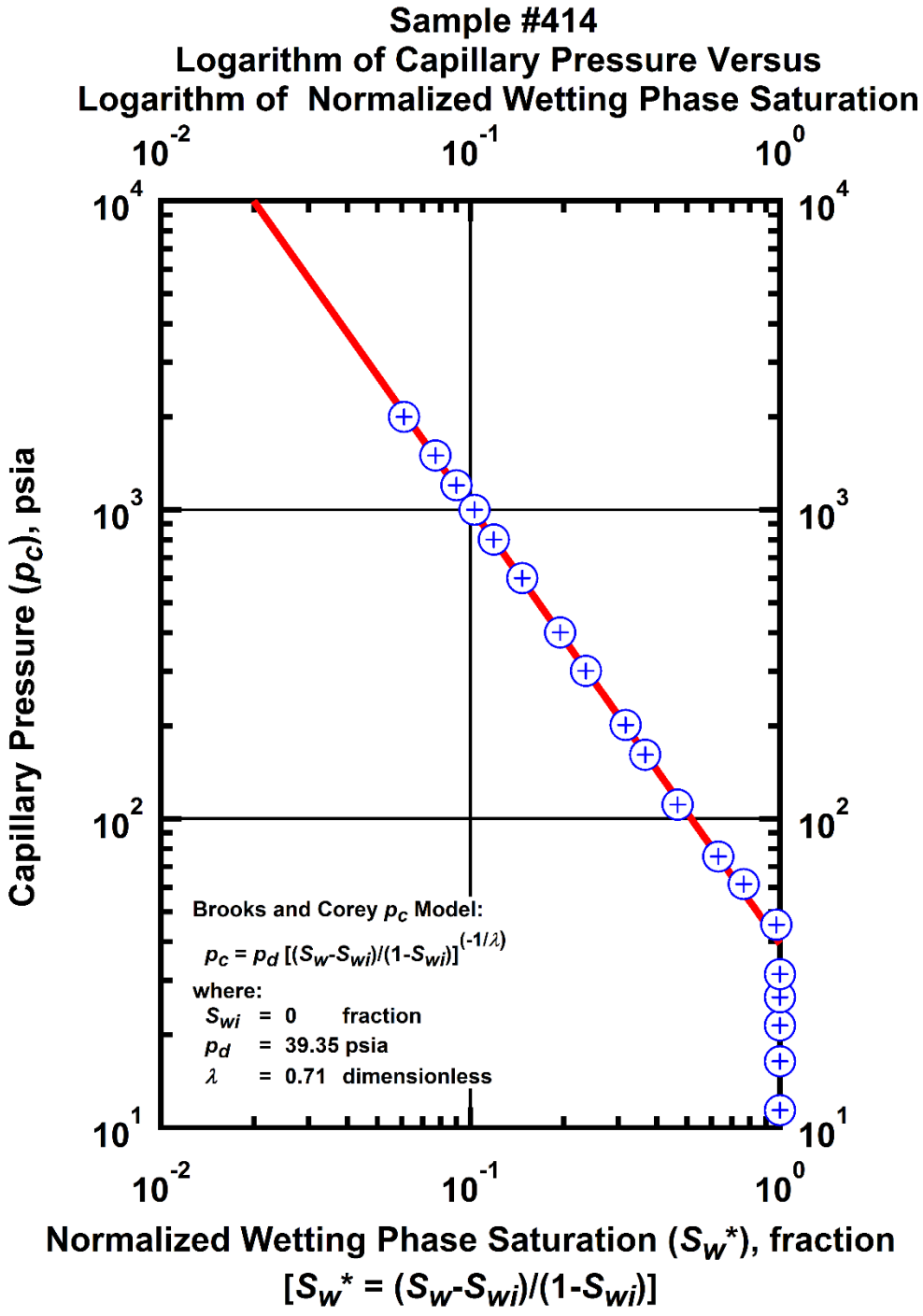

Figure I-23 — Plot of logarithm of capillary pressure vs. logarithm of normalized wetting phase saturation — Sample #414.

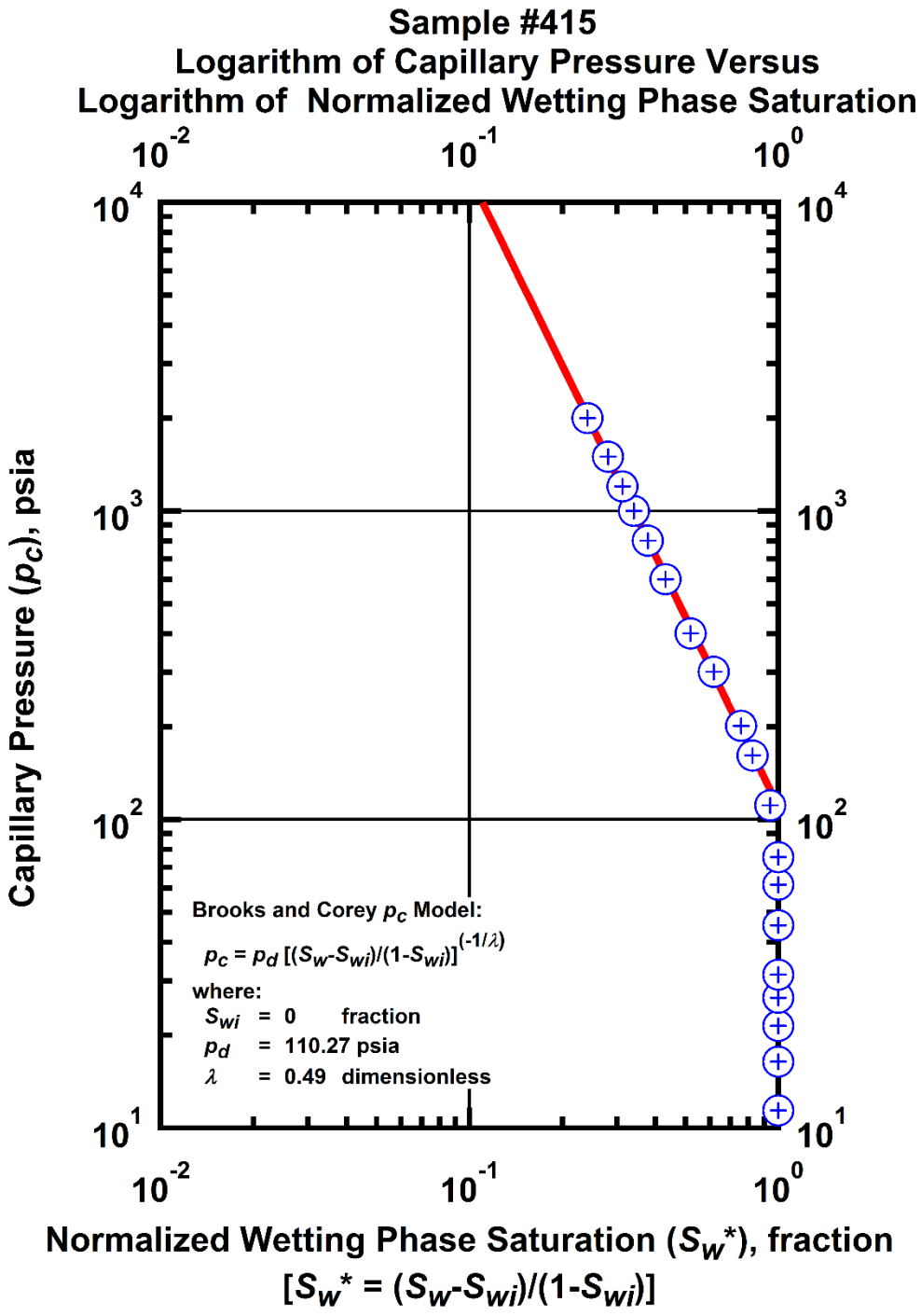

Figure I-24 — Plot of logarithm of capillary pressure vs. logarithm of normalized wetting phase saturation — Sample #415.

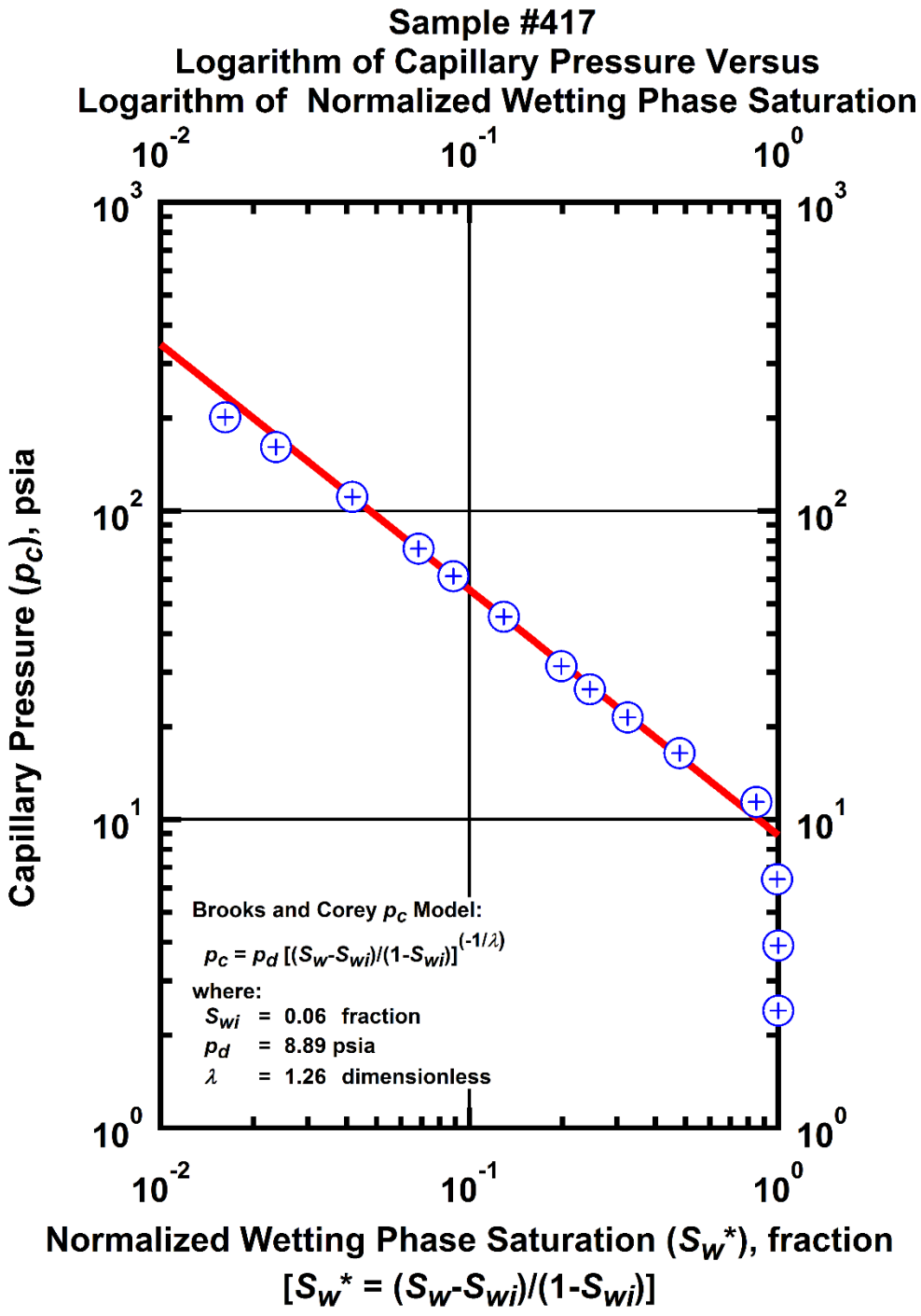

Figure I-25 — Plot of logarithm of capillary pressure vs. logarithm of normalized wetting phase saturation — Sample #417.

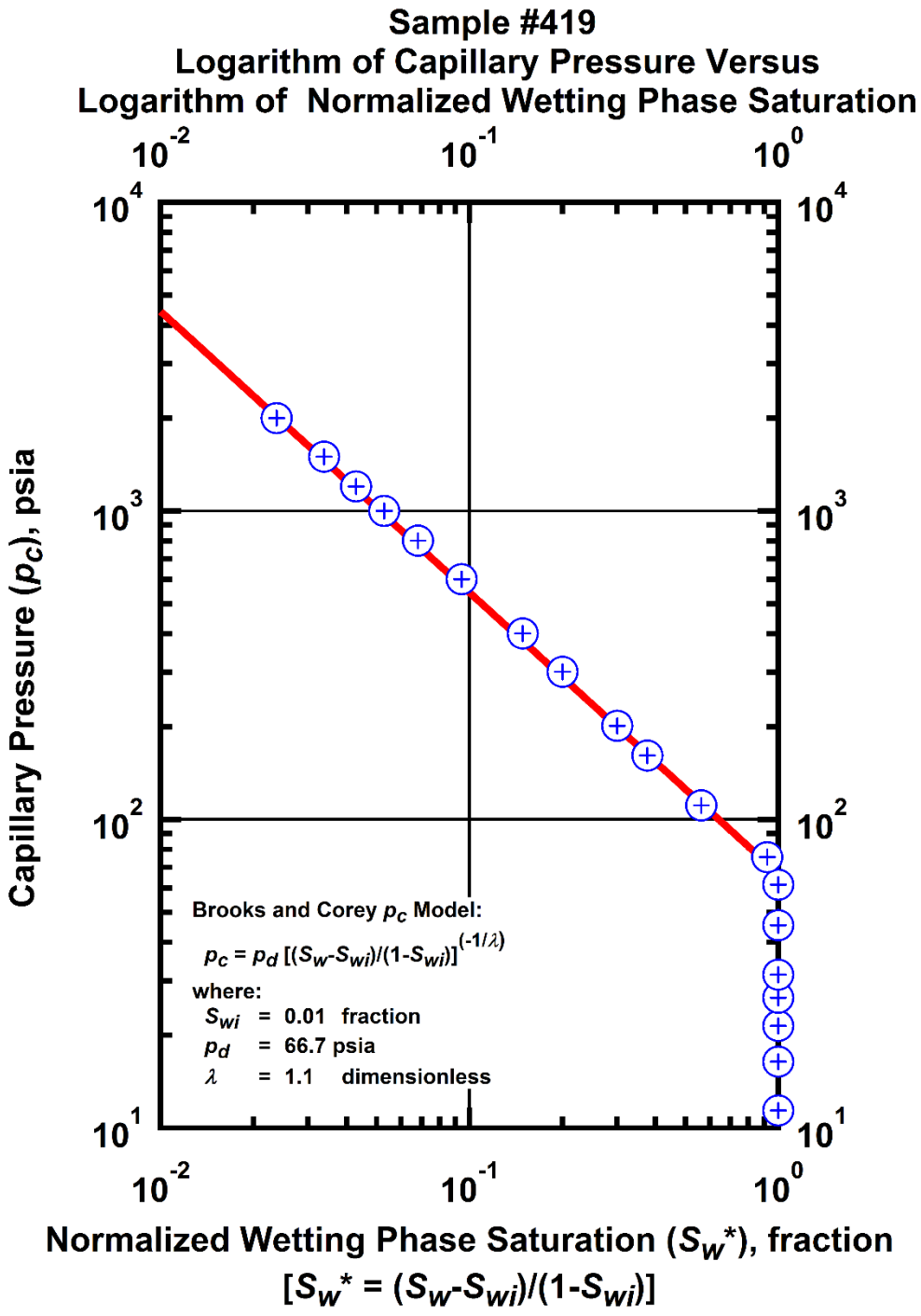

Figure I-26 — Plot of logarithm of capillary pressure vs. logarithm of normalized wetting phase saturation — Sample #419.

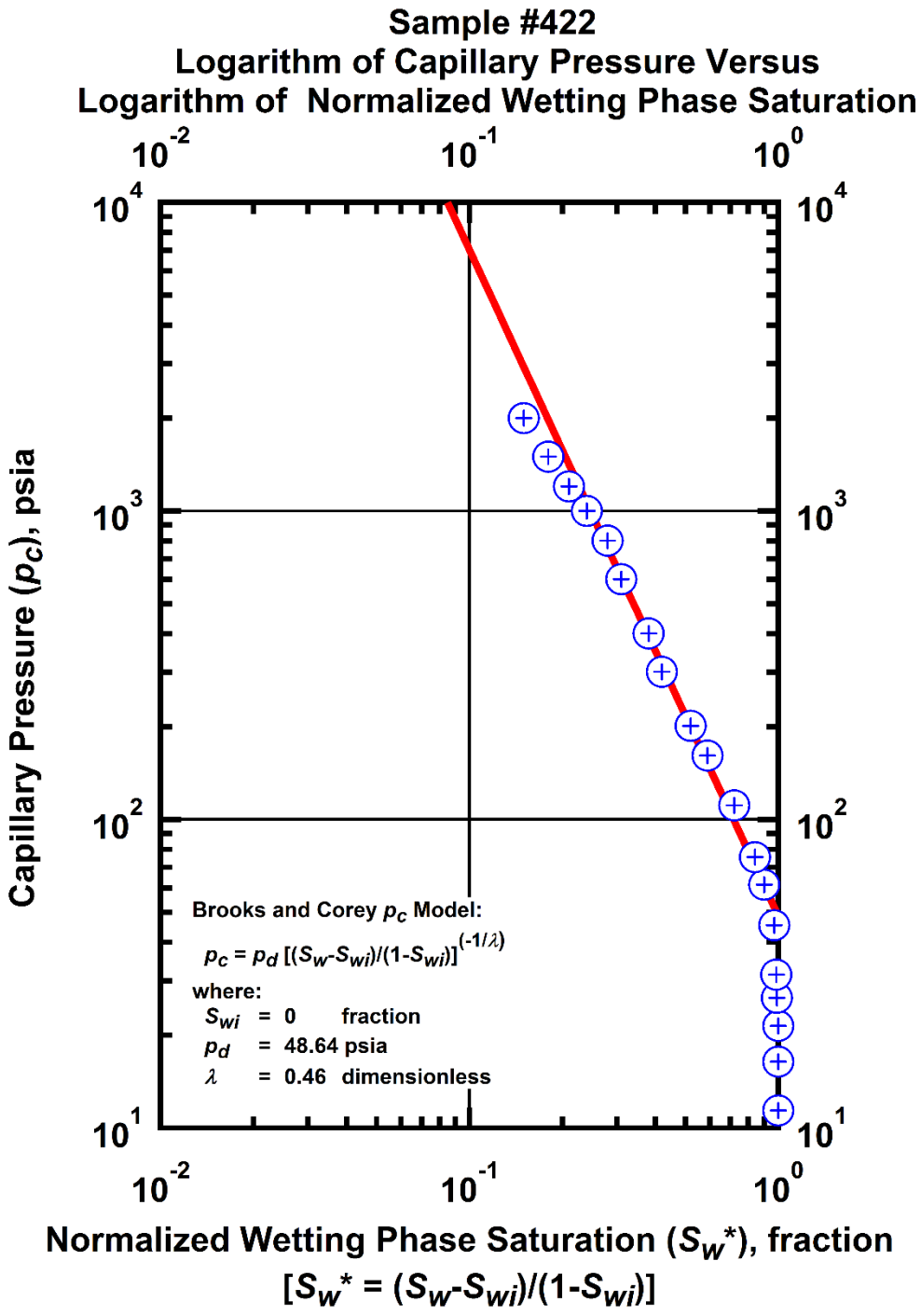

Figure I-27 — Plot of logarithm of capillary pressure vs. logarithm of normalized wetting phase saturation — Sample #422.

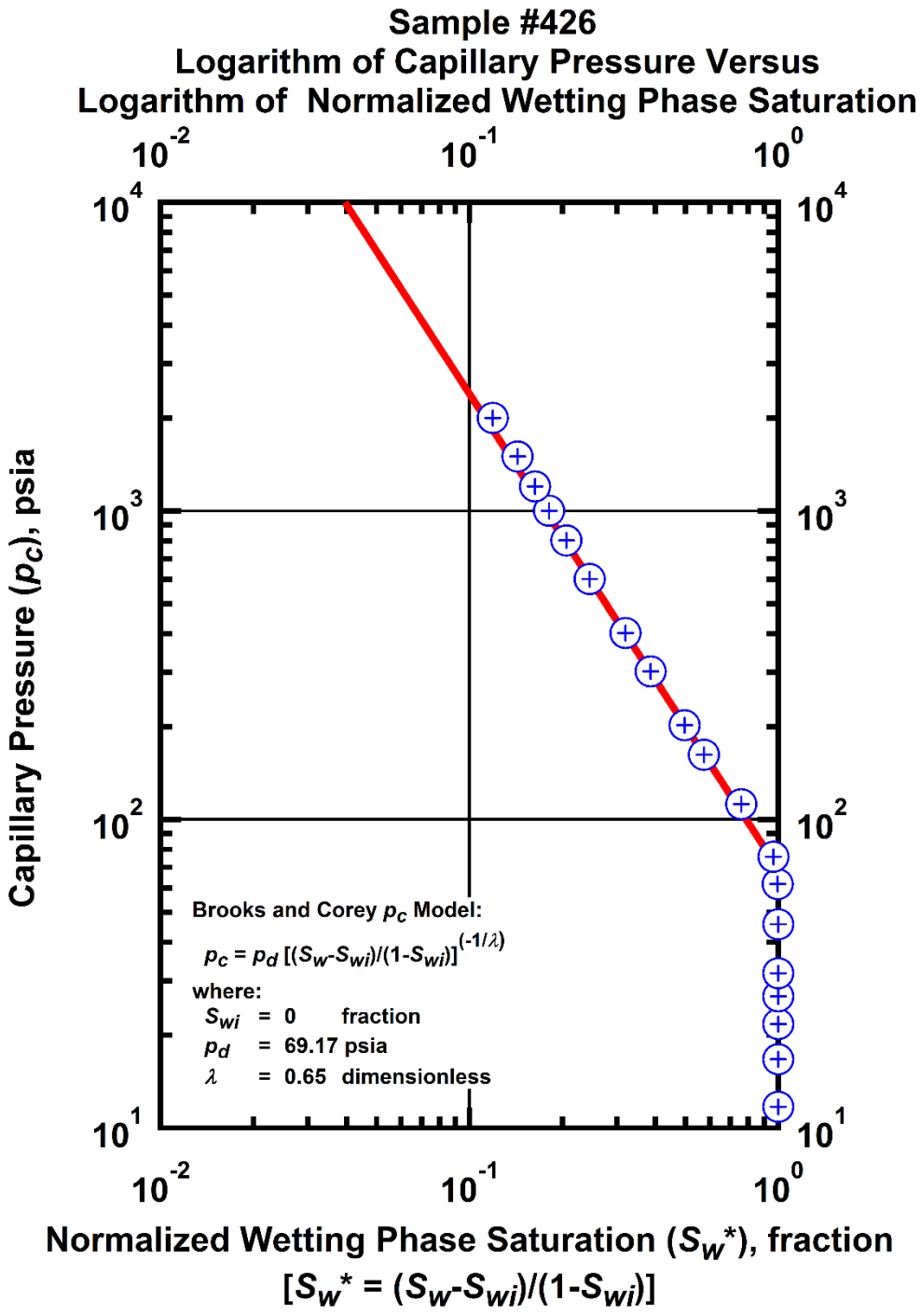

Figure I-28 — Plot of logarithm of capillary pressure vs. logarithm of normalized wetting phase saturation — Sample #426.

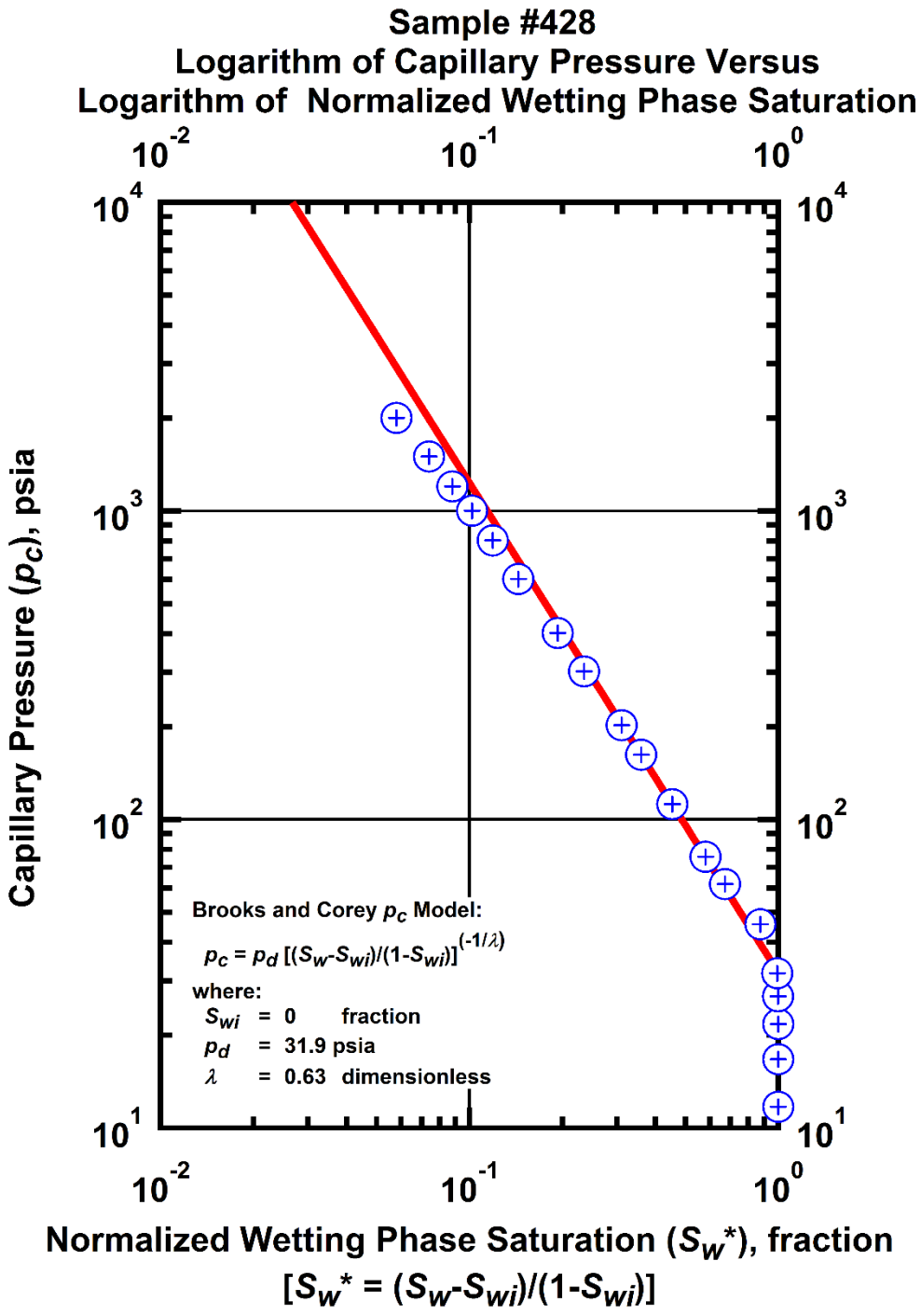

Figure I-29 — Plot of logarithm of capillary pressure vs. logarithm of normalized wetting phase saturation — Sample #428.

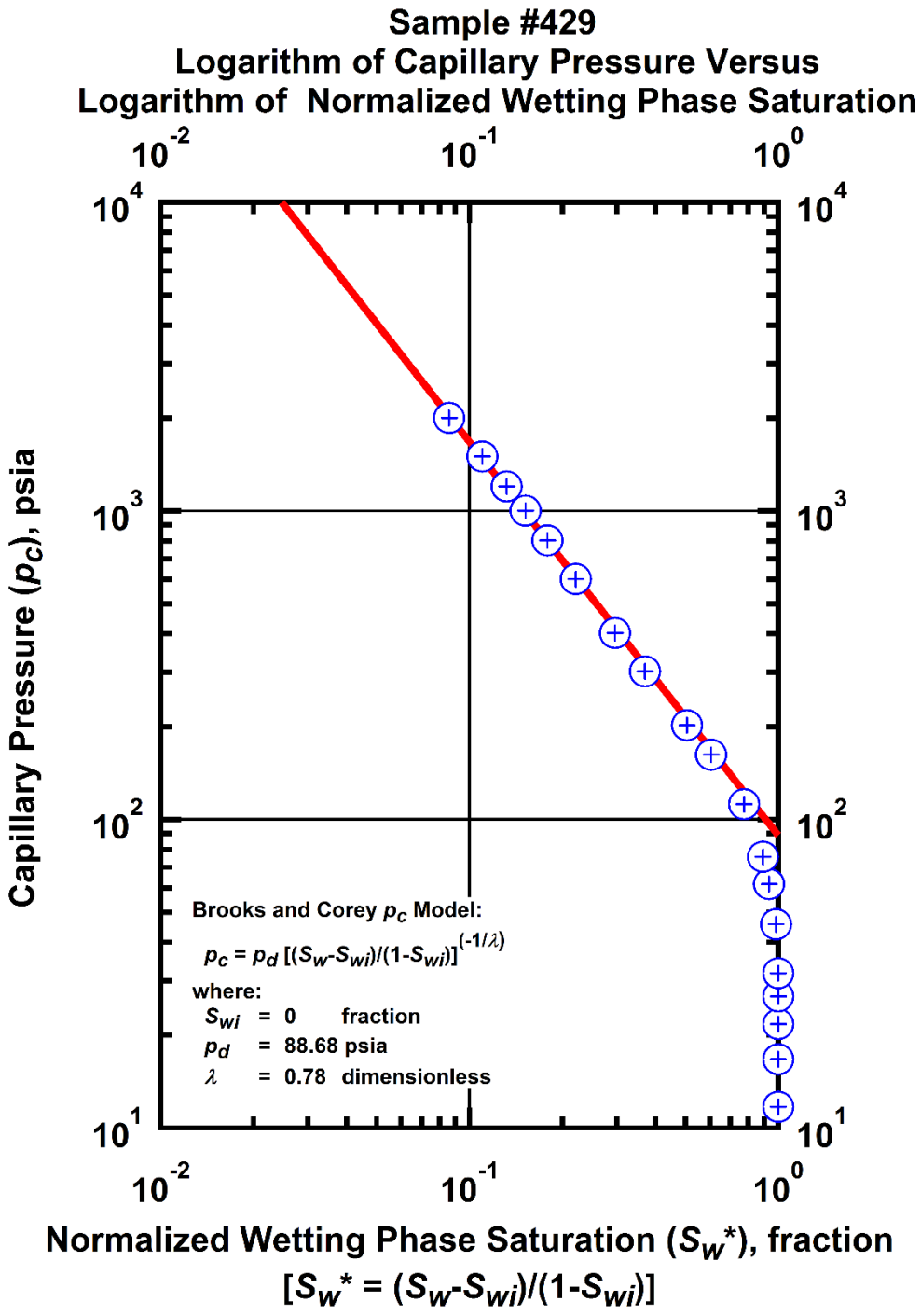

Figure I-30 — Plot of logarithm of capillary pressure vs. logarithm of normalized wetting phase saturation — Sample #429.

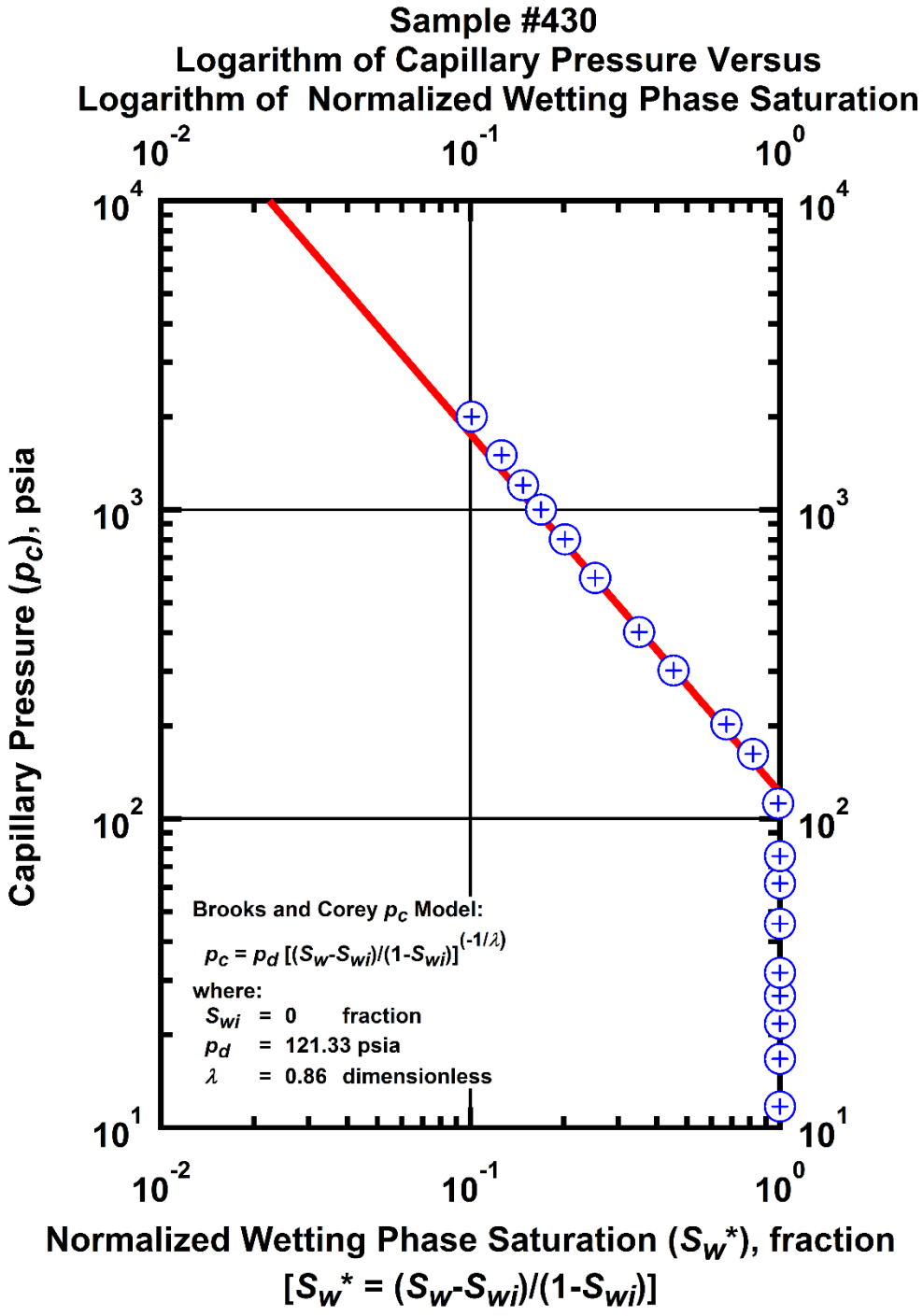

Figure I-31 — Plot of logarithm of capillary pressure vs. logarithm of normalized wetting phase saturation — Sample #430.

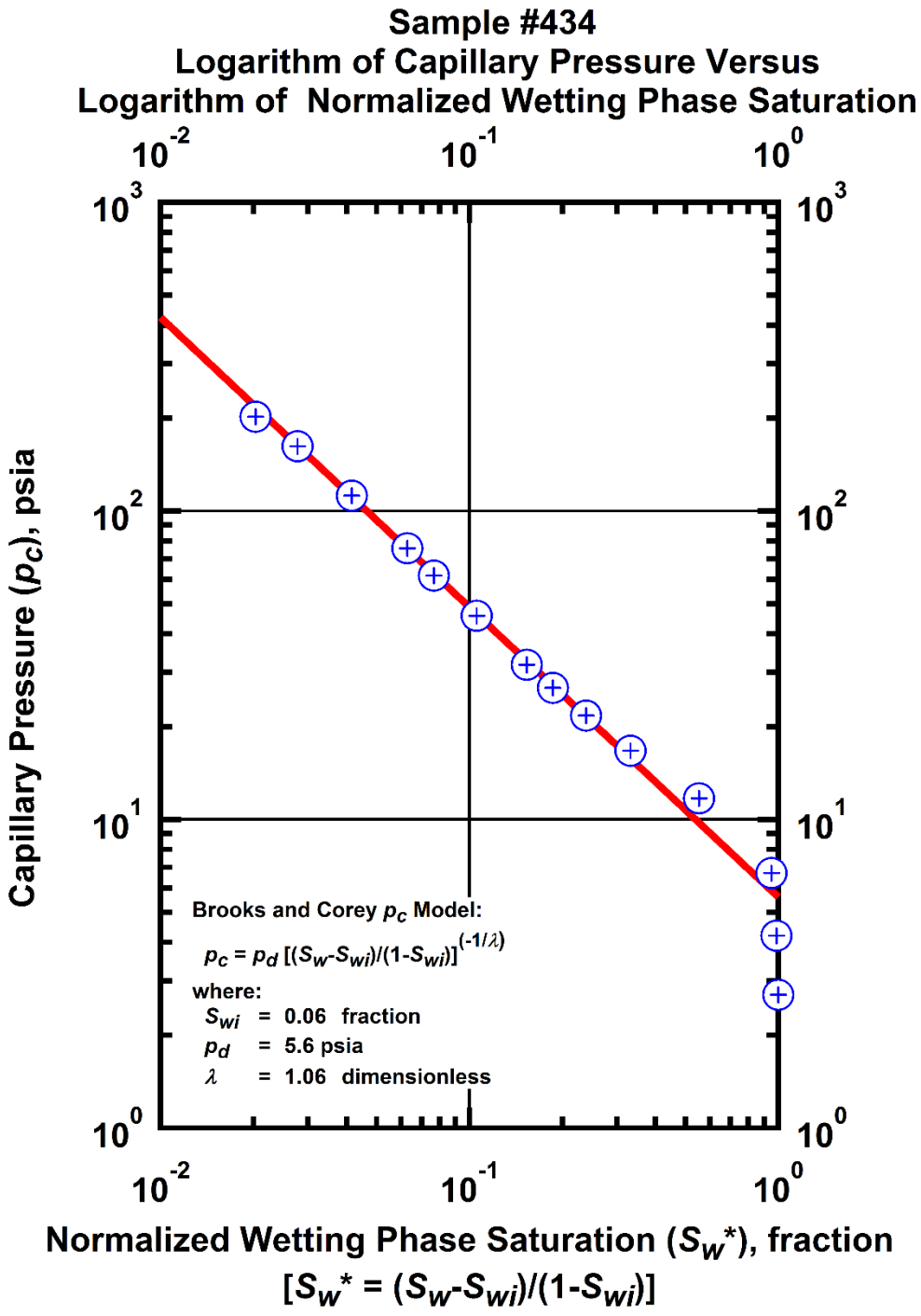

Figure I-32 — Plot of logarithm of capillary pressure vs. logarithm of normalized wetting phase saturation — Sample #434.

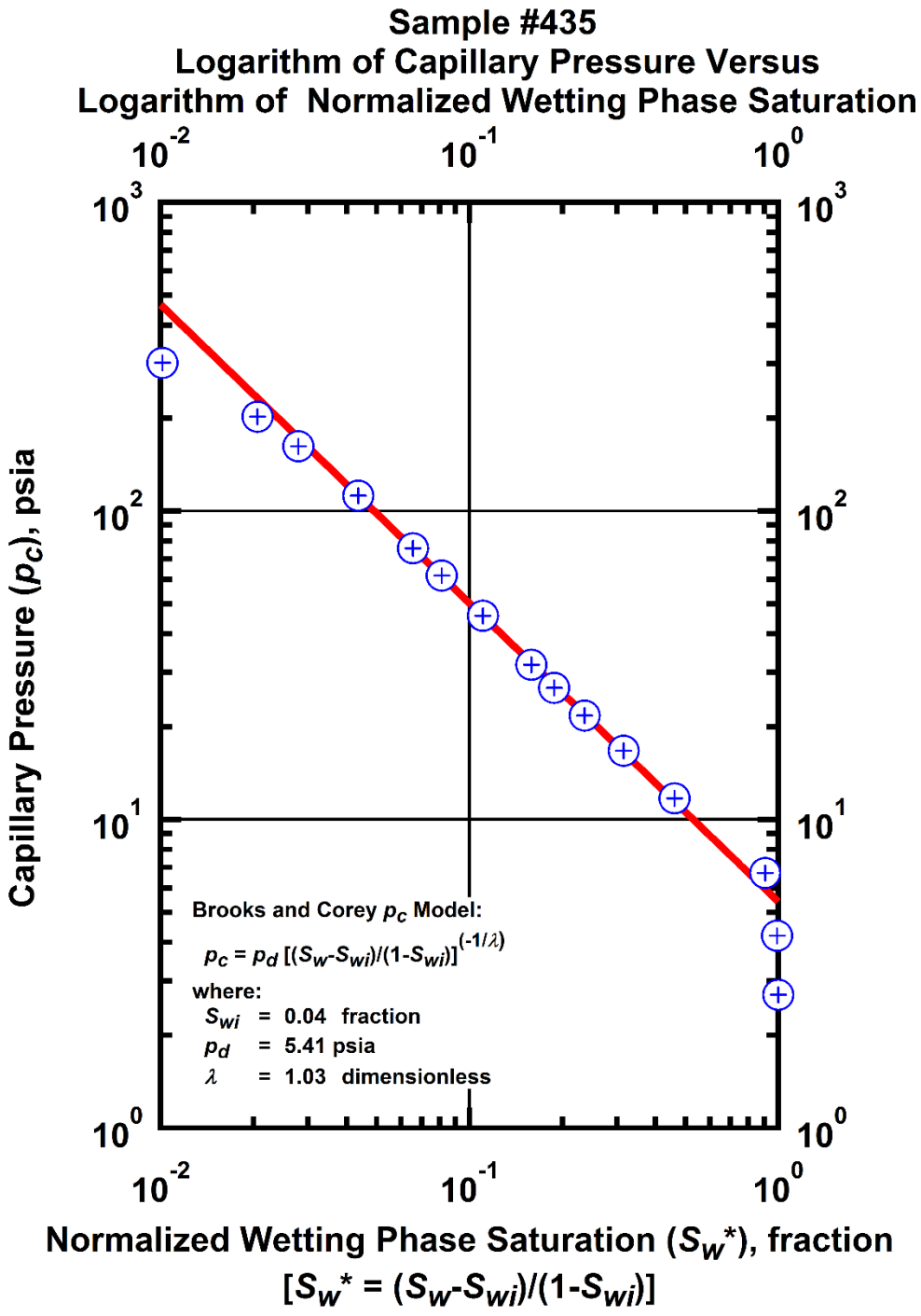

Figure I-33 — Plot of logarithm of capillary pressure vs. logarithm of normalized wetting phase saturation — Sample #435.

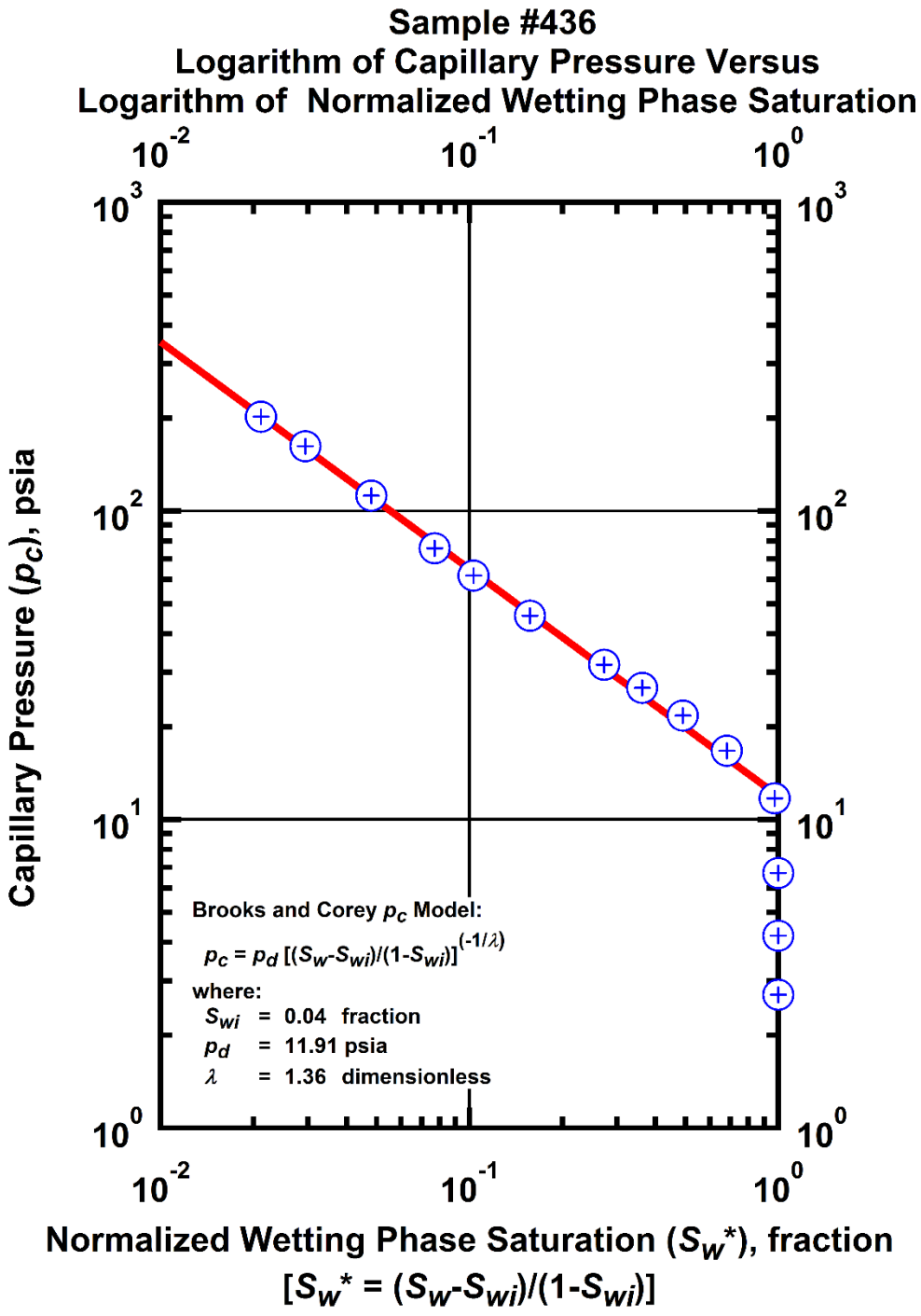

Figure I-34 — Plot of logarithm of capillary pressure vs. logarithm of normalized wetting phase saturation — Sample #436.

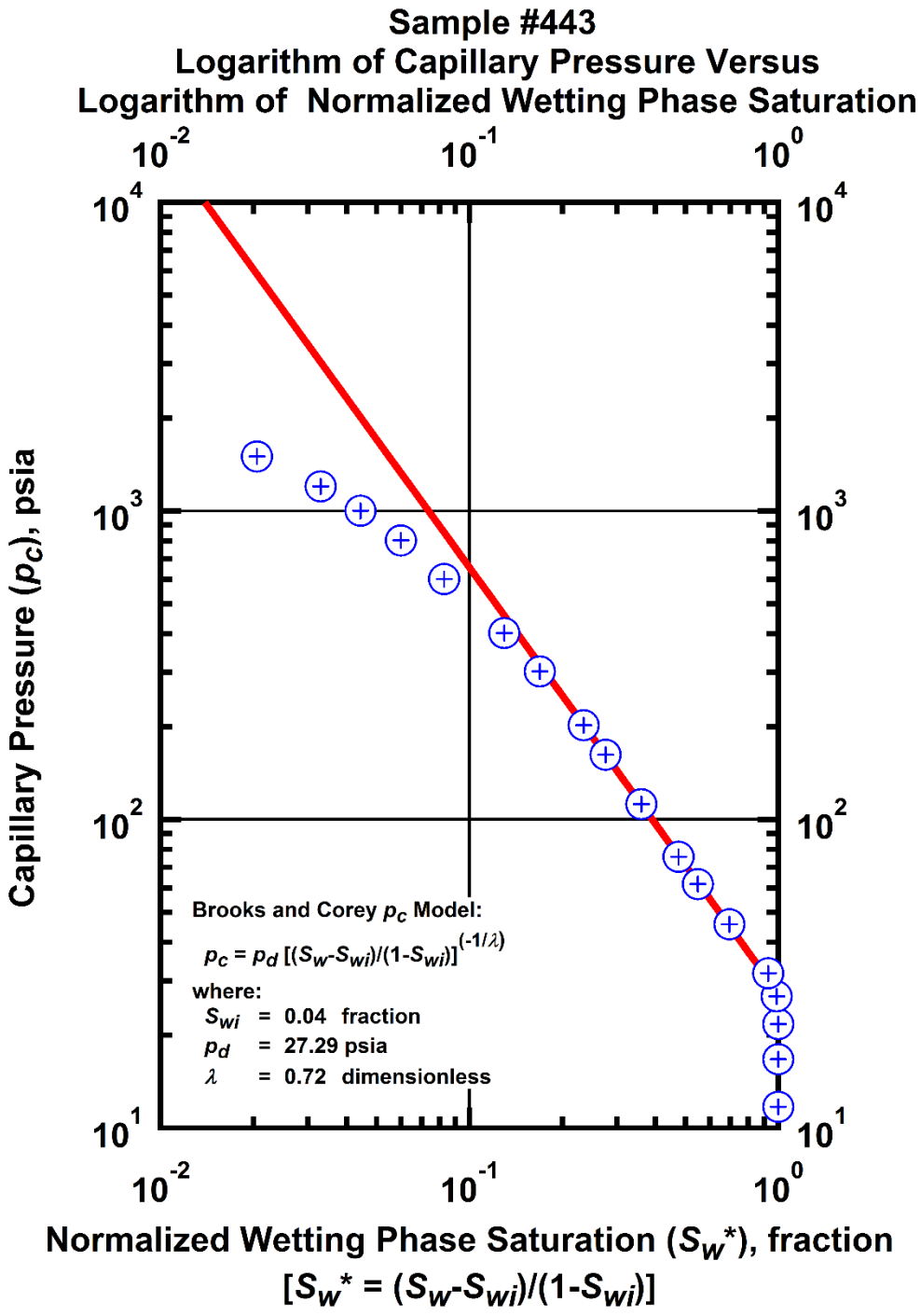

Figure I-35 — Plot of logarithm of capillary pressure vs. logarithm of normalized wetting phase saturation — Sample #443.

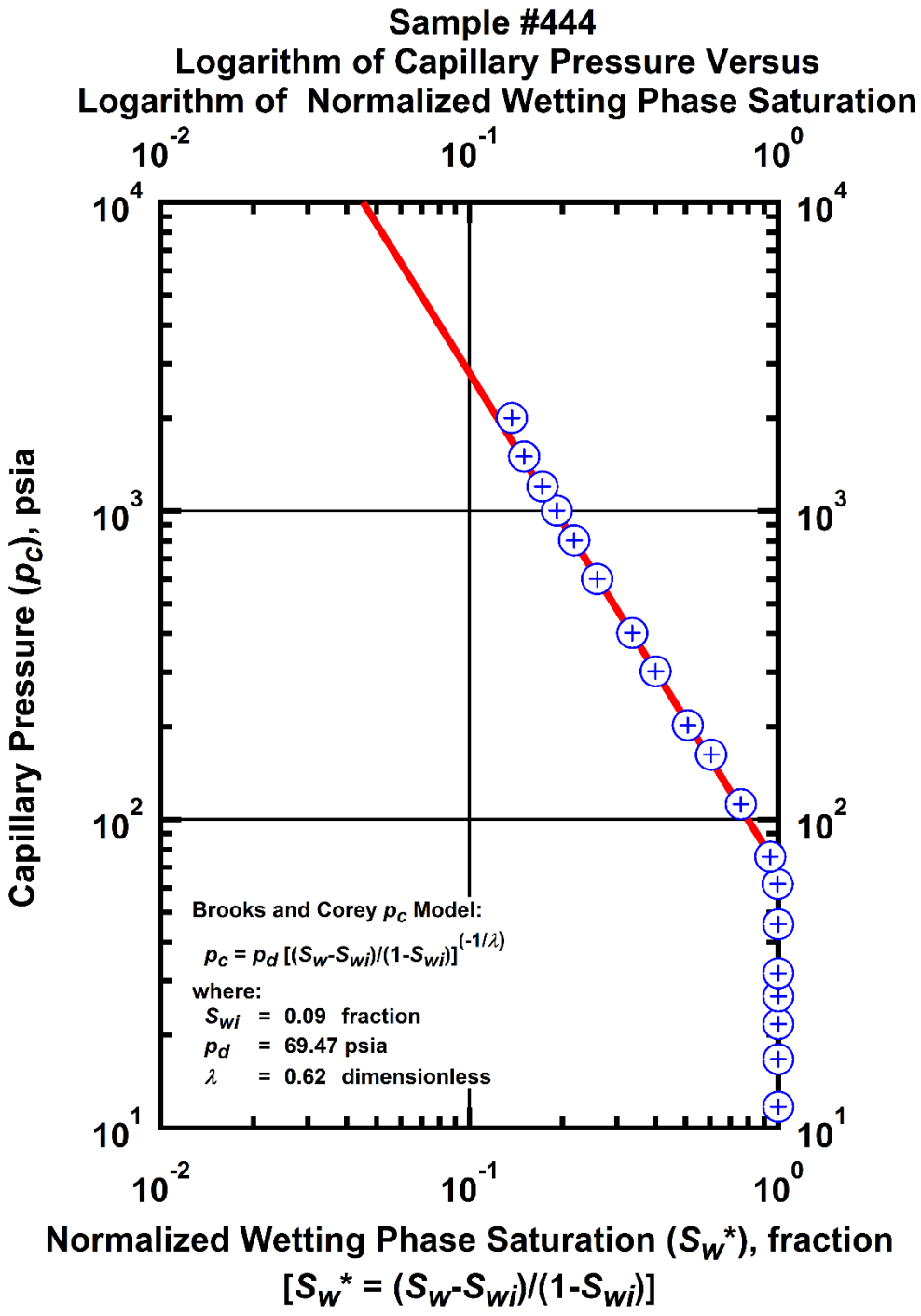

Figure I-36 — Plot of logarithm of capillary pressure vs. logarithm of normalized wetting phase saturation — Sample #444.

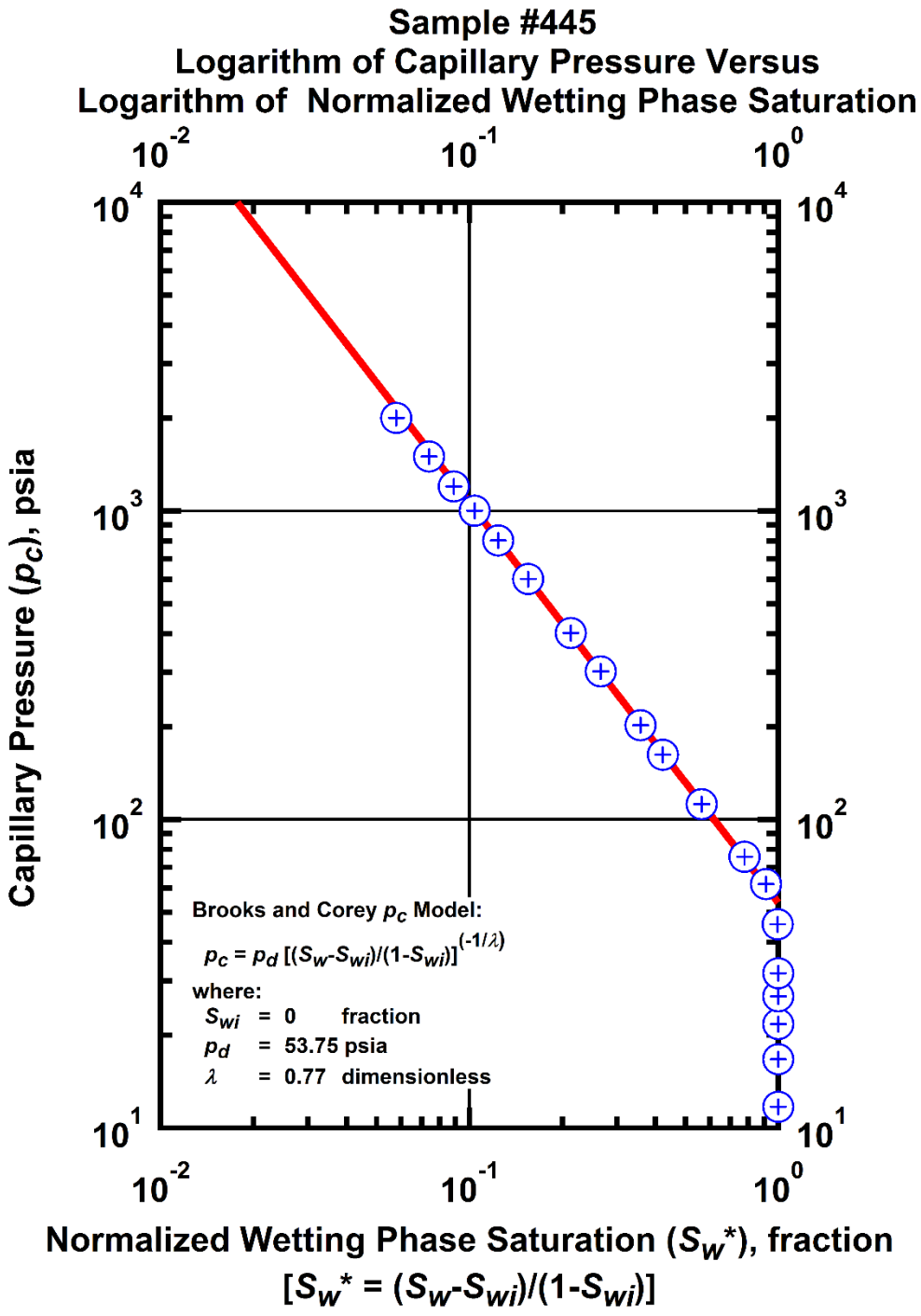

Figure I-37 — Plot of logarithm of capillary pressure vs. logarithm of normalized wetting phase saturation — Sample #445.

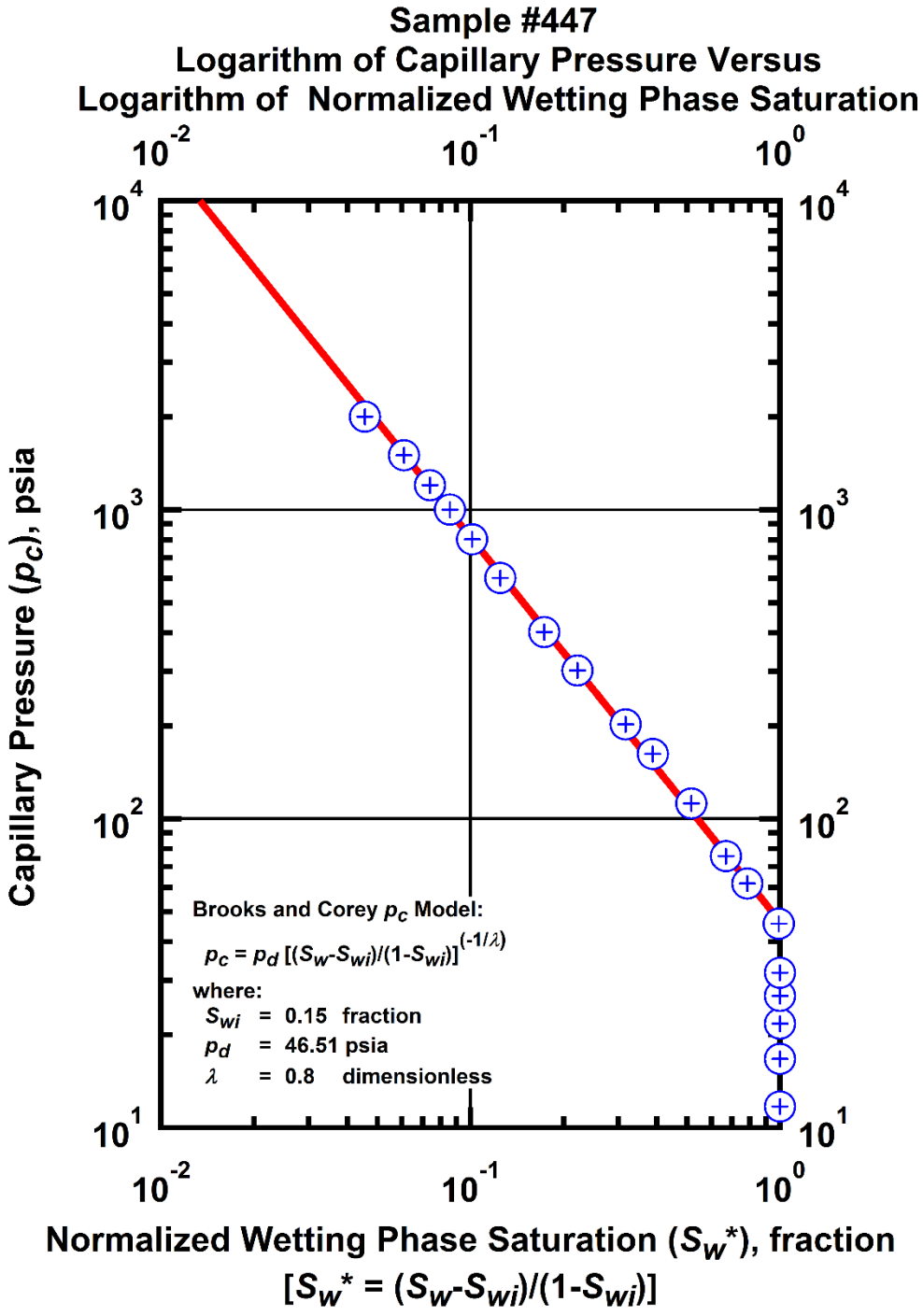

Figure I-38 — Plot of logarithm of capillary pressure vs. logarithm of normalized wetting phase saturation — Sample #447.

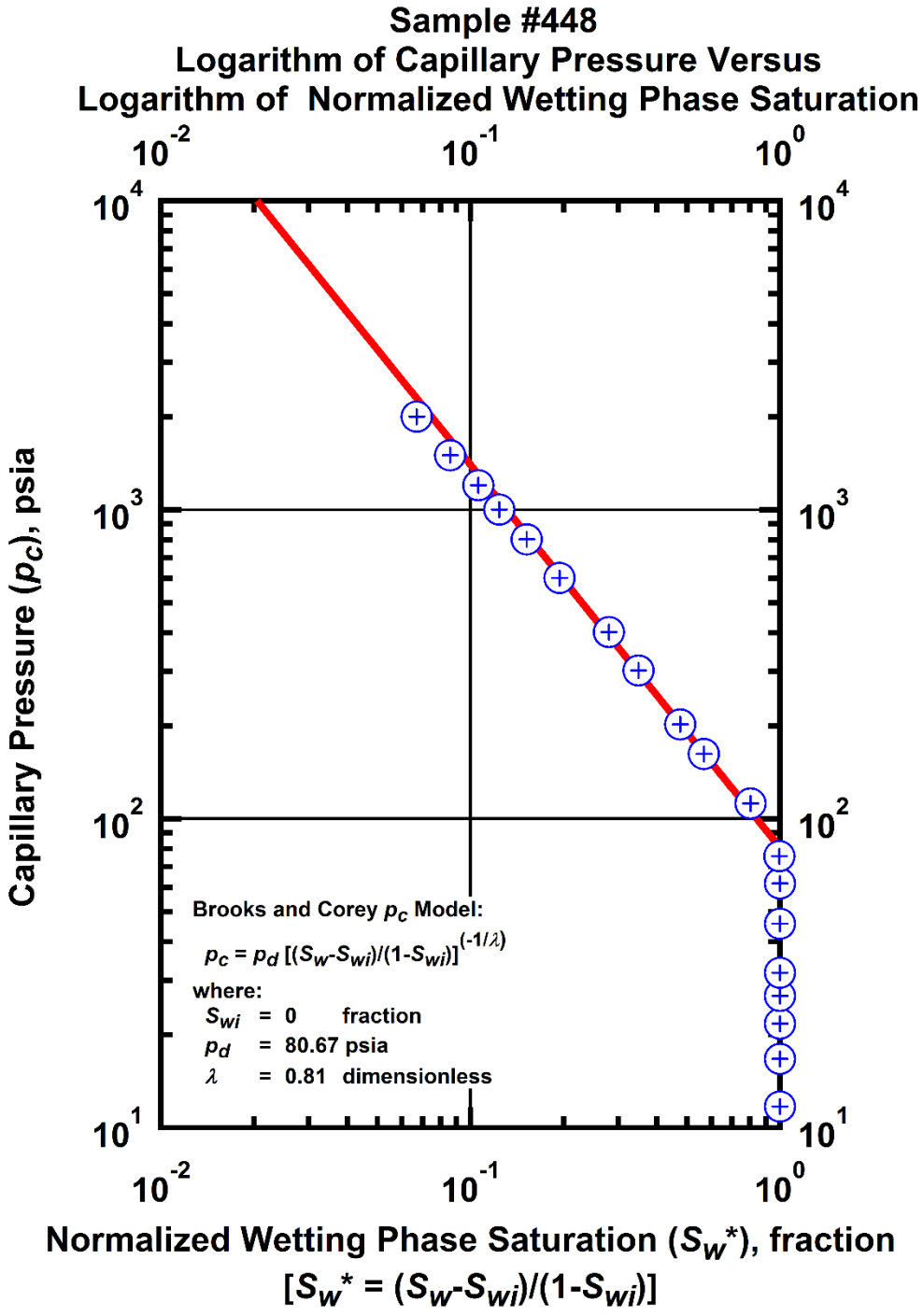

Figure I-39 — Plot of logarithm of capillary pressure vs. logarithm of normalized wetting phase saturation — Sample #448.

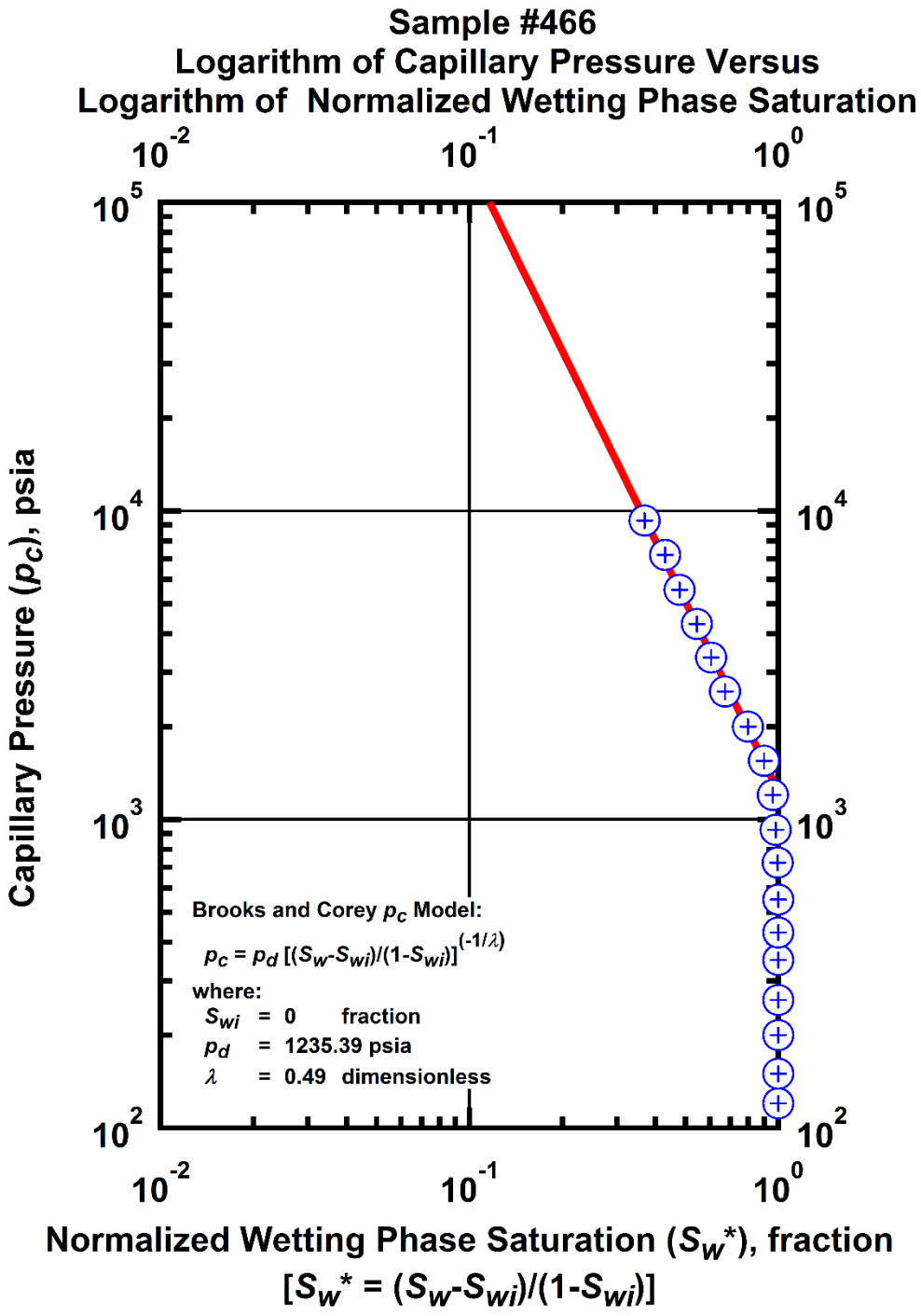

Figure I-40 — Plot of logarithm of capillary pressure vs. logarithm of normalized wetting phase saturation — Sample #466.

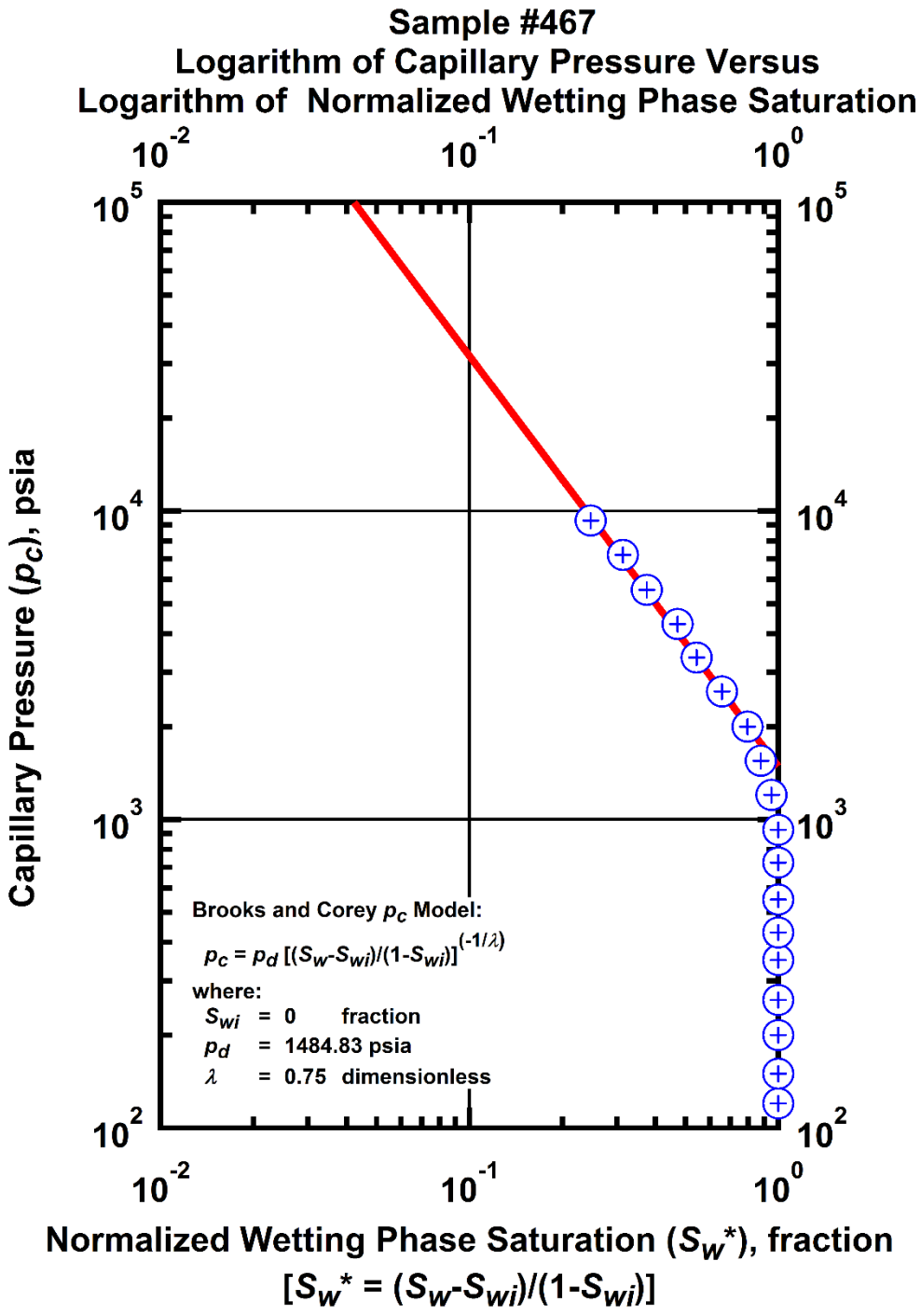

Figure I-41 — Plot of logarithm of capillary pressure vs. logarithm of normalized wetting phase saturation — Sample #467.

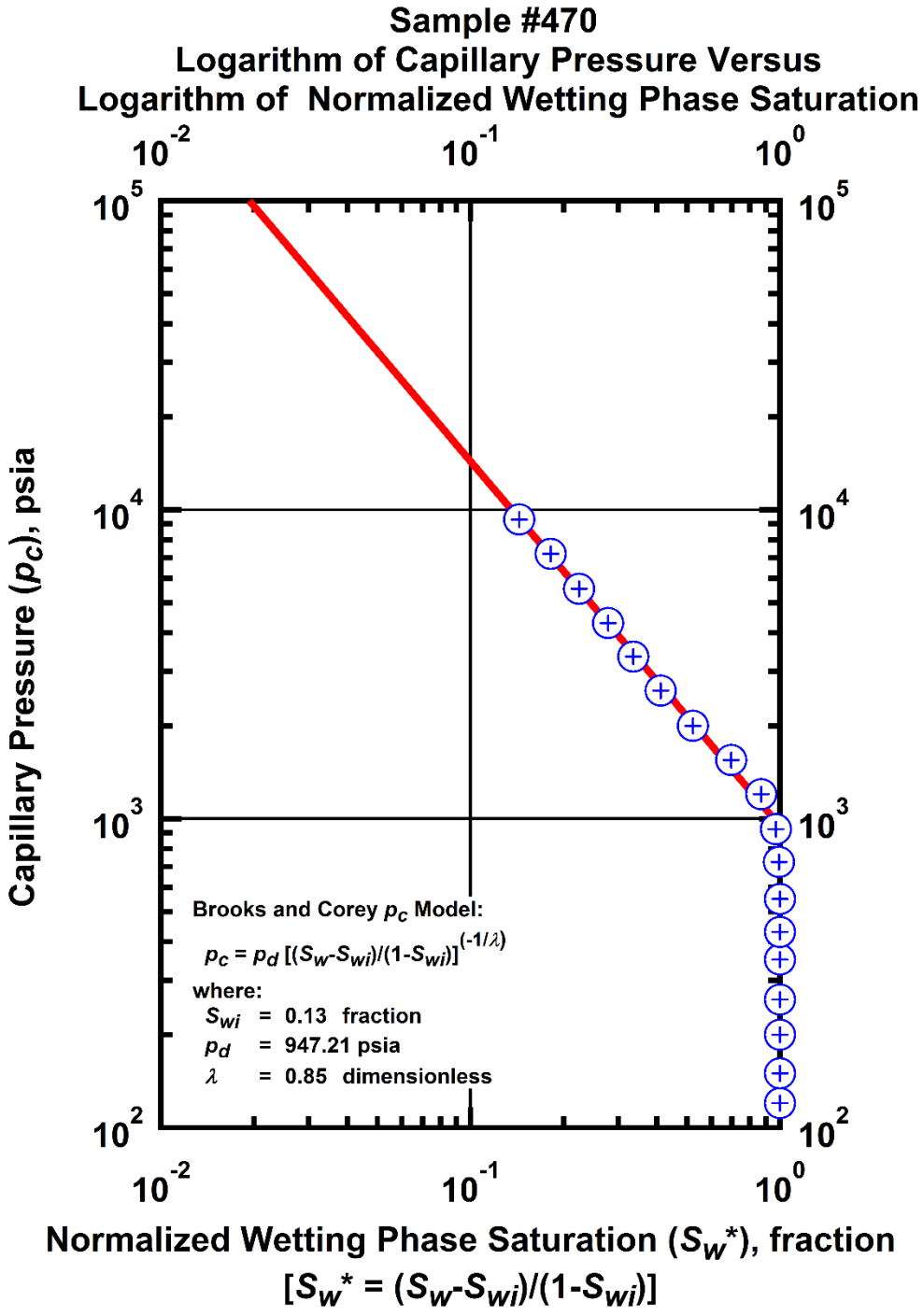

Figure I-42 — Plot of logarithm of capillary pressure vs. logarithm of normalized wetting phase saturation — Sample #470.

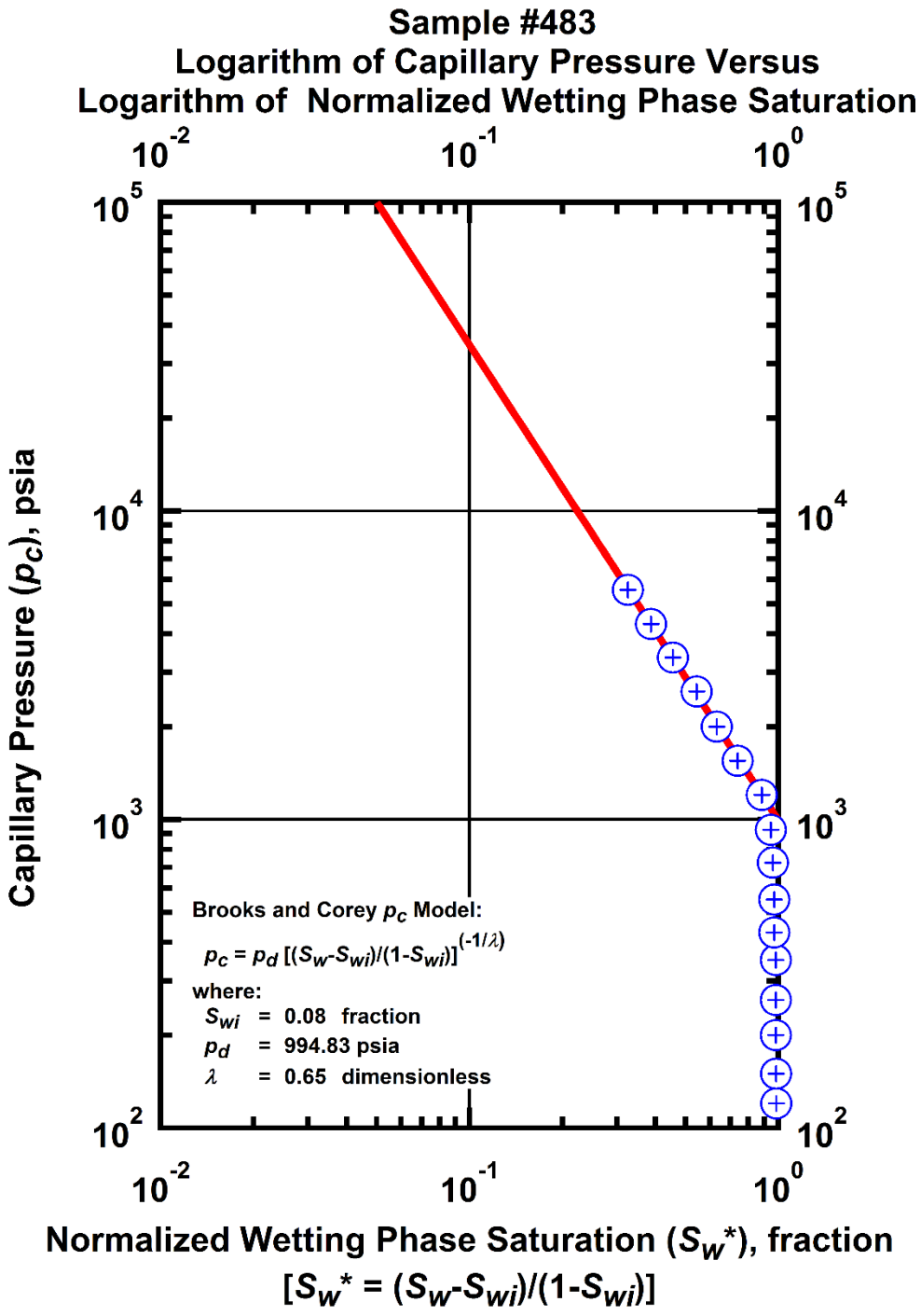

Figure I-43 — Plot of logarithm of capillary pressure vs. logarithm of normalized wetting phase saturation — Sample #483.

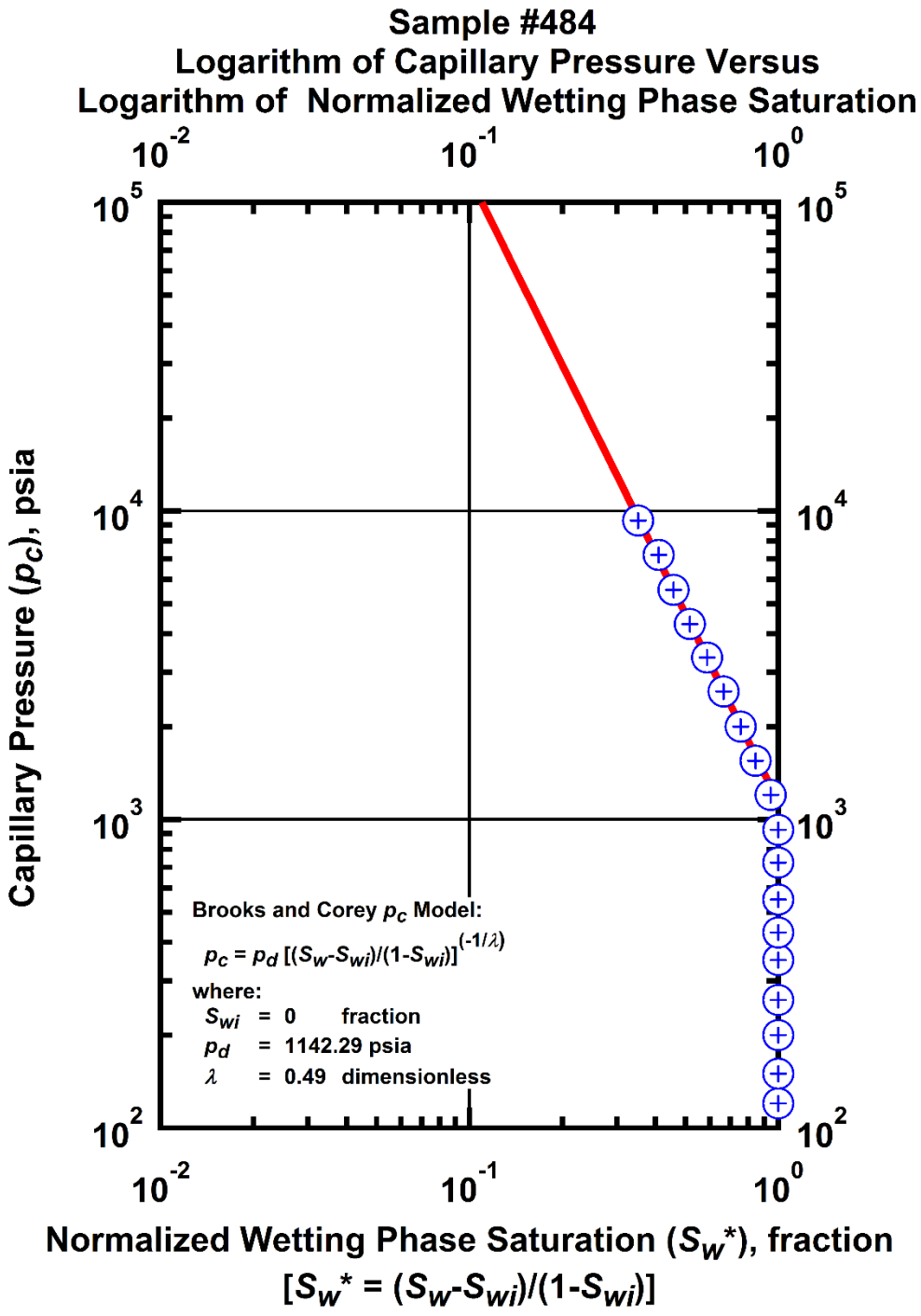

Figure I-44 — Plot of logarithm of capillary pressure vs. logarithm of normalized wetting phase saturation — Sample #484.

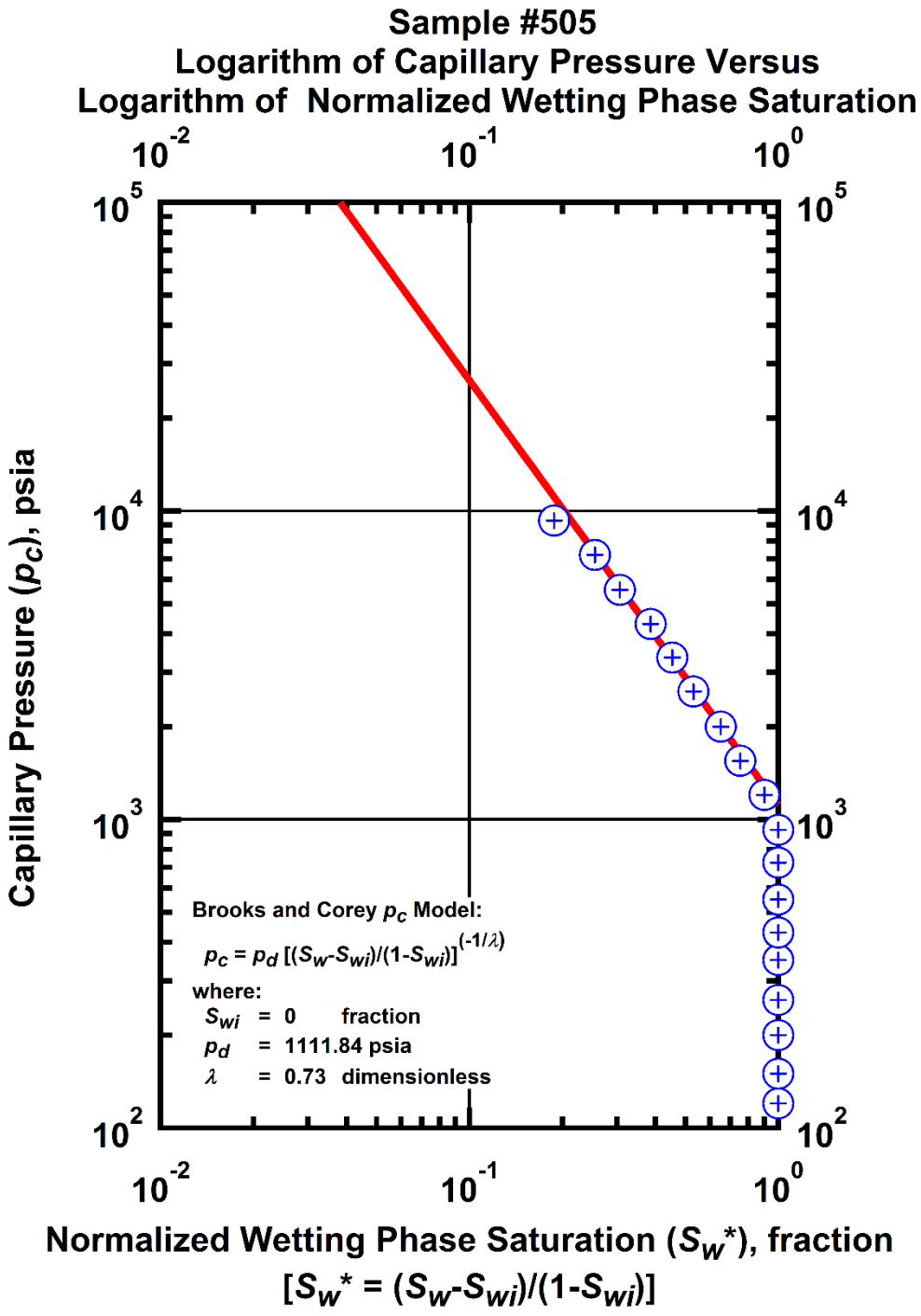

Figure I-45 — Plot of logarithm of capillary pressure vs. logarithm of normalized wetting phase saturation — Sample #505.

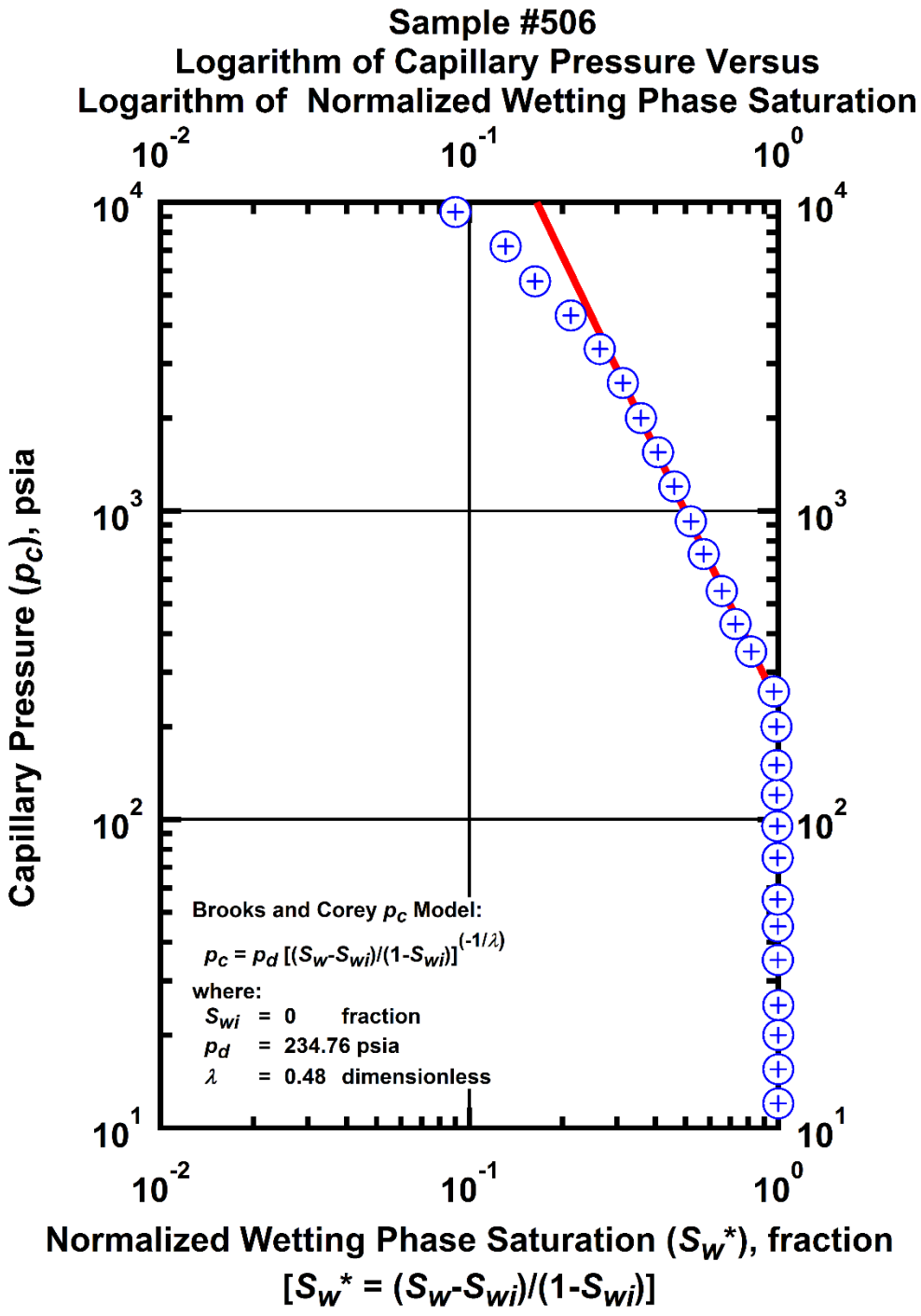

Figure I-46 — Plot of logarithm of capillary pressure vs. logarithm of normalized wetting phase saturation — Sample #506.

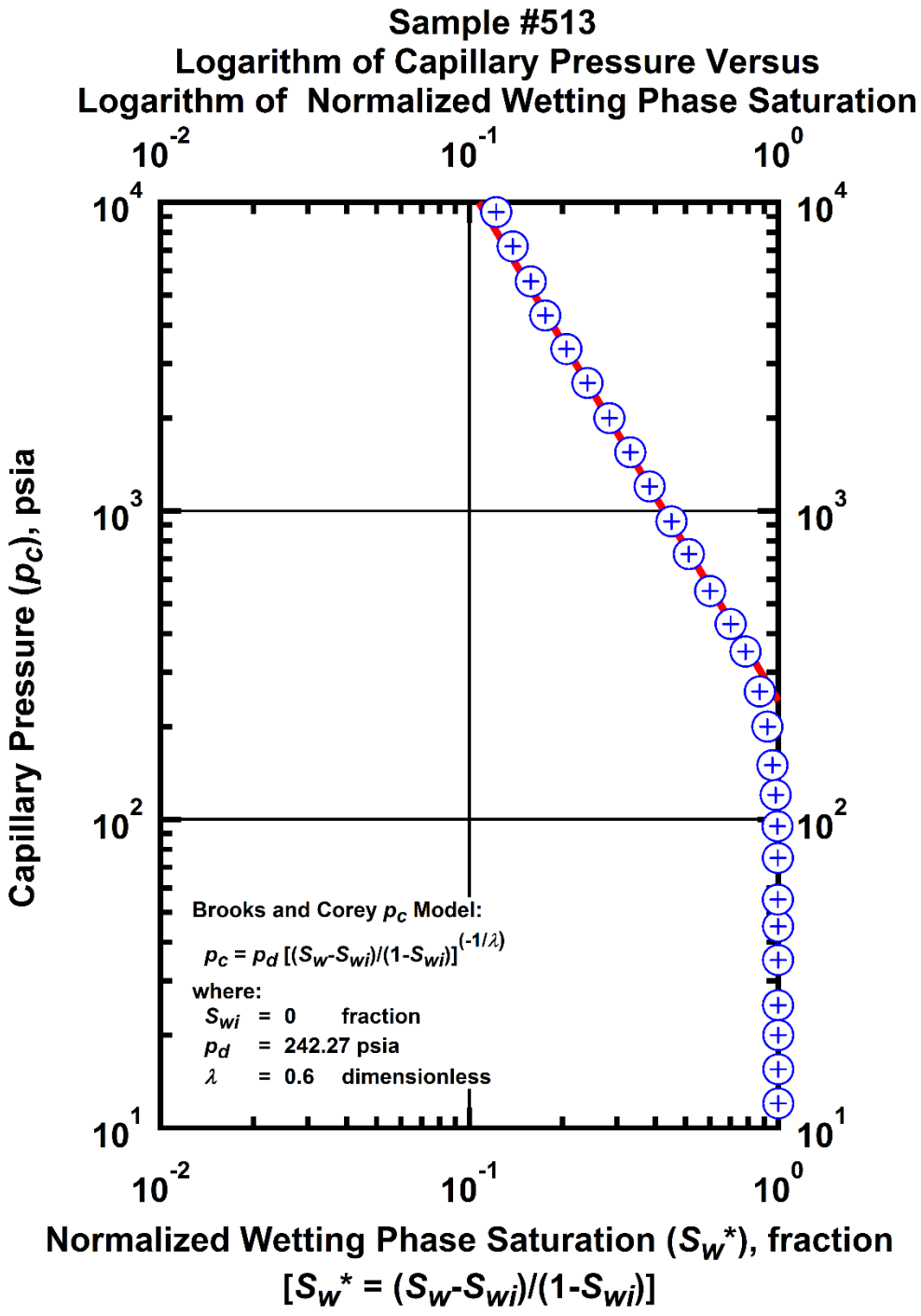

Figure I-47 — Plot of logarithm of capillary pressure vs. logarithm of normalized wetting phase saturation — Sample #513.

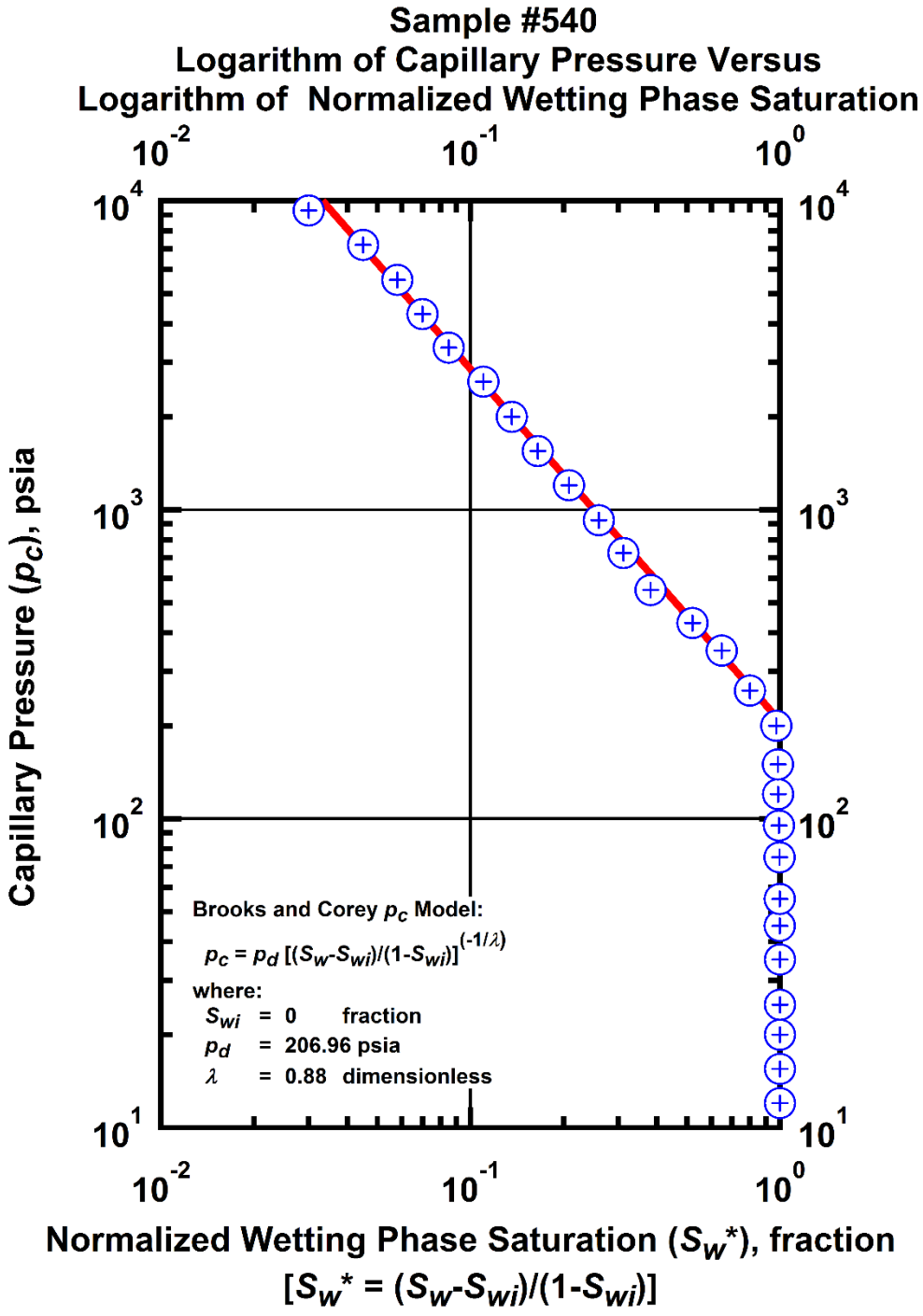

Figure I-48 — Plot of logarithm of capillary pressure vs. logarithm of normalized wetting phase saturation — Sample #540.

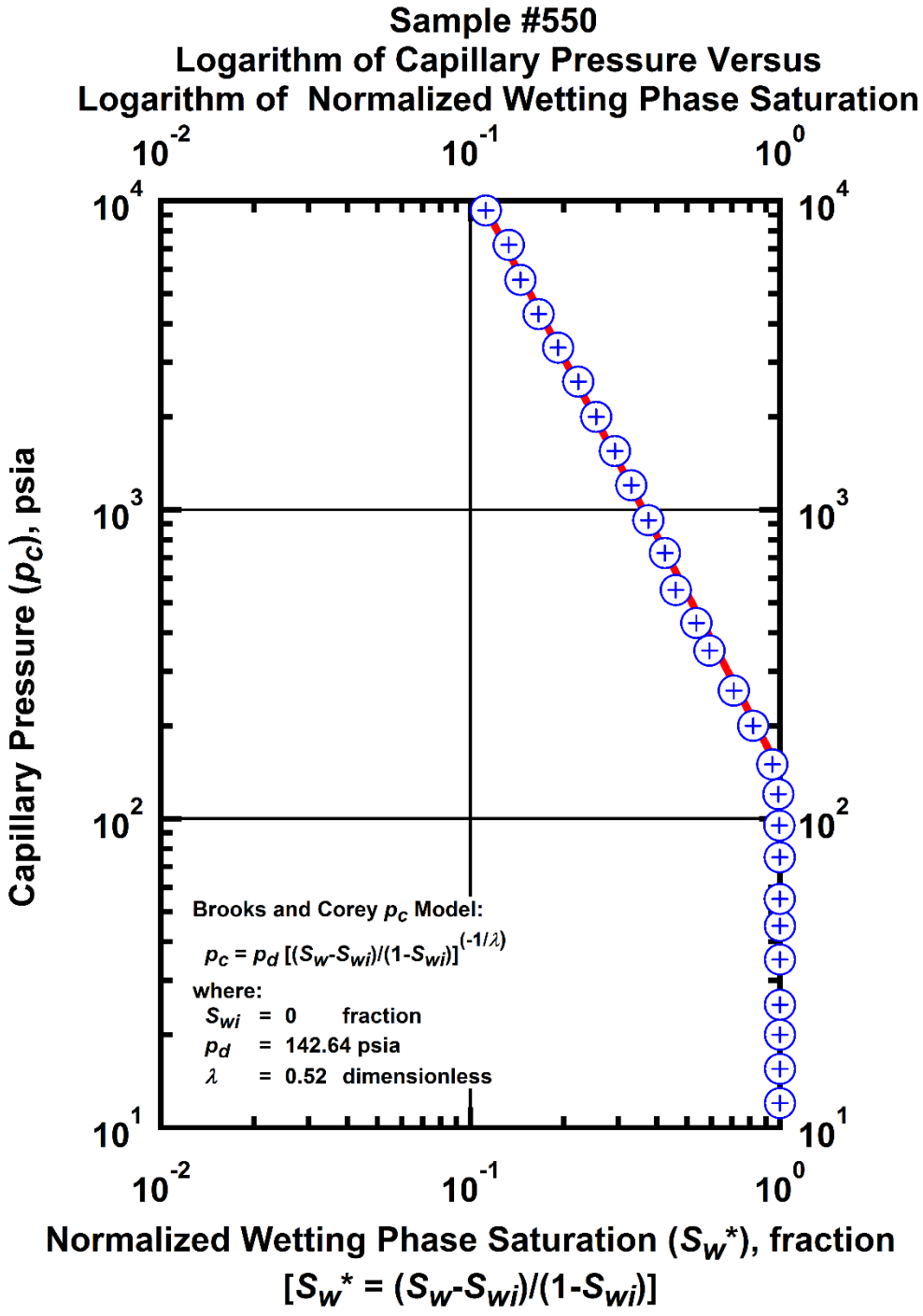

Figure I-49 — Plot of logarithm of capillary pressure vs. logarithm of normalized wetting phase saturation — Sample #550.

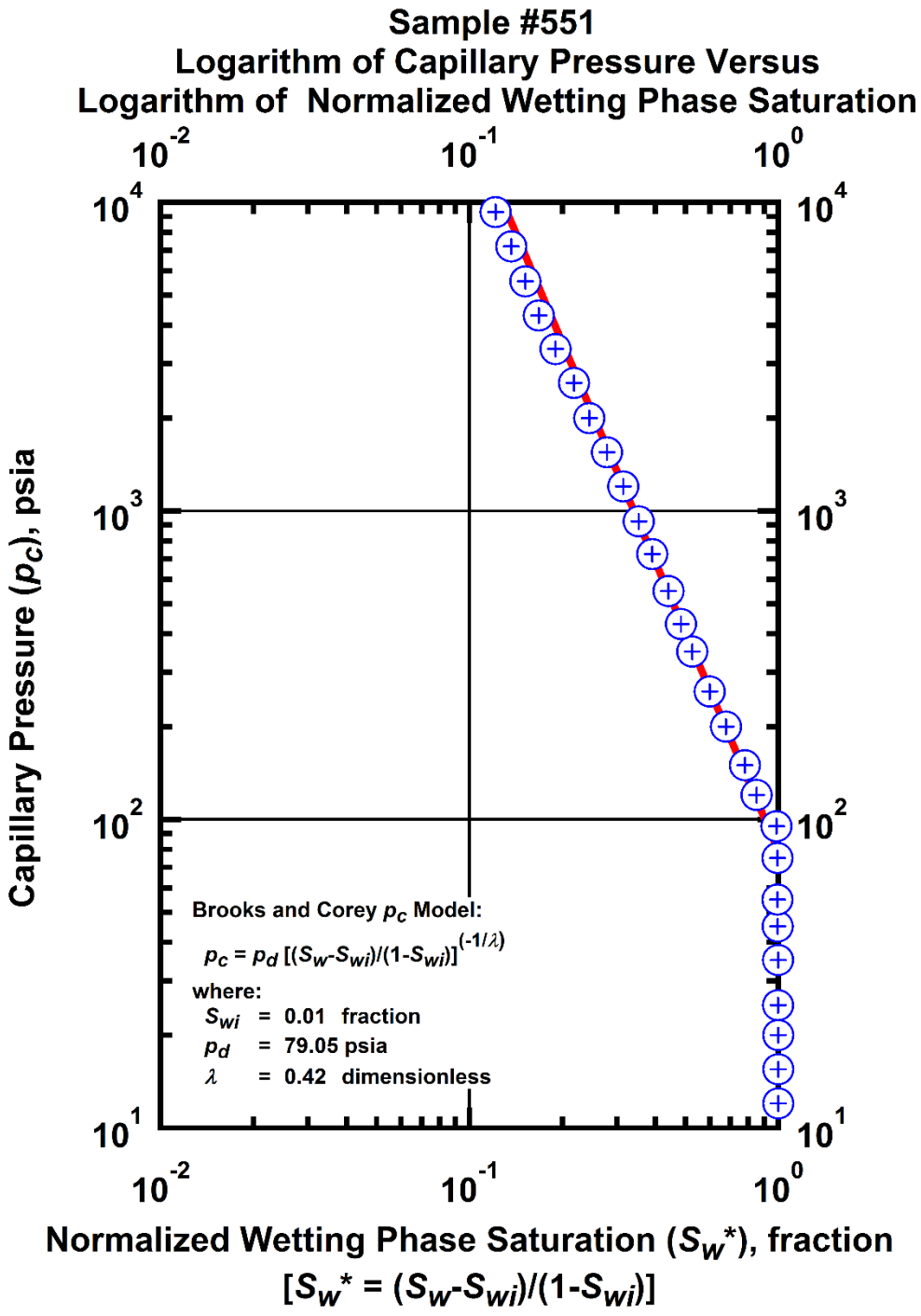

Figure I-50 — Plot of logarithm of capillary pressure vs. logarithm of normalized wetting phase saturation — Sample #551.